Numerical and analytical study of time-resolved luminescence in thin-film semiconductors

Dissertation

zur Erlangung des Doktorgrades der Naturwissenschaften

(*Dr. rer. nat.*)

der

Naturwissenschaftlichen Fakultät II
Chemie, Physik und Mathematik

der Martin-Luther-Universität
Halle-Wittenberg

vorgelegt von

Herrn Matthias Maiberg
geb. am 23.03.1988 in Bernburg (Saale)

Erstgutachter: Prof. Dr. Roland Scheer

Zweitgutachter: Prof. Dr. Steffen Trimper

Drittgutachter: Prof. Dr. Thomas Walter (Hochschule Ulm)

Datum der Einreichung: 22. August 2016

Datum der öffentlichen Verteidigung: 12. Dezember 2016

Mitglieder der Promotionskommission: Prof. Dr. Jochen Balbach (Vorsitz), PD. Dr. Otwin Breitenstein, Prof. Dr. Peter Dold, Prof. Dr. Ingrid Mertig, Prof. Dr. Jörg Schilling, Prof. Dr. Georg Schmidt

Abriss

In der vorliegenden Arbeit wird die zeitaufgelöste Lumineszenz an Dünnschichthalbleitern mithilfe analytischer und numerischer mathematischer Methoden studiert. Die Grundlage der Berechnungen bilden die Kontinuitätsgleichungen, die Stromgleichungen sowie die Poisson-Gleichung. Diese werden sowohl numerisch mit Hilfe des Softwarepakets Synopsys® TCAD, als auch approximativ analytisch gelöst. Untersucht wurde der Einfluss von Band-zu-Band und Shockley-Read-Hall-Rekombination im Volumen und an den Grenzflächen sowie der Einfluss von Drift- und Diffusionstransport von Ladungsträgern auf den zeitlichen Verlauf der Lumineszenz. Die Ergebnisse zeigen, dass für einzelne Absorberschichten unter geringen Anregungen ein exponentieller zeitlicher Verlauf der Lumineszenz zu erwarten ist. Dabei korreliert die Zeitkonstante des Abfalls mit der Leerlaufspannung der Solarzelle. Im konkreten Fall der Halbleiter $Cu(In,Ga)Se_2$ und $Cu_2ZnSnSe_4$ kann diese Korrelation jedoch nicht experimentell bestätigt werden. Dies ist unter anderem auf die Veränderung der Absorberschicht durch die darauffolgende Präparation zurückzuführen, was eine Charakterisierung des Absorbers am Ende des Zellprozesses sinnvoll macht. Es wird gezeigt, dass die dabei auftretenden Drifteffekte in einer spannungsabhängigen zeitaufgelösten Lumineszenzmessungen dahingehend ausgenutzt werden können, nicht nur die Lebensdauer sondern auch die Beweglichkeiten im Absorber zu charakterisieren. Damit bleibt jedoch der Ursprung von experimentell beobachteten multi-exponentiellen Transienten bei einzelnen Absorberschichten unklar. Um diesen auf den Grund zu gehen, wird die zeitaufgelöste Lumineszenz unter erhöhten Anregungen und Temperaturen in Experiment und Simulation studiert. Die gefundenen Abhängigkeiten können mit dem gängigen Modell aus Rekombination, Drift und Diffusion nicht beschrieben werden. Eine Erweiterung des Modells ist daher unabdingbar. Auf der Grundlage der Rechnungen wird gezeigt, dass die Hinzunahme von Potentialfluktuationen im Absorber nicht die gefundenen Transienten wiederspiegeln kann. Erst die Berücksichtigung flacher Haftstellen für Minoritätsladungsträger kann die Lumineszenzexperimente erklären. Als Folge geht im Einklang mit den experimentellen Befunden die Korrelation der Leerlaufspannung und der Zeitkonstante des Lumineszenzabfalls verloren.

Abstract

In this work, time-resolved luminescence on thin-film semiconductors is studied by means of analytical an numerical mathematical methods. The calculations are based on the continuity equations, the current equations as well as the poisson equation. These are solved both numerically using the simulation tool Synopsys® TCAD and approximate analytically. In course thereof, the effect of band-to-band and Shockley-Read-Hall-recombination in the bulk and at the surfaces, as well as the impact of drift and diffusion of charge carriers on the time-dependent decay of the luminescence are investigated. The results show that for single absorber layers under low injections, an exponential time-dependent decay of the luminescence is expected. Additionally, the time-constant of the decay is supposed to correlate with the open-circuit voltage of the solar cell. In the concrete case of the semiconductors $Cu(In,Ga)Se_2$ and $Cu_2ZnSnSe_4$, this correlation can not be confirmed, though. Among others, this can be traced back to a change of absorber properties by the subsequent processing. This makes a characterization of the absorber at the end of the cell processing more reasonable. It is revealed that drift effects, which thereby occur, can be exploited by time-resolved luminescence measurements under different bias voltages in that sense, that not only the lifetime but also the mobilities in the absorber are characterized. With that, the origin of experimentally observed multi-exponential decay curves on single absorber layers remains unclear. For clearification, time-resolved luminescence under elevated injection and temperature is studied in experiment and simulation. The observed dependencies cannot be described with the common model consisting of recombination, drift and diffusion. Therefore, the developement of a more general model is indispensable. Based on the calculations, it is shown that the additional consideration of potential fluctuations in the absorber cannot reflect the found decay curves. Only the consideration of shallow traps for minority carriers is capable to describe the luminescence experiments. In consequence of these trap states, the correlation of the open-circuit voltage and the time-constant of the luminescence decay becomes lost, in accordance with experimental findings.

List of publications

[Mai1]   M. Maiberg and R. Scheer. "Theoretical study of time-resolved luminescence in semi-conductors. 1. Decay from the steady state". In: *Journal of Applied Physics* 116 (2014), p. 123710.

[Mai2]   M. Maiberg and R. Scheer. "Theoretical study of time-resolved luminescence in semi-conductors. 2. Pulsed excitation". In: *Journal of Applied Physics* 116 (2014), p. 123711.

[Mai3]   M. Maiberg, T. Hölscher, S. Zahedi-Azad, and R. Scheer. "Theoretical study of time-resolved luminescence in semiconductors. 3. Trap states in the band gap". In: *Journal of Applied Physics* 118 (2015), p. 105701.

[Mai4]   M. Maiberg, F. Bertram, and R. Scheer. "Theoretical study of time-resolved luminescence in semiconductors. 4. Lateral inhomogeneities". In: *Journal of Applied Physics* (2016). submitted.

[Mai5]   M. Maiberg, C. Spindler, E. Jarzembowski, and R. Scheer. "Electrical characterization of Cu(In,Ga)Se$_2$-solar cells by voltage dependent time-resolved photoluminescence". In: *Thin Solid Films* 582 (2015), pp. 379–382.

[Mai6]   M. Maiberg, C. Spindler, E. Jarzembowski, and R. Scheer. "Characterization of Cu(In,Ga)Se$_2$-solar cells by voltage dependent time-resolved photoluminescence". unpublished.

[Mai7]   M. Maiberg, T. Hölscher, S. Zahedi-Azad, W. Fränzel, and R. Scheer. "Investigation of long lifetimes in Cu(In,Ga)Se$_2$ by time-resolved photoluminescence". In: *Applied Physics Letters* 107 (2015), p. 122104.

[Mai8]   M. Maiberg, T. Hölscher, S. Hartnauer, W. Fränzel, and R. Scheer. "Investigation of long lifetimes in Cu$_2$ZnSnSe$_4$ by time-resolved photoluminescence". unpublished.

[Mai9]   M. Maiberg, T. Hölscher, E. Jarzembowski, S. Hartnauer, S. Zahedi-Azad, W. Fränzel, and R. Scheer. "Verification of minority carrier traps in Cu(In,Ga)Se$_2$ and Cu$_2$ZnSnSe$_4$ by means of time-resolved photoluminescence". In: *Thin Solid Films* (2016). submitted.

[Mai10]   E. Jarzembowski, M. Maiberg, F. Obereigner, K. Kaufmann, S. Krause, and R. Scheer. "Optical and electrical characterization of Cu(In,Ga)Se$_2$ thin film solar cells with varied absorber layer thickness". In: *Thin Solid Films* 576 (2015), pp. 75–80.

[Mai11]   W. Witte, D. Abou-Ras, K. Albe, G. H. Bauer, F. Bertram, C. Boit, R. Brügge-mann, J. Christen, J. Dietrich, A. Eicke, D. Hariskos, M. Maiberg, R. Mainz, M. Meessen, M. Müller, O. Neumann, T. Orgis, S. Paetel, J. Pohl, H. Rodriguez-Alvarez, R. Scheer, H.-W. Schock, T. Unold, A. Weber, and M. Powalla. "Gallium gradients in Cu(In,Ga)Se$_2$ thin-film solar cells". In: *Progress in Photovoltaics: Research and Applications* 23 (2015), pp. 717–733.

[Mai12]   T. Orgis, M. Maiberg, and R. Scheer. "Influence of band gradients on Cu(In,Ga)Se$_2$ solar cell diode factors". In: *Journal of Applied Physics* 114 (2013), p. 214506.

Contents

1 Introduction

In the thin-film photovoltaic industry, semiconductor materials generally have to meet high qualities in terms of large charge carrier lifetimes and mobilities, and low densities of recombinative defects. These quantities must be determined during the preparation process as early as possible without altering the sample's properties. This not only enables the retrieval of malfunctions at an early stage, but also accelerates optimization. The conventional current-voltage or quantum efficiency measurements do not comply with these requirements, since a characterization is possible only at the end of the preparation and the deduced quantities only deliver a limited insight into the microscopic dynamics. Therefore, the demand arose for new non-destructive, fast, and sensitive characterization techniques with the potential for in-line application.

Traditionally, the following two techniques can be mentioned as the best-established: Hall measurements and transient photoconductivity measurements. Hall measurements allow the determination of the minority carrier mobility [1]. In fact, this method can be applied to blank absorbers, but it suffers from the disadvantage that the determined mobility values differ from those under solar cell conditions due to scattering in the magnetic field. Furthermore, neither defect properties nor minority carrier lifetimes can be determined. In order to assess these quantities likewise, a measurement of the transient photoconductivity can be performed. The lifetime is thereby determined from the transient decay of the photoconductivity after a pulsed excitation [2]. By additional illumination with bias light, also the density and energy of shallow defects can be determined [3].

The mentioned methods require an electrical contacting and - in case of transient photoconductivity - only allow time-resolutions larger than 100 ns [4]. Both facts militate against the application of the techniques to thin-film semiconductors. In the first instance, this is due to the metallic back contact on which thin-film semiconductors are typically grown. These do not allow the inductive measurement of the conductivity. Secondly, some thin-film semiconductors exhibit time-constants smaller than 100 ns, which is not experimentally resolvable.

A method, that may overcome this dilemma due to its contactless measurement with time-resolutions down to a few 10 ps is the measurement of time-resolved luminescence (TRL). Depending on the excitation, one can distinguish among others between time-resolved cathodoluminescence (TRCL), electroluminescence (TREL), and photoluminescence (TRPL). For convenience, TRPL is exemplarily investigated in this work. Differences

Figure 1.1: An electron jumps into a higher energy state by absorption of a photon γ. After a certain time the electron jumps back by emission of a photon.
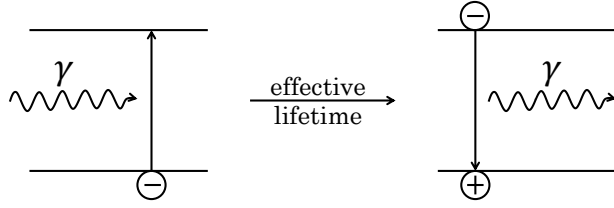
to the other methods are discussed when appropriate. For the purpose of TRL, a semi-conductor is excited, e.g. by light as drawn schematically in figure 1.1. The generated charge carriers recombine radiatively and the emission of photons is observed. In doing so, the average time between charge carrier generation and recombination can be measured. This is called the effective carrier lifetime. It is very sensitive to charge carrier recombination, drift, diffusion, and trapping processes, as well as to material inhomogeneities. Hence, TRL in principle can be used to detect small variations in many material properties. The samples are thereby not destroyed, because the measurement is non-destructive and non-invasive due to excitation with light. It can be applied to any semiconductor independent from the back contact, the substrate, or the number of semiconductor layers in the stack. Apart from that, the measurement setup is very simple, which led to an extensive application of TRL on photovoltaic thin-film semiconductors. In the course thereof, a correlation between the luminescence decay time and the solar cell efficiency has been reported for $Cu(In,Ga)Se_2$ (CIGSe) by Ohnesorge et al. [5] and by Keyes et al. [6]. Metzger et al. [7] showed similar results for CdTe. Since then, the luminescence decay was an important quantity for characterizations of photovoltaic devices. It was used to optimize the annealing temperature of $Zn_{1-x}Mg_xO/Cu(In,Ga)Se_2$ interfaces [8], or as a process monitor in CIGSe solar cell preparation [9, 10].

Despite the numerous successfull applications of TRL in photovoltaics, further experiments on the semiconductors $Cu(In,Ga)Se_2$ and $Cu_2ZnSnSe_4$ (CZTSe), which will be the working examples in this thesis, still pose lots of open questions. For instance, the luminescence decay can be mono- or bi-exponential, which is exemplified in figure 1.2 (a) for two different CZTSe absorbers. Such a characteristic of TRL has often been reported not only for CZTSe but also for CIGSe absorbers [11–15]. However, the origin of a luminescence decay with more than one time constant was still not clear and the time constants could not be related to the effective carrier lifetime either. Figure 1.2 (b) demonstrates two other pecularities mainly occuring on CIGSe absorbers. The figure shows the luminescence decay time for CIGSe absorbers (determined from the 1/e decay) plotted against the open-circuit voltage of the complete solar cell. First of all, decay times in the range of radiative recombination ($\sim 500\,$ns [16]) occur, in agreement with decay time values reported in literature [17]. This fact is not comprehensible, since CIGSe is a very defective semiconductor with estimated effective recombination lifetimes $\tau_{eff,r}$ of a few $10\,$ns.[1]

---

[1]This follows from simulations of $Voc(\tau_{eff,r})$ with values from Ref. [16]. It comes out, that the current record efficiency of a $Cu(In,Ga)Se_2$ solar cell of $22.6\,\%$ [18] may be achieved with $\tau_{eff,r} \approx 10\,$ns.
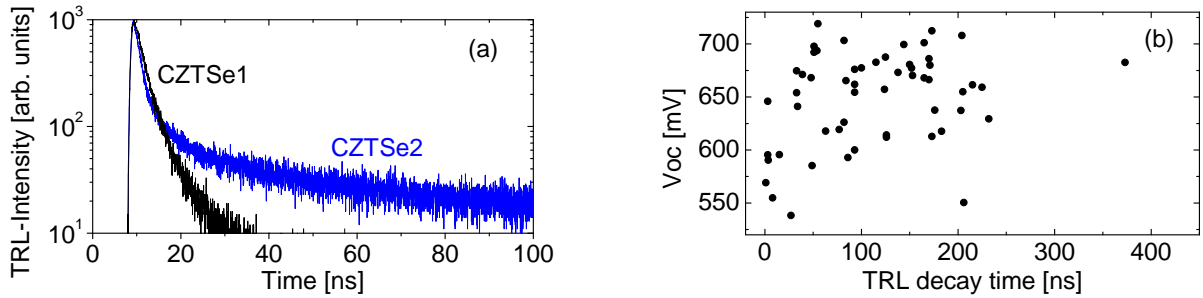
Figure 1.2: (a) Mono- and bi-exponential luminescence decay of two different $Cu_2ZnSnSe_4$ absorber layers and (b) luminescence decay time (determined from the $1/e$ decay) of $Cu(In,Ga)Se_2$ absorbers measured immediately after the preparation process vs. open-circuit voltage of the final solar cell. With kind permission of Stefan Hartnauer and Enrico Jarzembowski.

Furthermore, the figure shows that there is no clear correlation between the open-circuit voltage and the luminescence decay time in contrast to the above mentioned correlations reported for CIGSe and CdTe. This suggests that the luminescence time constant and the effective carrier lifetime are not equal. This is due to the large number of effects in polycrystalline thin-film semiconductors, that influence the luminescence decay thereby hindering the determination of the effective carrier lifetime. Actually, this variety of effects raises two more problems of the luminescence decay analysis: first, the time constant may strongly depend on experimental conditions such as excitation intensity or excitation duration, because the recombination and transport processes may become different. In consequence, material parameters determined under steady state excitation (e.g. open-circuit voltage measurement) cannot be extrapolated from measurements under pulsed excitation (TRL measurement). Secondly, an optimum experimental route must be designed aiming at the discrimination of each effect influencing the luminescence decay, which will then enable the isolation of the effective carrier lifetime. The definition of such an optimized experiment is still a big challenge for the TRL data analysis [19]. Therefore, at this time the data cannot be interpreted automatically by an algorithm applied to only one time-resolved luminescence measurement. This makes an in-line characterization by means of TRL difficult.

The claim for an "ideal" experimental route and an interpretation algorithm raises the demand for a broad theory of TRL, which was first provided by Richard K. Ahrenkiel for III-V semiconductors [20]. He calculated the luminescence time constants for radiative and non-radiative recombination and addressed its strong excitation dependence. Further, he explained that the time constant will be below the effective carrier lifetime, if the charge carriers are generated within an electric field. This has often been approved for solar cells by experiment [21–23] and by numerical solution of the semiconductor equations applied to a GaAs pn-junction [24]. A more detailed but mostly numerical analysis of charge recombination within an electric field was done by Kanevce et al. [25] by simulation of TRL on a CdTe solar cell.

On the basis of these preliminary results, the present thesis was written with the setted goal to characterize a thin-film semiconductor by time-resolved luminescence. For this purpose, the following milestones are defined: the present theoretical understanding of TRL in III-V semiconductors has to be adopted first to thin-film semiconductors in general. This includes the derivation of analytical formulae for the time constants of the luminescence governed by space charges, charge carrier transport, trapping, surface, or bulk recombination. As will be shown, the time constant of each effect exhibits a different dependence on excitation intensity and device temperature. Therefore, measurement scenarios can be figured out to discriminate each effect, and by using the formulae for the time constants, lifetimes, mobilities and recombination velocities can be quantified. Finally, a model of the semiconductor can be set up based on the determined values. Afterwards, this model must be approved or improved if necessary by loop-wise comparison of experimental and theoretical luminescence decay curves.

To attain these milestones, this cumulative thesis starts with a derivation of the basic semiconductor equations in chapter 2. This derivation is carried out explicitly to highlight the necessary assumptions, since these limit the reliability of the simulations. In the course of the derivation, the very important material parameter of the recombination lifetime occurs. Therefore, chapter 3 adresses time constants in general. After a few introductive definitions of decay times and lifetimes, their determination by means of TRL is described and problems are highlighted. Then, the method is compared to other lifetime measurement techniques, and advantages and disadvantages are pointed out. On the basis of chapters 2 and 3, TRL can be simulated. A description of the simulations and the numerical solution of the semiconductor equations will be carried out in chapter 4.

After establishing the basis of TRL in chapters 2−4, the results of the simulations and experiments are presented in chapter 5. First, the influence of drift, diffusion, bulk- and surface recombination on the luminescence decay is investigated for different injection levels by simulation. It turns out, that the luminescence decay in solar cells is mostly dominated by bulk recombination and drift transport. With this knowledge, the luminescence decay of a solar cell is measured to determine the charge carrier mobilities and the minority carrier lifetime of the absorber layer. The result is approved by comparison of experiment and simulation. Despite the good congruence, the theory of TRL at that point may not explain bi-exponential decays with decay times up to the radiative limit. Therefore, the model is extended to shallow defects that are defects close to the conduction or valence band. These are studied by simulation in general. Then, this extended model is used to approximate experimental TRL of absorbers which yields a good fit. The chapter ends with a generalization of the simulations to higher dimensions to account for the impact of lateral inhomogeneities on the luminescence decay. A short conclusion of the results with propositions for future work closes the thesis.

2 Charge carrier dynamics

In this chapter, the semiconductor equations required for the simulation and analyzation of time-resolved luminescence are introduced. Each equation will be derived or justified to point out the assumptions and the limitations of the model. First, the density of electrons and holes in a semiconductor is calculated using statistical quantum mechanics. Due to the mobile charge carriers, macroscopic electric fields may occur. Therefore, the Poisson equation is derived, which is one of the three basic semiconductor equations. It relates the electrostatic potential and the charge carrier densities. As a consequence of the electric field the charge carriers drift. For this reason, the current equations and the continuity equations are deduced from the semi-classical, bipolar Boltzmann equation. These are the second and the third fundamental semiconductor equations. An input of the continuity equation is the generation and recombination of electrons and holes - both are the basis for TRL. The rate of generation and recombination is calculated for band-to-band and free-to-bound transitions. In the end, all assumptions are summarized and discussed regarding the comparability of experimental and simulated time-resolved luminescence. This is intentionally not done at the place of application, since many assumptions are related to each other which makes an overall discussion more reasonable.

2.1 Charge carrier statistics

In this section, electrons in a compensated semiconductor with direct band gap are considered. The energy diagram is drawn schematically in figure 2.1 for the first Brillouin zone (1. BZ). According to the Born-Oppenheimer and the Hartree-Fock approximation [26, 27] the state of an electron can be described by three discrete quantum numbers: the band index ν, the pseudo-wavevector $k \in 1.\,\mathrm{BZ}$, and the spin s. Hence, the energy of an electron is denoted by $E_{\nu,s}(k)$. As stated in the introduction, the electrons change
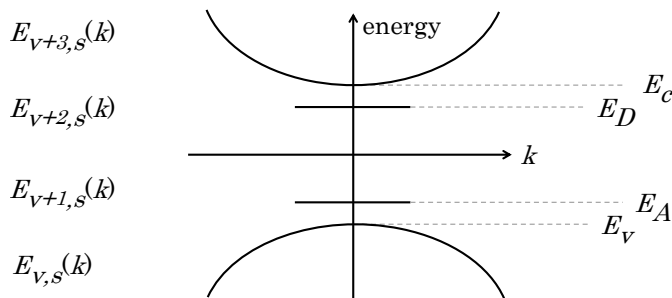

Figure 2.1: Schematic energy diagram of electrons in a compensated semiconductor in reduced zone scheme with valence band edge E_v, conduction band edge E_c, acceptor level E_A, and donor level E_D. Each state of electron can be denoted by the spin s, the pseudo-wavevector k and the main quantum number ν.

their energy state when being excited. The rate of transitions depends on the average occupation f of the quantum states which is deduced in the following. For macroscopic diameters of the semiconductor the number of electrons is $\sim 10^{23}$ and the derivation of f can be made by a statistical approach using the grand canonical partition function [27]. For non-degenerate energy states, the result is the Fermi-Dirac distribution

$$f\left(E_{\nu,s}(k)\right) = \left(1 + e^{\frac{E_{\nu,s}(k) - E_f}{k_B T}}\right)^{-1} \tag{2.1.1}$$

with the Boltzmann constant k_B and the Fermi-level E_f of electrons, that depends among others on the temperature T and on the energy levels $E_{\nu,s}(k)$. In particular, it depends on the total number of electrons N_e, and can be determined from the condition $N_e = \sum_{\nu,k,s} f\left(E_{\nu,s}(k)\right)$. This is comprehensible, since $f\left(E_{\nu,s}(k)\right)$ is the mean number of electrons in the quantum state $\{\nu, s, k\}$. Therefore, summation over all quantum states must equal the total number of electrons. By the volume V of the semiconductor, this condition can be rewritten for the total electron density n_e:

$$n_e = \frac{N_e}{V} = \sum_{\nu} \int_{\mathbb{R}} \underbrace{\left(\frac{1}{V} \sum_{k,s} \delta(E - E_{\nu,s}(k))\right)}_{=D_\nu(E)} f(E) \, \mathrm{d}E. \tag{2.1.2}$$

δ is the Dirac-distribution and $D_\nu(E)$ is the density-of-states of the ν-th energy band. It gives the number of quantum states in the ν-th energy band within the energy range $E \dots E + \mathrm{d}E$. For discrete acceptor levels, this can be easily calculated. For acceptor states it holds $E_{A,s}(k) = E_A$. If there are N_A acceptors in the semiconductor, each being able to capture only one electron, the degree of degeneracy of the energy level E_A will be N_A. Similarly, discrete donor levels with $E_{D,s}(k) = E_D$ can emit one electron and the energy level E_D is degenerated N_D-times. The density-of-states of acceptors and donors become

$$D_A(E) = n_A \, \delta\left(E - E_A\right) \tag{2.1.3a}$$

$$D_D(E) = n_D \, \delta\left(E - E_D\right) \tag{2.1.3b}$$

with $n_A = \frac{N_A}{V}$ and $n_D = \frac{N_D}{V}$ being the acceptor and donor density, respectively. The acceptor states are neutral (0) when being unoccupied by an electron. They are negatively charged ($-$) when being occupied by an electron. The probability of occupation is given by f. By contrast, the donor states are neutral (0) when being occupied and positively charged ($+$) when being unoccupied. The probability of unoccupation is given by the complementary function $1 - f$. The equilibrium densities n_A^- and n_D^+ of ionized dopants

follow from equation (2.1.2):

$$n_A^- = \int_{\mathbb{R}} D_A(E) f(E) \, \mathrm{d}E = \frac{n_A}{1 + \mathrm{e}^{\frac{E_A - E_f}{k_{\mathrm{B}} T}}} \stackrel{E_f - E_A > 3 \, k_{\mathrm{B}} T}{\approx} n_A \tag{2.1.4a}$$

$$n_D^+ = \int_{\mathbb{R}} D_D(E) \left(1 - f(E)\right) \, \mathrm{d}E = \frac{n_D}{1 + \mathrm{e}^{-\frac{E_D - E_f}{k_{\mathrm{B}} T}}} \stackrel{E_D - E_f > 3 \, k_{\mathrm{B}} T}{\approx} n_D. \tag{2.1.4b}$$

It turns out that most of the acceptors will be ionized if the Fermi-level lies far above E_A with respect to $k_{\mathrm{B}} T$. Analogously, almost all donors will be ionized if the Fermi-level lies far below E_D with respect to $k_{\mathrm{B}} T$. This is the so-called impurity exhaustion.

For broad energy bands, the inner sum in equation (2.1.2) is more difficult to evaluate. However, for large semiconductor diameters the pseudo-wavevectors are quasi-continuous and the sum over k can be transformed into an integral over the first Brillouin zone by $\sum_k \rightarrow \frac{V}{8 \, \pi^3} \int_{1.\mathrm{BZ}} \mathrm{d}k$. Hence, the density-of-states of the ν-th energy band can also be calculated by

$$D_\nu(E) = \frac{1}{8 \, \pi^3} \sum_s \int_{1.\mathrm{BZ}} \delta(E - E_{\nu,s}(k)) \, \mathrm{d}k. \tag{2.1.5}$$

For further evaluation the dispersion relation $E_{\nu,s}(k)$ must be known. From the k·p-theory it follows $E_{\nu,s}(k) \approx E_{\nu,s,0} + \frac{\hbar^2}{2 \, m_{\nu,s}^*} k^2$ for isotropic semiconductors. Here, $\hbar$ is the reduced Planck constant and $m_{\nu,s}^*$ is the effective mass of electrons in the ν-th energy band with spin s. The parabolic energy dispersion approximates the energy bands only close to the extrema; at the boundaries of the 1. BZ the error can become very large. In the following it is exemplified for the conduction band how this problem is circumvented. The conduction band is the lowest unoccupied energy band. Following the notation from figure 2.1, it is denoted by the subscript c. Additionally, the electrons shall have a positive effective mass independent of spin or direction: $m_{c,s}^* = m_c^* > 0$. It is now assumed that the number of electrons in the conduction band is small. Then, only energy states close to the conduction band minimum are occupied (due to energy minimization), and higher energy states (with poorly approximated energy dispersion) do not contribute to the electron density anyway. This is the keynote of the low-density-approximation. Actually, this allows an extension of the integration volume in (2.1.5) to $\mathbb{R}^3$. Consequently, the density-of-states of the conduction band becomes

$$D_c(E) = \frac{1}{2 \, \pi^2} \left(\frac{2 \, m_c^*}{\hbar^2}\right)^{3/2} \begin{cases} \sqrt{E - E_c}, & E \geq E_c \\ 0, & E < E_c. \end{cases} \tag{2.1.6}$$

Now, the equilibrium density n_0 of electrons in the conduction band can be calculated:

$$n_0 = \int_{\mathbb{R}} D_c(E) f(E) \, \mathrm{d}E = N_c \, F_{1/2}\left(\frac{E_c - E_f}{k_{\mathrm{B}} T}\right) \stackrel{E_c - E_f > 3 \, k_{\mathrm{B}} T}{\approx} N_c \, \mathrm{e}^{-\frac{E_c - E_f}{k_{\mathrm{B}} T}}. \tag{2.1.7}$$

$N_c = 2 \left(\frac{m_c^* k_B T}{2 \pi \hbar^2} \right)^{3/2}$ is the effective density-of-states of the conduction band. The function $F_{1/2}(\cdot)$ is the Fermi-Dirac integral which converges for large arguments against a Boltzmann distribution function. This is the so-called Boltzmann approximation and will be valid if the Fermi-level is far below the conduction band edge with respect to $k_B T$.

The highest occupied energy band is called valence band, is denoted by the subscript v, and the effective mass of electrons is negative and assumed to be independent of spin and direction: $m_{v,s}^* = -m_v^* < 0$. Due to the high occupation of the valence band it is more reasonable to study the unoccupied states - these are termed holes. By applying the low-density-approximation to the holes the density-of-states of the valence band becomes

$$D_v(E) = \frac{1}{2 \pi^2} \left(\frac{2 m_v^*}{\hbar^2} \right)^{3/2} \begin{cases} \sqrt{E_v - E} & E \le E_v \\ 0 & E > E_v. \end{cases} \tag{2.1.8}$$

The probability for unoccupation again is $1 - f$. Therewith, the equilibrium density p_0 of holes in the valence band becomes

$$p_0 = N_v F_{1/2} \left(\frac{E_f - E_v}{k_B T} \right) \overset{E_f - E_v > 3 k_B T}{\approx} N_v e^{-\frac{E_f - E_v}{k_B T}} \tag{2.1.9}$$

with the effective density-of-states of the valence band $N_v = 2 \left(\frac{m_v^* k_B T}{2 \pi \hbar^2} \right)^{3/2}$. Again, the Boltzmann approximation holds for Fermi-levels far above the valence band edge with respect to $k_B T$.

A consequence of equation (2.1.2) is the neutrality condition. For a temperature $T = 0$, only valence band and donor states are occupied by electrons. Hence, the total electron density becomes

$$n_e = n_D + \int_{\mathbb{R}} D_v(E) \, \mathrm{d}E. \tag{2.1.10}$$

By equation of (2.1.2) and (2.1.10) follows $n_0 + n_A^- = p_0 + n_D^+$. This neutrality condition determines the Fermi-level and thus all carrier densities by the equations (2.1.4), (2.1.7), and (2.1.9). Hence, in equilibrium the densities cannot be set independently. This changes for small perturbations from equilibrium, e.g. due to illumination. Then, the electron and hole densities n and p are still given by a Fermi-Dirac distribution, but each has its own Fermi-level E_{fn} and E_{fp}, respectively; thereby, enabling the independence of both:

$$n = N_c F_{1/2} \left(\frac{E_c - E_{fn}}{k_B T} \right) \overset{E_c - E_{fn} > 3 k_B T}{\approx} N_c e^{-\frac{E_c - E_{fn}}{k_B T}} \tag{2.1.11a}$$

$$p = N_v F_{1/2} \left(\frac{E_{fp} - E_v}{k_B T} \right) \overset{E_{fp} - E_v > 3 k_B T}{\approx} N_v e^{-\frac{E_{fp} - E_v}{k_B T}}. \tag{2.1.11b}$$

In contrast to electrons and holes, the density of ionized dopants in non-equilibrium can

no longer be described by a Fermi-Dirac distribution. Instead, the occupation of the dopants has to be determined from transition rates of electrons into or from the doping level (see sec. 2.4). This leads to a density of occupied dopants, which will be given later for the steady state by equation (2.4.15). It turns out that in the limit of the low-density-approximation impurity exhaustion $n_A^- \approx n_A$ and $n_D^+ \approx n_D$ can be assumed even in non-equilibrium.

2.2 Poisson equation

Due to the mobile charge carriers and immobile donors and acceptors, space charges may occur. The space and time dependent space charge density $\varrho(r,t)$ is given by

$$\varrho(r,t) = e_0 \left(p(r,t) - n(r,t) + n_D^+(r,t) - n_A^-(r,t) \right) \tag{2.2.1}$$

with the elementary electric charge $e_0 > 0$. Because of the impurity exhaustion approximation, it is $n_D^+(r,t) = n_D(r)$ and $n_A^-(r,t) = n_A(r)$. The space charge in equation (2.2.1) creates an electric field. The interplay of space charges and electric fields is described by Maxwell's equations which are used in the following form [28]:

$$\mathrm{div}\, D = \varrho \tag{2.2.2a}$$

$$\mathrm{div}\, B = 0 \tag{2.2.2b}$$

$$\mathrm{rot}\, E = -\frac{\partial}{\partial t} B \tag{2.2.2c}$$

$$\mathrm{rot}\, H = J + \frac{\partial}{\partial t} D. \tag{2.2.2d}$$

D is the displacement field, B is the magnetic field, E denotes the electric field, H is the magnetizing field, and J denotes the total current density. The equation (2.2.2b) is formally solved by $B = \mathrm{rot}\, A$ with the so-called vector potential A. Inserting this into equation (2.2.2c) yields the formal solution

$$E = -\nabla_r \varphi - \frac{\partial}{\partial t} A \tag{2.2.3}$$

with the gradient operator ∇_r acting on the scalar electric potential φ. The materials studied in this work are not magnetic. Therefore, magnetic effects are mostly neglected and the vector potential A becomes zero. Then, the electric field can be calculated from the electric potential by

$$E = -\nabla_r \varphi. \tag{2.2.4}$$

By equation (2.2.4), the calculation of the electric field has been transformed into the calculation of φ. As a conditional equation for φ, the first Maxwell equation (2.2.2a) is

used. For this purpose, the displacement field D is formally expanded by powers of E. For small electric fields it is $D = \varepsilon_0 \varepsilon_r E$, with the permittivity of vacuum ε_0 and the relative permittivity of the material ε_r. The relative permittivity ε_r is a tensor of second order. In this thesis, ε_r is assumed to be isotropic, piecewise homogeneous, and independent of time. This excludes ferroelectric and non-linear optic effects. Inserting $D = \varepsilon_0 \varepsilon_r E$, equation (2.2.3), and $\varepsilon_r = \text{const.}$ into the Maxwell equation (2.2.2a) yields the Poisson equation:

$$\Delta_r \varphi = -\frac{\varrho}{\varepsilon_0 \varepsilon_r} = -\frac{e_0}{\varepsilon_0\,\varepsilon_r}\left(p(r,t) - n(r,t) + n_D(r) - n_A(r)\right). \qquad (2.2.5)$$

This is a conditional equation for the electric potential φ and allows the determination of the electric field by equation (2.2.4).

2.3 Transport equations

Due to the electric field in equation (2.2.3) the charge carriers move. Knowledge about this motion is indispensable for a theory of time-resolved luminescence since the transport of charge carriers can enhance or reduce the recombination. The theory of charge carrier transport, whose derivation will be carried out in this section, is of statistical nature to account for the statistically distributed velocities of the charge carriers. In the end, the very important transport equations of electrons and holes will arise. However, before starting with the derivation the scope of the theory has to be defined: the basic transport equations of charge carriers in semicondutor devices can be distinguished by semi-classical and quantum mechanical approaches [26, 29]. The quantum mechanical approaches will become important, if the device size is in the range or even smaller than the characteristic lengths of carrier-carrier, carrier-lattice, or carrier-defect scattering. Since the devices in this thesis are larger than $500\,\text{nm}$ in diameter, quantum effects do not have to be considered and semi-classical approaches are sufficient and appropriate due to their calculation time saving properties. The semi-classical approaches in turn are divided into diffusive and hydrodynamic models depending on the characteristic lengths. Here, only the drift-diffusion model is studied, which is derived from the electron distribution function $f_{\nu,s}(r,k,t)$ - the subscripts s and ν in the following are left out. The starting point is $\frac{\mathrm{d}}{\mathrm{d}t}f(r(t),k(t),t) = 0$, which is a consequence of the Liouville theorem [26]. Evaluating the time derivative leads to

$$\frac{\partial}{\partial t}f + \frac{\mathrm{d}r}{\mathrm{d}t}\nabla_r f + \frac{\mathrm{d}k}{\mathrm{d}t}\nabla_k f = 0, \quad r \in \mathbb{R}^3,\ k \in 1.\text{BZ},\ t > 0. \qquad (2.3.1)$$

In accordance with k·p-theory it is $\frac{\mathrm{d}r}{\mathrm{d}t} = \frac{1}{\hbar}\nabla_k E(k)$ and $\frac{\mathrm{d}k}{\mathrm{d}t} = \frac{F}{\hbar}$, with F being the force acting on the charge carriers. F is a superposition of external forces F_{ex}, for example by an applied electric field, and inner forces F_{in} due to the scattering of electrons with phonons, impurities, or other charge carriers. Therefore, the unipolar Boltzmann transport equation

(2.3.1) is written in the form [28]

$$\partial_t f + \frac{1}{\hbar}\nabla_k E(k)\,\nabla_r f + \frac{F_{ex}}{\hbar}\,\nabla_k f = -\frac{F_{in}}{\hbar}\,\nabla_k f = Q(f), \qquad (2.3.2)$$

with Q being an operator acting on f; thereby, describing the net-collision of electrons. For the collision operator Q the following ansatz is made [30]:

$$Q(f) = \int_{\mathbb{R}^3 \times \mathbb{R}^3 \times \mathbb{R}} f(r',k',t')\,(1 - f(r,k,t))P(r',k',t';r,k,t)\mathrm{d}t'\mathrm{d}r'\mathrm{d}k'$$
$$- \int_{\mathbb{R}^3 \times \mathbb{R}^3 \times \mathbb{R}} f(r,k,t)\,(1 - f(r',k',t'))P(r,k,t;r',k',t')\mathrm{d}t'\mathrm{d}r'\mathrm{d}k'. \qquad (2.3.3)$$

$P(r',k',t';r,k,t)$ is the probability rate of electron scattering from the state (r',k',t') into the state (r,k,t). The equation (2.3.2) together with (2.3.3) is a semi-classical, microscopic integro-differential equation for the distribution function f. In general, it can only be solved numerically, e.g. by Monte-Carlo-methods. To obtain an approximate analytic solution, the following assumptions are made:

- The scattering is assumed to be localized and fast compared to macroscopic length and time scales: $P(r',k',t';r,k,t) = \delta(t - t')\,\delta(r - r')\,\Pi(r',k';k)$. The scatter probability rate Π is assumed to be independent of time.

- The electron temperature is homogeneous and equals the lattice temperature.

- Low occupation is assumed, in accordance with section 2.1. Low occupation means $f \ll 1$ and $1 - f \approx 1$. This will be true, if the Fermi-level is far below the electron energy with respect to $k_\mathrm{B}\,T$. Then, the equilibrium Fermi-Dirac distribution (2.1.1) is approximated by a Maxwell-Boltzmann distribution $f_{eq} = \mathrm{e}^{-\frac{E(r,k)-E_f}{k_\mathrm{B}\,T}}$.

- The energy dispersion is approximated by a parabola $E(r,k) = E_0(r) + \frac{\hbar^2}{2\,m^*}k^2$, since the high energy states (with poorly approximated energy) are not occupied.

- The deviations from equilibrium are small.

By using this, the Boltzmann equation (2.3.2) in low density and relaxation time approximation becomes

$$\partial_t f + \frac{\hbar}{m^*}k\,\nabla_r f + \frac{e_0}{\hbar}\,\nabla_r \varphi_{eff}\,\nabla_k f = Q_\tau(f) = -\frac{f - f_{eq}}{\tau_{rel}}. \qquad (2.3.4)$$

In equation (2.3.4), $\tau_{rel} = \tau_{rel}(r)$ is the relaxation time, $Q_\tau(f)$ is the relaxation time operator, and φ_{eff} is an effective electric potential to account for external forces. Equation (2.3.4) is a partial differential equation for the distribution function f of electrons with spin s in the ν-th energy band. It is pointed out that the electrons neither change the energy band (ν) nor the spin (s) when being scattered as a result of the special collision

operator (2.3.3). If the solution $f(r, k, t)$ of (2.3.4) was known, macroscopic quantities could be evaluated, e.g. the density of electrons in the conduction band by $n(r, t) = \frac{1}{V} \sum_{k,s} f_{c,s}(r, k, t)$ with the volume V of the semiconductor. To find an approximate solution of (2.3.4), dimensionless quantities $\widetilde{r}, \widetilde{k}, \widetilde{t}, \widetilde{\varphi}_{eff}, \widetilde{Q}_\tau$ are at first defined as follows:

$$r = \lambda \widetilde{r}, \quad t = \tau \widetilde{t}, \quad k = \frac{m^* u}{\hbar} \widetilde{k}, \quad u = \sqrt{\frac{k_B T}{m^*}}, \quad \varphi_{eff} = \frac{k_B T}{e_0} \widetilde{\varphi}_{eff},$$

$$\lambda_c = u\, \tau_c, \quad \tau = \frac{\lambda_c^2}{\lambda^2}\, \tau_c, \quad Q_\tau = \frac{1}{\tau_c} \widetilde{Q}_\tau, \quad \widetilde{f}_{eq} = \mathrm{e}^{-\frac{E_0 - E_f}{k_B T}}\, \mathrm{e}^{-\frac{\widetilde{k}^2}{2}}. \tag{2.3.5}$$

τ describes a macroscopic time and λ a macroscopic length, whereas τ_c describes the mean time between two scattering events and λ_c the mean free path. It is emphasized that even the equilibrium Maxwell-Boltzmann distribution function is scaled. By this scaling, equation (2.3.4) is rewritten as the scaled Boltzmann equation (the $\sim$ is left out)

$$\alpha^2\, \partial_t f_\alpha + \alpha \left(k\, \nabla_r f_\alpha + \nabla_r \varphi_{eff}\, \nabla_k f_\alpha \right) = -\frac{f_\alpha - f_{eq}}{\tau_{rel}}, \tag{2.3.6}$$

where the Knudsen-number α is defined by $\alpha = \frac{\lambda_c}{\lambda} = \sqrt{\frac{\tau_c}{\tau}}$. f_α denotes the solution of the scaled Boltzmann equation (2.3.6) parametrized by α. This thesis assumes time scales larger than the collision time and device diameters larger than the collision length. Thus, it is $\alpha \ll 1$. To solve (2.3.6) within the limit $\alpha \to 0$ the formal Chapman-Enskog-expansion $f_\alpha = f_{eq} + \alpha\, g_\alpha$ is made, which is motivated by the presumed small deviation from equilibrium. Insertion of this expansion into equation (2.3.6) yields a differential equation for the unknown function g_α. Within the limit $\alpha \to 0$ this equation becomes

$$Q\left(\lim_{\alpha \to 0} g_\alpha\right) = k\, \nabla_r f_{eq} + \nabla_r \varphi_{eff}\, \nabla_k f_{eq} \tag{2.3.7a}$$

$$\Rightarrow g := \lim_{\alpha \to 0} g_\alpha = f_{eq} - \tau_{rel} \left(k\, \nabla_r f_{eq} + \nabla_r \varphi_{eff}\, \nabla_k f_{eq} \right). \tag{2.3.7b}$$

The last step before formulating the transport equations restarts with equation (2.3.6). The sought function $f = \lim_{\alpha \to 0} f_\alpha$ is formally known from the Chapman-Enskog-expansion, since g_α is known in the limit $\alpha \to 0$ from equation (2.3.7). However, for the scope of this work an exact expression for f is not of interest because only the average motion of charge carriers is important anyway. Therefore, the Chapman-Enskog expansion is inserted into equation (2.3.6) and the whole equation is integrated in k-space. Then, the transition $\alpha \to 0$ is performed. With the notation $\langle h(k) \rangle := \frac{1}{8\pi^3} \int_{\mathbb{R}^3} \sum_s h(k)\, \mathrm{d}k$ the result reads

$$\partial_t \langle f_{eq} \rangle + \mathrm{div}_r \langle k\, g \rangle + \langle \nabla_k g \rangle\, \nabla_r \varphi_{eff} = 0. \tag{2.3.8}$$

Each term in (2.3.8) only depends on the equilibrium distribution f_{eq} which is given by the scaled Maxwell-Boltzmann distribution (2.3.5). For electrons in the conduction band,

this can be expressed by $f_{eq} = \frac{n}{N_c} \mathrm{e}^{-\frac{k^2}{2}}$, using the result (2.1.7) for the electron density n. Considering this as well as the definition (2.3.7) of g, equation (2.3.8) can be further evaluated:

$$\partial_t n - \mathrm{div}_r \tau_{rel} \left(\nabla_r n - n \nabla_r \varphi_{eff} \right) = 0. \tag{2.3.9}$$

This is the transport equation of electrons in a scaled, dimensionless form. Scaling back and introducing the electron mobility $\mu_n = \frac{e_0 \tau_{rel}}{m_n^*} > 0$, the electron diffusion constant $D_n = \frac{k_B T}{e_0} \mu_n > 0$, and the effective potential $\varphi_{eff} = \varphi + \frac{1}{e_0} \chi$ with the electron affinity χ yields the unscaled drift-diffusion equation of electrons

$$\partial_t n + \mathrm{div}_r \Gamma_n = 0, \qquad \Gamma_n = -D_n \nabla_r n + \mu_n n \nabla_r \varphi + \frac{\mu_n n}{e_0} \nabla_r \chi. \tag{2.3.10}$$

Γ_n is the current density of electrons. With the hole mobility $\mu_p = \frac{e_0 \tau_{rel}}{m_p^*} > 0$, the hole diffusion constant $D_p = \frac{k_B T}{e_0} \mu_p > 0$, and the effective potential $\varphi_{eff} = \varphi + \frac{1}{e_0} \chi + \frac{1}{e_0} E_g$ with the band gap E_g, a similar drift-diffusion equation for holes can be derived, relating the hole density p and the hole current density Γ_p:

$$\partial_t p + \mathrm{div}_r \Gamma_p = 0, \qquad \Gamma_p = -D_p \nabla_r p - \mu_p p \nabla_r \varphi - \frac{\mu_p p}{e_0} \nabla_r \chi - \frac{\mu_p p}{e_0} \nabla_r E_g. \tag{2.3.11}$$

The equations (2.3.10) and (2.3.11) are the transport equations for electrons and holes. Throughout the derivation, two restricting assumptions about the scattering were made: the scattering of electrons in the ν-th energy band is not influenced by the occupation of other energy bands, and the electrons cannot be scattered into other energy bands either. More precisely the charge carriers in different energy bands do not interact. In semiconductors, however, this is unsustainable because transitions of electrons between different energy bands always occur. The energy bands of particular importance are the conduction and the valence band. Accounting for transitions between these two bands leads to the bipolar Boltzmann equation for electrons in the conduction band[2]

$$\partial_t f_c + \frac{1}{\hbar} \nabla_k E_c(k) \nabla_r f_c + \frac{e_0}{\hbar} \nabla_r \varphi_{eff,c} \nabla_k f_c = Q_{\tau,c}(f_c) + I_n(f_c, f_v) \tag{2.3.12a}$$

$$\text{with } I_n(f_c, f_v) = \int_{\mathbb{R}^3} \left(g_n(r, k'; k)(1 - f_c)(1 - f_v') - r_n(r, k; k') f_c f_v' \right) \mathrm{d}k'. \tag{2.3.12b}$$

Now, the scattering processes are the sum of intraband transitions ($Q_{\tau,c}$) and additional interband transitions (I_n) from or into the valence band. These interband transitions also depend on the occupation distribution f_v of holes in the valence band. The quantity r_n describes the probability rate for an electron transition from an occupied state k in the conduction band into an empty state k' in the valence band. This is termed recombination. Similarily, g_n describes the probability rate for the transition of an electron from an

---

[2]A similar equation holds for holes in the valence band.

occupied state k' in the valence band into an empty state k in the conduction band. This process is termed generation. The bipolar Boltzmann equation (2.3.12) is a coupled, non-linear integro-differential equation. The approximate solution of (2.3.12) is similar to the above procedure: First, the low-density and the relaxation time approximation are assumed and the Boltzmann equation is scaled. Then, the Chapman-Enskog-expansion is inserted and finally the integration over k-space is performed. The result reads

$$\partial_t n + \text{div}_r \Gamma_n = - \left(n\, p - n_i^2 \right) \cdot \xi(r, t) \qquad (2.3.13a)$$

$$\partial_t p + \text{div}_r \Gamma_p = - \left(n\, p - n_i^2 \right) \cdot \xi(r, t). \qquad (2.3.13b)$$

ξ is a function containing information on the transition probabilities, and $n_i^2 = n_0\, p_0$ is the product of the equilibrium electron and hole densities from equation (2.1.7) and (2.1.9). Γ_n and Γ_p are the electron and hole current densities from equation (2.3.10) and (2.3.11). The equations (2.3.13) are termed the continuity equations of electrons and holes.[3] The right-hand sides are the net-recombination rates - the difference of generation and re-combination - written in a general form for band-to-band recombination. For radiative band-to-band recombination, the function ξ is calculated in the next section. After this, the recombination process is generalized to transitions via energy states in the band gap within the framework of the Shockley-Read-Hall theory.

2.4 Charge carrier recombination

In the course of the derivation of the continuity equations (2.3.13), the terms genera-tion and recombination have been introduced. Recombination of an electron means the transition of an electron from the conduction band into an unoccupied state with lower energy. In analogy, recombination of a hole means the transition of a hole from the va-lence band into an occupied state with higher energy. Depending on the involved energy states, the recombination processes are divided into band-to-band recombination, defect assisted recombination, and Auger recombination. The excess energy is either transferred to phonons of the crystal lattice or emitted by photons. This leads to another classification into radiative and non-radiative recombination processes.

2.4.1 Radiative band-to-band recombination

If an electron e in the conduction band recombines with a hole h in the valence band, the energy difference will either be used to generate phonons (a few ten at room temperature), or to be emitted by a photon γ. The latter process in general is more likely than the

---

[3]The continuity equations have been derived under the assumption of the Boltzmann-approximation. It is worth mentioning that the same continuity equations can be derived also for Fermi-Dirac statistics. In that case, additional terms in the current densities of electrons and holes occur.

non-radiative phonon generation because only three particles are included. Multi-photon events are, however, excluded throught the whole thesis. The generation of one photon may occur by spontaneous emission $e + h \rightarrow \gamma$ or by stimulated emission $\gamma + e + h \rightarrow \gamma + \gamma$. The rate of spontaneous emission of a photon with energy $\hbar\omega$ is arranged by

$$r_{sp}(\hbar\omega) = \sum_{s,k_c,k_v} A_{c\rightarrow v}\, \delta\left(E_c(k_c) - E_v(k_v) - \hbar\omega\right)\, f_c(E_c(k_c)))\, f_v(E_v(k_v)). \qquad (2.4.1)$$

$A_{c\rightarrow v}$ is the transition rate of electrons in the conduction band with pseudo-wavevector k_c transferred into an unoccupied state in the valence band with pseudo-wavevector k_v. The δ-distribution ensures that the energy difference of the electron $E_c(k_c) - E_v(k_v)$ equals the photon energy $\hbar\omega$. At last, the state in the conduction band must be occupied and the state in the valence band must be unoccupied, which is provided by the Fermi-Dirac distributions f_c and f_v of the conduction and the valence band. The transition rate $A_{c\rightarrow v}$ is hard to evaluate directly. Therefore, it is related to Einstein's coefficient $B_{c\rightarrow v}$ for stimulated emission, which can be calculated easier using Fermi's Golden rule. From detailed balance follows [31]

$$A_{c\rightarrow v} = D_{op}(\hbar\omega)\, B_{c\rightarrow v} \qquad (2.4.2)$$

with the optical density-of-states $D_{op}(\hbar\omega) = \frac{n_r^3\,(\hbar\omega)^2}{\pi^2\,\hbar^3\,c_0^3}$, the refractive index n_r, and the vacuum speed of light c_0. The transition rate $B_{c\rightarrow v}$ can be calculated using Fermi's Golden rule $B_{c\rightarrow v} = \frac{2\pi}{\hbar}\,|\langle c\,|H'|\,v\rangle|^2$ with the Bloch functions of the electron $|c\rangle$ and $|v\rangle$, and the perturbation Hamiltonian H'. Since the transition into the valence band is due to the interaction of the electron with the electric field of an electromagnetic wave, the perturbation Hamiltonian reads [31]

$$H' = -\frac{e_0}{m_0} A\, p + \frac{e_0^2}{2\,m_0} A^2 \qquad (2.4.3)$$

with the dipole momentum p. It is $A = \frac{1}{2} A_0\, \widehat{e}\, e^{i\,k_{op}\,r}$ the vector potential (see sec. 2.2) of the electromagnetic wave with polarization vector $\widehat{e}$ and amplitude A_0. By assuming small optical intensities $|e_0 A| \ll |p|$ and long optical wavelengths $|k_{op}| \ll |k_c|,\,|k_v|$, the perturbation Hamiltonian becomes $H' \approx -\frac{e_0}{2m_0} A_0\, \widehat{e}\, p$. The transition rate is given by

$$B_{c\rightarrow v} = \frac{1}{V} C_0\, \delta_{k_c,k_v}\, |\widehat{e}\, p_{cv}|^2 \qquad \text{with} \qquad C_0 = \frac{2\,\pi}{\hbar}\frac{e_0^2\,A_0^2}{4\,m_0^2} V = \frac{\pi\,e_0^2}{n_r^2\,\varepsilon_0\,m_0^2\,\omega}. \qquad (2.4.4)$$

It is pointed out that the electrons do not change the pseudo-wavevector because of the negligible photon momentum. It remains the calculation of the squared interband momentum matrix element $|\widehat{e}\, p_{cv}|^2$. To this end, the semiconductor again is assumed to be isotropic with parabolic energy bands - the latter again presumes the low density approximation. Kane's formalism then yields a momentum matrix element being independent

from k:

$$M_{cv} := |\widehat{e}\,p_{cv}|^2 = \left(\frac{m_0}{m_n^*} - 1\right) \frac{m_0\,E_g\,(E_g + \Delta)}{6\left(E_g + \frac{2}{3}\Delta\right)}. \tag{2.4.5}$$

In (2.4.5), Δ is the split-off energy to account for light and heavy holes. With (2.4.2) - (2.4.5) the rate of spontaneous emission of a photon with energy $\hbar\omega$ becomes

$$r_{sp}(\hbar\omega) = D_{opt}(\hbar\omega)\,\frac{C_0}{V}\,M_{cv}\sum_{k,s}\delta\left(E_c - E_v - \hbar\omega\right)f_c(E_c)\left(1 - f_v(E_v)\right) \tag{2.4.6}$$

with the abbreviations $E_c = E_c(k)$ and $E_v = E_v(k)$. In order to calculate the sum over k and s it is advisable to introduce a new energy $E_r := E_c(k) - E_v(k) - E_g$. For parabolic bands it is $E_r = \frac{\hbar^2}{2\,\mu_r}k^2$ with the reciprocal of the reduced effective mass $\mu_r^{-1} = \frac{1}{m_n^*} + \frac{1}{m_p^*}$. Similar to section 2.1, the pseudo-wavevectors k are quasi-continuous and the sum can be transformed into an integral by the substitution $\sum_{k,s} \to \frac{V}{4\pi^3}\int \mathrm{d}k$. To perform the integration, it is convenient to define the reduced density-of-states by

$$D_r(E_r) = \frac{1}{2\pi^2}\left(\frac{2\,\mu_r}{\hbar^2}\right)^{3/2}\sqrt{E_r}, \quad E_r \geq 0. \tag{2.4.7}$$

The reduced density-of-states gives the density of energy states in the conduction and valence band, whose energetic distance is $E_r \dots E_r + \mathrm{d}E_r$. By this, the integration over k can be done without difficulties and the rate of spontaneous emission is expressed by

$$r_{sp}(\hbar\omega) = C_0\,M_{cv}\,D_{opt}(\hbar\omega)\,D_r(\hbar\omega - E_g)\,f_c\left(E_{c0} + \frac{\mu_r}{m_n^*}\left(\hbar\omega - E_g\right)\right)\times$$

$$\times\left(1 - f_v\left(E_{v0} - \frac{\mu_r}{m_p^*}\left(\hbar\omega - E_g\right)\right)\right). \tag{2.4.8}$$

The quantity r_{sp} is the number of photons with energy $\hbar\omega \dots \hbar\omega + \mathrm{d}\hbar\omega$ emitted per time and per volume by spontaneous emission. For the continuity equations (2.3.13), the total spontaneous recombination rate R_{sp} is needed. This is obtained by integration of r_{sp} with respect to $\hbar\omega$:

$$R_{sp} = \int_{E_g}^\infty r_{sp}(\hbar\omega)\mathrm{d}\hbar\omega. \tag{2.4.9}$$

In general, the expression (2.4.9) can only be calculated numerically. However, in the low-density-approximation f_c and f_v equal the Maxwell-Boltzmann distribution and the integration can be performed analytically:

$$R_{sp} = \underbrace{\frac{e_0^2\,M_{cv}\,n_r\left(E_g + \frac{3}{2}k_B T\right)}{\pi\,\hbar^2\,c_0^3\,m_0^2\,\varepsilon_0}\,\frac{1}{2}\left(\frac{2\,\pi\,\hbar^2}{(m_n^* + m_p^*)\,k_B T}\right)^{3/2}}_{B}\,n\,p =: R_{rad}. \tag{2.4.10}$$

B is a material constant depending on the temperature according to $T^{-3/2}$. It contains

information on the transition probabilities and corresponds to the function ξ in equation (2.3.13), as will be shown next.

Equation (2.4.10) gives the total rate of radiative band-to-band recombination. For the continuity equations (2.3.13), however, the net-recombination rate is needed. Therefore, the rate of the reverse process must be known meaning the generation of electron-hole pairs by absorption of photons. This generation rate is commonly separated into a generation by illumination G_{ph} and into a generation by irradiation from the environment G_{th}. The first is usually treated separately (see section 2.5.1). Therefore, the radiative net-recombination rate here is defined by $R_{rad,net} = R_{rad} - G_{th}$. In equilibrium, the generation by the environment must equal the recombination, which implies $G_{th} = B \, n_0 \, p_0$. Thus, the radiative net-recombination rate becomes

$$R_{rad,net} = B \, (n \, p - n_0 \, p_0) \,. \tag{2.4.11}$$

2.4.2 Defect assisted recombination

In the previous section, the rate of radiative band-to-band recombination was derived. Now, recombination is considered, which is assisted by additional energy levels in the band gap. These energy levels are caused by defects of the semiconductor crystal, e.g. by acceptor and donor levels, as they have been introduced in section 2.1. The defect levels can be close to the conduction or valence band (shallow defects) or in the middle of the energy gap (deep defects). As for dopants, these defects can be charged by capturing or emitting an electron or a hole. The rates of these capture and emission processes are derived in the following for a single defect level with energy E_t. Assuming the low-density-approximation, the derivation is mostly similar to that of radiative band-to-band recombination (see eq. 2.4.10). Thus, the capture and emission rates are linear in the involved charge carrier densities [32, 33]:

$$C_n = \sigma_n \, v_n \, (N_t - n_t) \, n \tag{2.4.12a}$$

$$C_p = \sigma_p \, v_p \, n_t \, p \tag{2.4.12b}$$

$$E_n = \beta_n \, n_t \tag{2.4.12c}$$

$$E_p = \beta_p \, (N_t - n_t) \,. \tag{2.4.12d}$$

C_n and C_p are the capture rates of electrons and holes, and E_n and E_p are the emission rates of electrons and holes. Further, it is v the thermal velocity, σ the capture cross-section, and β the emission coefficient of electrons and holes, respectively. n_t denotes the density of occupied defects and N_t the density of all defects where each defect can capture only one charge carrier.

For now, the semiconductor is in equilibrium. Then, the defect occupation n_{t0} is determined by the Fermi-Dirac distribution (2.1.1): $n_{t0} = N_t \, f(E_t)$. Furthermore, detailed

balance requires "electron capture = electron emission" and "hole capture = hole emission". This yields the emission coefficients which come out as

$$\beta_n = \sigma_n \, v_n \, N_c \, e^{-\frac{E_c - E_t}{k_B \, T}} = \sigma_n \, v_n \, n^* \tag{2.4.13a}$$

$$\beta_p = \sigma_p \, v_p \, N_v \, e^{-\frac{E_t - E_v}{k_B \, T}} = \sigma_p \, v_p \, p^*. \tag{2.4.13b}$$

$n^* = N_c \, e^{-\frac{E_c - E_t}{k_B \, T}}$ and $p^* = N_v \, e^{-\frac{E_t - E_v}{k_B \, T}}$ will be the carrier densities if the Fermi-level lies in the defect level E_t.

Now, non-equilibrium is considered. To this end, the semiconductor is excited homogeneously with a generation rate G of electron-hole pairs. Since for this derivation the semiconductor is assumed to be homogeneous and any other recombination path shall be neglected, the continuity equations (2.3.13) become

$$\frac{\partial}{\partial t} n = G + E_n - C_n \tag{2.4.14a}$$

$$\frac{\partial}{\partial t} p = G + E_p - C_p \tag{2.4.14b}$$

$$\frac{\partial}{\partial t} n_t = C_n - E_n + E_p - C_p. \tag{2.4.14c}$$

The quantity $C_n - E_n$ is the net-transition rate of electrons from the conduction band into an energy state with lower energy, thus, the net-recombination rate.[4] For its determination, the quantities β_n, β_p, and n_t must be known. The emission coefficients are approximated by the equilibrium values in equation (2.4.13), since the deviation from equilibrium will be small if the excitation is small. The non-equilibrium density of occupied defects n_t has to be determined from (2.4.14c) which is a non-linear differential equation. By using the steady state condition $\frac{\partial}{\partial t} n_t \big|_{steady} = 0$, at least the steady state occupied defect density can be calculated:

$$n_t \big|_{steady} = \frac{N_t \, (\sigma_n \, v_n \, n + \sigma_p \, v_p \, p^*)}{\sigma_n \, v_n \, (n + n^*) + \sigma_p \, v_p \, (p + p^*)}. \tag{2.4.15}$$

Now, the net-recombination rate under steady state conditions $(C_n - E_n)\big|_{steady}$ can be calculated. In honor of the authors of the original papers [32, 33], this is termed the Shockley-Read-Hall-(SRH)-recombination rate R_{srh}. By using the equations (2.4.12), (2.4.13), and (2.4.15), the SRH-recombination rate becomes

$$R_{srh} := (C_n - E_n)\big|_{steady} = \frac{n \, p - n_0 \, p_0}{\frac{1}{\sigma_p \, v_p \, N_t} \, (n + n^*) + \frac{1}{\sigma_n \, v_n \, N_t} \, (p + p^*)}. \tag{2.4.16}$$

The same result will arise if $(C_p - E_p)\big|_{steady}$ is considered. Therefore, in steady state the electron and hole recombination rates are equal.

---

[4]It shall be mentioned that in the nomenclature of this work the recombination of an electron does not imply the recombination of a hole because the transition rates $C_n - E_n$ and $C_p - E_p$ are not necessarily equal.

The defect density N_t in (2.4.16) has the dimension of a volume density, if the defects are within the semiconductor bulk. Then, $\frac{1}{\sigma_n v_n N_t}$ and $\frac{1}{\sigma_p v_p N_t}$ have the dimension of a lifetime. Therefore, the minimum lifetimes $\tau_{n0} := \frac{1}{\sigma_n v_n N_t}$ and $\tau_{p0} := \frac{1}{\sigma_p v_p N_t}$ are defined and the SRH-recombination rate for bulk-defects is rewritten by

$$R_{srh} = \frac{n\,p - n_0\,p_0}{\tau_{p0}\,(n + n^*) + \tau_{n0}\,(p + p^*)}. \tag{2.4.17}$$

For interface-defects, N_t has the dimension of an area density and $\sigma_n v_n N_t$ and $\sigma_p v_p N_t$ have the dimension of a velocity. Therefore, the recombination velocities $S_{n0} := \sigma_n v_n N_t$ and $S_{p0} := \sigma_p v_p N_t$ are defined and the SRH-recombination rate for interface defects becomes

$$R_{srh} = \frac{n\,p - n_0\,p_0}{\frac{1}{S_{p0}}\,(n + n^*) + \frac{1}{S_{n0}}\,(p + p^*)}. \tag{2.4.18}$$

Especially for deep interface defects in a p-type semiconductor, one finds for low excitations ($p \approx p_0$)

$$R_{srh} = S_{n0}\,(n - n_0) = S_{p0}\,(p - p_0). \tag{2.4.19}$$

At last, the temperature dependence of the SRH-recombination is studied. Apart from the carrier densities n_0, p_0, n, p, n^*, p^*, also the minimum lifetimes and recombination velocities are temperature dependent due to the temperature dependence of the thermal velocity and the capture cross-section. A common ansatz is a power law [Mai3, Mai7]

$$\tau_{n0},\ \tau_{p0} \sim T^{-b_{n,p}} \tag{2.4.20a}$$

$$S_{n0},\ S_{p0} \sim T^{b_{n,p}} \tag{2.4.20b}$$

with a constant $b_{n,p} > 0$ depending on the material, the doping, and the defect.

Radiative vs. non-radiative defect assisted recombination
The above derivation of the SRH-recombination rate is based on the semi-classical rate equations (2.4.12) for electrons and holes, and disregards the energy transfer to photons or phonons. The treatment of the interaction with photons is similar to that described in section 2.4.1. For dealing with the coupling with phonons, the influence of the semiconductor lattice has to be taken into consideration. For a specification of a lattice state, the configuration coordinate Q is introduced, which for example may be the distance of an intrinsic defect to the next neighbours. In harmonic approximation, the lattice potential then comes out parabolic in Q. In the following, two energy parabolae are considered: one for an electron in the conduction band E_c and one for an electron captured by the defect E_t. These are shown in figure 2.2 (a). Both parabolae are shifted on the energy axis due to the energy loss when the electron is captured. The equilibrium configuration in the two cases (electron in conduction band or electron in defect state) depends on the
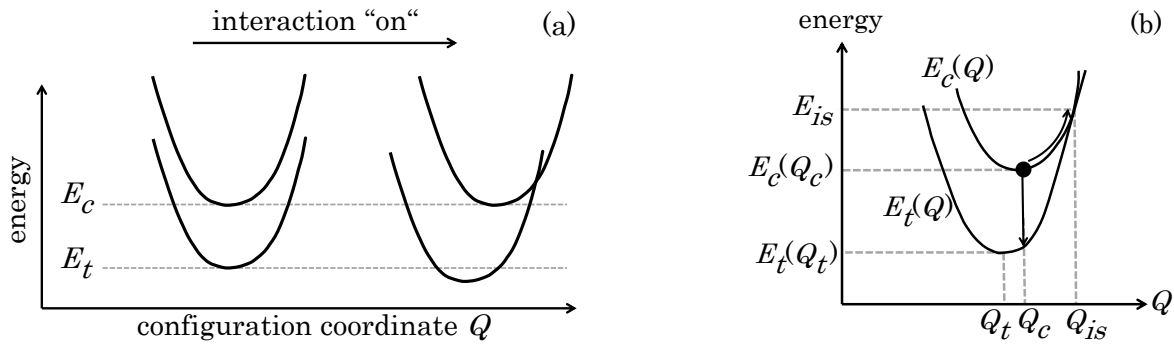
Figure 2.2: (a) Energy parabolae in a configuration coordinate diagramm with and without electron-lattice inter-
action. (b) Due to the interaction, the minima $(Q_t, E_t(Q_t))$ and $(Q_c, E_c(Q_c))$ of the parabolae are
not equal and both intersect in a point (Q_{is}, E_{is}). The figures are adapted from ref. [34].

electron-lattice interaction. If both do not interact, the equilibrium configuration will be
equal for both states. However, if the electron and the lattice interact, the lattice will
deform due to the charge of the defect by the captured electron and a new equilibrium
configuration will materialize. Therefore, the parabolae of the free and the captured elec-
tron are also shifted on the Q axis and both intersect. Due to this intersection there are
two possibilities for an electron transition from $(Q_c, E_c(Q_c))$ in the conduction band into
$(Q_t, E_t(Q_t))$ in the defect state (see fig. 2.2 (b)):

If the electron-lattice interaction is strong or if the defect is close to the conduction band,
the energy difference $E_{is} - E_c(Q_c)$ will be small. Therefore, the electron in the conduction
band can be thermally excited into the state (Q_{is}, E_{is}). Here, the energy parabolae of
the conduction band and the defect intersect. Thus, the transition probability is not van-
ishing and the electron can get from $E_c(Q_{is})$ into $E_t(Q_{is})$. Then, it thermalizes into the
minimum $E_t(Q_t)$ by emission of phonons which is why this transition is a non-radiative
process.

If the coupling of the defect with the surrounding lattice is small or if the defect is far
below the conduction band (and close to the valence band), the activation energy of the
state (Q_{is}, E_{is}) will become large. Hence, it is more likely that the electron jumps from
$(Q_c, E_c(Q_c))$ into the defect state $(Q_c, E_t(Q_c))$ by emission of a photon, and then ther-
malizes by phonon emission into the minimum $(Q_t, E_t(Q_t))$. Since now also a photon is
emitted, this process is a radiative electron transition.

Following these considerations, radiative transitions of electrons dominate for weak inter-
actions ($Q_c \approx Q_t$) or for defects far below the conduction band ($E_t(Q_t) \ll E_c(Q_c)$). This
is revealed by the following equation for the ratio of radiative and non-radiative electron
transitions, which has been derived for the special case $E_c(Q_t) > E_c(Q_c), E_c(Q_{is}), E_t(Q_t)$
[35]:

$$\frac{\text{radiative transitions}}{\text{non-radiative transitions}} = \left(1 - 2\frac{E_c(Q_t) - E_c(Q_c)}{E_c(Q_t) - E_t(Q_t)}\right)^2. \qquad (2.4.21)$$

The mechanism of capturing holes in the valence band by a defect is similar to the above described electron capture. Therefore, the following conclusions are drawn: if the defect is close to the conduction or valence band, the recombination will be radiative since for the first case the holes are captured radiatively and for the latter case the electrons are captured radiatively. But, if the defect is in the middle of the band gap, electrons and holes will be captured non-radiatively and the recombination will be non-radiative, too.

Charge carrier trapping vs. recombination

As it was the case in the above considerations, a defect always (except from a few special cases) enhances the steady state recombination of electron-hole pairs, independent from the defect density or the defect energy. This becomes obvious from the SRH-recombination rate in equation (2.4.16), which is always positive. The steady state behavior of defects, however, is of minor importance for this work, since the scope are transient processes. Hence, transient charging and discharging of defects is investigated in the following. Prior to that, a discrimination of defects is appropriate which is justified through the following preliminary consideration.

If an electron is captured by a defect, there will be two possibilities: the electron can recombine with a captured hole or it can be thermally reexcited to the conduction band. In the first case, the defect is referred to as a recombination center. In the latter case, the defect is called an electron trap due to the temporary preservation of the electron from recombination. This trapping of charge carriers is a pecularity of time-dependent processes and will become very important in the course of this thesis. Therefore, it is reasonable to have criteria for the discrimination between recombination centers and electron traps. These can be found by the hole capture and electron emission rate (2.4.12), which are equal only in the steady state. The defect is designated as an electron trap, if the electron emission rate is larger than the hole capture rate. This leads to the electron trap condition:

$$E_n > C_p \quad \Rightarrow \quad \frac{\sigma_n \, v_n}{\sigma_p \, v_p} > \frac{p}{n^*}. \tag{2.4.22}$$

For a p-type semiconductor with a defect near the conduction band ($p \gg n^*$) and with similar thermal velocities ($v_n \approx v_p$), the hole capture cross-section must be much smaller than the electron capture-cross section to obtain an electron trap. This is characteristic for donor like traps meaning they are uncharged when being occupied [36, 37].

The above thoughts on electron traps can be transferred one-to-one to holes. This yields the hole trap condition:

$$E_p > C_n \quad \Rightarrow \quad \frac{\sigma_p \, v_p}{\sigma_n \, v_n} > \frac{n}{p^*}. \tag{2.4.23}$$

For defects that fulfill the trap condition, the charge carrier capturing as well as emission must be determined from the rate equations (2.4.12). For recombination centers, meaning defects that do not fulfill the trap conditions, the net-recombination of electrons $C_n - E_n$

and holes $C_p - E_p$ is given by the SRH-recombination rate (2.4.16) only in steady state. Hence, in general they must be determined from the rate equations, too. This needs knowledge about the defect occupation n_t; therefore the solution of the rate equation for n_t. This is laborious and very inconvenient. Hence, the net-recombination rates of electrons and holes under transient conditions are often approximated by the steady state net-recombination rate R_{srh} (2.4.16). This will be possible, if $(C_n - E_n) \approx (C_n - E_n)|_{steady}$ and $(C_p - E_p) \approx (C_p - E_p)|_{steady}$ hold. Evaluating this for example for electrons leads to the simple condition

$$n_t \approx n_t|_{steady}. \tag{2.4.24}$$

In other words, at any time the occupation must equal the steady state occupation (2.4.15) for the given electron and hole density. This will be true if the densities n and p vary on a larger time scale than n_t. Then, the defect will be in a quasi-steady state. To quantify this, a relaxation time constant of the occupation of recombination centers is calculated. Therefore, it is assumed that the system is in a steady state "1" with the charge carrier densities n_1 and p_1. The steady state occupation n_{t1} results from the condition $\frac{\partial}{\partial t} n_t|_{steady1} = 0$. Omitting the emission rates, which are negligible for recombination centers, yields

$$n_{t1} = \frac{\sigma_n v_n N_t n_1}{\sigma_n v_n n_1 + \sigma_p v_p p_1}. \tag{2.4.25}$$

Now, the steady state is perturbed by a small, instantaneous change of the electron density $n_1 \to n_1 + \delta n$ with $\delta n \ll n_1$ for example by a generation of electrons.[5] As a consequence, the hole capturing is over- or undercompensated by the electron capturing and the system evolves into a new steady state "2" with the carrier densities $n_2 = n_1 + \delta n$, $p_2 = p_1$, and

$$n_{t2} = \frac{\sigma_n v_n N_t (n_1 + \delta n)}{\sigma_n v_n (n_1 + \delta n) + \sigma_p v_p p_1}. \tag{2.4.26}$$

The relaxation time δt is the time, which the defect with steady state occupation n_{t1} needs to reach the new steady state occupation n_{t2}. This time is extrapolated from the rate equation (2.4.12) by replacing the time derivative by the difference quotient:

$$\frac{n_{t2} - n_{t1}}{\delta t} \approx \frac{d}{dt} n_t \approx C_n - C_p = \sigma_n v_n (n_1 + \delta n)(N_t - n_{t1}) - \sigma_p v_p p_1 n_{t1} \tag{2.4.27a}$$

$$\Rightarrow \delta t \approx (\sigma_n v_n n + \sigma_p v_p p)^{-1}. \tag{2.4.27b}$$

Now, the recombination center will be in quasi-steady state - and therefore $(C_n - E_n) \approx R_{srh}$ will hold -, if δt is much smaller than the time scale of variation of the electron and the hole density. In other words, the relaxation time must be smaller than the effective carrier lifetimes, that will be defined in chapter 3.

---

[5]A perturbation of the hole density p instead of the electron density yields the same result (2.4.27).

2.4.3 Alternative recombination paths

To conclude this section about charge recombination in semiconductors and for the sake of completeness, other recombination processes are discussed. As they have only a minor influence on the room temperature TRL in thin-film semiconductors, they are only explained shortly.

At the beginning of this section the radiative band-to-band recombination was described. This was generalized to the recombination of free charge carriers assisted by one defect in the band gap, which arises the denomination "free-to-bound" recombination. Going one step further leads to the bound-to-bound or donor-acceptor (DA) recombination, where an electron captured by a donor recombines radiatively with a hole captured by an acceptor. This situation is shown in the spatial energy diagramm in figure 2.3 (a). Before the recombination, the donor is neutrally charged due to the occupation by the electron and the acceptor is neutrally charged due to the occupation by a hole. After the recombination, however, the donor and acceptor are ionized and interact with each other. For large distances R between both, the Coulomb interaction contributes the major part to the interaction energy. For smaller distances an additional interaction term $J(R)$ must be taken into consideration due to the overlap of the wavefunctions. Therefore, the energy of the emitted photon becomes:

$$\hbar\omega = E_g - (E_A + E_D) + \frac{e^2}{4\,\pi\,\varepsilon_0\,\varepsilon_r\,R} - J(R). \qquad (2.4.28)$$

The derivation of the total rate R_{DA} of radiative DA-recombination is similar to that of radiative band-to-band-recombination (2.4.10), if the low-density-approximation is applied and if the donor and acceptor state are treated as energy bands with infinity effective mass. The result reads [34]

$$R_{DA} = T_{DA}\,n_D\,n_A. \qquad (2.4.29)$$

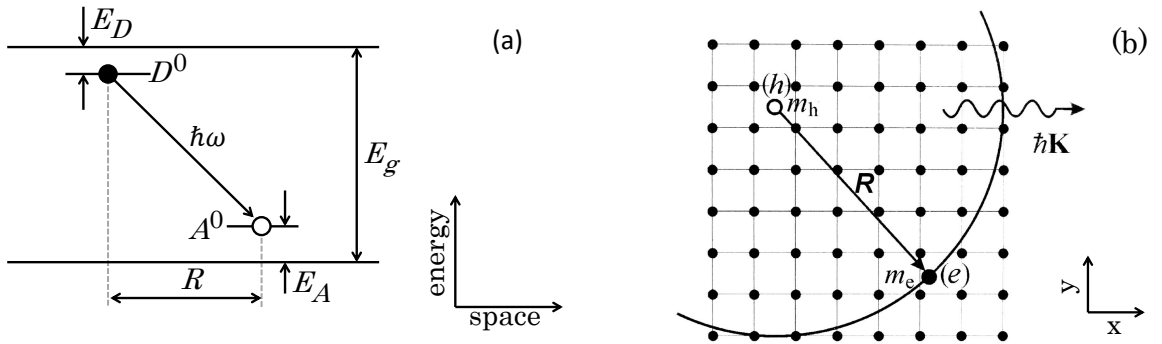In equation (2.4.29), n_A is the density of neutral acceptors, n_D is the density of neutral

Figure 2.3: (a) Recombination of an electron bound to a donor (D^0) with a hole bound to an acceptor (A^0) by emission of a photon $h\,\omega$. Donor and acceptor have a distance R. (b) A hole and an electron are bound together within a distance R. The joint centre of mass moves with the momentum $\hbar\,K$. [38]

donors, and T_{DA} is the coefficient of DA-recombination, depending among others on the donor and acceptor levels E_D and E_A, and on the dielectric permittivity ε_r.

Another recombination mechanism, being predominant in highly doped semiconductors, is the Auger recombination. Thereby, an electron-hole pair recombines and the excess energy is transferred by a photon to a third charge carrier. If this charge carrier is a second electron, this will be excited into higher states of the conduction band. Then, it thermalizes non-radiatively into the conduction band minimum. If the charge carrier is a second hole, this will be excited into deeper states of the valence band, and then thermalizes non-radiatively to the valence band maximum. Due to the complete conversion of the photon into phonons, the Auger recombination is another non-radiative recombination mechanism. Again, the transition rates are arranged linearly in the participating carrier densities. Thus, the rate of Auger recombinationen for which the energy is transferred to a second electron is arranged by $A_n\, n^2\, p$ with the Auger coefficient A_n for electrons. The rate for which the energy is transferred to a second hole is arranged by $A_p\, n\, p^2$ with the hole Auger coefficient A_p. Hence, the total rate of Auger recombination becomes

$$R_{Aug} = A_n\, n^2\, p + A_p\, n\, p^2. \tag{2.4.30}$$

In the preceeding cases, recombination of charge carriers was considered that are either free or bound to defects. However, there is also the possibility that charge carriers are attracted to each other. An electron and a hole which are bound to each other are called an exciton. This is demonstrated in figure 2.3 (b). Here, the electron and hole are bound within a distance R and the joint center of mass moves with the pseudo-wavevector K. The energy of the exciton then is discretized similarly to the hydrogen atom according to

$$E_n(K) = E_g - \frac{m_n^*\, m_p^*}{m_n^* + m_p^*} \frac{Ry}{m_0\, \varepsilon^2\, n^2} + \frac{\hbar^2\, K^2}{2\,(m_n^* + m_p^*)}, \quad n \in \mathbb{N} \tag{2.4.31}$$

with the Rydberg energy $Ry \approx 13.6\,\text{eV}$. From equation (2.4.31) it becomes obvious, that the binding energy of the exciton is large only for large dielectric permittivities ε. Otherwise, the binding energy is small and most of the excitons are thermally dissociated at room temperature.

If the bound electron and hole recombine, a photon with energy $\hbar\,\omega = E_n(K) < E_g$ will be emitted. In the low-density-approximation, the net-rate R_{ex} of exciton recombination is arranged linearly in the exciton densities $n_{ex,0}$ and n_{ex} in equilibrium and non-equilibrium, respectively, by the ansatz [39]

$$R_{ex} = \frac{1}{\tau_{ex}}\,(n_{ex} - n_{ex,0}). \tag{2.4.32}$$

τ_{ex} is the so-called exciton lifetime (see chapter 3).

2.5 Generation of free charge carriers

The variety of charge carrier generation mechanisms is as wide as the the possibilities for recombination. Free electrons and holes can be generated by excitation with light, by thermal irradiation or by excitation with electrons. These mechanisms are discussed in this section. Other possibilities like heating and doping of the semiconductor, or the injection of charge carriers are not studied here, since they are of minor importance for time-resolved luminescence experiments.

2.5.1 Generation by absorption of light

As a photon with energy $\hbar\omega > E_g$ is emitted by radiative recombination of an electron-hole pair, free charge carriers can be generated by the reverse process: the absorption of a photon $\gamma \rightarrow e + h$ with an energy $\hbar\omega > E_g$. The number of absorbed photons and thus the number of generated electron-hole pairs strongly depends on the light intensity. Therefore, knowledge about the propagation of light is indispensable for the calculation of the generation rate. The derivation of this is carried out in the following. For reasons of simplicity, monochromatic light propagating in z-direction and incidenting perpendicular to the semiconductor surface is considered. As light is an electromagnetic wave, it is described by Maxwell's equations (2.2.2). The wave equation for the electric field reads

$$\frac{\partial^2}{\partial t^2} E + \frac{\sigma}{\varepsilon_0\,\varepsilon_r}\,\frac{\partial}{\partial t} E - c^2\,\frac{\partial^2}{\partial z^2} E + c^2 \operatorname{grad} \operatorname{div} E = 0, \qquad (2.5.1)$$

with the speed of light $c = c_0/\sqrt{\varepsilon_r}$ in matter, the speed of light in vacuum c_0, and the conductivity σ. Again, ε_r is the isotropic, homogeneous relative permittivity of the material, that does not depend on the field E. It is further assumed, that the semiconductor is uncharged ($\operatorname{div} E = 0$). Equation (2.5.1) then is solved by

$$E(t,z) = \operatorname{Re}\left(\widetilde{E}_0\,\mathrm{e}^{-i\,\omega\,t - i\,\widetilde{k}\,z}\right) \quad \text{with} \quad \widetilde{k} = \pm\frac{\omega}{c_0}\,\sqrt{\varepsilon_r + i\,\frac{\sigma}{\varepsilon_0\,\omega}}. \qquad (2.5.2)$$

$\operatorname{Re}(\cdot)$ means the real part of the argument, i is defined by $i = \sqrt{-1}$, and $\widetilde{E}_0$ is a complex constant. Obviously, $\widetilde{k}$ is a complex function depending on the angular frequency ω and on the material parameters σ and ε_r. Decomposing $\widetilde{k}$ into the real and imaginary part, it can be written as $\widetilde{k} = k_{z0} \cdot (n_r - i\,\kappa)$ with the wavenumber $k_{z0} = \frac{\omega}{c_0}$ in vacuum. The complex function $n := n_r - i\,\kappa$ is called the complex refractive index, with the refractive index n_r and the extinction coefficient κ, both depending on ω, σ and ε_r.[6] [7] Thus, the

---

[6]It is worth mentioning that n_r and κ are not independent, but have to fulfill a Kramers-Kronig-relation since n is a meromorphic function [40].

[7]The complex refractive index depends on the conductivity and thus, on the density of free charge carriers. For reasons of simplicity, this relationship is disregarded in this work.

general, monochromatic plane-wave solution of (2.5.1) is

$$E(t, z) = \text{Re}\left(E_0(t)\, e^{-k_{z0}\,\kappa\, z}\, e^{-i\, k_{z0}\, n_r\, z}\right), \qquad (2.5.3)$$

with $E_0(t) = \widetilde{E}_0\, e^{-i\,\omega\, t}$. The electric field of the electromagnetic wave must now be related to the intensity I because this determines the number of photons; therefore, the generation of charge carriers. In non-magnetic materials, as supposed for this thesis, the intensity is calculated from the electric field $E(t, z)$ by the absolute value of the Poynting-vector averaged over time: $I(z) = \frac{1}{\mu_0}\langle |E \times B|\rangle_t$. Prior to that, the magnetic field B must be calculated from the third Maxwell equation (2.2.2c). Using the electric field $E(t, z)$ in equation (2.5.3) this yields

$$B(t, z) = \frac{1}{c_0}\, e^{-k_{z0}\,\kappa\, z}\, \text{Re}\left((n_r + i\,\kappa)\, E_0(t)\, e^{i\, n_r\, k_{z0}\, z}\right). \qquad (2.5.4)$$

Evaluating the cross-product $E \times B$ and the time-average $\langle\cdot\rangle_t$ the intensity becomes

$$\Rightarrow I(z) = \frac{1}{2}\, n_r\, \varepsilon_0\, c_0\, \left|\widetilde{E}_0\right|^2\, e^{-2\,\kappa\, k_0\, z}. \qquad (2.5.5)$$

The results show that the light intensity decays exponentially in direction of propagation. This is Lambert-Beer's law of light absorption. For its derivation, the amplitude $\widetilde{E}_0$ was assumed to be time-independent, that is, the intensity of incident light is constant in time. Otherwise, (2.5.3) would not be a solution of the wave equation. In luminescence experiments, however, the intensity of incident light varies with time (see chapter 3). If the time scale of intensity variation is $\gg \omega^{-1}$, equation (2.5.3) will still be a solution of the wave equation, but with a time-dependent amplitude $\widetilde{E}_0(t)$. The intensity (2.5.5) then will also be time-dependent

$$I(z, t) = \frac{1}{2}\, n_r\, \varepsilon_0\, c_0\, \left|\widetilde{E}_0(t)\right|^2\, e^{-2\,\kappa\, k_0\, z}. \qquad (2.5.6)$$

Normalizing to $z = 0$ and dividing by the photon energy, equation (2.5.6) can also be written for the photon current density

$$j_\gamma(z, t) = j_\gamma(z = 0, t)\, e^{-\alpha\, z}. \qquad (2.5.7)$$

This is Lambert-Beer's law written for the photon current density j_γ. It is only valid for small electric fields, since ε_r was assumed to be independent from E. The absorption of photons is characterized by the absorption constant $\alpha := 2\,\kappa\, k_0$. Just like the extinction, it depends on the frequency, as well as on the relative permittivity ε_r and on the conductivity σ.

As the current density of photons is known now as a function of time and space, the generation rate of electron-hole pairs can be calculated. For this purpose, a small volume

$\Delta V = [x, x + \Delta x] \times [y, y + \Delta y] \times [z, z + \Delta z]$ and the time interval $[t, t + \Delta t]$ is considered. The number of photons being absorbed in ΔV within the time $[t, t + \Delta t]$ is achieved by integration of (2.5.7) with the result $\Delta N_\gamma = j_\gamma(z, t) \left(1 - e^{-\alpha \Delta z}\right) \Delta x \, \Delta y \, \Delta t$. Each of the absorbed photons is assumed to generate one electron and one hole if the photon energy is larger than the band gap. Hence, the number ΔN_n, ΔN_p of generated electrons and holes is related to the number of absorbed photons by: $\Delta N_n = \Delta N_p = \Delta N_\gamma \, \Theta(\hbar \omega - E_g)$. Here, Θ denotes the Heaviside function.

The generation rate is the number of charge carriers generated per time per volume. Therefore, the generation rate of free electron-hole pairs by light becomes

$$G_{ph}(z, t) = \lim_{\Delta V, \Delta t \to 0} \frac{\Delta N_n}{\Delta V \, \Delta t} = \alpha \, j_\gamma(z, t) \, \Theta(\hbar \omega - E_g). \tag{2.5.8}$$

This equation gives the generation rate for a given photon current density $j_\gamma(z, t)$. The photon current density does not necessarily need to meet (2.5.7), but can be an arbitrary function of space. This will become relevant, if the considered device structures have reflecting interfaces. In this thesis, there are at least two: the semiconductor front and back surface. The reflection and transmission of a plane wave at an interface between two materials with different optical constants is described by Fresnel's formulae which are derived from boundary conditions for the electric and the displacement field.

A plane wave is assumed to propagate in a medium with complex refractive index $n_{r1} - i \, \kappa_1$. It falls perpendicular on an interface to a second medium with complex refractive index $n_{r2} - i \, \kappa_2$. The amplitude of the incident, reflected and transmitted wave shall be E^{inc}, E^r, and E^t respectively. Then, the reflection coefficient r_{12} and the transmission coefficient t_{12} are given by

$$\frac{E^r}{E^{inc}} = r_{12} = \frac{n_{r1} - i \, \kappa_1 - n_{r2} + i \, \kappa_2}{n_{r1} - i \, \kappa_1 + n_{r1} - i \, \kappa_1} \tag{2.5.9a}$$

$$\frac{E^t}{E^{inc}} = t_{12} = 2 \, \frac{n_{r1} - i \, \kappa_1}{n_{r1} - i \, \kappa_1 + n_{r2} - i \, \kappa_2}. \tag{2.5.9b}$$

Due to the reflection, the electric field is a superposition of plane waves propagating in opposite directions. Therefore, the electric field in each layer is given by $E(t, z) = \mathrm{Re}(E_0(t) \, (A(z) + B(z)))$ with complex functions $A(z)$ and $B(z)$ describing the local dependence of the incident and reflected wave respectively, in each layer. They are calculated by the Transfer-Matrix-Method (see chapter 4). From this, the magnetic field and the Poynting-vector are calculated. This leads to the total photon current density

$$j_\gamma(z) = j_{\gamma,0} \, \frac{n_r}{n_{r0}} \, |A(z) + B(z)|^2 , \tag{2.5.10}$$

with the incident photon current density $j_{\gamma,0}$, and the refractive indices n_r and n_{r0} of the layer and the medium of incidence, respectively.

2.5.2 Generation by thermal irradiation

A special case of the generation of electron-hole pairs by absorption of an electromagnetic wave is the generation by thermal irradiation, which is not least an electromagnetic wave, either. The spectrum $j_{th}(\hbar\omega)$ of such a temperature irradiation is given by Planck's law. Using equation (2.5.8) for $z = 0$ and $j_\gamma(z = 0, t) = j_{th}(\hbar\omega)$, the generation rate G_{th} becomes [16]

$$G_{th} = \frac{16\,\pi^4\,n_r^2}{c_0^2\,\hbar^3} \int_{E_g}^{\infty} \frac{\alpha(\hbar\omega)\,(\hbar\omega)^2}{e^{\frac{\hbar\omega}{k_B T}} - 1} \mathrm{d}\hbar\omega. \tag{2.5.11}$$

In equilibrium, the absorption of thermal photons must equal the emission of thermal photons. The latter is given by $R_{rad} = B\,n_0\,p_0$ (see equations (2.4.10) and (2.4.11)). Then follows from detailed balance

$$B = \frac{G_{th}}{n_0\,p_0} = \frac{16\,\pi^4\,n_r^2}{c_0^2\,\hbar^3\,n_0\,p_0} \int_{E_g}^{\infty} \frac{\alpha(\hbar\omega)\,(\hbar\omega)^2}{e^{\frac{\hbar\omega}{k_B T}} - 1} \mathrm{d}\hbar\omega. \tag{2.5.12}$$

Therewith, the material constant B can be calculated from the absorption coefficient α.

2.5.3 Generation by impact ionization

Apart from the generation due to irradiation with an electromagnetic wave, electron-hole pairs may also be generated by collision of particles with electrons - this is the reverse process to the Auger recombination. This so-called "impact ionization" is often used for cathodoluminescence measurements in an electron microscope. To this end, an electron beam excites electrons from the valence band into the conduction band; thereby, creating an electron-hole pair. For excitation, the incoming electrons must have sufficient kinetic energy. Hence, the generation rate depends on the velocity and thus, on the current densitiy of the electron beam. Therefore, the generation rate by impact ionization G_{imp} is arranged by

$$G_{imp}(t, z) = \alpha_n\,\Gamma_{n,beam}(t, z), \tag{2.5.13}$$

with $\Gamma_{n,beam}$ being the electron current density of the incident electron beam. α_n is the impact ionization rate defined as the number of electron-hole pairs, generated by electrons per unit distance traveled with the velocity v_n [41]:

$$\alpha_n = \frac{1}{n_{beam}} \frac{\mathrm{d}n}{\mathrm{d}(t\,v_n)} = \frac{1}{\Gamma_{n,beam}} \frac{\mathrm{d}n}{\mathrm{d}t}. \tag{2.5.14}$$

It is worth mentioning, that the generation rate due to impact ionization (2.5.13) is completely analogue to the generation rate by a photon current density (see equation (2.5.8)). In this case, however, the profile $\Gamma_{n,beam}(r)$ is difficult to calculate and will not be studied here.

2.5.4 Generation by reabsorption

As a conclusion of this section, radiative recombination of charge carriers is studied again. After a photon is created, it moves through the semiconductor. On its way to the surfaces it may be reabsorbed. Due to this self-absorbtion or photon-recycling, electron-hole pairs may be generated without external generation, but only due to the radiative recombination. This effect can be accounted for by an additional generation term $G_{PR}(r,t)$ in the continuity equations (2.3.13) [42]. For $G_{PR}(r,t)$ the photon current density must be
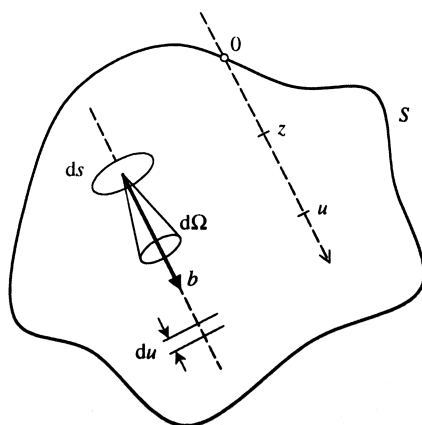
Figure 2.4: A spectral photon flux density b is created at a position z within a volume S. Along the trajectory, photons are absorbed and emitted within the path du which effects a change of the spectral photon flux density db [42]

known at each position and at each time. The calculation of this is illustrated in figure 2.4. The spectral photon flux density b,

$$b := \frac{\mathrm{d}^2 j_\gamma}{\mathrm{d}E\,\mathrm{d}\Omega}, \tag{2.5.15}$$

is defined by the photon current density per energy E, which is emitted from an area s per solid angle Ω. As the photons travel through the semiconductor, they can be absorbed with a rate A^{ph}; thereby, generating electron-hole pairs. Alternatively, also new photons can be generated with the rate G^{ph} by radiative recombination.[8] Within the resulting continuity equation for photons,

$$\frac{\mathrm{d}b}{\mathrm{d}u} = G^{ph} - A^{ph}, \tag{2.5.16}$$

u describes a length along the photon trajectory (see fig. 2.4). The spectral photon flux b is here determined as a function of space, time, energy and solid angle. Knowing b, the electron-hole pair generation rate per energy and solid angle becomes $\mathrm{d}^2 G_{PR} = \alpha\,\mathrm{d}^2 j_\gamma = \alpha\,b\,\mathrm{d}E\,\mathrm{d}\Omega$ (see equation (2.5.8) and (2.5.15)). Hence, integration over all Ω and E yields the total generation rate G_{PR} of charge carriers due to photon recycling

$$G_{PR} = \int \alpha\,b\,\mathrm{d}E\,\mathrm{d}\Omega. \tag{2.5.17}$$

---

[8]It is pointed out, that the rates are also defined per energy E and per solid angle Ω as well as per length u.

2.6 Boundary conditions

The continuity equations of electrons and holes (2.3.13), together with the Poisson equation (2.2.5), are the three fundamental semiconductor equations. For their numerical solution (see chapter 4) boundary conditions must be definied, more precisely three conditions for each boundary. These are provided by the model of ohmic contacts [28]. This treatment assumes a contact, which is always in thermal equilibrium and without of space charges. More explicit, it is $n\,p = n_0\,p_0$ and $n - p = n_D^+ - n_A^-$. Using Boltzmann statistics and the impurity exhaustion, this can be transformed into a Dirichlet boundary condition for the electrostatic potential

$$\varphi|_{boundary} = \frac{k_{\mathrm{B}}\,T}{e_0}\,\mathrm{asinh}\left(\frac{N_D - N_A}{2\,n_i}\right) + U|_{boundary}\,, \tag{2.6.1}$$

where $U|_{boundary}$ means the outer applied voltage. For the boundary conditions of the two continuity equations, the following consideration is taken as a basis: the interface between the semiconductor and the contact is very defective and leads to a high interface recombination rate with recombination velocities S_{n0} and S_{p0} (see (2.4.19)). This recombination locally reduces the charge carrier density and causes a charge carrier transport to the contact. Thereby, only as many charge carriers can recombine as are transported to the contact. Hence, the constraint becomes $\Gamma|_{boundary} = R_{SRH}|_{boundary}$ with the current density Γ and the interface recombination rate R_{SRH}. By using equation (2.4.19) for the interface recombination rate, this boundary condition becomes

$$\widehat{n} \cdot \Gamma_n|_{boundary} = S_{n0}\,\left(n - n_0\right)|_{boundary} \tag{2.6.2a}$$

$$\widehat{n} \cdot \Gamma_p|_{boundary} = S_{p0}\,\left(p - p_0\right)|_{boundary}\,, \tag{2.6.2b}$$

in which $\widehat{n}$ is the outer normal vector.

2.7 Reliability of the simulations

In the above sections and subsections, all relevant equations for the simulation of room-temperature time-resolved luminescence in thin-film semiconductors have been derived. Throughout the derivation, many assumptions were necessary to simplify the calculations and to obtain analytical expressions. For the most important assumptions, the justification and the consequences for TRL simulation will be discussed in the following.

The low-density-approximation has been used for the derivation of the charge carrier densities, for the continuity equations, and for the recombination rates. It includes the Boltzmann approximation of the charge carrier distribution, the parabolic energy band approximation, the impurity exhaustion, and the requirement of small deviations from equilibrium. All these assumptions require low electron and hole densities. In the fol-

lowing, this requirement is quantified by the estimation of an upper limit to the charge carrier densities.

For the Boltzmann approximation, the Fermi-level must not be closer than approximately $3\,k_B\,T$ from the energy band edges. By the effective density-of-states $N_{c,v} = 2 \times 10^{18}\,\mathrm{cm}^{-3}$ [16], equation (2.1.11) then yields an upper limit of n, $p < 10^{17}\,\mathrm{cm}^{-3}$. For the parabolic band approximation, the maximum pseudo-wavevector of electrons in the conduction band is defined by the highest occupied conduction band energy state, which is approximately $E_{c,max} \approx E_c + 5.67\,k_B\,T$.[9] Assuming an effective electron mass $m_n^* \approx m_0$ [16], the parabolic energy dispersion yields a maximum pseudo-wavevector $k_{max} \approx 5 \times 10^9\,\mathrm{m}^{-1}$, which is much smaller than the size of the Brillouin zone (typically $5 \times 10^{10}\,\mathrm{m}^{-1}$ [16]). Therefore, 99% of the electrons in the conduction band are close to the conduction band minimum which is the presupposition of the parabolic band approximation. Now, it remains the impurity exhaustion. To this end, the electron density always must be smaller than n^* and the hole density must be smaller than p^* (see equation (2.4.13)). For donors close to the conduction band and acceptors close to the valence band, it is n^*, $p^* \approx 10^{17}\,\mathrm{cm}^{-3}$. This again leads to the condition n, $p < 10^{17}\,\mathrm{cm}^{-3}$.

Apart from the amount of generated charge carriers, the time scale in the simulations is restricted. The derivation of the transport equations from the Boltzmann equation presumed a macroscopic time scale being larger than the scattering time of charge carriers, which is in the range of femtoseconds. Therefore, throughout the whole simulations the charge carriers are in thermal equilibrium with the crystal lattice. This excludes the simulation of thermalization processes. Another constraint on the time scale arose from the derivation of Lambert-Beer's law: the optical intensity of the excitation must vary slower than the inverse frequency of the light. For the light considered in this thesis (wavelength 638.9 nm), the time period is 1 fs. Therefore, the length of a pulsed excitation must not be smaller than approximately 10 fs. Additionally, it follows a wavenumber of the light of $k_{op} \sim 10^7\,\mathrm{m}^{-1}$. This is much smaller than the maximum pseudo-wavevector of electrons. Therefore, the photon momentum is much smaller than the charge carrier momenta and all charge carrier transitions can be assumed vertical.

The next point adresses the homogeneity and isotropy. The permittivity, temperature, and effective mass were assumed to be homogeneous. The effective mass, permittivity, carrier scattering, and transition matrices were assumed to be isotropic. Further, the surfaces are plain and not rough, so the light is coherent. In general, there is no justification for these assumptions. Thin-film semiconductors especially like $Cu(In,Ga)Se_2$ or $Cu_2ZnSnSe_4$ are polycrystalline materials with material properties being neither homogeneous nor isotropic. Therefore, homogeneity and isotropy are maintained for convenience, but they always must be questioned depending on the context.

---

[9]For the estimation of $E_{c,max}$, the energy range $[E_c, E_{c,max}]$ in the conduction band, which encloses 99% of the free electrons is calculated. This results from equation (2.1.7) by $\int_{E_c}^{E_{c,max}} D_c(E) f(E)\,\mathrm{d}E = 0.99\,n_0$.

A further restriction to the simulations is the omission of Auger-, donor-acceptor-, and exciton recombination. In contrast to the above points, the neglect of these recombination mechanisms is no consequence of the derivations in this chapter. Instead, this is due to a reduced complexity of the simulations. A justification for this approach is carried out in the following:

For the materials studied in this thesis, the Auger-coefficient is $A \approx 10^{-28}\,\mathrm{cm^{-6}\,s^{-1}}$ [37]. In consequence, Auger recombination becomes critical for doping densities in the range of $10^{18}\,\mathrm{cm^{-3}}$ or above [16]. However, all doping densities in the simulations in this work are smaller than $10^{17}\,\mathrm{cm^{-3}}$. Hence, Auger-recombination is of minor importance and can be neglected. The exciton recombination as an alternative radiative recombination path can be disregarded, since excitons are dissociated at room-temperature. It remains the donor-acceptor-recombination. The defects included in this recombination path are shallow defects with small activation energies. It follows, that the interaction of the donors and acceptors with the conduction and the valence band, respectively, is fast at room-temperature. Then, recombination via two defects can be dealt with by the approach of Shockley, Read, and Hall using effective charge carrier lifetimes.

The last point concerns the calculation of the luminescence intensity. By a specification of the simulation tool, only band-to-band recombination may contribute to the luminescence intensity. Recombination via defects is always non-radiative. However, this does not influence the luminescence decay, since radiative defect recombination is assisted by shallow defects, which reveal a time constant being similar to the band-to-band recombination (see ref. [Mai3]).

To conclude this discussion on the limitations of the TRL simulations in this thesis, the main consequences are summarized:

- The charge carrier densities must be $n,\,p \ll 10^{17}\,\mathrm{cm^{-3}}$.

- The minimum time resolution of the simulation is about $10\,\mathrm{fs}$. The length of a pulsed excitation must be larger than $10\,\mathrm{fs}$.

- Inhomogeneities of permittivity, temperature, and effective mass, as well as anisotropy of effective mass, permittivity, carrier scattering and transition matrices are not simulated.

- Auger-, donor-acceptor-, and exciton-recombination are neglected.

- The doping density must be below $10^{18}\,\mathrm{cm^{-3}}$.

- Only band-to-band recombination contributes to the luminescence intensity.

3 Lifetimes and techniques for their measurement

In the previous chapter, numerous properties of semiconductors have been described. The most important of these for photovoltaic applications is the possibility of charge carrier generation and recombination. In equilibrium, both equal each other in accordance with detailed balance. Hence, the net-recombination vanishes. But, in non-equilibrium there may be a noticible net-recombination of charge carriers. Assuming, the electron and hole densities are equal, these net-rates may become very different depending on the underlying recombination mechanism. Therefore, a recombination lifetime is assigned to each recombination mechanism which is thought to be independent from the charge carrier densities. Thus, dominant recombination processes are easier to retrieve. The concept and the measurement of these lifetimes will be the issue of this chapter.

First, the recombination lifetimes are motivated and exactly defined. Because of the high relevance, techniques for their measurement have been developed, which are reviewed below. One of these is the measurement of the time-resolved luminescence. This is of particular importance for this work. Hence, it is explained and discussed in detail exemplarily for time-resolved photoluminescence. Thereby, also the problems that already have been touched on in the introduction are picked up. In the end, TRL is compared with other lifetime measurement techniques, especially with the measurement of the photoconductivity decay, which is probably the most competing method.

3.1 Definitions of lifetimes

The strength of recombination processes depends on "the deviation from equilibrium", thus, on the difference of the charge carrier densities n and p to the equilibrium values n_0 and p_0. Therefore, it is reasonable to introduce excess carrier densities Δn and Δp of electrons and holes by

$$\Delta n := n - n_0 \qquad \text{and} \qquad \Delta p := p - p_0. \tag{3.1.1}$$

In the following, $R_{i,(n,p)}$ denotes the net-recombination rate of electrons or holes by a recombination mechanism i. In equilibrium then holds $\Delta n = \Delta p = 0$ and $R_{i,(n,p)} = 0$, as a consequence of detailed balance; in non-equilibrium holds Δn, $\Delta p \neq 0$ and $R_{i,(n,p)} \neq 0$.

Therefore, a factorial correlation between Δn and Δp, and $R_{i,(n,p)}$ can be presumed and it is reasonable to arrange the net-recombination rates by

$$R_{i,n} = \frac{1}{\tau_{i,n}} \Delta n \qquad \text{and} \qquad R_{i,p} = \frac{1}{\tau_{i,p}} \Delta p. \qquad (3.1.2)$$

Each net-recombination rate can always be written in this form because the factors $1/\tau_{i,n}$ and $1/\tau_{i,p}$ are arbitrary and can be chosen properly, so that (3.1.2) is fulfilled. The quantities $\tau_{i,n}$ and $\tau_{i,p}$ are called the recombination lifetimes of electrons and holes. By $\tau_{i,n} = \Delta n/R_{i,n}$ and $\tau_{i,p} = \Delta p/R_{i,p}$ a unique lifetime can be always attributed to each recombination mechanism. Therefore, the characterization of the recombination can be exchanged for the characterization of the recombination lifetime. The advantage is that this facilitates the requirements on the experiment since in first approximation the lifetimes are independent from excitation.[10] For multiple recombination paths, the effective recombination lifetime $\tau_{eff,r,(n,p)}$ is defined by

$$R_{total,net} = R_{1,net} + R_{2,net} + \ldots \Rightarrow \frac{1}{\tau_{eff,r,(n,p)}} := \frac{1}{\tau_{1,(n,p)}} + \frac{1}{\tau_{2,(n,p)}} + \ldots . \qquad (3.1.3)$$

If recombination is not exactly compensated by generation of charge carriers, it will lead to a decay of the charge carrier density. To make this clear, it is assumed that an excess electron density is generated by any mechanism within a homogeneous semiconductor. These excess electrons shall recombine by only one recombination mechanism with a constant recombination lifetime $\tau_{r,n}$. Then follows $\frac{\mathrm{d}}{\mathrm{d}t}\Delta n(t) = -\frac{\Delta n}{\tau_{r,n}}$ from the continuity equation and the time-dependence of the excess electron density becomes

$$\Delta n(t) = \Delta n(t=0)\, \mathrm{e}^{-\frac{t}{\tau_{r,n}}}. \qquad (3.1.4)$$

This shows that the excess electron density decays exponentially and the effective electron lifetime $\tau_{eff,n}$ - the time-constant of the decay - equals the recombination lifetime $\tau_{r,n}$. A second important finding of equation (3.1.4) is that the electrons do not recombine simultaneously, but at different times after the generation. This means, the electrons do not have a distinct lifetime but a distribution of lifetimes according to a certain probability density function $f_{\tau,n}(\tau)$ (see figure 3.1). For the calculation of $f_{\tau,n}$ it is pointed out, that within the time $[t, t+\Delta t]$ after the generation all of the electrons recombine which have a lifetime $\tau \in [t, t+\Delta t]$. Therefore, it holds

$$\Delta n(t+\Delta t) - \Delta n(t) = -f_{\tau,n}(t)\,\Delta t\,\Delta n(t=0) \qquad (3.1.5a)$$

$$\Rightarrow f_{\tau,n}(\tau) = -\frac{\mathrm{d}}{\mathrm{d}t}\frac{\Delta n(t)}{\Delta n(t=0)}\bigg|_{t=\tau}. \qquad (3.1.5b)$$

---

[10]One should be aware that this is only true in first approximation. In general, the recombination lifetimes are not constant but may be functions of Δn and Δp, too.
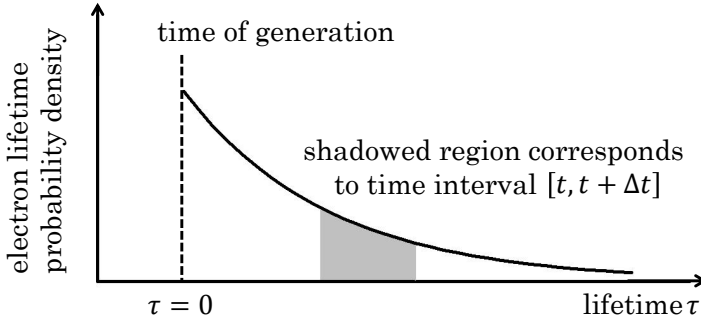
Figure 3.1: Electron lifetime probability density $f_{\tau,n}$. The electron density $\Delta n(t = 0)$ is generated at the time $t = 0$, thus, recombination at $t = 0$ corresponds to $\tau = 0$. Analoguously, within the time $[t,\, t + \Delta t]$ all electrons recombine that have a lifetime $\tau \in [t,\, t + \Delta t]$.

For the special result (3.1.4), the electron lifetime probability density becomes an exponential distribution

$$f_{\tau,n}(\tau) = \frac{1}{\tau_{r,n}}\, e^{-\frac{\tau}{\tau_{r,n}}}. \tag{3.1.6}$$

Taking $\tau_{r,n} = \tau_{eff,n}$ into consideration, it turns out for this special case that the effective electron lifetime is the expected value with respect to all electrons.

The one-exponential decay of electrons like in equation (3.1.4) is not the general case, especially, if the electrons trap. To account for such non-exponential decays, the effective carrier lifetime $\tau_{eff,(n,p)}$ (not to be confused with the effective recombination lifetime $\tau_{eff,r,(n,p)}$!) is defined on the basis of equation (3.1.4) by

$$\tau_{eff,n}^{-1} = -\frac{\mathrm{d}}{\mathrm{d}t} \log \Delta n(t) \qquad \text{and} \qquad \tau_{eff,p}^{-1} = -\frac{\mathrm{d}}{\mathrm{d}t} \log \Delta p(t). \tag{3.1.7}$$

It is pointed out, that the effective carrier lifetime in these definitions will be time-dependent if the decay of the excess carrier density is not mono-exponential.

When the charge carriers recombine, the net-rate of radiative recombination decreases and consequently the luminescence intensity I decays.[11] This luminescence decay can be mono- or bi-exponential or even curved (see chapter 5). Therefore, the time-constant for the decay - the so-called decay time - has to be defined similar to the effective carrier lifetime in equation (3.1.7). Due to this, the decay time may become time-dependent. In some cases, however, the indication of a time-dependent decay time is very inconvenient. Therefore, the luminescence decay is also often characterized by the 1/e decay of the intensity. This leads to two different definitions of the decay time:

$$\tau_{decay} := -\frac{\mathrm{d}}{\mathrm{d}t} \log I(t) \qquad \text{or by the condition} \qquad I\left(\tau_{decay}\right) = \frac{1}{e} I_{max}. \tag{3.1.8}$$

From the context it should be always clear, which definition is used. It shall be mentioned, that both definitions are equivalent for exponential decays.

To conclude this section, the numerous lifetime definitions are exemplified for radiative band-to-band recombination. To this end, the net-recombination rate (2.4.11) is expressed by the excess carrier densities by $R_{rad,net} = B \left(n_0\, \Delta p + p_0\, \Delta n + \Delta n\, \Delta p\right)$. It is now assumed,

---

[11]Of course only in non-steady state when the recombination is not exactly compensated by a generation.

that the electrons and holes have equal effective lifetimes. This is mostly true for semi-conductors without charge carrier traps and without space charges (see chapter 5). Then, $\Delta n = \Delta p$ can be assumed. Further, p-doping is presumed ($n_0 \ll p_0$) and the excitation shall be small ($\Delta p \ll p_0$). Then, the inverse of the recombination lifetime of electrons becomes

$$\tau_{rad,n}^{-1} = B\,p_0. \tag{3.1.9}$$

By solving the continuity equation, the time-dependent excess electron density becomes

$$\Delta n(t) = \Delta n(t=0)\,\mathrm{e}^{-\frac{t}{B\,p_0}} \qquad \Rightarrow \qquad \tau_{eff,n}^{-1} = B\,p_0. \tag{3.1.10}$$

Finally, the luminescence decay time is calculated. The luminescence intensity is proportional to the radiative recombination. By using (3.1.10), the luminescence intensity becomes

$$I(t) \sim B\,p_0\,\mathrm{e}^{-\frac{t}{B\,p_0}} \qquad \Rightarrow \qquad \tau_{decay}^{-1} = B\,p_0. \tag{3.1.11}$$

The result of a time-resolved luminescence measurement is the decay time. However, as the equations (3.1.9) - (3.1.11) show, this decay time is equal to the effective electron lifetime and in particular equal to the recombination lifetime. Hence, the recombination can be easily characterized from the luminescence decay, which led to the considerable attention to this method.

3.2 Time-resolved luminescence

The key message of the section above is that recombination lifetimes are supposed to be determined from the decay of the luminescence intensity. In order to do so, charge carriers must be generated first, as demonstrated in figure 3.2. Depending on the generation mechanism, the luminescence is distinguished by cathodoluminescence (generation by impact ionization with electrons), by electroluminescence (generation by application of a voltage), or by photoluminescence (generation by absorption of light). After the generation G is turned off, a part of the charge carriers recombines by radiative band-to-band recombination with the intensity I_B, the rest recombines via defects; thereby, emitting luminescence of the intensity I_M. The sum of both - I_B and I_M - then gives the time-resolved luminescence intensity I, which is recorded.

A general advantage of this procedure is the contactless measurement of the luminescence. In particular, the luminescence decay only depends on the rate of excitation. Thus, each of the above mentioned techniques will basically yield the same luminescence decay as long as the generation rates are equal. For the scope of this work, however, photoluminescence enables a simpler calculation of the generation rate. Thus, for convenience the following will focus on photoluminescence measurement techniques only.
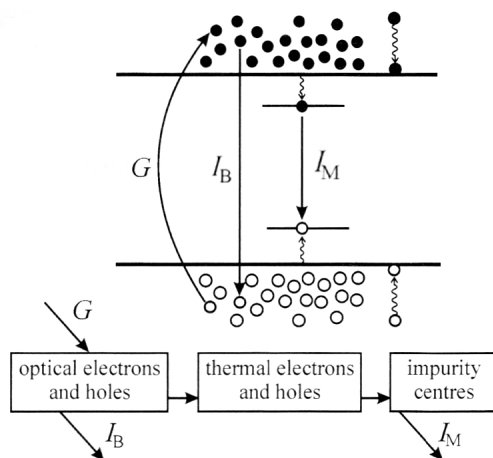
Figure 3.2: Principle procedure of a time-resolved luminescence experiment. Charge carriers are generated with a rate G. They recombine by band-to-band-recombination with intensity I_B or thermalize and recombine by impurity recombination with intensity I_M. Figure is adapted from ref. [38].

The options for measuring the time-resolved photoluminescence are various. In the direct imaging method, the semiconductor is excited by a pulsed laser. The luminescence is detected by a photomultiplier, whose output is displayed on the Y-axis of an oscilloscope and swept in time by its horizontal time base. Then, the luminescence decay can be observed on a screen or on a computer and the decay time can be determined. This method is very simple. However, the instrument response functions of all components (mainly photomultiplier, excitation source, and oscilloscope) must be short enough for a sufficient time resolution.

In the phase shift method, the excitation intensitiy is modulated sinusoidally with an angular frequency ω. Therefore, the photoluminescence response is also modulated sinusoidally with the same frequency but with a phase shift ϕ, due to the finite lifetime of the charge carriers. If a single exponential decay with one time constant τ_{decay} is presumed, it holds [38]

$$\tan \phi = \omega \tau_{decay}. \tag{3.2.1}$$

Therefore, the decay time can be easily determined from the phase-shift. The disadvantage of this method is that it does not account for multi-exponential decays nor it makes a statement about their contribution to the total luminescence intensity.[12]

In this work, the time-correlated single photon counting (TCSPC) method with the setup illustrated in figure 3.3 (a) is used for measurement of the luminescence decay. A laser generates a pulse of photons directed to the sample. The absorption of these photons generates charge carriers, which then recombine radiatively. The luminescence is collected and directed to a photomultiplier for detection.[13] For each detected photon, the time between emission of the laser pulse and detection of the photon is measured. In order to do this, the laser pulse serves as the start signal and the photon detection serves as a stop signal. Hence, only one photon can be detected for each laser pulse. In order to detect a large number of photons for statistical reasons this procedure must be often repeated.

---

[12]For further details on theses methods, reference is made at this point to reference [38].
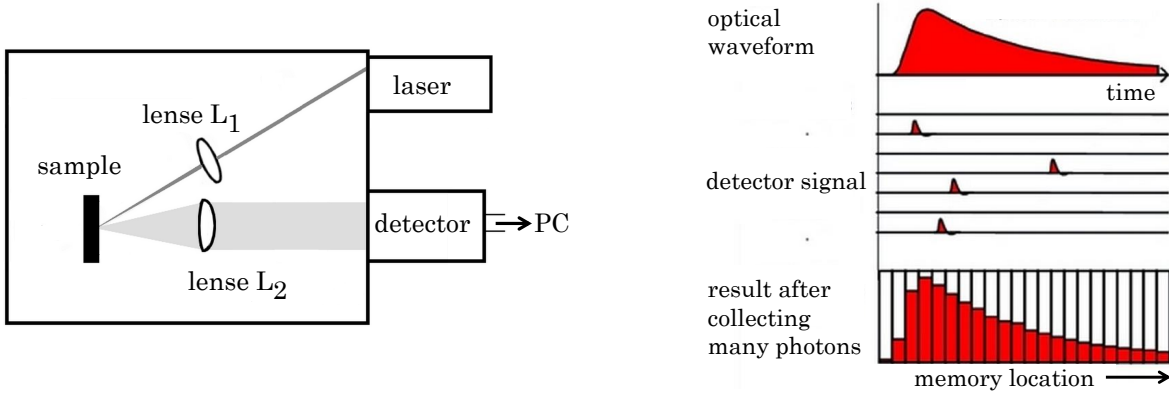[13]For further information on the setup see reference [Mai5].

Figure 3.3: (a) Experimental setup for measuring TRPL. The light is focused on the sample by a lens L_1. The photoluminescence is collected by a second lens L_2 and directed to the detector. (b) Principle of the time-correlated single photon counting method. The luminescence transient is gradually reconstructed by repeatedly measuring the luminescence photons. Figure is adapted from ref. [43]

Due to the finite time resolution, the time scale is separated into channels j of width Δt (see fig. 3.3 (b)). After the time for the detection of the photon is measured, a counter in the corresponding channel $[t_j, t_j + \Delta t)$ is increased by one. Hence, the counter gives the number of detected photons for which the time between generation and detection is between t_j and $t_j + \Delta t$. In accordance with equation (3.1.11), the luminescence intensity $I(t)$ is the number of photons, emitted per time. Therefore, $\int_{t_j}^{t_j+\Delta t} I(t)\mathrm{d}t \approx I(t_j)\,\Delta t$ is the number of photons for which the time between generation and emission is between t_j and $t_j + \Delta t$. However, except a scaling, this is the value of the counter of the channel j. Therefore, the histogramm in figure 3.3 (b) approximates the time-resolved luminescence. Hence, TCSPC is capable to record the full luminescence decay in contrast to other methods like the phase-shift method. This is a prerequisite for understanding the full recombination kinetics.

3.3 The problem of determining material parameters from TRL

Up to now, time-resolved (photo)luminescence turned out to be easily measured by means of TCSPC and the luminescence decay can be easily analyzed, because the equations $(3.1.9)-(3.1.11)$ show that the decay time equals the recombination lifetime. Unfortunately, this is not the general case but only valid for low-injection levels and negligible defect-enhanced recombination. To make this clear, the presumption of low-injection levels is dropped now. Then, the net-rate of radiative recombination and the inverse of the recombination lifetime of electrons in a p-type semiconductor with $p_0 \ll n_0$ and $\Delta n = \Delta p$ become

$$R_{rad,net} = B\,\Delta n\,(p_0 + \Delta n) \qquad \text{and} \qquad \tau_{rad,n}^{-1} = B\,(p_0 + \Delta n)\,. \qquad (3.3.1)$$

It is obvious, that the recombinaton lifetime is not constant but may implicitly depend

on the excitation by the excess carrier density Δn. By solving the continuity equation, the time-dependent excess electron density Δn can be calculated as a function of time. Knowing $\Delta n(t)$, also the luminescence intensity $I(t)$ can be determined. The effective electron lifetime, the radiative recombination lifetime, and the decay time come out as

$$\tau_{eff,n}^{-1} = B\, p_0 \, \frac{p_0 + \Delta n(t=0)}{p_0 + \Delta n(t=0) - \Delta n(t=0)\, \mathrm{e}^{-B\, p_0\, t}} = \tau_{rad,n}^{-1} \qquad (3.3.2a)$$

$$\tau_{decay}^{-1} = B\, p_0 \, \frac{p_0 + \Delta n(t=0) + \Delta n(t=0)\, \mathrm{e}^{-B\, p_0\, t}}{p_0 + \Delta n(t=0) - \Delta n(t=0)\, \mathrm{e}^{-B\, p_0\, t}} \neq \tau_{rad,n}^{-1}. \qquad (3.3.2b)$$

This shows that the decay of the electron density is not exponential since the effective electron lifetime depends on time. Further, this shows that the decay time is neither equal to the effective electron lifetime nor to the radiative recombination lifetime.[14]

Another problem addresses the discrimination of different recombination paths by TRL. Therefore, it is assumed that there are two recombination mechanisms with constant recombination lifetimes $\tau_{r1,n}$ and $\tau_{r2,n}$. The effective electron lifetime and the decay time then are

$$\tau_{decay}^{-1} = \tau_{r1,n}^{-1} + \tau_{r2,n}^{-1} = \tau_{eff,n}^{-1} = \tau_{eff,r,n}^{-1}. \qquad (3.3.3)$$

Now, only the sum of the inverse recombination lifetimes can be determined from the decay time. It is not possible, to calculate $\tau_{r1,n}$ and $\tau_{r2,n}$ separately. For this purpose, at least two decay times are needed, which may come out from TRL measurements at different experimental conditions, e.g. different excitation levels or temperatures.

3.4 Alternative lifetime measurement techniques

The above sections can be summarized as follows: The measurement of time-resolved luminescence is easy and straight forward. From the decay of the luminescence a decay time can be determined, which is supposed to characterize the recombination. Unfortunately, this decay time can only be related to recombination lifetimes in exceptional cases. In general, analytical formulae and experimental variations are necessary for the semiconductor characterization. Therefore, alternative lifetime measurement techniques have been developed which are introduced and compared with TRL in the following. One possibility is to measure the so-called diffusion length L_x, which is defined by

$$L_x = \sqrt{D_x\, \tau_{eff,r,x}}, \quad x = n,\, p, \qquad (3.4.1)$$

with the charge carrier diffusion constant D_x and the effective recombination lifetime $\tau_{eff,r,x}$. This diffusion length can be measured in EBIC measurements on a pn-junction [44]. In order to do so, a charge carrier density is locally generated. By diffusion, a certain

---

[14]Therefore, it is misleading to call the decay time a lifetime.

amount of charge carriers reaches the collecting space charge region of the pn-junction and generates a photo current. By the variation of the distance of generation to the space charge region, the diffusion profile and, thus, the diffusion length can be measured. The advantage of this method is the rather simple analysis. But the measurement is stationary which means transient effects like charge carrier trapping cannot be observed. Furthermore, the charge carrier mobility must be known and a charge carrier collecting junction is needed. Therefore, EBIC measurements cannot be applied to sole absorbers. Both are considerable disadvantages compared to TRL.

Another possibility is to apply a forward voltage to a solar cell [45]. Thereby, minority charge carriers are injected. Then, the sign of the voltage is changed almost instantaneously. Due to the finite lifetime of the charge carriers, a large reverse current (due to the injected charge carriers) flows which decays in time. From this, the effective minority carrier lifetime is determined. The advantage is that due to the transient measurement transient effects can be observed. However, again blank absorbers cannot be characterized since complete solar cells are needed, which additionally have to be electrically contacted. Further, the analyzation is very difficult due to the complex currents and the interaction with internal electric fields.

Probably the most competing method is the measurement of the photoconductivity [2, 37]. Therefore, charge carriers, for example electrons, are generated and the conductivity σ_n is measured either contactless by an inductivity or by application of a voltage. Then, the electron density can be determined from the conductivity as a function of time by

$$n(t) = \frac{\sigma_n(t)}{e_0\,\mu_n}. \tag{3.4.2}$$

Due to the factorial relation, the decay of the electron density and, thus, the effective electron lifetime can be directly measured without knowledge of the electron mobility. This is an important advantage compared to TRL, where $\tau_{eff,n}$ has to be determined from the decay time in a roundabout way. Furthermore, this method is also applicable to blank absorber layers and also to semiconductors that have poor luminescence properties. Main disadvantages of this method are the limited time resolution of approximately $100\,\mathrm{ns}$ [4] and the required absence of a metallic back contact due to the inductive measurement.

4 Simulation of TRL with Synopsys® TCAD

In chapter 3, the measurement of TRL has been explained. For its description, all necessary equations are provided in chapter 2. Hence, all requirements for the simulation of a TRL experiment are fulfilled. How this is done using the tool Synopsys® TCAD will be the issue of this chapter. For a better understanding, the basic procedure for running a simulation is explained first. Then, strategies for each individual step - which is the discretization of the semiconductor, the calculation of the generation, and the numerical solution of the semiconductor equations - are presented without going into a detailed mathematical description. The output of the simulations will be the electrostatic potential, the electron density, and the hole density as a function of space and time. From these quantities, any other quantity can be calculated, e.g. the rate of radiative recombination. By its numerical integration over space for each time step, the TRL intensity can be determined as a function of time.

4.1 The workflow of a TRL simulation

At the beginning, the basic simulation procedure of TRL with Synopsys® TCAD is described. Afterwards, a more mathematical analysis will be given.

Defining the geometry, material profiles, and the mesh
First of all, the geometry and the boundaries of the device under simulation are defined using the Sentaurus Structure Editor. Here, the dimensionality of the simulation is chosen, lengths are specified, regions with specific materials are definied, and ohmic contacts are assigned to the boundaries. Further, profiles of material properties, such as the doping density, the band gap or the SRH-lifetime are definied. In the end, the mathematical grid for the numerical solution of the semiconductor equations is calculated (see section 4.2) according to user defined specifications, e.g. mesh refinements next to interfaces, maximum grid distances, etc.

Generation of parameter files
Each vertex (grid point of the mesh) contains information on the material at this position. The properties of these materials are stored in parameter files. For semiconducting materials, these contain at least the electron affinity, the complex refractive index as a

numerical table of the wavelength, the effective densities-of-states, the charge carrier mobilities, the constant for radiative recombination, and the trap parameters. If not given by a profile, they also contain the SRH-lifetimes and the band gap.

In order to account for the pulse shape, the pulse width, the number of excitation pulses, and the excitation frequency, another file is created providing a numerical table for the time-dependence of a scaling factor $[0, 1]$ for the generation function (see section 4.3). The advantage is that the generation function does not need to be recalculated but can be used for each time step again.

Performing the simulation

With the mesh file and the parameter files, it remains the specification of the boundary conditions and the physical models, prior to being able of performing the simulation. This means, the applied voltages and the contact recombination velocities have to be assigned to each ohmic contact and recombination processes, mobility models or temperature dependencies must be defined. Afterwards, the simulation starts with the calculation of the generation function. In this thesis, an optical excitation is chosen with specified wavelength, intensity, time-dependence, angle of incidence, and method for calculation (see section 4.3). Then, an equilibrium solution as a starting point for the transient simulation is calculated by solution of the Poisson equation with previously defined options for the numerical solver.[15] Afterwards, the simulation of the experiment is performed, which in this work is the transient simulation of the luminescence. Thereby, the solution of the coupled Poisson and continuity equations is calculated at each time-step (see sections 4.4 and 4.5). In doing so, the time-discretization, the number of steps, and the final time can be set individually.

Postprocessing of the simulation output

The output of the simulation are the electrostatic potential, and the electron and hole densities (or equivalently the quasi-Fermi levels) at each grid point at each time-step. From these, almost any other quantity can be calculated as a function of space and time, in particular the rate of radiative recombination. For each time-step, this rate is integrated numerically over space. Following the discussion in section 2.7, the result of this integration is taken as the luminescence intensity, which can be processed further (see section 4.6). For example, it can be convoluted with an experimentally determined instrument-response-function to approximate experimental time-resolved luminescence. Alternatively, it can be fitted exponentially in order to determine decay times.

---

[15] For the initial equilibrium solution, the continuity equations are purposely not solved due to a pecularity of the simulation tool: Independent from the time-dependence of the optical scaling, a maximum generation is assumed at $t = 0$. Thus, the solution of the continuity equations then would lead to a large amount of charge carriers and a non-equilibrium state of the device.

4.2 Delaunay triangulation for mesh generation

The first step in performing a simulation is the generation of the mesh in order to descretize the semiconductor equations. The mesh generator reads the input geometry from a file and generates a set of N_m vertices $\{v_1, v_2, \ldots\}$ according to user specified requirements (refinements near interfaces etc.). Then, a so-called axis aligned Delaunay triangulation is used in order to interconnect the vertices. The resulting mesh confines triangles (or tetrahedra in three dimensions[16]) fully covering the semiconductor without overlap.

The mesh, however, is not arbitrary since it must fulfill the Delaunay condition. For its revisal, the circumcircle is determined for each triangle. If there are no vertices in the interior of the circumcircles, the Delaunay condition will be fulfilled. This is exemplified
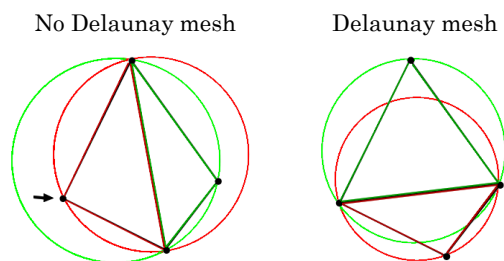
Figure 4.1: Two different options of the triangulation of four vertices. In the left figure, the Delaunay condition is not fulfilled, since the green circumcircle contains vertices (marked by an arrow) apart from the three of the corresponding green triangle. In the right figure, the Delaunay condition is fulfilled.

in figure 4.1 for a triangulation of four vertices. Here, the green and the red circle are the circumcircles of the green and the red triangle, respectively. On the left-hand side, the Delaunay condition is not fulfilled since the green circle contains, besides the green triangle, other vertices marked by an arrow. In contrast, for the same vertices the triangulation shown on the right-hand side complies with the Delaunay condition.

This Delaunay triangulation brings several numerical advantages along. For instance, it maximizes the internal angles of the triangles, which minimizes rounding errors when the semiconductor equations are solved.

4.3 Calculation of the generation function

The next step in the simulation process is the calculation of the generation function. In this work, the generation of charge carriers is achieved by an optical excitation. The calculation of the corresponding generation function is done by two ways: by RayTracing or by the Transfer-Matrix-Method (TMM). Both are described in the following.

4.3.1 RayTracing

For RayTracing, the incident light is simulated by a set of starting rays that is distributed randomly on the surface of incidence. These rays propagate through the material and

---

[16]The three dimensional terminology will be disregarded in the following.
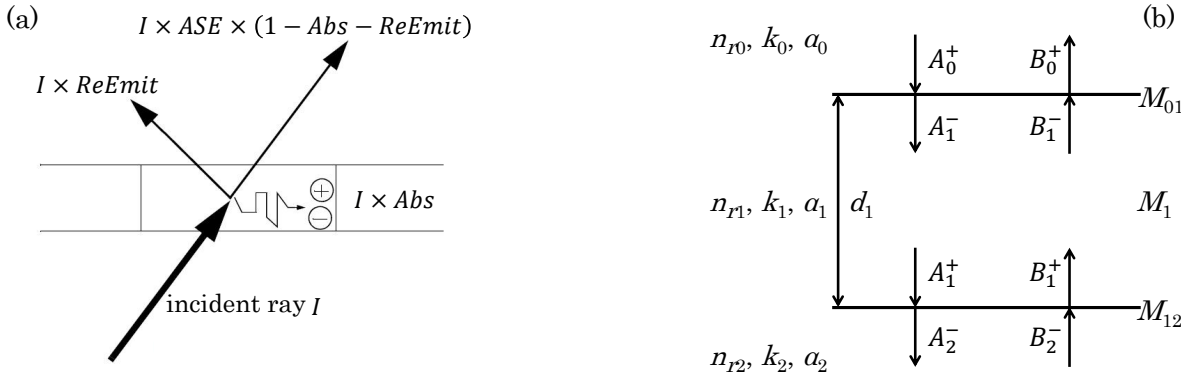
Figure 4.2: (a) Schematic illustration for the consideration of photon recycling by RayTracing. By crossing an optically active layer, a ray emitted by spontaneous recombination is absorbed (Abs), absorbed and instantaneously reemitted into another direction ($ReEmit$), and the rest is amplified by stimulated emission (ASE). The figure is adapted from ref. [39]. (b) Illustration of forward and backward waves in a stack of three materials with optical constants n_r, κ, α. M_{01} and M_{12} are the interface matrices relating the incident, transmitted, and reflected intensity, and M_1 is the transfer matrix of the layer.

they are reflected and transmitted at interfaces; thereby, being split into two new rays. From the resulting ray tree, the generation function can be calculated from the absorption of each ray. The advantage is that this method allows non-planar surfaces and interfaces. Furthermore, it enables the calculation of the generation due to photon recycling. To this end, a second ray tree is generated, where the starting rays originate from a spontaneous emission process. If such a ray with intensity I passes an optically active layer such as in figure 4.2 (a), the fraction Abs will be absorbed in the layer, the fraction $ReEmit$ will be absorbed and instantaneously reemitted into another direction, and the rest $1 - Abs - ReEmit$ will be amplified by stimulated emission with the coefficient $ASE \geq 1$. If the incident ray carries a rate number N_{ph} of photons, the net-generation rate due to photon recycling will become

$$G_{PR} = N_{ph} \left((ASE - 1) \left(1 - Abs - ReEmit \right) - Abs \right). \tag{4.3.1}$$

In doing so, photon recycling can be easily accounted for in the simulations without solving the photon equation (2.5.16). A major disadvantage, especially for thin-film semiconductors, is that the rays do not carry information on the phase. Thus, interference effects are not modeled by RayTracing. Apart from this, photon recycling has only a minor influence on the TRL decay anyway according to paper [Mai1].

4.3.2 Transfer-Matrix-Method

To account for interference effects, the Transfer-Matrix-Method described in the following is more appropriate. The electric field strength of incident, reflected, and transmitted light at each interface is thereby related by matrices. For their derivation, a layer of thickness d_1 with optical constants n_{r1}, κ_1, α_1 is presumed (see figure 4.2 (b)). This layer shall be

surrounded by two (other) materials with optical constants n_{r0}, κ_0, α_0 and n_{r2}, κ_2, α_2. Due to internal reflections, there is light propagating in forward and backward direction with the complex electric field strengths A and B. These are related in Fresnel's equations (2.5.9) by

$$B_0^+ = r_{01} A_0^+ + t_{10} B_1^-, \qquad A_1^- = t_{01} A_0^+ + r_{10} B_1^-. \qquad (4.3.2)$$

This system of equations is now arranged in matrix form by

$$\begin{pmatrix} A_0^+ \\ B_0^+ \end{pmatrix} = M_{01} \begin{pmatrix} A_1^- \\ B_1^- \end{pmatrix} \qquad \Rightarrow \qquad M_{01} := \frac{1}{t_{01}} \begin{pmatrix} 1 & r_{01} \\ r_{01} & 1 \end{pmatrix}, \qquad (4.3.3)$$

which defines the interface matrix M_{01}. The propagation of the forward and backward waves through layer 1 is described by the solution (2.5.3) of Maxwell's equations:

$$B_1^- = e^{-\frac{\alpha_1}{2} d_1} e^{i k_0 n_{r1} d_1} B_1^+, \qquad A_1^- = e^{\frac{\alpha_1}{2} d_1} e^{i k_0 n_{r1} d_1} A_1^+. \qquad (4.3.4)$$

Again, this equation system can be arranged in matrix form by

$$\begin{pmatrix} A_1^- \\ B_1^- \end{pmatrix} = M_1 \begin{pmatrix} A_1^+ \\ B_1^+ \end{pmatrix} \qquad \Rightarrow \qquad M_1 := \begin{pmatrix} e^{-\frac{\alpha_1}{2} d_1} e^{i k_0 n_{r1} d_1} & 0 \\ 0 & e^{\frac{\alpha_1}{2} d_1} e^{-i k_0 n_{r1} d_1} \end{pmatrix}, \qquad (4.3.5)$$

which defines the transfer matrix M_1. Both, the interface matrix and the transfer matrix can be determined for any other interface or layer in the same way. The combination of equation (4.3.3) and (4.3.5) then yields

$$\begin{pmatrix} A_0^+ \\ B_0^+ \end{pmatrix} = M_{01} \begin{pmatrix} A_1^- \\ B_1^- \end{pmatrix} = M_{01} M_1 \begin{pmatrix} A_1^+ \\ B_1^+ \end{pmatrix} = M_{01} M_1 M_{12} \begin{pmatrix} A_2^- \\ B_2^- \end{pmatrix} = \dots . \qquad (4.3.6)$$

This is continued up to the last interface N, for which the boundary conditions $A_N^- = 0$ and $A_0^+ = E_0(t)$ hold. Equation (4.3.5) then is a linear system of equations for the unknown quantities $B_0^+ = E_{reflected}$ and $B_N^- = E_{transmitted}$. By its solution, the photon current density can be calculated at any depth using equation (2.5.10), and from this the generation function is known after equation (2.5.8).

4.4 Linearization of the semiconductor equations using the box discretization and the TRBDF composite method

After the calculation of the generation function, the semiconductor equations are solved numerically. In order to do so, the equations are discretized by the box discretization [39]. A box is thereby designed around each of the N_m vertices (see figure 4.3 (a)). The box Ω_i around the vertex v_i is confined by the perpendicular bisectors of the mesh elements.[17]

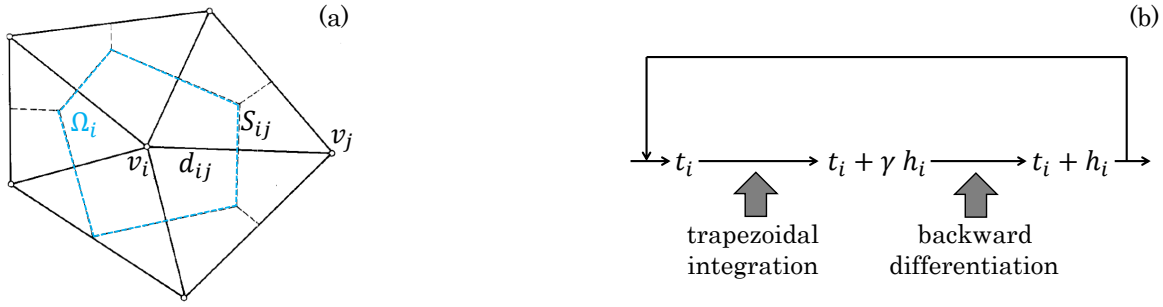[17]For the existence and the convexity of the box the mesh must fulfill the Delaunay criterion.

Figure 4.3: (a) Delaunay mesh (black lines) around a vertex v_i. The box Ω_i (blue lines) of vertex v_i is constructed by determining the perpendicular bisectors of interconnections d_{ij}. The length of the bisector on d_{ij} (or the area in three dimensions) is denoted by S_{ij}. The figure is adapted from [46]. (b) Schematic illustration of a time-discretization. To get from time t_i to time $t_i + h_i$, an intermediate time-step $t_i + \gamma\, h_i$ is inserted. Then, in the first step the continuity equations are solved by trapezoidal integration. In the second step the time derivative is approximated by the backward differentiation rule.

The semiconductor equations then are solved within each box Ω_i. To this end, they are arranged in the form

$$\mathrm{div}\left(\varepsilon_0\,\varepsilon_r\,\nabla_r\varphi\right) = -\varrho \tag{4.4.1a}$$

$$\mathrm{div}\Gamma_n = G_n - R_n - \frac{\partial}{\partial t}n \tag{4.4.1b}$$

$$\mathrm{div}\Gamma_p = G_p - R_p - \frac{\partial}{\partial t}p. \tag{4.4.1c}$$

Hence, each equation can be written as $\mathrm{div}F = g$ with a vector function F and a scalar function g. These then are integrated over the box Ω_i and Gauss's theorem is applied to the divergency term. If $\partial\Omega_i$ denotes the boundary of the box and $\widehat{n}$ the outer normal vector on $\partial\Omega_i$, the result will become

$$\int_{\partial\Omega_i} F\,\widehat{n}\,\mathrm{d}S = \int_{\Omega_i} g\,\mathrm{d}r. \tag{4.4.2}$$

It is now assumed that the box is small since the mesh is fine. Then, the function g can be assumed constant in Ω_i and equation (4.4.2) becomes

$$\int_{\partial\Omega_i} F\,\widehat{n}\,\mathrm{d}S \approx \mu(\Omega_i)\,g_i. \tag{4.4.3}$$

Here and in the following, the index i means that the function is evaluated at the vertex v_i, thus, it is $g_i = g_i(t) = g(v_i, t)$. Further, $\mu(\Omega_i)$ denotes the measure of the box Ω_i. The surface $\partial\Omega_i$ is now decomposed into the segments S_{ij} which are the bisectors between vertex v_i and its connected vertices v_j (see figure 4.3 (a)). Then, it follows from equation (4.4.3)

$$\sum_{\substack{j \\ v_j \text{ connected to } v_i}} \int_{S_{ij}} F\,\widehat{n}\,\mathrm{d}S \approx \mu(\Omega_i)\,g_i. \tag{4.4.4}$$

It is again assumed, that Ω_i is small. Hence, the surface is small, too. Therefore, F can

be assumed constant on each S_{ij} and it follows

$$\sum_{\substack{j \\ v_j \text{ connected to } v_i}} \mu(S_{ij})\ F\,\widehat{n}|_{S_{ij}} \approx \mu(\Omega_i)\,g_i, \tag{4.4.5}$$

with $\mu(S_{ij})$ being the measure of S_{ij}. It remains the calculation of $F\,\widehat{n}|_{S_{ij}}$ which must be done seperately for each of the three equations (4.4.1a)$-$(4.4.1c).

For the Poisson equation it is $g = -\varrho$ and $F\,\widehat{n}|_{S_{ij}} = \varepsilon_0\,\varepsilon_r\ (\widehat{n}\,\nabla_r\varphi)|_{S_{ij}}$. The latter is the directional derivative of the electrostatic potential and can be approximated by finite differences. This yields the following discretization of the Poisson equation:

$$\sum_{\substack{j \\ v_j \text{ connected to } v_i}} \mu(S_{ij})\,\varepsilon_0\,\varepsilon_r\,\frac{\varphi_j - \varphi_i}{d_{ij}} = -\mu(\Omega_i)\,\varrho_i, \quad \forall i = 1, \dots, N_m. \tag{4.4.6}$$

The same procedure can be applied to the continuity equations. For the electron continuity equation especially follows $g_i = G_{n,i} - R_{n,i} - \frac{\partial}{\partial t}n_i$ and $F\,\widehat{n}|_{S_{ij}} = -D_n\ (\widehat{n}\,\nabla_r\,n)|_{S_{ij}} - \mu_n\ (n\,\widehat{n}\,\nabla_r\,\varphi)|_{S_{ij}}$. However, in this case the directional derivative cannot be approximated by finite differences since these may lead to numerical oscillations [47]. Besides, negative charge carrier densities could result, if the drift dominates the diffusion [29]. Thus, a Scharfetter-Gummel approach is used instead [48] which presumes a constant electric field and a constant current density along d_{ij}. This defines a differential equation for the electron density $n(r)$ with the boundaries $n(v_i) = n_i$ and $n(v_j) = n_j$. By its solution the projection of $F = \Gamma_n$ on $\widehat{n}$ becomes

$$F\,\widehat{n}|_{S_{ij}} = \frac{D_n}{d_{ij}}\left(n_i\,B\left(\frac{e_0}{k_{\mathrm{B}}\,T}(\varphi_i - \varphi_j)\right) - n_j\,B\left(\frac{e_0}{k_{\mathrm{B}}\,T}(\varphi_j - \varphi_i)\right)\right) \tag{4.4.7}$$

with the Bernoulli function $B(x) = x/(\mathrm{e}^x - 1)$. With that, the spatial discretization of the electron continuity equation becomes

$$\sum_{\substack{j \\ v_j \text{ connected to } v_i}} \mu(S_{ij})\,\frac{D_n}{d_{ij}}\left(n_i\,B\left(\frac{e_0}{k_{\mathrm{B}}\,T}(\varphi_i - \varphi_j)\right) - n_j\,B\left(\frac{e_0}{k_{\mathrm{B}}\,T}(\varphi_j - \varphi_i)\right)\right)$$

$$\approx \mu(\Omega_i)\left(G_{n,i} - R_{n,i} - \frac{\partial}{\partial t}n_i\right), \quad \forall i = 1, \dots, N_m. \tag{4.4.8}$$

A similar discretization can be derived for the hole continuity equation:

$$\sum_{\substack{j \\ v_j \text{ connected to } v_i}} \mu(S_{ij})\,\frac{D_p}{d_{ij}}\left(p_j\,B\left(\frac{e_0}{k_{\mathrm{B}}\,T}(\varphi_j - \varphi_i)\right) - p_i\,B\left(\frac{e_0}{k_{\mathrm{B}}\,T}(\varphi_i - \varphi_j)\right)\right)$$

$$\approx \mu(\Omega_i)\left(G_{p,i} - R_{p,i} - \frac{\partial}{\partial t}p_i\right), \quad \forall i = 1, \dots, N_m. \tag{4.4.9}$$

The equations (4.4.6), (4.4.8), and (4.4.9) are the spatial discretization of the Poisson

and the continuity equations. In other words, instead of calculating the functions $n(r,t)$, $p(r,t)$, $\varphi(r,t)$, only the values at the vertices $n(v_i,t)$, $p(v_i,t)$, $\varphi(v_i,t)$ are determined by $3\,N_m$ implicit equations.

In accordance with the spatial dependence, also the time dependence must be discretized within a transient simulation. In order to do so, it is pointed out that the two continuity equations (4.4.8) and (4.4.9) in discretized form can be written as

$$\frac{\partial}{\partial t}q_i(t) = f_i(t) \qquad \text{with} \qquad q_i = n_i,\,p_i. \tag{4.4.10}$$

As the equations were integrated over boxes for the spatial discretization, equation (4.4.10) can be integrated over time intervals $[t_n,\,t_n+h_n)$. However, it turns out that the results will be more stable in a numerical sense, if an intermediate step $[t_n,t_n+\gamma\,h_n,t_n+h_n)$ with $\gamma = 2-\sqrt{2}$ is inserted (see figure 4.3 (b)). The integration over one time interval then is

$$\int_{t_n}^{t_n+\gamma\,h_n} \frac{\partial}{\partial t}q_i(t) = \int_{t_n}^{t_n+\gamma\,h_n} f_i(t)\mathrm{d}t \tag{4.4.11a}$$

$$\int_{t_n+\gamma\,h_n}^{t_{n+1}} \frac{\partial}{\partial t}q_i(t) = \int_{t_n+\gamma\,h_n}^{t_{n+1}} f_i(t)\mathrm{d}t. \tag{4.4.11b}$$

The right-hand side of equation (4.4.11a) is solved by trapezoidal integration, the right-hand side of equation (4.4.11b) is solved by the backward differentiation method [49, 50]. This yields

$$2\,q_i(t_n+\gamma\,h_n) - \gamma\,h_n\,f_i(t_n+\gamma\,h_n) = 2\,q_i(t_n) + \gamma\,h_n\,f_i(t_n) \tag{4.4.12a}$$

$$q_i(t_{n+1}) - \frac{1-\gamma}{2-\gamma}\,h_n\,f_i(t_{n+1}) = \frac{1}{\gamma\,(2-\gamma)}\,q_i(t_n+\gamma\,h_n) - \frac{(1-\gamma)^2}{\gamma\,(2-\gamma)}\,q_i(t_n). \tag{4.4.12b}$$

With $q_i = n_i,\,p_i$ and f_i from equation (4.4.8) or (4.4.9), these are the time- and space discretized continuity equations. Equation (4.4.12a) is an implicit equation for the unknown $n_i(t_n+\gamma\,h_n)$ or $p_i(t_n+\gamma\,h_n)$ that can be determined from $n_i(t_n)$ and $p_i(t_n)$, and from that $n_i(t_n+h_n)$ and $p_i(t_n+h_n)$ can be calculated from the implicit equation (4.4.12b). Thus, the state of the system at any time step is determined from the previous time step.

4.5 Numerical solution of the semiconductor equations using the Bank-Rose-algorithm

For each time step t_n and for each vertex v_i there are three implicit equations for the three unknown quantities $n_i(t_n)$, $p_i(t_n)$, $\varphi_i(t_n)$. Thus, for N_m vertices, $3\,N_m$ implicit equations for the unknown quantities $n_1(t_n),\ldots,n_{N_m}(t_n),p_1(t_n),\ldots,p_{N_m}(t_n),\varphi_1(t_n),\ldots,\varphi_{N_m}(t_n)$ must be solved for each time step. These $3\,N_m$ unknowns can be arranged in a $3\,N_m$ dimensional vector $u_n := (n_1(t_n),\ldots,n_{N_m}(t_n),p_1(t_n),\ldots,p_{N_m}(t_n),\varphi_1(t_n),\ldots,\varphi_{N_m}(t_n))$,

where the index n denotes the time step. In analogy, the $3\,N_m$ implicit equations can be arranged in a $3\,N_m$ dimensional vector function T_n. Therefore, the system of equations is compactly written as:

$$T_n\left(u_n\right) = 0, \quad \forall t_n. \tag{4.5.1}$$

For the solution of the system (4.5.1), a global and damped Newton method is applied [51]. If T'_n denotes the Jacobian matrix of T_n, the Newton iteration will read

$$x_{n,k}\, T'_n(u_{n,k}) = -T_n(u_{n,k}), \quad u_{n,k+1} = u_{n,k} + \omega_{n,k}\, x_{n,k} \quad k \in \mathbb{N},\, \forall t_n. \tag{4.5.2}$$

According to this, the solution u_n is calculated iteratively for each time step t_n with a certain damping parameter $\omega_{n,k}$. For each iteration step k, (4.5.2) is a linear system of equations for the unknown $x_{n,k}$. Its solution can either be done directly or again iteratively using the three different solvers provided in Synopsys® TCAD.

The PARDISO and the SUPER solvers are direct methods calculating a LU factorization of the sparse coefficient matrix $T'_n(u_{n,k})$. Both yield very long calculation times for high dimensions of the matrix $T'_n(u_{n,k})$ and for a large number of non-zero entries. Thus, their application is only convenient for a number of vertices below 10000 which is not appropriate for three dimensional simulations.

Therefore, in this work an iterative linear solver (ILS) is used, more precisely the method of the generalized minimal residual (GMRES) [52]; this gives the best results in terms of the number of iterations, time to compute the solution, and reliability. Thereby, the approximation $x_{n,k}^m$ of the solution $x_{n,k}$ in the m-th iteration step is arranged by $x_{n,k}^m = x_{n,k}^0 + V_m\, y^m$, where V_m is a matrix of m basis vectors that have to be chosen properly. $x_{n,k}^0$ is arranged by $x_{n,k}^0 = -T_n(u_{n,k})$. y^m then is determined so that the eucledian norm of the residuum $||x_{n,k}^m\, T'_n(u_{n,k}) + T_n(u_{n,k})||_2$ is minimal. If the residuum complies with a specified tolerance, the algorithm will stop. Otherwise the procedure is repeated with $m+1$ basis vectors.

To improve the convergence velocity of the GMRES method and in order to reduce calculation times, the equation system (4.5.2) is preconditioned. Therefore, an incomplete LU factorization of $T'_n(u_{n,k})$ is calculated so that $T'_n(u_{n,k}) \approx L\,U$.[18] If the equation system (4.5.2) then is multiplied from the right with $(L\,U)^{-1}$, it will be

$$x_{n,k}\, \underbrace{T'_n(u_{n,k})\, (L\,U)^{-1}}_{\approx\text{unity matrix}} = -T_n(u_{n,k})\, (L\,U)^{-1}. \tag{4.5.3}$$

Therefore, the preconditioned coefficient matrix is already close to the unity matrix; therefore, the starting value $x_{n,k}^0 = -T_n(u_{n,k})\, (L\,U)^{-1}$ of the GMRES method is close to the solution $x_{n,k}$, which reduces the number of iterations significantly.

---

[18]The factorization is incomplete in the sense that elements smaller than a parameter ϵ are disregarded, which saves memory and computation times. The smaller ε is, the more accurate the preconditioner becomes.

Finally, to enhance the calculation of the incomplete LU factorization, the matrix $T'_n(u_{n,k})$ is ordered non-symmetrically to improve the condition of the matrix that means the problem is more stable concerning numerical errors. The result then is re-ordered symmetrically to reduce the fill-in in the preconditioner [28].

4.6 Calculation of the TRL intensity

In the end, the postprocessing of the simulation is shortly described. The output of the simulations are the electrostatic potential, and the electron and hole densities at each vertex and time step: $n_i(t_n)$, $p_i(t_n)$, $\varphi_i(t_n)$ for all $i = 1, \ldots, N_m$. From this, the spontaneous recombination rate or the radiative recombination rate can be determined after equation (2.4.10). The numerical integration over the device volume V yields the luminescence intensity $I(t_n)$ at each time step:

$$I(t_n) = \int_V R_{sp}(r, t_n)\mathrm{d}V \quad \text{or} \quad I(t_n) = \int_V R_{rad}(r, t_n)\mathrm{d}V. \quad (4.6.1)$$

Following the discretization methods in section 4.4, it is for example

$$I(t_n) \approx B \sum_i^{N_m} \mu(\Omega_i)\, n_i(t_n)\, p_i(t_n). \quad (4.6.2)$$

This is the number of photons which are generated per time in the whole device. It is worth mentioning that this definition of the luminescence in the simulations does not account for limited collection of the luminescence.

The result (4.6.2) can be processed further. For example it can be convoluted with a theoretically or experimentally determined instrument response function IRF such as [53]

$$I_{conv}(t) = \int_{-\infty}^{+\infty} I(\tau)\, IRF(t - \tau)\, \mathrm{d}\tau, \quad \text{with} \quad IRF(t) = \mathrm{e}^{-\frac{(t-t_0)^2}{\tau_{IRF}^2}}. \quad (4.6.3)$$

This is very important when simulated luminescence decays are compared with experimental TRL in order to account for the limited time resolution of an experimental setup.

5 Results of the TRL simulations and experiments

After establishing the basis for the measurement and the simulation of TRL, this chapter presents the results of this work by means of peer-reviewed articles and focuses on the open questions and problems of luminescence decay introduced in chapter 3:

- The reason for bi- and multi-exponential decays is not accurately known.

- Material parameters cannot be determined from one single luminescence decay due to ambiguities.

- Reasons for decay times in the range of the radiative lifetime are not clarified.

- The reason for the non-correlation of the open-circuit voltage and the decay time is not exactly known.

- The relation of the steady state of a solar cell under operation to its response in TRL is still unclear, especially concerning similar carrier densities and defect occupation.

A strategy for dealing with these problems has already been proposed in the introduction: The first step is to study the luminescence decay for all imaginable charge carrier eliminating processes, and to derive analytical formulae for the decay time as function of the injection level or the temperature. This is attended by the transfer of the theory by Ahrenkiel [20] on the impact of space charges, charge carrier transport, and surface and bulk recombination from III-V semiconductors to thin-film semiconductors. All this has been carried out in [Mai1, Mai2], which is summarized and discussed with regard to solar cell characterization in the subsequent section 5.1.

With the findings on the TRL in thin-film semiconductors, the decay curves of a CIGSe solar cell can be measured and analyzed. This has been demonstrated in [Mai5, Mai6], which is the focus of section 5.2. It is shown that the current understanding of TRL under the influence of space charges and bulk-recombination is approved by the measurements, which becomes apparent through the good approximation of experimental decay curves by simulated ones. Under these circumstances, an analytical formula is derived which allows the determination of the minority carrier lifetime and the calculation of an upper limit for the charge carrier mobilities from the measured decay times. Both give reasonable values that are in accordance with literature data.

Despite the successful application and analyzation of TRL on solar cells, at this point the theory is not capable of reliably answering the reason for bi-exponential decays with decay times in the range of the radiative limit; neither it is able to satisfactorily explain the non-correlation of the decay time and the open-circuit voltage. This is due to an important material property that up to that point has not been considered - charge carrier traps. For this reason, a general theory of the impact of traps on the TRL has been derived in ref. [Mai3]. The results are summarized in section 5.3. It is shown, that the TRL under the influence of traps has a unique dependence on the excitation intensity and the temperature. Based on this result, it is proposed to detect charge carrier traps by means of an injection and temperature dependent TRL, which has been examined exemplarily on CIGSe and CZTSe absorbers in [Mai7, Mai8]. In doing so, traps can be verified for both materials. By the reproduction of the decay curves in simulations, also the trap properties can be determined.

Another important issue that has not been dealt with so far, is the problem of material inhomogeneities on the lateral scale, which are predominant in thin-film semiconductors. For this reason, the simulations are generalized to higher dimensions in the last section 5.4, and the effect of inhomogeneous charge carrier lifetimes, doping densities, band gaps, and excitations are studied in order to specify the limits of the one-dimensional simulations.

5.1 General considerations on the TRL decay

At first, the time-resolved luminescence decay has been studied in general by combination of simulations and analytical calculations for a steady state excitation in [Mai1] and for a pulsed excitation in [Mai2]. In doing so, charge carrier diffusion, charge carrier drift, surface recombination, bulk recombination, and photon recycling have been investigated. For these effects, an impact on the charge carrier density (and thus on the luminescence intensity) is expected, which is expressed by the continuity equation. First, photon recycling has been studied. This is an artificial effect since it obscures the real charge carrier kinetics. It mostly occurs in luminescent materials due to their high absorptivity, for which reason photon recycling may become very important for TRL experiments. A proof of this strong influence of reabsorption on the TRL decay has been obtained by Ahrenkiel et al. by means of theoretical calculations combined with experimental TRL on GaAs [20]. Because of the similar absorptivity of CIGSe and GaAs, such strong impact of photon recycling on TRL is also expected for thin-film semiconductors. However, according to the results in ref. [Mai1], photon recycling in CIGSe should be negligible due to the following reasons:

- The spectrum of the luminescence reveals peak energies below the energy band gap [11]. For these energies the absorption coefficient is small [Mai10], which makes reabsorption improbable.

- Photon recycling bends TRL decay curves during the homogenization of charge carriers. The time for homogenization of the charge carriers is close to or even below the time resolution of the experimental setup used in this work. For this reason, bending of luminescence transients due to photon recycling cannot be detected.

- The recombination of charge carriers in thin-film semiconductors is mostly mediated by non-radiative defect recombination. This reduces the photons for reabsorption.

On the basis of these findings, the effect of photon recycling has been omitted throughout the following simulations, which enabled faster simulation times.

In the listing above, surface and bulk-recombination have been adressed. Both govern a luminescence decay which has been studied for a p-doped semiconductor in [Mai1, Mai2]. By doing so, only radiative band-to-band recombination according to equation (2.4.11), and non-radiative defect assisted Shockley-Read-Hall recombination according to equation (2.4.17) have been considered.[19] Following the definition in section 3.1, bulk recombination lifetimes have been deduced for thin-film semiconductors [Mai1, Mai2] that equal the results of Ahrenkiel et al. for III-V semiconductors [20]. The obtained equations revealed an excitation dependence of the recombination lifetimes. For a systematic investigation of the recombination mechanisms, low and high excitation levels therefore had to be distinguished. For a low excitation, the density of majority carriers remains almost unchanged and only the density of minority carriers is substantially changed. Then, the bulk-recombination lifetimes are equal to the TRL decay times. For recombination of charge carriers at surfaces, the related decay time τ_s is not equal to the recombination lifetime, since surface recombination is mediated by the diffusive transport of charge carriers which requires a solution of the whole transport equation. This led to a transcendental eigenvalue equation for τ_s [Mai2], which is equal to that derived by Hooft [54] and Ahrenkiel [55] for GaAs. While Sproul et al. suggest a graphical solution [56], in [Mai2] an approximation by a Laurant series is proposed which yields an algebraic equation for τ_s. In consequence, analytical expressions for the lifetimes of recombination in the bulk and at the surfaces are known and the total decay time under low injection comes out as

$$\tau_{decay} = \left(\frac{1}{\tau_{rad}} + \frac{1}{\tau_{SRH}} + \frac{1}{\tau_s} \right)^{-1} = \tau_{eff,r}. \tag{5.1.1}$$

At this point, a few remarks will be made. First of all, equation (5.1.1) shows that the decay time under low excitation equals the effective recombination lifetime $\tau_{eff,r}$ whose determination from the TRL of the semiconductor thereby becomes straight forward. This allows a deeper investigation of material properties by means of TRL, which is the starting point for this theoretical work. For instance, the surface degradation of a freshly

---

[19]It is always assumed that the deep defect relaxation time δt (see equation (2.4.27)) is smaller than the effective charge carrier lifetimes.

prepared semiconductor that is exposed to air can be investigated. It is expected that the semiconductor surface then becomes more defective as the time passes. Consequently, τ_s should decrease and the decay time should decline by time in accordance to equation (5.1.1) and figure 5.1 (a). This has been revealed for a CIGSe layer by Metzger et al. [17] whose results are given in Fig. 5.1 (d). Further he found that the decline of the decay time due to the surface degradation is attended by a decrease of the solar cell parameters. Here, the solar cell parameters are the short-circuit current density J_{sc} and the open-circuit voltage V_{oc}. For both holds [16]

$$\frac{\mathrm{d}V_{oc}}{\mathrm{d}\tau_{eff,r}} > 0 \qquad \text{and} \qquad \frac{\mathrm{d}J_{sc}}{\mathrm{d}\tau_{eff,r}} > 0. \tag{5.1.2}$$

Accordingly, the efficiency of the cell increases with increasing effective recombination lifetime. Taking equation (5.1.1) into account this means that absorbers with larger decay times will also yield solar cells with higher efficiencies. In other words, the decay time and the solar cell parameters correlate as it has been numerously confirmed experimentally for thin-film semiconductors such as CdTe [7] and CIGSe [5, 6, 8, 11, 14]. This is the crucial factor for the realization of TRL experiments since they enable a fast characterization of the cell already after the absorber preparation.

But for all that, a differentiation of different recombination mechanisms by low injection TRL is not possible, because there is only one decay time for the various unknowns. To obtain such a discrimination one may use the different excitation dependencies of the recombination lifetimes under high excitations. In ref. [Mai1, Mai2] it has been calculated that the SRH-recombination lifetime increases with excitation as shown schematically in fig. 5.1 (b). In figure 5.1 (e) it is illustrated that this lifetime increase being calculated for thin-film semiconductors is in agreement with experimental findings on AlGaAs [57]. The additional fast decay at the beginning of the decay curve is due to bimolecular recombination. This bimolecular recombination is a term for band-to-band recombination in highly excited semiconductors. In contrast to SRH-recombination, for band-to-band recombination the lifetime declines with increasing excitation [Mai1, Mai2]. Due to this, the luminescence decay becomes curved under high excitations as shown schematically in figure 5.1 (c). This is in agreement with experimental findings on GaAs [23], CZTSe [15], and CIGSe [17, 23, 58], as exemplified in figure 5.1 (f).

By this bimolecular recombination another influence on the TRL decay is mediated - the diffusion of charge carriers as a consequence of the generation profile. Although this diffusion keeps the number of charge carriers constant, it may reduce the luminescence intensity. This is a pecularity of bimolecular recombination for which reason an impact of diffusion requires high excitations. Furthermore, it has been shown in [Mai1, Mai2] that diffusion only affects the TRL decay if the excitation duration is below the homogenization time $\tau_{Diff,car}$. This quantity is defined by that time which the charge carriers
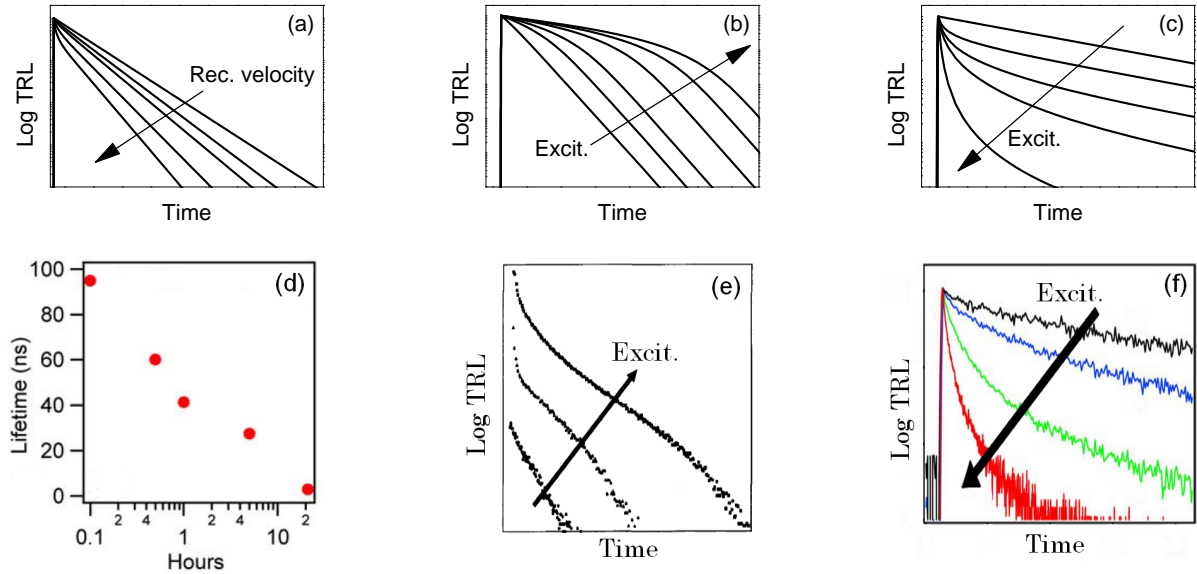
Figure 5.1: (a) Schematic of the increased TRL decay under increasing front surface recombination velocity (b) Schematic of the increased TRL decay time due to deep defect saturation under increasing excitation (c) Schematic of the TRL decay due to bi-molecular recombination under increasing excitation (d) Experimentally observed decrease of the decay time after air exposure of a CIGSe absorber layer [23] (e) Luminescence decay of a AlGaAs layer under increasing excitation [57] (f) Experimental TRL on a CIGSe absorber layer under increasing excitation [23]. The subfigures (d)-(f) have been modified for better visibility.

need after their generation to take on a homogeneous profile. In [Mai2], $\tau_{Diff,car}$ has been calculated from a solution of the transport equation. On the basis of this solution, in [Mai2] also the decay time τ_{Diff} due to diffusion in thin-film semiconductors has been calculated, which again is in agreement with the results of Ahrenkiel for GaAs [20].

The last effect being discussed in [Mai1, Mai2] is the drift of charge carriers in the electric field of a junction, e.g. a solar cell. Electrons and holes thereby become locally separated. In consequence of the absence of recombination partners, the recombination rate is small yielding a more pronounced luminescence decay. This has been already verified by comparison of the TRL of an absorber and a solar cell by experiment for CIGSe [9, 17] and GaAs [59], and by simulation as well for GaAs [24, 59] and CdTe [25]. Apart from the confirmation of these findings especially for CIGSe, in [Mai1, Mai2] also the impact of excitation duration and intensity on the drift effects has been investigated.

In [Mai2] it is shown, that the three decay times of a TRL decay in a solar cell can be assigned to (see fig. 5.2 (a)) ① drift in the space charge region ② recombination in the quasi-neutral region, and ③ diffusion across the space charge region. Due to the strong drift, the initial decay time is much smaller than that of the sole absorber. For that reason it does not reflect the recombination in the absorber. Instead, the second decay time being related to recombination in the quasi-neutral region can be used. As there is no electric field, the corresponding decay time ② in fig. 5.2 (a) reveals the effective recombination lifetime of the absorber. In course of the charge separation, electrons are
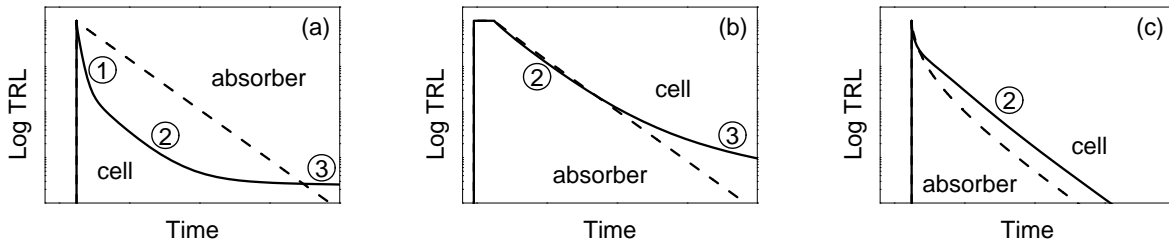
Figure 5.2: Schematic TRL decay of an absorber and a solar cell for (a) a pulsed, low excitation, (b) a steady-state low excitation, and (c) a pulsed, high excitation.

collected in the n-type semiconductor (positive space charge) and holes are collected in the p-type semiconductor (negative space charge), thereby screening the electric field. This enables a diffusive recombination current of charge carriers across the potential barrier. Following the model of Dashdorj [60], this is similar to the leakage current of a capacity. In [Mai1], the time-dependent leakage current and the related luminescence decay have been calculated. It turns out that the decay may become very slow for low excitations as shown by ③ in fig. 5.2 (a).

Both, the charge separation and the discharge of the capacity can be obscured by an extended [Mai1] or by an increased excitation [Mai2]. In case of an extended excitation, the charge separation will be already finished when the excitation is turned off. Then, the TRL will not reveal a fast initial decay as figure 5.2 (b) shows. Furthermore, more charge carriers will accumulate at the boundaries of the space charge region. This reduces the discharge of the capacity (compare ③ in Fig. 5.2 (a) and (b)). In case of an increased excitation, again more charge carriers accumulate leading to an almost completely screened electric field. Consequently, the TRL at high excitations does not exhibit a fast decay being related to drift (Fig. 5.2 (c)). Hence, the decay time increases with increasing excitation in agreement with experimental observations on CIGSe solar cells [17, 58].

In conclusion, in [Mai1, Mai2] the theory of TRL in bulk semiconductors has been transferred to thin-film semiconductors. The deduced analytical expressions for the time-constants are equal for thin-film and bulk semiconductors. The predicted decays are in agreement with experimental observations. For low excitations of a single semiconductor, the TRL is expected to decay mono-exponentially with a decay time being correlated to the solar cell efficiency. In this regard, the experimentally observed non-correlation of the open-circuit voltage and the decay time could not be solved by the simulations. In the first instance, this may be due to a change of the absorber properties during cell preparation. Hence, it appears reasonable to characterize an absorber after the cell preparation. This will be the focus of the next section 5.2.

Theoretical study of time-resolved luminescence in semiconductors. I. Decay from the steady state

Matthias Maiberg[a)] and Roland Scheer
Institute of Physics, Martin-Luther-University Halle-Wittenberg, 06120 Halle, Germany

Time-resolved luminescence (TRL) is a non-destructive, non-invasive, and contactless characterization method. We studied TRL decay on semiconductor layers and thin film homostructures after a steady state illumination by simulation with Synopsys TCAD® and by analytical approximate solution of the appropriate equations. First, we show that the luminescence decay time in general equals the minority carrier lifetime only for a homogeneous and time-independent carrier lifetime. Then, we investigate the influence of photon recycling, injection level, charge carrier diffusion, defects in the bulk and at the surfaces, as well as space charge on the TRL decay separately by quasi one-dimensional simulations of semiconductor layers and semiconductor homostructures. We further study the influence of sample non-homogeneity as may be found in polycrystalline semiconductors. We show how carrier lifetime can be extracted from the TRL transients and how the samples can be characterized by excitation dependent measurements in the open circuit case. We can explain some effects found in luminescence experiments, like a decrease of the decay time with an increasing excitation, a maximum in the decay time due to saturated bulk-defects and curved luminescence transients due to high injections or sample inhomogeneities. Furthermore, we are focussing on the question, how single layers within a semiconductor stack can be characterized. © 2014 AIP Publishing LLC. [http://dx.doi.org/10.1063/1.4896483]

I. INTRODUCTION

Time-resolved luminescence (TRL) can be used to investigate carrier dynamics and recombination processes in semiconductors. In solar cells, it may give access to an important 3rd level parameter, which is the minority carrier lifetime.[1] This parameter is linked to second level parameters such as open circuit voltage V_{OC} and short circuit current J_{SC} and finally to the 1st level parameter being the energy conversion efficiency η of the cell.

There are already many publications about transient luminescence experiments on semiconductor layers and thin film solar cells. It has been revealed that the TRL decay time correlates with the open circuit voltage V_{OC} and the cell efficiency.[2–4] Furthermore, charge separation dynamics was investigated by TRL to show that the absorber bulk of a heterostructure solar cell can be characterized by TRL under high excitation.[5,6] However, there are only a few theoretical approaches to understand experimental TRL decay curves, especially the shape of the transients and their dependence on excitation.[6,7] To fill this gap and to provide a more quantitative theory, we performed quasi one-dimensional simulations of the luminescence decay in combination with analytical approximate solution of the appropriate equations. In the first part of this series, the sample is illuminated to a steady state until the illumination is turned off instantaneously and the decay of the luminescence signal is observed. Experimentally, this decay from a quasi-steady state is realized in transient cathodoluminescence (CL) measurements.[8] We show, how defect densities in the bulk and at the surfaces

can be studied and how minority carrier lifetimes can be determined. In the second part, we present simulations calculated for a short excitation accounting for short laser pulses in photoluminescence (PL) measurements.

For simulation, we used Synopsys TCAD® which solves the Poisson equation and the continuity equation by finite elements methods (FEM) and finite difference methods (FDM). The absorption and reflection were calculated with the transfer matrix method (TMM). The radiation of luminescence was calculated by RayTracing. Bulk defects were introduced as deep traps and ohmic boundary conditions were used to account for surface defects.[9] The semiconductor $CuIn_{1-x}Ga_xSe_2$ is considered as a working example with material parameters typical for highly efficient solar cells.

II. SEMICONDUCTOR AND EXCITATION PARAMETERS

We simulated the experiment with monochromatic light at room temperature (300 K). The generation profile is exponential with a characteristic length of $1/\alpha$ where the absorption coefficient α is $3.805 \, \mu m^{-1}$. This corresponds to a wavelength of 900 nm in the semiconductor $CuIn_{0.7}Ga_{0.3}Se_2$ with $E_g = 1.15$ eV where E_g is the bandgap.[10] The mobilities of electrons and holes are assumed to be equal and set to $\mu_n = \mu_p = 20 \, cm^2 \, V^{-1} \, s^{-1}$. The value of the material parameter B describing the radiative recombination was set to $1.67 \times 10^{-10} \, cm^3 \, s^{-1}$.[10] The doping of the semiconductor is p-type with an acceptor concentration $N_A = 10^{16} \, cm^{-3}$. The capture cross sections of deep defects were set to be $\sigma_n = 10^{-13} \, cm \, s^{-1}$ for electrons and $\sigma_p = 10^{-15} \, cm \, s^{-1}$ for holes if not stated otherwise.[10] The thickness of the semiconductor slab was chosen to be $3 \, \mu m$. Except for distinct cases, the

a)matthias.maiberg@physik.uni-halle.de

surfaces of the semiconductor were passivated leading to equal electron and hole surface recombination velocities of $0\,\mathrm{cm\ s^{-1}}$. If photon recycling was included, the probability of reabsorption of an emitted ray crossing a finite element of the semiconductor layer was 0.2.

Finally, a process i which effects a recombination of a carrier density Δn with the rate R_i can be described by $\tau_i = \frac{\Delta n}{R_i}$, where τ_i is the lifetime of the recombination process. However, the decay time τ of the luminescence signal is defined by $I(t_0 + \tau) = I(t_0)/\mathrm{e}$ for an arbitrary chosen t_0. In the following, if not stated otherwise, t_0 will be equal to zero. Both τ_i and τ need not to be constant in time, for instance if the decay is multi-exponential. At last, we define the lifetime τ_n of an excess carrier density Δn by $\Delta n(t = \tau_n) = \Delta n(t = 0)/\mathrm{e}$.

III. THE IDEAL CASE

First, we deduce mathematically necessary conditions for the direct extraction of the carrier lifetime from TRL decay measurements. We use the model of Ahrenkiel[7] and extend it by photon recycling. We start with the continuity equation for electrons

$$\frac{\partial}{\partial t} n + \mathrm{div}\Gamma_n = G_{\mathrm{ext}} + G_{\mathrm{PR}} - R_{\mathrm{rad}} - R_{\mathrm{nrad}}. \quad (1)$$

Here, n is the electron density, Γ_n is the electron current density, G_{ext} is the generation due to external illumination, G_{PR} is the generation due to photon recycling, R_{rad} is the radiative net-recombination, and R_{nrad} is the non-radiative net-recombination. All quantities first depend on time t and position $\mathbf{r}$. In experiments often a transient excitation is used, which means the generation function becomes

$$G_{\mathrm{ext}}(t, \mathbf{r}) = \begin{cases} >0 & \text{for} \quad t < 0 \\ =0 & \text{for} \quad t \geq 0 \end{cases}, \quad (2)$$

and the excess electron density $\Delta n(t = 0, \mathbf{r})$ turns out to be greater than 0. Accordingly, for $t > 0$ Δn fulfills the equation

$$\frac{\partial}{\partial t} \Delta n + \mathrm{div}\Gamma_n = G_{\mathrm{PR}} - R_{\mathrm{rad}} - R_{\mathrm{nrad}}. \quad (3)$$

Integration of (3) over the volume V of the sample (including its surfaces) and requiring no carrier flux out of the specimen leads to

$$\int_V (R_{\mathrm{rad}} - G_{\mathrm{PR}})\mathrm{d}\mathbf{r} = -\int_V \left(\frac{\partial}{\partial t} \Delta n + R_{\mathrm{nrad}}\right)\mathrm{d}\mathbf{r}. \quad (4)$$

The left-hand side equals the number of luminescence-photons emitted per time $I(t)$. The right-hand side can be transformed using the lifetimes $\tau_{\mathrm{rad}} = \frac{\Delta n}{R_{\mathrm{rad}}}$ and $\tau_{\mathrm{nrad}} = \frac{\Delta n}{R_{\mathrm{nrad}}}$ of radiative and non-radiative recombination, respectively. In general, τ_{rad} and τ_{nrad} depend on time and position. Evaluation of (4) leads to

$$I(t) = -\int_V \left(\frac{\partial}{\partial t} \Delta n + \frac{\Delta n}{\tau_{\mathrm{nrad}}}\right)\mathrm{d}\mathbf{r}. \quad (5)$$

Up to now, we have only assumed that the sample is isolated that means $\int_{\partial V} \Gamma_n \mathrm{d}\mathbf{S} = 0$, where $\mathbf{S}$ is a surface element. Apart

from this, there are no restrictions concerning internal currents.

Without loss of generality the decay of the excess carrier density can be written by $\Delta n(t, \mathbf{r}) = \Delta n(0, \mathbf{r})\,\mathrm{e}^{-\frac{t}{\tau_n(t, \mathbf{r})}}$ for $t \geq 0$. Inserting this into (5) reveals

$$I(t) = \int_V \left(\frac{1}{\tau_n} - \frac{1}{\tau_{\mathrm{nrad}}}\right)\mathrm{e}^{-\frac{t}{\tau_n}} \Delta n(0, \mathbf{r})\mathrm{d}\mathbf{r}$$
$$-t \int_V \frac{\frac{\partial}{\partial t}\tau_n}{\tau_n^2} \mathrm{e}^{-\frac{t}{\tau_n}} \Delta n(0, \mathbf{r})\mathrm{d}\mathbf{r}. \quad (6)$$

From Eq. (6), it becomes clear that in general the transient evolution of Δn and I is different leading to distinct decay times, $\tau_n \neq \tau$. For example, if the lifetime is homogeneous and time-dependent, it follows from Eq. (6)

$$I(t) = \left(\frac{1}{\tau_n} - \frac{1}{\tau_{\mathrm{nrad}}} - t\frac{\frac{\partial}{\partial t}\tau_n}{\tau_n^2}\right)\mathrm{e}^{-\frac{t}{\tau_n}}\int_V \Delta n(0, \mathbf{r})\mathrm{d}\mathbf{r}. \quad (7)$$

Then, the decays of $I(t)$ and Δn are only identical for $\tau_n(t) \propto \frac{1}{\log t}$.

Concerning the special case of a time and space independent lifetime τ_n Eq. (6) can be simplified to

$$I(t) = \left(\frac{1}{\tau_n} - \frac{1}{\tau_{\mathrm{nrad}}}\right)\mathrm{e}^{-\frac{t}{\tau_n}}\int_V \Delta n(0, \mathbf{r})\mathrm{d}\mathbf{r}. \quad (8)$$

Equation (8) shows that in this particular case the decays of the minority carrier density and the luminescence are equal. As will be shown later, a time and position independent carrier lifetime can be realized in a homogeneous semiconductor layer under low excitation conditions. For further evaluation of (8) photon recycling has to be modeled: The number of reabsorbed photons is assumed to be proportional to the number of spontaneously emitted photons, hence $G_{\mathrm{PR}} \approx \alpha R_{\mathrm{rad}}$ with $0 \leq \alpha < 1$ can be assumed. In fact, this is an approximation, because the photons are not reabsorbed instantaneously, thus in an exact theory the photon-rate-equation must be used.[11] The carrier lifetime then reads

$$\frac{1}{\tau_n} = \frac{1}{\tau_{\mathrm{nrad}}} + \frac{1 - \alpha}{\tau_{\mathrm{rad}}}. \quad (9)$$

Inserting (9) into (8) finally leads to

$$I(t) = \frac{1 - \alpha}{\tau_{\mathrm{rad}}} \mathrm{e}^{-\frac{t}{\tau_n}}\int_V \Delta n(0, \mathbf{r})\mathrm{d}\mathbf{r}. \quad (10)$$

Equation (10) shows that the luminescence decay time τ equals the carrier lifetime τ_n if the sample is isolated and if the carrier lifetime is homogeneous and time-independent. Furthermore, (9) shows that the influence of photon recycling on the carrier lifetime becomes smaller if there is non-radiative recombination.

IV. ISOLATION OF EFFECTS

Luminescence decay may not only reflect the carrier lifetime but also may be influenced by other effects, e.g.,

photon reabsorption, diffusion of charge carriers and space charges. In the following, we treat these effects separately.

A. Photon recycling

As was explained at the beginning, reabsorption of photons can decrease the luminescence-intensity and increase the decay time. Photon recycling according to our simulations only plays a role if the excitation is lower than used in this study (see Figure 2). This can be explained with the spatial exponential profile of the excess carrier density into the sample as a consequence of the inhomogeneous generation. Therefore, most of the luminescence-photons are generated near the surface of the semiconductor and they can be directly emitted without reabsorption. Increasing the excitation increases the absolute difference of photons generated near the surface and deep in the bulk. Hence, an increasing part of photons can be emitted without reabsorption and the effect of photon recycling vanishes.

If non-radiative recombination takes place the number of luminescence-photons decreases, thus further reducing reabsorption and photon recycling. Hence, in the following, we neglect photon recycling in our simulations.

B. Dependence on excitation intensity

First, we excited a homogenous semiconductor layer homogenously with different generation rates. The semiconductor layer was ideal, meaning there were no defects at the surfaces or in the bulk and there was no current flowing out of the sample. Figure 1 shows calculated TRL transients. It is obvious that the luminescence-signal falls off exponentially in case of low excitations and non-exponentially for short times and high excitations. The reason is the increasing contribution of the parabolic term to the radiative net-recombination

$$R_{\mathrm{rad}} = \underbrace{B\,(n_0 + p_0)\,\Delta n}_{\text{low excitation}} + \underbrace{B\,\Delta n^2}_{\text{high excitation}}, \qquad (11)$$

where B is a constant and n_0 and p_0 are the equilibrium electron- and hole-densities, respectively. If the excitation
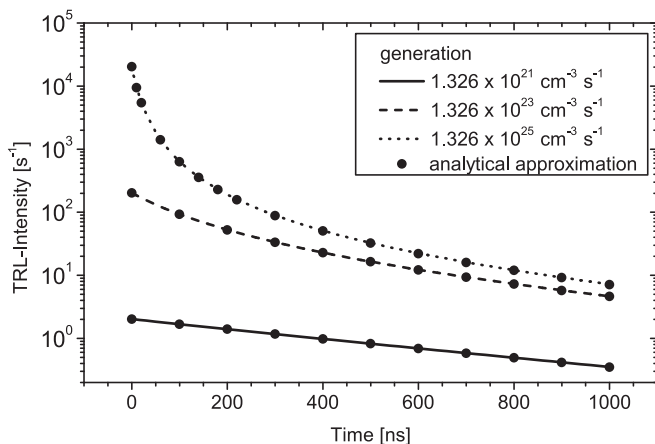
FIG. 1. TRL-transients of a homogeneous and homogeneously excited semiconductor slab without defects for different generation rates G. Analytical approximation after Eq. (12).

increases, not only the number of electrons but also the number of holes increases. For $\Delta p \geq p_0$, there is a transition from monomolecular to bimolecular recombination, which leads to a decrease in the decay time. This is called the high-injection case in the following.

Solving the continuity Eq. (3) leads to

$$\Delta n(t) = \frac{(n_0 + p_0)\,\Delta n(0)}{\left(\Delta n(0) + n_0 + p_0\right) e^{B\,(n_0 + p_0)\,t} - \Delta n(0)}, \qquad (12)$$

and with

$$I(t) = \int_V R_{\mathrm{rad}}(t,\,\mathbf{r})\,\mathrm{d}\mathbf{r}, \qquad (13)$$

it holds

$$I(t) \sim \frac{e^{B\,(n_0 + p_0)\,t}}{\left(\Delta n(0) - \left(\Delta n(0) + n_0 + p_0\right) e^{B\,(n_0 + p_0)\,t}\right)^2}. \qquad (14)$$

With (14) the transients can be described very well, as shown in Figure 1. The exponential luminescence decay comes out as

$$I(t) \sim e^{-B\,(n_0 + p_0)\,t}, \qquad (15)$$

for $\Delta n(0) \ll n_0 + p_0$. The non-exponential decay in case of high excitation becomes apparent for $\Delta n(0) \gg n_0 + p_0$

$$I(t) \sim \frac{1}{\sinh\!\left(\frac{1}{2}\,B\,(n_0 + p_0)\,t\right)^2}. \qquad (16)$$

It can be seen that the decay time for low injection $\tau = \frac{1}{B\,(n_0 + p_0)} = \tau_{\mathrm{rad}}$ is excitation-independent. This further proves the equality of the decay time and the carrier lifetime for low injection levels.

C. Excitation profile

Next, we show that diffusion of charge carriers due to an inhomogeneous generation profile does not influence the luminescence-decay in case of a homogeneous absorber layer. To this end, we illuminated only one side of the layer with different intensities. The calculated transients are shown in Figure 2. The intensity decay qualitatively has the same form as in the case of a homogeneous generation since we start from a stationary state. If the mobilities are large, then most of the inhomogeneities of charge carriers are already vanished due to diffusion at the time the excitation is turned off. The diffusion currents are small because of the small gradients in the carrier densities. However, if the mobilities are small, then the grade of inhomogeneity is larger, but diffusion is still inhibited due to the reduced mobility. Altogether, diffusion currents are small for a wide range of carrier mobility values above $0.01\ \mathrm{cm^2\,V^{-1}\,s^{-1}}$. That means, the full homogenization of excess minority carriers due to diffusion runs on a much longer timescale than the recombination of the carriers.

Now, we assume that the inhomogeneous minority excess carrier density after an inhomogeneous excitation is
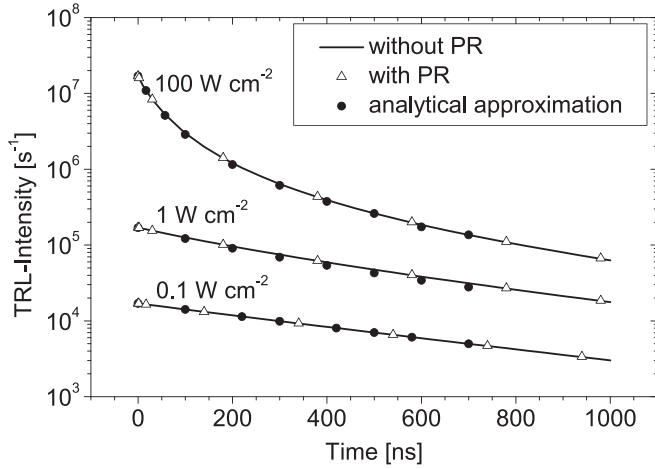
FIG. 2. Simulated and approximated luminescence-transients of an inhomogenously excited semiconductor layer without defects for different injection levels with and without photon recycling. Analytical approximation after Eq. (17).

known and denoted by $\Delta n(0, \mathbf{r})$. The function $\Delta n(0, \mathbf{r})$ can be calculated by solving the inhomogeneous, time-independent diffusion equation numerically, e.g., with direct methods of variational calculus. According to the considerations above, we neglect the diffusion current. Then, Eq. (12) can be adapted,

$$\Delta n(t, \mathbf{r}) = \frac{(n_0 + p_0)\, \Delta n(0, \mathbf{r})}{(\Delta n(0, \mathbf{r}) + n_0 + p_0)\, e^{B\,(n_0+p_0)\,t} - \Delta n(0, \mathbf{r})}.$$

(17)

Calculating the TRL signal with (13) and (17) and comparing with the simulated results (Fig. 2) further proves the assumption of a negligible influence of diffusion on the TRL decay. Hence, the exponential as well as the non-exponential decay can be explained with the mono- and bimolecular recombination in the low and the high injection case, respectively. In consequence provided that diffusion and photon recycling are negligible, CL and PL experiments should give the same carrier lifetime value. The dependence of the shape of the transients on the illumination intensity was already found experimentally.[5]

The fact that diffusion does not influence the luminescence decay is still true for defective absorber layers, as will be shown below. However, for charge separation processes in an internal electric field zone, diffusion and drift of charge carriers play a role (see Sec. IV G).

D. Deep bulk defects

The most relevant application of TRL is the characterization of deep defects in semiconductors. By spatial-resolved measurements local inhomogeneities or especially the spatial density distribution of deep defects can be determined, whereas the resolution is determined by the carrier mobilities.[12] In the following, we show that the density of deep defects can be estimated using different excitation levels. In Figure 3, we calculated two maps showing the influence of excitation density and defect density on the decay time for different defect capture cross sections. First, we
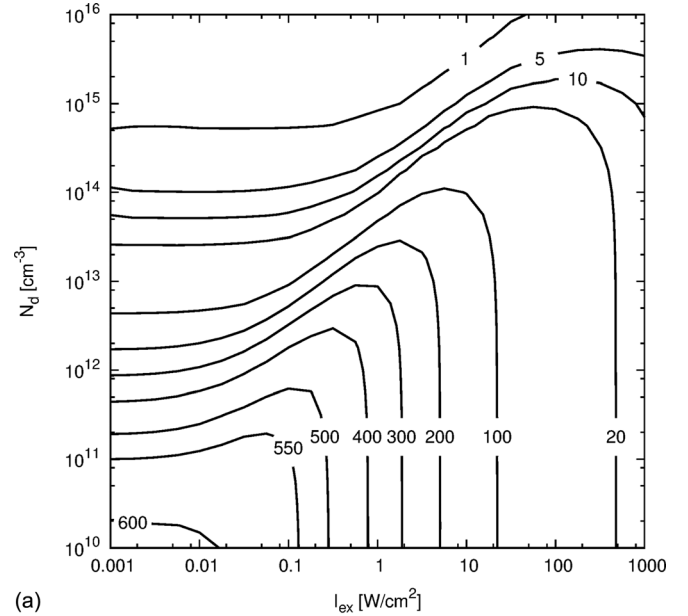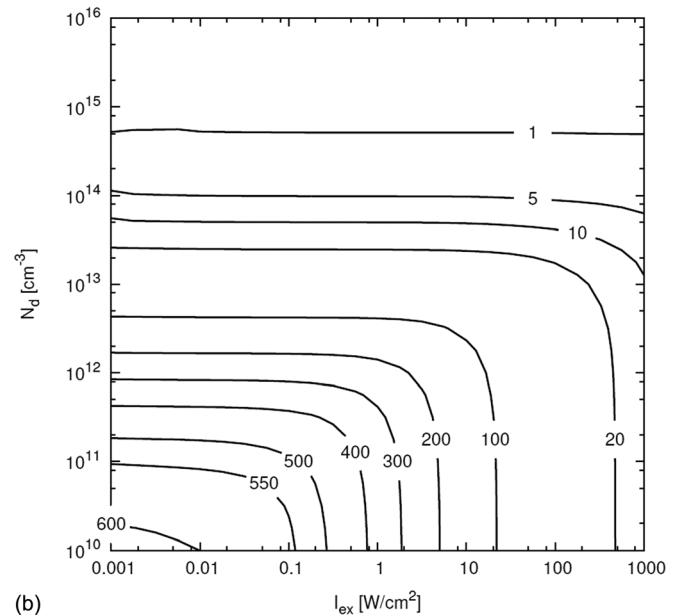
FIG. 3. Contour map of decay times in nanoseconds depending on the excitation, I_{ex}, and the density of deep defects, N_d, in an homogeneous semiconductor slab for capture cross sections $\sigma_p = \sigma_n = 10^{-13}$ cm s^{-1} and $\sigma_p = 100\,\sigma_n = 10^{-13}$ cm s^{-1}.

look at Figure 3(a) (asymmetric capture). Two different effects can be found: With increasing excitation, the decay time initially increases. This is so because the minority excess carrier density increases, depending on the majority carrier lifetime the defects become negatively charged, and the Shockley-Read-Hall recombination (SRH) becomes kinetically inhibited. For exceedingly higher excitation, the decay time again decreases due to bimolecular recombination. Hence, a maximum of the decay time is formed for a certain excitation density. With increasing defect density, this maximum shifts to higher excitation.

Now, we look at Figure 3(b) (symmetric capture). The intersection of the isolines with the coordinate axes is the same as in Figure 3(a), but in contrast no initial increase of

the decay time with increasing excitation can be found, since now also the majority carrier lifetime is quite small. Hence, SRH-recombination does not become inhibited and the decay time stays small. However, the excitation for which bimolecular recombination becomes apparent depends on the defect density.

The well known equation after Shockley, Read, and Hall describing non-radiative recombination reads

$$R_{\mathrm{SRH}} = \frac{n\,p - n_0\,p_0}{\tau_{n0}\,(p + p^*) + \tau_{p0}\,(n + n^*)}. \qquad (18)$$

Here, n^* and p^* are the electron and hole density, if the Fermi-level lies on the defect level. τ_{n0} and τ_{p0} denote the minimal SRH-lifetimes of electrons and holes, respectively. The lifetimes can be rewritten as $\tau_{n0} = 1/N_d\,\sigma_n\,v_n$ and $\tau_{p0} = 1/N_d\,\sigma_p\,v_p$, where N_d is the defect density, σ_n and σ_p are the capture-cross sections, and v_n and v_p are the thermal velocities.

If there is no trapping, it is $\Delta n \approx \Delta p$. Then follows from Eq. (18) for a p-doped semiconductor

$$R_{\mathrm{SRH}}(\Delta n) = \frac{p_0 + \Delta n}{(\tau_{n0} + \tau_{p0})\,\Delta n + \tau_{n0}\,(p_0 + p^*) + \tau_{p0}\,n^*}\,\Delta n$$
$$\Rightarrow \tau_{\mathrm{SRH}}(\Delta n) = \frac{(\tau_{n0} + \tau_{p0})\,\Delta n + \tau_{n0}\,(p_0 + p^*) + \tau_{p0}\,n^*}{p_0 + \Delta n}. \qquad (19)$$

By means of excitation dependent TRL the lifetimes τ_{n0} and τ_{p0} can be estimated by analyzing the TRL transients as shown in the following.

1. Low defect densities

For low excitation $\Delta n \ll p_0/\left(1 + \frac{\tau_{p0}}{\tau_{n0}}\right) < p_0$, it is (see Eqs. (15) and (19))

$$\tau_{\mathrm{SRH}} \approx \tau_{n0}, \quad \tau_{\mathrm{rad}} \approx \frac{1}{B\,p_0}. \qquad (20)$$

Because of (20) there is mathematically the same dependence of R_{SRH} und R_{rad} on Δn. Thus, for low excitations there is still only a single exponential decay. Moreover, the electron lifetime is time-independent that means due to the considerations in III the decay time equals the electron lifetime.

If the excitation increases, the minority lifetime increases, too, because of $\frac{d}{d\Delta n}\tau_{\mathrm{SRH}}(\Delta n) \approx \frac{\tau_{p0}\,p_0}{(p_0 + \Delta n)^2} > 0$. Depending on the value of τ_{p0}, this leads to an initial increase of the decay time (Figure 3(a)) or virtually no increase in the decay time (Figure 3(b)).

If the excitation becomes further increased, the minority carrier density becomes $\Delta n \gg p_0$. Then one finds

$$\tau_{\mathrm{rad}} \approx \frac{1}{B\,\Delta n}, \qquad (21)$$

$$\tau_{\mathrm{SRH}} \approx \tau_{n0} + \tau_{p0} \approx \begin{cases} \tau_{n0} & \text{for } \sigma_n \approx \sigma_p \\ \tau_{p0} & \text{for } \sigma_n \gg \sigma_p \end{cases}. \qquad (22)$$

Comparing the SRH-lifetimes in (20) and (22) it becomes obvious that the SRH-lifetime increases heavily, if it is

$\sigma_n \gg \sigma_p$ and hence $\tau_{p0} \gg \tau_{n0}$. In this case, one finds a distinct rise in the luminescence-decay time (Figure 3(a)). On the contrary, the increase is comparably small if it is $\tau_{p0} \approx \tau_{n0}$ (Figure 3(b)).

From now on the decay time becomes again reduced with increasing excitation, since we are in the high injection case as governed by Eq. (16). Due to Eq. (22), there is an exponential decay for high and due to Eq. (21) a non-exponential decay for very high excitations.

With $\Delta n, p_0 \gg n^*, p^*, n_0, \sigma_n \gg \sigma_p$, and a negligible diffusion current, the continuity equation

$$\frac{d}{dt}\Delta n = -\left(B + \frac{1}{\tau_{p0}\,\Delta n + \tau_{n0}\,p_0}\right)\Delta n\,(p_0 + \Delta n), \qquad (23)$$

has to be solved, where Δn depends on time t and position $\mathbf{r}$. There is no analytical solution. The numerically approximated data calculated by a numerical solution of Eq. (23) are shown in Figure 4.

By distinguishing the low and the high injection case, Eq. (23) can be solved analytically with the approximations (20) and (22). The result reads

$$\Delta n(t,\mathbf{r}) \approx \Delta n(0,\mathbf{r})\,e^{-\left(B\,p_0 + \frac{1}{\tau_{n0}}\right)t}, \qquad (24)$$

for the low injection case $\Delta n \ll p_0/\left(1 + \frac{\tau_{p0}}{\tau_{n0}}\right) < p_0$ and

$$\Delta n(t,\mathbf{r}) \approx \frac{e^{B\,p_0\,t} - e^{\frac{t}{\tau_{p0}}}\,p_0\,\dfrac{1 + B\,\Delta n(0,\mathbf{r})\,\tau_{p0}}{\Delta n(0,\mathbf{r}) + p_0}}{-B\,\tau_{p0}\,e^{B\,p_0\,t} + e^{\frac{t}{\tau_{p0}}}\,\dfrac{1 + B\,\Delta n(0,\mathbf{r})\,\tau_{p0}}{\Delta n(0,\mathbf{r}) + p_0}}, \qquad (25)$$

for the high injection case $\Delta n \gg p_0$.

2. High defect densities

If the density of defects is above $10^{14}\,\mathrm{cm^{-3}}$, the TRL decay time is very small and increases only for very high excitations as shown in Figure 5. The SRH-recombination
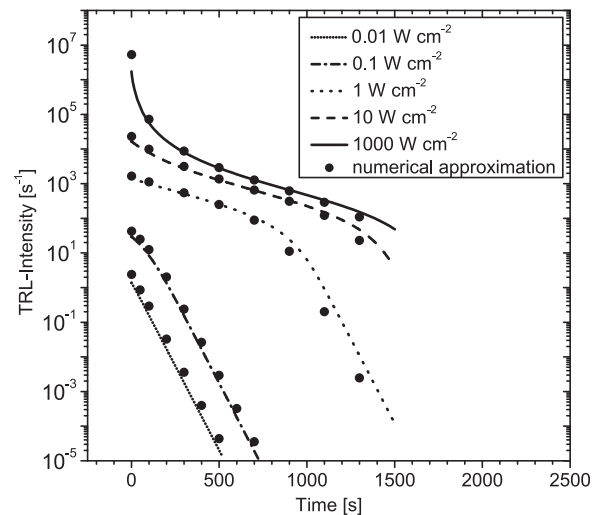

FIG. 4. Simulated and approximated TRL-transients of a semiconductor layer with a bulk defect density of $10^{13}\,\mathrm{cm^{-3}}$ for different excitations. Depth dependent (exponential) generation function. Numerical approximation after Eq. (23).
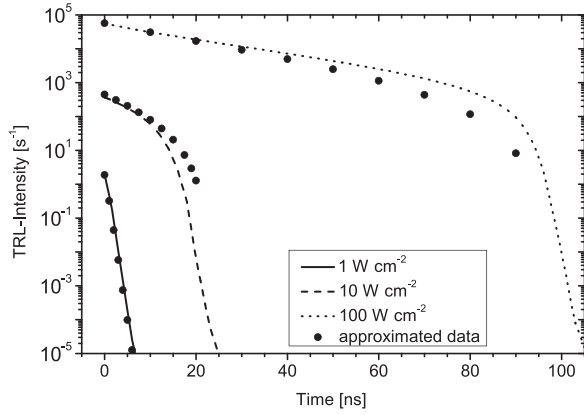
FIG. 5. Simulated and approximated TRL-transients of an absorber layer with a bulk defect density of $10^{15}\,\mathrm{cm}^{-3}$ for different excitations. Depth dependent (exponential) generation. Numerical approximation after Eq. (23).

dominates for low excitations, so (20) is still valid and there is only a single exponential decay with a small decay time.

If the excitation increases, SRH-recombination saturates and the decay time increases and becomes limited by $\tau_{n0} + \tau_{p0}$. After a certain time, the excess minority carrier density is reduced, and the defects are not saturated anymore. Then, the TRL intensity decays with a second (much smaller) decay time τ_{n0} and a multi-exponential decay can be found. The SRH-lifetime can be determined by TRL for low injection levels and small observation times.

In the case of high defect densities, the TRL transients can again be approximated by a numerical solution of the continuity equation neglecting the diffusion current. However, an analytical approximate solution is not reasonable, since in this case the assumptions above make only sense for a small time range.

E. Specimen non-homogeneity

In many experiments it was found that the luminescence decays non-exponentially.[13–15] Especially in polycrystalline materials there are multiple grains, each contributing another decay time to the TRL signal due to varying defect densities. In the following, we give a short illustration, how the distribution of lifetimes can be determined. We further investigate how different distributions perturb a single-exponential decay.

Assume a measured TRL intensity $I(t)$. This can be represented by a Laplacian transformation[13]

$$I(t) = \int_0^\infty H(k)\, e^{-kt}\mathrm{d}k. \tag{26}$$

By the transformation $k = \tau^{-1}$, Eq. (26) leads to

$$I(t) = I_0 \int_0^\infty f(\tau)\, e^{-\frac{t}{\tau}}\mathrm{d}\tau, \tag{27}$$

$$f(\tau) = \frac{1}{I_0\,\tau^2}\, H\left(\frac{1}{\tau}\right), \tag{28}$$

with $I_0 = I(t=0)$. Hence, $I(t)$ can be seen as a sum of transients with a continuous spectrum of decay times and $f(\tau)$ is

the probability density of a certain decay time. By the inverse Laplacian transformation

$$H(k) = \frac{1}{2\,\pi\,i} \int_{-i\infty}^{+i\infty} I(t)\, e^{kt}\mathrm{d}t, \tag{29}$$

the function $H(k)$ can be determined, and by Eq. (28) $f(\tau)$ is determined, too. However, the evaluation of (29) is numerically ill conditioned.[13]

Therefore, in the following we suppose different distributions $f(\tau)$ and calculate the corresponding TRL intensity $I(t)$. In principle, the calculated $f(\tau)$ can be distinct from the spatial distribution of τ, since the charge carriers can diffuse. However, following the considerations in Sec. IV C the diffusion currents shall be small.

1. Gaussian distribution of lifetimes

In the following, we assume a Gaussian distribution of SRH-lifetimes with the average $\bar\tau = \langle\tau\rangle$ and the standard deviation σ_τ:

$$f(\tau) = \frac{1}{\sqrt{2\,\pi}\,\sigma_\tau}\, e^{-\frac{(\tau-\bar\tau)^2}{2\sigma_\tau^2}}. \tag{30}$$

Equation (30) is only meaningful if $\bar\tau \geq 3\,\sigma_\tau$, otherwise also negative decay times would be allowed. In the following the integral:

$$I(t) = \frac{I_0}{\sqrt{2\,\pi}\,\sigma} \int_0^\infty e^{-\frac{(\tau-\bar\tau)^2}{2\sigma^2}}\, e^{-\frac{t}{\tau}}\mathrm{d}\tau, \tag{31}$$

has to be evaluated. This is not possible analytically. Because of the fast decay of f next to $\tau = \bar\tau$, it is sufficient to know $e^{-\frac{t}{\tau}}$ in the vicinity of $\bar\tau$. Hence, $e^{-\frac{t}{\tau}}$ is approximated by a Taylor polynomial of order 4 around $\tau = \bar\tau$. This is inserted into Eq. (31). Considering $\bar\tau > 3\,\sigma_\tau$, the integration can be extended to $\mathbb{R}$, so the odd terms become zero.

By introducing the scaling $t = \bar\tau\,T$ the result reads

$$I(\bar\tau\,T) \approx I_0\, e^{-T} \left(1 + \frac{T\,(T-2)}{2}\left(\frac{\sigma_\tau}{\bar\tau}\right)^2 \right.$$
$$\left. + \frac{T\,(T^3 - 12T^2 + 36\,T - 24)}{8}\left(\frac{\sigma_\tau}{\bar\tau}\right)^4\right). \tag{32}$$

From Eq. (32), it can be seen that the deviation of $I(t)$ from a single exponential decay depends on the powers of $\frac{\sigma_\tau}{\bar\tau}$. Hence, for $3\,\sigma_\tau < \bar\tau$, the perturbance is very small. Therefore, a Gaussian distribution of SRH-lifetimes cannot explain a strong non-exponential decay.

2. Equal distribution of lifetimes

Now, we assume an equal distribution of decay times

$$f(\tau) = \begin{cases} \dfrac{1}{\tau_2 - \tau_1}, & \tau_1 \leq \tau \leq \tau_2 \\ 0, & \text{elsewhere.} \end{cases} \tag{33}$$

The decay times τ_1 and τ_2 can be expressed by

$$\tau_1 = \bar{\tau} - \sqrt{3}\,\sigma_\tau \quad \tau_2 = \bar{\tau} + \sqrt{3}\,\sigma_\tau, \tag{34}$$

where $\bar{\tau}$ and σ_τ are the average and the standard deviation, respectively. Since the decay times have to be positive $\bar{\tau} \geq \sqrt{3}\,\sigma_\tau$ must be fulfilled. Again the integral (27) has to be evaluated. $e^{-\frac{t}{\tau}}$ is approximated by a Taylor polynomial of order 4 in the vicinity of $\bar{\tau}$. Then it follows with $t = \bar{\tau}\,T$:

$$I(\bar{\tau}\,T) \approx I_0\,e^{-T}\left(1 + \frac{T(T-2)}{2}\left(\frac{\sigma_\tau}{\bar{\tau}}\right)^2 \right.$$
$$\left. + \frac{3\,T(T^3 - 12T^2 + 36T - 24)}{40}\left(\frac{\sigma_\tau}{\bar{\tau}}\right)^4\right). \tag{35}$$

Again the perturbation depends on the powers of $\frac{\sigma_\tau}{\bar{\tau}}$. Since it is $\sqrt{3}\,\sigma_\tau \leq \bar{\tau}$ the perturbation is small, so an equal distribution of decay times has only a little impact on the single-exponential decay.

3. Equal distribution of defect densities

Now, we investigate the case that the decay times comply with a Pareto distribution

$$f(\tau) = \frac{\tau_1\,\tau_2}{\tau_1 + \tau_2}\frac{1}{\tau^2}, \quad \tau_1 \leq \tau \leq \tau_2. \tag{36}$$

This is valid, if the density of deep defects N_d complies with an equal distribution and so the probability density distribution of $\tau_{n0} = (\sigma_n\,v_n\,N_d)^{-1}$ follows (36). The integral (27) can be evaluated analytically. It holds

$$I(t) = I_0\,\frac{\tau_1\,\tau_2}{\tau_1 - \tau_2}\frac{e^{-\frac{t}{\tau_1}} - e^{-\frac{t}{\tau_2}}}{t}. \tag{37}$$

By the curvature of $I(t)$ for small times the variation of SRH-lifetimes can be determined.

4. Gaussian distribution of defect densities

Finally, we consider the case that the defect densities comply with a Gaussian distribution with average μ_d and standard deviation σ_d. Then, one finds by transformation

$$f(\tau) = \frac{1}{\sqrt{2\pi}\,\sigma_d\,\sigma_n\,v_n\,\tau^2}\,e^{-\frac{\left(\frac{1}{\sigma_n v_n \tau} - \mu_d\right)^2}{2\sigma_d^2}}. \tag{38}$$

Evaluating the integral in (27) leads to

$$I(t) = I_0\,e^{-\mu_d\,\sigma_n\,v_n\,t}\,e^{\frac{1}{2}\sigma_d^2\,\sigma_n^2\,v_n^2\,t^2}. \tag{39}$$

It can be seen that the decay is non-exponential, if σ_d is large. This is the case, if the distribution of defects is broad.

The above calculations show that common distributions of lifetimes cannot explain curved luminescence decay, since the spectra are not broad enough. It is a variation in the defect density that causes a curved luminescence decay. Because of the reciprocity $\tau_{n0} = (\sigma_n\,v_n\,N_d)^{-1}$, small variations in N_d are sufficient to cause a large variation of τ_{n0} and hence a curved decay.

F. Dependence on surface defects

In the following, we show the influence of deep defects at the contacts or surfaces of a semiconductor slab. Assume that we have $S_{n0} = S_{p0} = S$. Then, the surface SRH-recombination rate becomes[12]

$$R_{s,\mathrm{SRH}} = S\,\Delta n_s\,\frac{p_0 + \Delta n_s}{p_0 + 2\,\Delta n_s}, \tag{40}$$

where the subscript s denotes the value at the surface. Due to surface recombination, the excess minority carrier density is locally reduced and $\Delta n_s \ll p_0$ is fulfilled even for high illumination intensities up to $10\,\mathrm{W\,cm^{-2}}$. Therefore, Eq. (40) leads to

$$R_{s,\mathrm{SRH}} = S\,\Delta n_s. \tag{41}$$

From Eq. (41), it follows an excitation independent sSRH-lifetime, so no saturation effects can be found. Furthermore, it follows the boundary condition

$$\mathbf{j}_{n,s}\,\mathbf{n} = e_0\,S_n\,\Delta n_s, \tag{42}$$

where $\mathbf{n}$ is the inner surface vector. The carriers for recombination at the surfaces are collected from all sample depths. Assuming that the depth dependent collection probability is constant, which is the case for not too small carrier mobilities, than the surface SRH-recombination (41) can be transformed into a bulk-recombination rate

$$\tilde{R}_{\mathrm{sSRH}} = \frac{S}{d}\,\Delta n_s, \tag{43}$$

where d denotes the thickness of the sample. The carrier densities are reduced only near the surfaces. One can estimate $\Delta n \approx \left(1 + \frac{2dS}{5D_n}\right)\Delta n_s$ by solving the continuity equation for a homogeneous generation. Thereby, Eq. (43) leads to

$$\tilde{R}_{\mathrm{sSRH}} = \frac{S}{d\left(1 + \frac{2dS}{5D_n}\right)}\,\Delta n. \tag{44}$$

Therefore, one finds the sSRH-lifetime

$$\frac{1}{\tau_{\mathrm{sSRH}}} = \frac{S_f}{d\left(1 + \frac{2dS_f}{5D_n}\right)} + \frac{S_b}{d\left(1 + \frac{2dS_b}{5D_n}\right)}, \tag{45}$$

where the subscripts f and b denote the recombination at the front and the back side, respectively. Equation (45) shows that for $S_{b/f} \gtrsim 10^5\,\mathrm{cm\,s^{-1}}$ the sSRH-lifetime becomes saturated, because with the provided mobility value of $20\,\mathrm{cm^2\,V^{-1}\,s^{-1}}$ the transport of the carriers towards the surfaces is limited by diffusion.

Figure 6 shows some simulated TRL-transients of a semiconductor layer including surface recombination using the boundary condition (42), as well as some analytically approximated data after Eq. (44). In this case, there were no defects in the bulk.

It can be seen that surface recombination reduces the decay time. Because of the constant sSRH-lifetime, a high
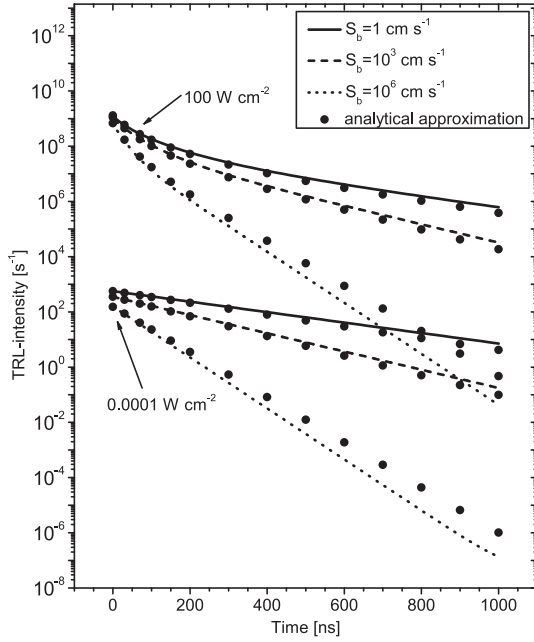
FIG. 6. Simulated and approximated TRL-transients of a semiconductor layer with a recombination velocity $S_f = 10^3$ cm s^{-1} at the front contact and different recombination velocities at the back contact. Analytical approximation after Eq. (44).

injection case can still be found, but no saturation of surface defects. So we state that surface recombination does reduce the decay time, but does not change the shape of the luminescence-transients. This will be shown in Sec. V A.

G. Space charge

Finally, we discuss the impact of space charge or in general the effect of an electric field on the TRL-decay. Space charge can result from junction regions, charged grain boundaries or surfaces. Figure 7 shows TRL-transients calculated for an np-homojunction in the open circuit case with no external current. Here, defects in the bulk or at the surfaces
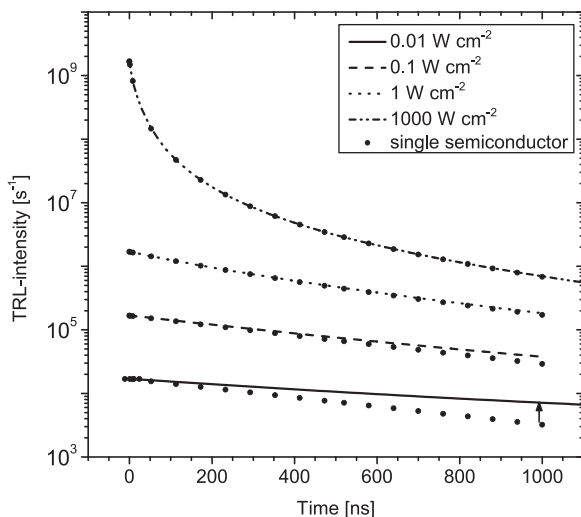
FIG. 7. Simulated TRL-transients of an np homojunction with $N_D = N_A = 10^{16}$ cm^{-3}, $d_p = 2.5$ μm, $d_n = 500$ nm (lines) and of a single semiconductor layer (dots) without surface or bulk-defect recombination.

are initially excluded. For sufficiently low injection, the decay time is large compared to that of a single semiconductor slab. If the excitation increases, the decay time decreases. This is contrary to the behavior found by Metzger et al.[5,6] for pulsed excitation. We consider the low and the high injection case separately.

1. Low injection

For low excitations, the few photogenerated carriers are separated by the electric field and accumulate at the edges of the space charge region (SCR) where they are majorities. When the steady state is reached, we turn off the illumination and start to simulate the TRL-transients. At this time, there are charge carriers in the SCR, which are separated by the electric field within a few 10 ps after the excitation is turned off. Since the lifetime is comparatively long und the number of charge carriers in the SCR is negligible for low injection levels, the transients do not reflect a fast initial decay due to the separation. Hence the largest part of the charge carriers are majorities at the edges of the space charge region and only a few minority carriers are within the SCR or in the quasi-neutral region (QNR) (see Figure 8).

Due to the low excitation, the dark space charge is only partly screened by the accumulated charge carriers and a small open circuit voltage is built up (see Figure 9). Therefore, a small dark diffusion current of majorities flows across the SCR into the QNR, where the carriers become minorities and recombine. Since the open circuit voltage is comparatively small, the diffusion current is small, too. This in turn means that the charge carriers are stored for a long time. Moreover, the recombination and hence the luminescence is determined by the dark diffusion current (Figure 9). This leads to a large decay time of the open circuit voltage and a large decay time of the TRL intensity compared to the case of a bare semiconductor slab (see Figures 8 and 9).

The semiconductor junction can be recognised as a charged capacity and the diffusion current as a leakage current. It is

$$\frac{d|Q|}{dU} = -\sqrt{\frac{e_0\,\varepsilon_0\,\varepsilon_r}{2}\,\frac{N_D\,N_A}{N_D + N_A}}\,\frac{1}{\sqrt{U_D - U}}, \qquad (46)$$

where U_D is the diffusion voltage and Q is the charge per area of unscreened ionized dopants. The charge $d|Q|$
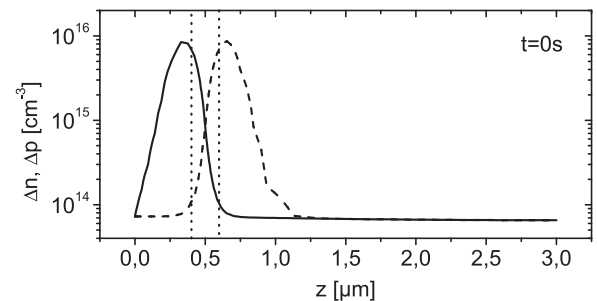

FIG. 8. Excess electron (solid) and hole (dashed) distribution in a CIGS/CIGS-homojunction for an illumination intensity of 0.01 W cm^{-2} immediately after excitation is turned off. The edges of SCR (dotted) are calculated according to the Schottky approximation.

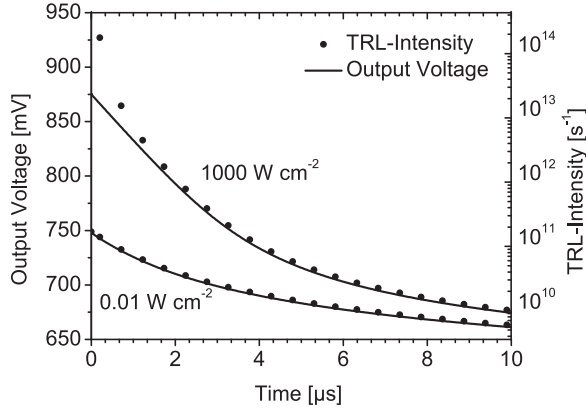FIG. 9. TRL intensity (dots) and transient open circuit voltage (lines) for an illumination intensity of 0.01 W cm^{-2} and 1000 W cm^{-2}.

increases with time due to a diffusion current j of electrons and holes with the saturation current density j_0: $d|Q| = |j| \, dt$. Hence, it is

$$\frac{d}{dt} U(t) = -|j_0| \sqrt{\frac{2}{e_0 \, \varepsilon_0 \, \varepsilon_r} \frac{N_D + N_A}{N_D \, N_A}}$$
$$\times \sqrt{U_D - U(t)} \left(e^{\frac{e_0 U(t)}{kT}} - 1 \right). \qquad (47)$$

As can be seen in Figure 9, it is $U(t) \gg \frac{kT}{e_0}$ for reasonable times. Hence, it is $e^{\frac{e_0 U(t)}{kT}} \gg 1$ and Eq. (47) yields

$$\frac{d}{dt} U(t) = -M \sqrt{U_D - U(t)} \, e^{\frac{e_0 U(t)}{kT}}$$
$$M = |j_0| \sqrt{\frac{2}{e_0 \, \varepsilon_0 \, \varepsilon_r} \frac{N_D + N_A}{N_D \, N_A}}. \qquad (48)$$

The solution of Eq. (48) fulfills the equation

$$\mathrm{erf} \sqrt{\frac{e_0}{kT} (U(t) - U_D)} = i \sqrt{\frac{e_0}{\pi \, kT}} M \, e^{\frac{e_0 U_D}{kT}} \, t$$
$$+ \, \mathrm{erf} \sqrt{\frac{e_0}{kT} (U_0 - U_D)}, \qquad (49)$$

where "erf" denotes the error function. For short times, it is $U(t) \approx U_0$ and further evaluation of Eq. (49) leads to

$$U(t) = -\frac{kT}{e_0} \log \left(e^{-\frac{e_0 U_0}{kT}} + \frac{e_0 M}{kT} \sqrt{U_D - U_0} \, t \right). \qquad (50)$$

Equation (50) describes the decay of the open-circuit voltage. The TRL-signal then is proportional to the radiative recombination which is determined by the diffusion current. Hence, it is

$$I(t) = \frac{A}{e_0} |j(t)| = \frac{|j_0| A}{e_0} \left(e^{-\frac{e_0 U_0}{kT}} + \frac{e_0 M}{kT} \sqrt{U_D - U_0} \, t \right)^{-1}, \qquad (51)$$

where A is the cross section of the sample. It can be seen that the decay time is small if the constant M is large. Looking at the definition (48) this is the case for large saturation current densities $|j_0|$ and small electric fields.

2. High injection

Increasing of the excitation has the following effects: The space charge of ionized dopants becomes further screened, since there are more majority carriers accumulating at the edges of the SCR lowering the diffusion barrier. Now, there is fairly no charge separation and the charge carriers have the same distribution as in a single semiconductor layer (Fig. 10). Hence, bulk recombination and the bulk-lifetime can be observed in the TRL-signal. The recombination is not determined by the dark diffusion current (see Figure 9), which in turn gives rise to a decay that is the same as in the case of a semiconductor slab including high injection effects (Fig. 7). This is in agreement with the findings of Metzger et al.[5,6]

After a certain time all minority carriers in the quasi-neutral regions have been recombined and only the majority carriers stored at the edges of the SCR remain (Fig. 10). Then, recombination is again limited by the diffusion of majority carriers across the SCR (see Figure 9) and TRL is limited by the diffusion current.

3. Influence of mobility

At last, we investigate the influence of the carrier mobility on the TRL-decay of a junction in the low injection case. A lowering of the mobility has two effects:

- A smaller carrier mobility gives rise to a smaller dark saturation current density.
- The open circuit voltage increases due to a lowered dark saturation current (see Fig. 11).

Since it holds $j \approx j_0 \, e^{\frac{e_0 V_{OC}}{kT}}$ for the dark diffusion current a decrease in j_0 is compensated by an increase in V_{OC}. Hence both effects cancel each other and the total dark diffusion current j is nearly unchanged by the mobility. Since the TRL-intensity is determined by the dark diffusion current, the luminescence's transients are unchanged, too (see Fig. 11).

To compare the influence of the mobility on the transient's decay, we varied the illumination intensity such that the initial open circuit voltage is equal for each provided carrier mobility. Again it holds $j \approx j_0 \, e^{\frac{e_0 V_{OC}}{kT}}$ for the dark current, but now V_{OC} is fixed and only j_0 varies. The results are shown in Figure 12. Due to an increase in j_0 with increasing carrier mobility, the decay of the open circuit voltage is faster and in turn the dark current decays faster, too. Because of the limitation of the TRL-intensity by the dark current, the TRL decay time also decreases. Furthermore, the dark current density increases with increasing mobility and fixed open circuit voltage. Therefore the TRL-intensity becomes larger with increasing mobility.

V. COMBINATION OF EFFECTS

A. Bulk and surface defects

More realistic is the case where deep defects are present in the bulk and at the surfaces of a semiconductor layer. We have already mentioned that in this case the dependence of
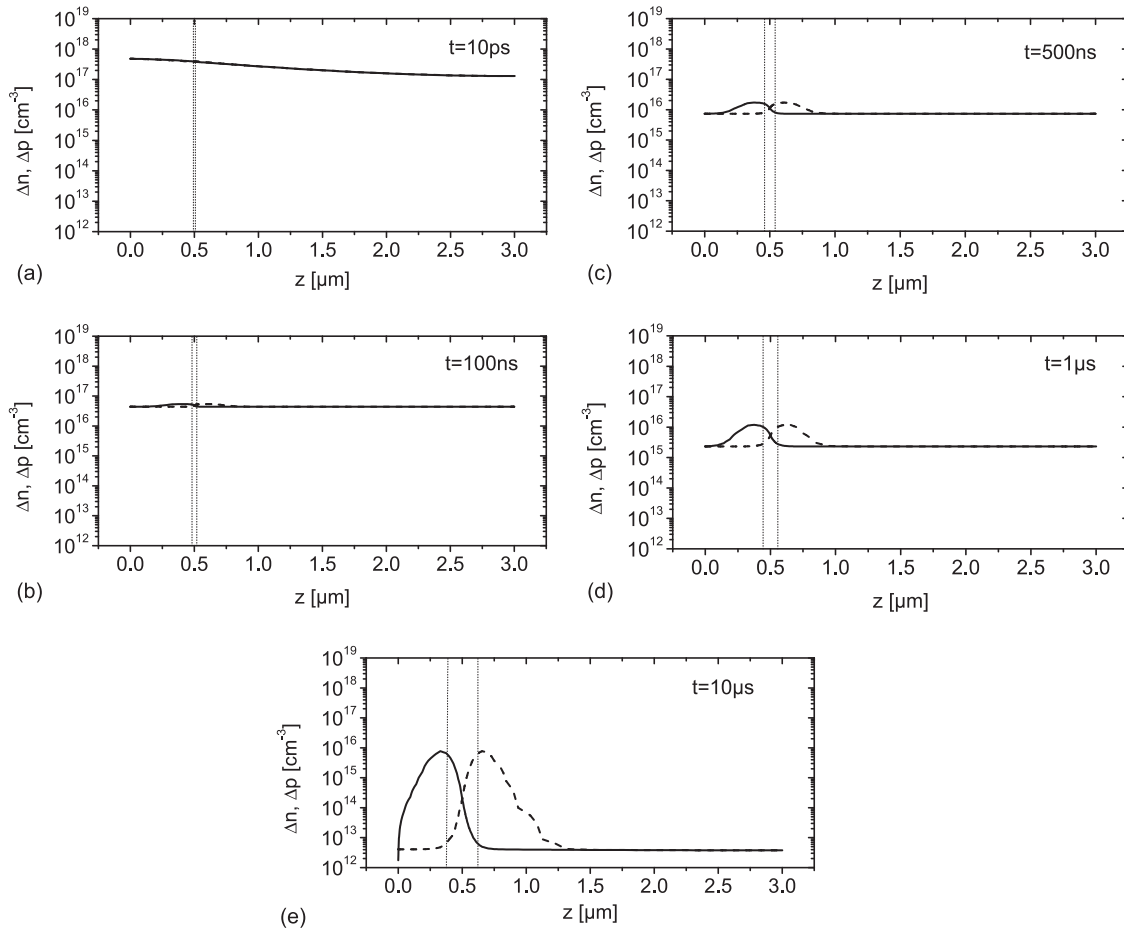
FIG. 10. Excess electron (solid) and hole (dashed) distribution in a CIGS/CIGS-homojunction for an illumination with 1000 W cm^{-2} at different times after excitation. The edges of SCR (dotted) are calculated with Schottky approximation.

the measured decay time on the excitation is similar as in the case without surface recombination. Indeed the maps in Figure 13 show that the trend of the decay time does not change qualitatively with S_f. However, decay time values are systematically reduced (compare also Fig. 3 with $S_f = S_b = 0$). Because of the decrease of the carrier density by surface recombination, the maximum of the decay time at a given defect density is shifted to higher excitations, meaning higher intensities are necessary to reach saturation of

bulk defects and onset of bimolecular recombination. For surface recombination velocities above about 10^5 cm s^{-1} a further increase of S does not affect the decay time anymore, since the transport of charge carriers towards the surfaces is limited by diffusion.

Assuming a certain defect density N_d and excess carrier density Δn, there is a unique relation between the absolute value of the decay time and the surface recombination velocity, since it is
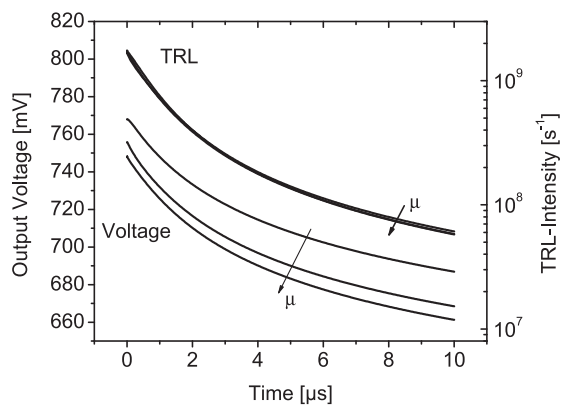
FIG. 11. TRL- and V_{OC}-transients for an illumination intensity of 0.01 W cm^{-2} and for carrier mobilities $\mu = 0.2$ cm^2 V^{-1} s^{-1}, 2 cm^2 V^{-1} s^{-1}, and 20 cm^2 V^{-1} s^{-1}.
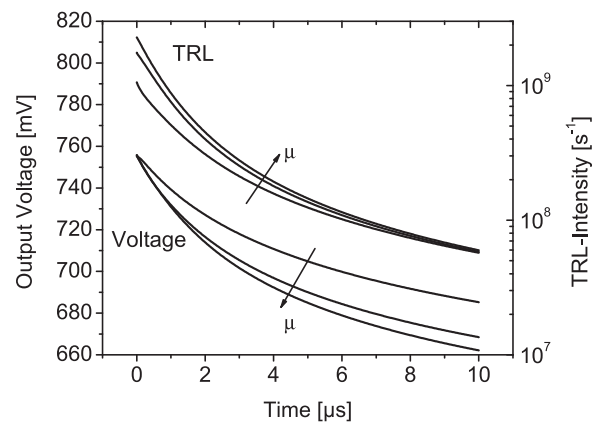
FIG. 12. TRL- and V_{OC}-transients for carrier mobilities 0.2 cm^2 V^{-1} s^{-1}, 2 cm^2 V^{-1} s^{-1}, and 20 cm^2 V^{-1} s^{-1} and varying illumination intensity such that $V_{OC}(t = 0)$ is constant.
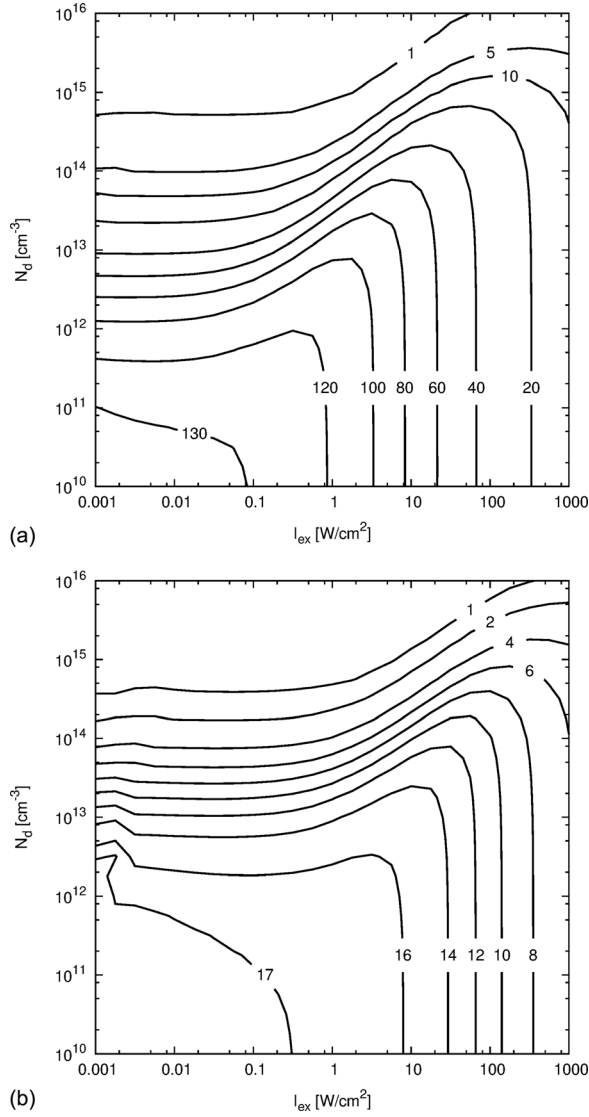
FIG. 13. Dependence of TRL-decay time in nanoseconds on the excitation and the density of deep defects in an homogeneous semiconductor slab for different surface recombination velocities.

$$\frac{1}{\tau(\Delta n)} = \frac{1}{\tau_{\text{SRH}}(\Delta n)} + \frac{1}{\tau_{\text{rad}}(\Delta n)} + \frac{1}{\tau_{\text{sSRH}}(S)}, \quad (52)$$

$$\frac{\text{d}}{\text{d}S}\tau_{\text{sSRH}} \neq 0. \quad (53)$$

If one assumes a certain surface recombination velocity, there is a biunique relation between the excess carrier density Δn_m at the decay time maximum and the defect density, since it follows from $\frac{\text{d}}{\text{d}\Delta n_m}\tau(\Delta n) = 0$

$$\Delta n_m = \frac{-C p_0 \sigma_p + \sigma_n \sqrt{B N_d p_0 \sigma_p v_n}}{C (\sigma_n + \sigma_p)} > 0. \quad (54)$$

Equation (54) also shows that the maximum does only exist for $N_d > \frac{C p_0 \sigma_p}{v_n \sigma_n^2}$, as was already explained. Hence the functions $S(\tau)$ and $N_d(\Delta n_m)$ exist and the values can be determined, if Δn_m is known. This can be determined for example with microwave conductivity.

For higher accuracy, the TRL-decay time can be measured depending on excitation and the parameter values can be calculated by fitting the data with (52).

B. Space charge and bulk defects

In practical terms, we will often have a combination of bulk defects and a space charge region, the latter being either the result of a pn junction or surface band bending. Again, we calculated a map showing the decay time depending on the bulk-defect density and on the excitation intensity. This is displayed in Fig. 14. That the bulk recombination can be observed for high injection levels is still valid. This becomes clear, if Fig. 3 is compared with Fig. 14. In the following, we investigate the dependence of the decay time on excitation for different defect densities separately.

1. Low defect densities $\leq 10^{12}$ cm^{-3}

For low defect densities, the isolines in Fig. 14 are largely parallel to the ordinate. Hence, SRH-recombination does not affect the TRL-signal. For low injection levels, the TRL-signal is determined by the dynamics of the small diffusion current across the space charge region. For high excitation, the excess carrier densities decay from more homogeneous distributions, recombination in the quasi-neutral regions becomes dominant, and is of bimolecular type. Hence, the decay time decreases.

2. Defect densities between 10^{12} cm^{-3} and 10^{14} cm^{-3}

For low injection levels, the diffusion current determines the TRL-signal and the decay time is high. For high excitations, again recombination in the quasi-neutral regions determines the TRL-signal. First, the number of electron-hole-pairs is low and SRH-recombination is dominating. Hence, the decay time is small. If the excitation is further increased, the defects are saturated and the decay time increases. For very high excitations, the bimolecular recombination lowers the TRL-decay time again.
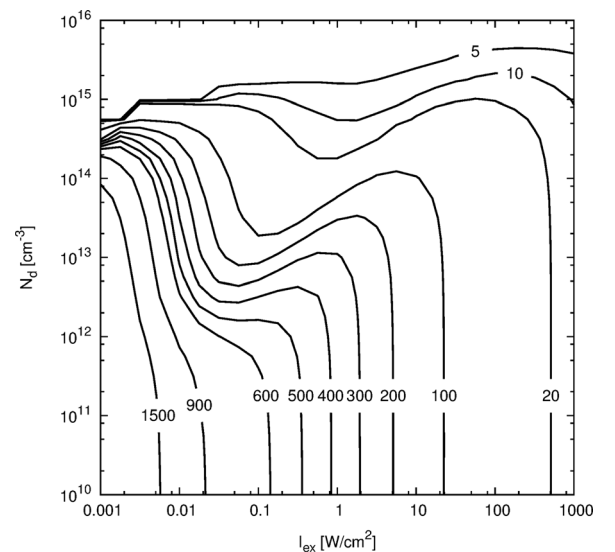
FIG. 14. TRL-decay time in nanoseconds of an np-homojunction with $N_D = N_A = 10^{16}$ cm^{-3}, $d_p = 2.5$ μm, $d_n = 500$ nm depending on excitation intensity I_{ex}, and the density of deep defects N_d.

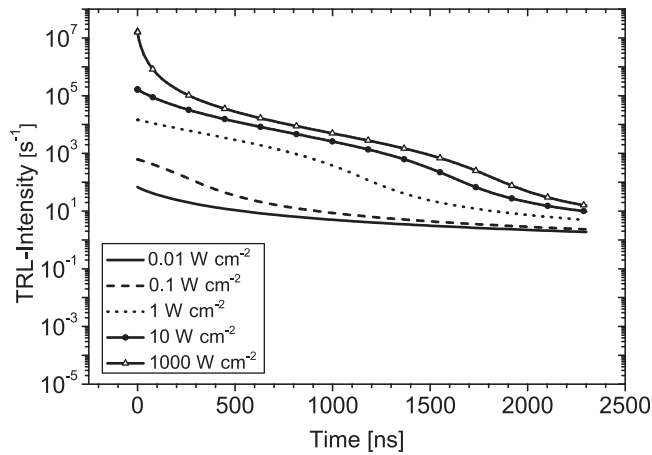FIG. 15. TRL-transients of an np-homojunction with $N_D = N_A = 10^{16}$ cm^{-3}, $d_p = 2.5$ μm, $d_n = 500$ nm, and $N_d = 5 \times 10^{13}$ cm^{-3} for different injection levels.
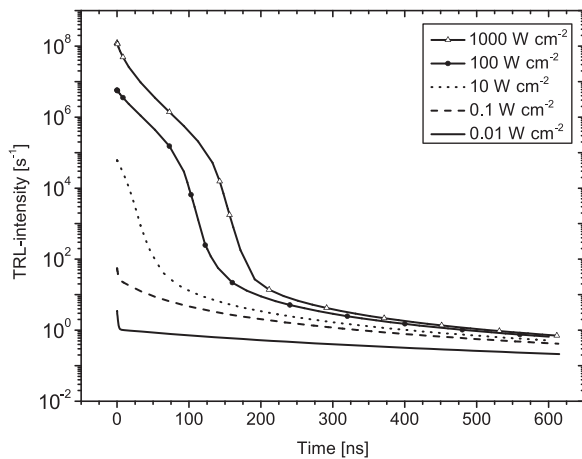
FIG. 16. TRL-transients of an np-homojunction with $N_D = N_A = 10^{16}$ cm^{-3}, $d_p = 2.5$ μm, $d_n = 500$ nm, and $N_d = 10^{15}$ cm^{-3} for different injection levels.

In the case of high excitations and short observation times, the TRL-transients in Fig. 15 have the same shape as the transients in Fig. 4. This reflects the fact that the PL-decay shows the recombination in the quasi-neutral regions.

3. High defect densities $\geq 10^{15}$ cm^{-3}

Some TRL-transients calculated for high defect densities are shown in Fig. 16. As can be seen, there is a fast decay for small times and low injection levels. This causes the very small TRL-decay times shown in the map of Figure 14. The electron-hole-pairs that are in the space charge region at the time the excitation is turned off, recombine before they can be separated. After a short time the space charge region is depleted of mobile charge carriers and the TRL-signal again is determined by the diffusion current.

For high injection levels once more, recombination in the quasi-neutral regions dominates, and because of the large defect density the fast decay of the PL-signal persists.

VI. CONCLUSION AND OUTLOOK

In this study, we could explain the behavior of the TRL transient's shape with varying excitation. We could replicate some experimental findings, as well as findings of other theoretical works.

We have shown that the TRL intensity of an homogeneous semiconductor slab decays non-exponentially for high injection levels due to bimolecular recombination in agreement with Metzger et al.[5] The decay time decreases with increasing excitation. This is still valid if there are deep defects in the bulk or at the surfaces of the layer.

Multi-exponential decays can be explained by parallel radiative and non-radiative recombination processes. Both dominate for a certain range of excess carrier densities. During a TRL decay the number of excess carriers changes and the dominating recombination process changes, too. The transition of recombination processes depends on the density of deep defects. Only if the number of defects is small ($<10^{14}$ cm^{-3}), the defects can be saturated and the SRH recombination can become limited by majority carrier capture. If one has a spatial distribution of defect densities, the TRL decay can also be multi-exponential where we find that the largest deviation from mono-exponential decay arises from a distribution of defect densities.

Further, we could show that the absorber layer of a complete solar cell can be studied under high excitation intensities. Therefore, we could reproduce the work of Metzger et al.[5,6] However, for low excitation we calculated different transients. This can be explained with the different initial state: Under a stationary illumination the dynamics of charge separation is not reflected in the decay curves. This will be different under short laser pulses which are investigated in the second part of this work.

[1] R. K. Ahrenkiel, N. Call, S. W. Johnston, and W. K. Metzger, Sol. Energy Mater. Sol. Cells **94**, 2197–2204 (2010).
[2] S.-I. Shimakawa, K. Kitani, S. Hayashi, T. Satoh, Y. Hashimoto, Y. Takahashi, and T. Negami, Phys. Status Solidi **203**, 2630 (2006).
[3] S. Shirakata and T. Nakada, Thin Solid Films **515**, 6151 (2007).
[4] W. K. Metzger, I. L. Repins, M. Romero, P. Dippo, R. N. Contreras, and D. Levi, Thin Solid Films **517**, 2360–2364 (2009).
[5] W. K. Metzger, I. L. Repins, and M. A. Contreras, Appl. Phys. Lett. **93**, 022110 (2008).
[6] W. K. Metzger, R. K. Ahrenkiel, J. Dashdorj, and D. J. Friedman, Phys. Rev. B **71**, 035301-1–035301-9 (2005).
[7] R. K. Ahrenkiel, Solid-State Electron. **35**, 239 (1992).
[8] I. Yamakawa, M. Ichida, S. V. Sorokin, A. A. Toropov, A. Titkov, S. V. Ivanov, and A. Nakamura, J. Lumin. 87–89, **384** (2000).
[9] Sentaurus Device User Guide, Synopsys®, 2011.
[10] R. Scheer and H.-W. Schock, Chalcogenide Photovoltaics: Physics, Technologies, and Thin Film Devices (Wiley-VCH, 2011).
[11] J. L. Balenzategui and A. Mart, Sol. Energy Mater. Sol. Cells **90**, 1068 (2006).
[12] S. Zott, "Optische Charakterisierung von CuInSe$_2$-Dünnschichten mittels stationärer zeitaufgelöster Photolumineszenz," Ph.D. dissertation, Technische Universität Dresden, 1997.
[13] M. N. Berberan-Santos, E. N. Bodunov, and B. Valeur, Chem. Phys. **315**, 171–182 (2005).
[14] D. C. Johnston, Phys. Rev. B **74**, 184430-1–184430-6 (2006).
[15] R. Chen, J. Lumin. **102–103**, 510–518 (2003).

Theoretical study of time-resolved luminescence in semiconductors. II. Pulsed excitation

Matthias Maiberg[a] and Roland Scheer
Institute of Physics, Martin-Luther-University Halle-Wittenberg, 06120 Halle, Germany

In the second part of this series, we studied TRL decay on semiconductor layers and thin film homostructures after a pulsed excitation by simulation with Synopsys TCAD® and by mathematical approximation. Again, our working example is Cu(In,Ga)Se$_2$. We investigate the influence of the excitation pulse length, axial diffusion, bulk-defects, and defects at the contacts, as well as space charge on the TRL-decay separately by quasi one-dimensional simulations of semiconductor layers and semiconductor homostructures. Material parameters like defect density, carrier mobility, and surface recombination velocity are varied in a wide range, such that the calculations are applicable to other semiconductors. We further study the influence of multi-pulse excitation. We show how material parameters such as carrier lifetime and carrier mobility can be extracted from the TRL transients and how the samples can be characterized by excitation dependent measurements in the open circuit case. We can explain some effects found in luminescence experiments, like an increased decay in semiconductor junctions due to the electric field in the space charge region. However, we also discuss the effect of charge storage which may lead to decreased decay. It is revealed that under high injection conditions single layers within a semiconductor stack can be characterized in terms of carrier lifetime. © *2014 AIP Publishing LLC*. [http://dx.doi.org/10.1063/1.4896484]

I. INTRODUCTION

In the first part of this work, we have investigated the influence of excitation, defects, and space charges on the transient luminescence signal by simulation with Synopsys TCAD®.[1] For systematic reasons, we have chosen a steady state illumination as an initial state. Thereby, we could eliminate the influence of experimental quantities like the excitation pulse length and at the same time could simulate the principle effects in cathodoluminescence decay experiments.[2]

In the second part of this work, we will present results on time-resolved luminescence (TRL) calculated for a pulsed excitation of Cu(In,Ga)Se$_2$ as a working example. This method also known as time-resolved photoluminescence (TRPL) has been used in numerous experimental studies of semiconductors.[3–10] First, we address the comparability of TRL experiments with different pulse properties such as pulse length and intensity. Then, we tie in with the results in the first part of this work and investigate the influence of axial diffusion and defects in semiconductor layers. We show that both can lead to curved TRPL transients, which is often observed in TRPL experiments.[5,6,10] We give an analytic formula that describes bimolecular recombination, axial diffusion, bulk, and surface recombination. These are distinct from those of Ahrenkiel,[11] where bimolecular recombination is not included. Then, we study the different influences of space charges in semiconductor devices. We show that the TRPL decay time can decrease due to charge separation[6] and it can increase as a result of multi-pulse excitation.[3] At the moment, there are already several works concerning simulation of charge separation effects

with focus on the time dependent carrier distribution, for example, in a GaAs-junction[12] and in CdTe solar cells.[13] We also show such simulation complemented with calculations of the photovoltage that builds up for different carrier lifetimes and excitation frequencies.

All our simulations are one-dimensional. However, comparison with TRPL-experiments is possible as long as the experimental focus diameter is much larger than the diffusion length. Additionally, the influence of grain boundaries that are not included in our simulations can be estimated by an effective bulk-lifetime. The one-dimensional simulations reach their limits, if lateral effects cannot be neglected, that is, for inhomogeneous charge carrier lifetimes, band gaps, or charge carrier mobilities. Furthermore, we again neglect the influence of Photon Recycling, since most of the luminescence photons are generated at the front side of the semiconductor and can by directly emitted before reabsorption.

II. PROVIDED QUANTITIES

The main semiconductor parameters have been given in the first part of this series. In the present part II, the time dependent excitation is realized by a time dependent photon flux density $j_\gamma(t)$ incident on the sample (after front surface reflection). $j_\gamma(t)$ fulfills a Gaussian time dependence

$$j_\gamma(t) = \frac{n_\gamma}{\sqrt{\pi}\,\tau_p}\, e^{-\frac{(t-t_0)^2}{\tau_p^2}}, \qquad (1)$$

where t_0 can be an arbitrary time, τ_p is the length of the pulse, and n_γ is the number of photons incident per area per pulse. If not stated otherwise, it is $\tau_p = 100$ fs and $t_0 = 1$ ps.

[a]Electronic mail: matthias.maiberg@physik.uni-halle.de

    116, 123711-1

III. SOME BASIC DEFINITIONS

In order to compare different TRL transients being obtained from experiment or simulation, one has to clarify the impact of different experimental conditions. Most important in this context are different excitation lengths and intensities. We will show that it is necessary to define a unique initial state of excitation. Another aspect of concern is the depth resolution of TRL. We will show how the experimental requirements are related to material parameters such as absorption coefficient and charge carrier mobility.

A. The influence of pulse length

Experimentally, the pulse length today can be varied in a wide range. Since the photon flux follows a Gaussian distribution, most of the charge carriers are generated within the time range $[t_0 - 3\tau_p, t_0 + 3\tau_p]$ (compare Eq. (1)). As t_0 is arbitrary, we set $t_0 = 3\tau_p$ and approximate the pulse start at time $t = 0$ and pulse end at time $t = 6\tau_p$. Assuming no substantial axial diffusion and recombination for times $t < 6\tau_p$, the continuity equation reads

$$\frac{\partial}{\partial t} \Delta n(t,z) \approx \alpha j_\gamma(t) \, e^{-\alpha z}, \quad 0 < t < 6\tau_p. \qquad (2)$$

Integration of (2) up to $t \approx 6\tau_p$ yields

$$\Delta n(z) \approx \alpha n_\gamma e^{-\alpha z}. \qquad (3)$$

The generated carrier density increases linearly with photon density n_γ but does hardly depend on the pulse length. Naturally, these conclusions are only valid as long as the above assumptions are fulfilled. Errors are made for high carrier mobilities, when the pulse length is in the range of the diffusion time (see Sec. III B).

B. Axial diffusion time

Next, we investigate the rearrangement of photogenerated carriers due to an inhomogeneous generation. We want to clarify, on which timescale axial diffusion takes place. Hence, recombination in the bulk and at the surfaces was excluded. The excitation density as well as the mobility of the charge carriers was varied. As a measure of inhomogeneity, we calculated the ratio of the carrier density at the front and at the back surface.

Figure 1 shows that the homogenization of the carriers is independent of the excitation and depends only on the mobility. Furthermore, the inhomogeneities are reduced with a characteristic time constant $\tau_{Dif,car}$ of 10^{-10} s…10^{-8} s for all chosen mobilities. Below, we give calculated values of $\tau_{Dif,car}$. Thus, in general, axial diffusion effects mostly take place long times after the excitation pulse. This approves the assumption above, that for the investigated mobilities there is no diffusion during the excitation.

The axial diffusion effects can be described with analytical expressions. Since we are only interested in diffusion, we neglect recombination and solve the continuity equation with the initial value (3) and the boundary conditions $\frac{\partial}{\partial z} \Delta n(t,0) = \frac{\partial}{\partial z} \Delta n(t,d) = 0$, where d is the slab thickness. The result reads
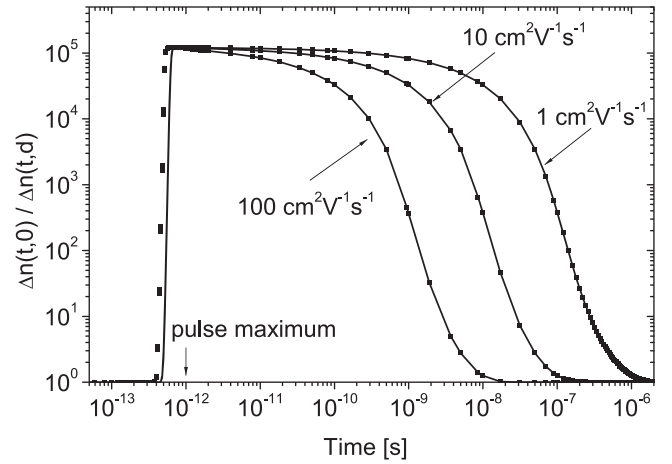

FIG. 1. Ratio $\frac{\Delta n(t,0)}{\Delta n(t,d)}$ for carrier mobilities $1\,\text{cm}^2\,\text{V}^{-1}\,\text{s}^{-1}$, $10\,\text{cm}^2\,\text{V}^{-1}\,\text{s}^{-1}$, and $100\,\text{cm}^2\,\text{V}^{-1}\,\text{s}^{-1}$, photon doses $n_\gamma = 10^9\,\text{cm}^{-2}$ (lines) and $n_\gamma = 10^{13}\,\text{cm}^{-2}$ (dots). The absorption coefficient is $\alpha = 3.805\,\mu\text{m}^{-1}$ and the slab thickness is $d = 3\,\mu\text{m}$. Carrier recombination is turned off.

$$\Delta n(t,z) = A_0 + \sum_{k=1}^{\infty} A_k \, e^{-\frac{D\pi^2 k^2}{d^2} t} \cos\left(\frac{\pi}{d} k z\right), \qquad (4)$$

$$A_0 = \frac{n_\gamma (1 - e^{-\alpha d})}{d},$$

$$A_k = \frac{2 n_\gamma}{d} \frac{1 - (-1)^k e^{-\alpha d}}{1 + \left(\frac{k\pi}{\alpha d}\right)^2}.$$

In Eq. (4), D denotes the diffusion coefficient. The coefficients A_0 and A_k are linear in n_γ and hence $\Delta n(t,z)$ is linear in n_γ, which means, we can write $\Delta n(t, z; n_\gamma, D, d, \alpha) = n_\gamma \cdot f(t, z; D, d, \alpha)$. Thus, the ratio $r(t) = \Delta n(t, 0)/\Delta n(t, d)$ indeed is independent from the photon density n_γ in agreement with Figure 1.

Next, we calculate the time scale on which diffusion takes place. To this end, we suppose an exponential time decay of the ratio $r(t)$ and calculate the decay time of diffusion $\tau_{Dif,car}$ from the time derivative of the logarithm of this ratio, that is,

$$\frac{1}{\tau_{Dif,car}} = -\left. \frac{d}{dt} \log r(t) \right|_{t \approx 0}. \qquad (5)$$

If x is defined by $x = \alpha d$ and y is defined by $y = e^{-\frac{D\pi^2 t}{d^2}}$, then Eq. (5) can be rewritten as

$$\frac{1}{\tau_{Dif,car}} = \frac{2D\pi^2 x^2}{d^2} \left(\frac{\displaystyle\sum_{k=1}^{\infty} \frac{(-1)^k - e^{-x}}{x^2 + (k\pi)^2} k^2 y^{k^2}}{1 - e^{-x} + 2x^2 \displaystyle\sum_{k=1}^{\infty} \frac{(-1)^k - e^{-x}}{x^2 + (k\pi)^2} y^{k^2}} \right.$$
$$\left. - \frac{\displaystyle\sum_{k=1}^{\infty} \frac{1 - (-1)^k e^{-x}}{x^2 + (k\pi)^2} k^2 y^{k^2}}{1 - e^{-x} + 2x^2 \displaystyle\sum_{k=1}^{\infty} \frac{1 - (-1)^k e^{-x}}{x^2 + (k\pi)^2} y^{k^2}} \right). \qquad (6)$$

Numerical evaluation of (6) for small times ($t \ll \frac{d^2}{D\pi^2}$ $\iff y \approx 0.99$) leads to

$$\frac{1}{\tau_{Dif,car}} \approx \frac{2D\pi^2}{d^2} 1.8\,\alpha\,d. \tag{7}$$

Inserting the parameter values of Figure 1 ($\alpha d \approx 3.6$) reveals $\tau_{Dif,car} \approx 27$ ns for $\mu = 1\,\text{cm}^2\,\text{V}^{-1}\,\text{s}^{-1}$, $\tau_{Dif,car} \approx 2.7$ ns for $\mu = 10\,\text{cm}^2\,\text{V}^{-1}\,\text{s}^{-1}$ and $\tau_{Dif,car} \approx 0.27$ ns for $\mu = 100\,\text{cm}^2$ $\text{V}^{-1}\,\text{s}^{-1}$. This fits the data in Fig. 1.

Due to the considerations above, a pulse length $\tau_p < \tau_{Dif,car}$ should be chosen to exclude substantial axial diffusion during the excitation. Then, the electron density directly after the excitation ($t \approx t_0 + 3\tau_p$) can easily be calculated and is a good criterion for comparison of TRL-experiments.

C. Depth resolution

Finally, we ask for the depth of luminescence generation. According to Eq. (3), the photogenerated carrier density at $t \approx t_0$ decays exponentially into the absorber layer for monochromatic light excitation. Hence, nearly all electrons are in a thin layer of $3\lambda_\alpha$ thickness from the illuminated surface, where $\lambda_\alpha = 1/\alpha$ is the absorption length. Therefore, the main part of the radiative recombination takes place near the front surface up to that time at which the electrons are homogeneously distributed. Hence, one can state that luminescence comes from

the front surface for $t < \tau_{Dif,car}$ and from the whole slab for $t > \tau_{Dif,car}$.

IV. ISOLATION OF EFFECTS

A. Impact of axial diffusion

First, we discuss the influence of axial diffusion on the TRL decay. Therefore, we investigate the slope of $I(t)$, where $I(t)$ is the total number of generated luminescence photons per time. For a semiconductor slab with thickness d, the slope $\frac{d}{dt}I(t)$ can be calculated from

$$\begin{aligned}\frac{d}{dt}I(t) &= \frac{d}{dt}\int_0^d R_{rad}(t,z)dz \\ &= \int_0^d \frac{\partial}{\partial t}R_{rad}(t,z)dz \\ &= B\int_0^d \left(n(t,z)\frac{\partial}{\partial t}p(t,z) + p(t,z)\frac{\partial}{\partial t}n(t,z)\right)dz,\end{aligned} \tag{8}$$

where R_{rad} is the radiative net-recombination rate and B is the radiative constant. Inserting the continuity equations for electrons and holes leads to

$$\frac{d}{dt}I(t) = \underbrace{-B\int_0^d (nR_p + pR_n)dz}_{(a)} \underbrace{-BS_n p\,\Delta n|_{z=d} - BS_n p\,\Delta n|_{z=0} - BS_p n\,\Delta p|_{z=d} - BS_p n\,\Delta p|_{z=0}}_{(b)} \\ \underbrace{+B\int_0^d E\left(\mu_p p\frac{\partial}{\partial z}n - \mu_n n\frac{\partial}{\partial z}p\right)dz}_{(c)} \underbrace{-B\int_0^d (D_n + D_p)\frac{\partial}{\partial z}n\frac{\partial}{\partial z}p\,dz}_{(d)}, \tag{9}$$

where D, μ, R, and S denote the diffusion coefficient, mobility, bulk-recombination rate, and surface recombination velocity of electrons and holes, respectively. E denotes the electric field strength.

Since R, p, and n are positive quantities, (a) in Eq. (9) is always negative. This means bulk-recombination of charge carriers leads to a decay of the luminescence intensity. All terms in (b) are negative, because S, n, p, Δn, and Δp are always positive. Hence, surface recombination further reduces the decay time. The third term describes the influence of drift effects on $\frac{d}{dt}I(t)$, for example, in the space charge region of a solar cell. The last term in Eq. (9) describes axial diffusion effects. Its sign is not unique which means diffusion of charge carriers can increase or decrease the decay time of the luminescence. In general, it is $\frac{\partial}{\partial z}n \approx \frac{\partial}{\partial z}p$. Then, diffusion effects further decrease the luminescence decay time. However, as will be shown below, term (d) is only relevant compared to term (a) for high injection levels.

Now, we look at the calculated TRL-transients in Figure 2 starting with low excitation (see label (1)). There is only one decay time due to radiative recombination. Though diffusion takes place, it does not affect the decay,

since the minority carrier lifetime is homogeneous. That means, it is not important, where the charge carriers recombine. If we look at the net-radiative recombination we have
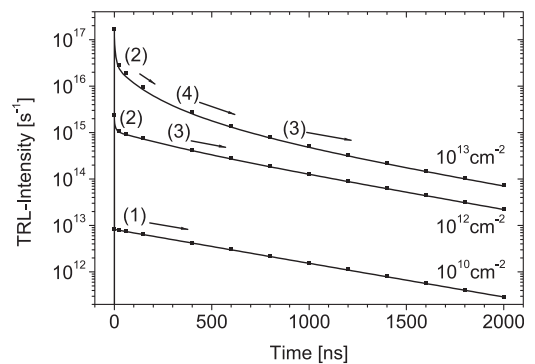
$$R_{rad}(t,z) \approx B\,p_0\,\Delta n(t,z), \tag{10}$$

FIG. 2. TRL-transients of a semiconductor slab without defects and with a carrier mobility of $20\,\text{cm}^2\,\text{V}^{-1}\text{s}^{-1}$ for different injection levels. The solid lines represent simulated data, the dots represent approximated data.

since we have a low photogenerated carrier density. p_0 is the equilibrium hole density. If we calculate the TRL-intensity, it holds

$$I(t) = \int_0^d R_{rad}(t,z)\mathrm{d}z = B\, p_0 \int_0^d \Delta n(t,z)\mathrm{d}z. \qquad (11)$$

According to Eq. (11), the intensity is proportional to the total number of generated carriers and hence not influenced by diffusion, because the rearrangement of electrons does not change their number. This can be traced back to the recombination probability of the electrons as minority charge carriers. The recombination of one electron depends only on the number of holes. Since the hole density is homogeneous for low injection levels ($p(z) \approx p_0$), the recombination probability is equally distributed. Therefore, the recombination of the whole electron population is independent of its distribution.

If the excitation increases, the quadratic term in

$$R_{rad}(t,z) = B\,(n_0 + p_0)\Delta n(t,z) + B\,\Delta n(t,z)^2, \qquad (12)$$

where n_0 is the equilibrium electron density, becomes important (bimolecular recombination). Now, the TRL-intensity decays very fast because of diffusion (label (2)). Again, the recombination probability depends on the hole density, that is inhomogeneous for high injection levels ($p(z) \approx \Delta p(z)$). If one electron is removed from a region of high hole density to a region of low hole density, its recombination probability decreases leading to a reduced recombination rate. In conclusion, a reduction of the recombination rate causes a decay of the luminescence intensity. After homogenization, the electrons are minorities and Eq. (11) can again be applied: The measured decay time equals the radiative lifetime (label (3)).

For even higher injection levels, diffusion again initially reduces the decay time. As shown above, the homogenization process is finished after a few nanoseconds. Now, the electron density is equally distributed, but equals the doping concentrations. That means, we are still in the limit of bimolecular recombination and the transient is curved (label (4)). After a certain time, the electrons become minorities and recombine in the limit of monomolecular recombination, where the TRL-decay is exponential and the decay time equals the radiative lifetime.

To approximate the data in Figure 2 by an analytical expression, one can utilise that axial diffusion takes place on a much shorter timescale than radiative recombination. Therefore, we first solve the continuity equation without recombination and the result is inserted as an initial value for the continuity equation with recombination, but without the diffusion term. The result reads

$$\Delta n(t,z) = \frac{p_0\, \Delta n_0(t,z)}{(p_0 + \Delta n_0(t,z))\mathrm{e}^{B p_0 t} - \Delta n_0(t,z)} \qquad (13)$$

where $\Delta n_0(t,z)$ equals the expression of $\Delta n(t,z)$ in Eq. (4). In Figure 2, it can be seen that (13) fits the data. Furthermore, one can prove the above considerations evaluating Eq. (13) for the different cases. Under low injection, it is $\Delta n_0(t,z) \ll p_0$ and it follows:

$$I(t) = \int_0^d R_{rad}(t,z)\mathrm{d}z \approx p_0\, A_0\, d\, \mathrm{e}^{-B p_0 t}. \qquad (14)$$

The decay time becomes $\tau = \frac{1}{B p_0} = \tau_{rad}$, which equals the minority carrier lifetime.

If we consider a high injection level and short times $t \ll \frac{1}{B p_0}$ it follows:

$$R_{rad}(t,z) \approx B\, \Delta n_0(t,z)\,(p_0 + \Delta n_0(t,z)), \qquad (15)$$

which means that the decay of radiative recombination is due to the decay of $\Delta n_0(t,z)$ and hence due to diffusion. To analyze for which injection levels axial diffusion becomes apparent, we integrate Eq. (15)

$$
\begin{aligned}
I(t) &= \int_0^d R_{rad}(t,z)\mathrm{d}z \\
&= B\, d\left(A_0\, p_0 + A_0^2 + \frac{A_1^2}{2}\, \mathrm{e}^{-\frac{2 D \pi^2}{d^2} t} + \cdots\right).
\end{aligned} \qquad (16)
$$

Since it is $|A_1| > |A_2| > \dots$, the time-dependence of $I(t)$ in Eq. (16) becomes only apparent, if it is $\frac{A_1^2}{2} \gtrsim A_0\,(p_0 + A_0)$. Evaluation of the ratio leads to

$$\frac{\frac{A_1^2}{2}}{A_0\,(p_0 + A_0)}
\begin{cases}
\approx \dfrac{2\, n_\gamma}{d\, p_0 + n_\gamma} & \text{for} \quad \alpha d \gg 1, \\[2mm]
\ll 1 & \text{for} \quad \alpha d \lesssim 1 \text{ and arbitrary } n_\gamma.
\end{cases} \qquad (17)$$

This shows that the appearance of diffusion effects does not only depend on the injection level but also on the value of αd. If it is $\alpha d \gg 1$, then follows from (17) for the minimum photon density per pulse for the appearance of diffusion effects

$$n_\gamma \gtrsim d\, p_0 \quad \text{for } \alpha d \gg 1. \qquad (18)$$

This proves mathematically that axial diffusion effects can only be seen for high injection levels. Additionally, according to Eq. (16), we can define a decay time of the luminescence intensity due to diffusion by

$$\tau_{Diff} = \frac{d^2}{2\,\pi^2 D}. \qquad (19)$$

We point out, that τ_{Diff} in Eq. (19) has to be distinguished from $\tau_{Dif.car}$ in Eq. (7).

Finally, we consider high injection levels and long times. Then one has $\Delta n_0(t,z) \approx A_0$, which is time-independent, and it follows a combination of bi- and monomolecular recombination according to the considerations in the first part of this series.

B. Impact of surface defects

Now, we want to investigate the influence of surface defects. To this end, we simulated some TRL-transients for different back surface recombination velocities and different injection levels. The recombination velocity at the front surface was set to $S_f = 10^3\ \mathrm{cm\ s^{-1}}$. As can be seen in Figure 3 and by comparison with Figure 2, in principle, the transient's decay does not change. For low injection levels, one still has
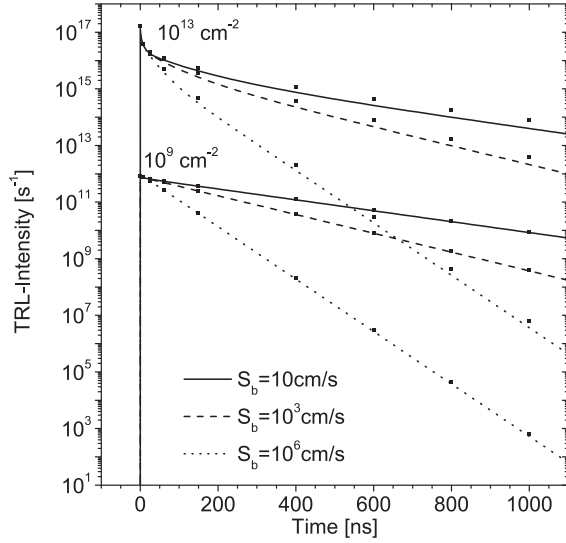
FIG. 3. TRL-transients of a semiconductor layer without bulk defects for different injection levels and different back surface recombination velocities S_b. The front surface recombination velocity was $S_f = 10^3$ cm s^{-1}. The lines represent simulated data, the dots approximated data.

a single-exponential decay, whereas the decay is multi-exponential for high injection levels due to diffusion, bimolecular recombination, and monomolecular recombination. Thus, surface recombination adds a lifetime to the carrier lifetime, which is nearly independent of the charge carrier density and hence independent of time and space.

To fit the data, we use the above mentioned model. First, we solve the diffusion equation with the boundary conditions

$$S_f \Delta n_0(t, 0) = D \frac{\partial}{\partial z} \Delta n_0(t, 0) \qquad (20)$$

$$S_b \Delta n_0(t, d) = -D \frac{\partial}{\partial z} \Delta n_0(t, d). \qquad (21)$$

The solution can be represented by

$$\Delta n_0(t, z) = A_0 + \sum_{k=1}^{\infty} A_k U_k(z) e^{-D \beta_k^2 t} \qquad (22)$$

with

$$U_k(z) = \cos \beta_k z + \frac{S_f}{D \beta_k} \sin \beta_k z. \qquad (23)$$

The set $\{\beta_k\}$ with $0 = \beta_0 < \beta_1 < \beta_2 < \ldots$ is the set of solutions of the well known eigenvalue equation[14]

$$\tan \beta_k d = -\frac{D (S_b + S_f) \beta_k}{S_b S_f - D^2 \beta_k^2} \qquad (24)$$

and has to be determined numerically. Since the $U_k(z)$ in Eq. (23) represent an orthogonal basis on $[0, d]$, one can determine the A_k by integration of the initial value

$$A_k = \alpha n_\gamma \frac{\int_0^d e^{-\alpha z} U_k(z) dz}{\int_0^d U_k(z)^2 dz}. \qquad (25)$$

For A_0, it holds

$$A_0 = \begin{cases} \dfrac{n_\gamma (1 - e^{-\alpha d})}{d}, & S_f = S_b = 0 \\ 0, & \text{else.} \end{cases} \qquad (26)$$

This makes sense, since it is $\lim_{t \to \infty} \Delta n(t, z) = A_0$. If there is a current across the surfaces ($S_f, S_b \neq 0$), the total number of electrons decreases, until all carriers are flown out and $A_0 = \lim_{t \to \infty} \Delta n(t, z) = 0$. If there is no carrier current across the contacts, the total number of electrons is conserved and it is $A_0 = \lim_{t \to \infty} \Delta n(t, z) > 0$. Furthermore, it can be seen that $\Delta n_0(t, z; n_\gamma, d, D, \alpha) = n_\gamma \cdot f(t, z; d, D, \alpha)$ still holds, which means that diffusion times are again independent of the injection level n_γ.

Now, $\Delta n_0(t, z)$ is inserted as an initial value into the continuity equation without diffusion, but only with radiative bulk recombination. Again the solution is Eq. (13). As can be seen in Figure 3, the data calculated with (13) fit the simulated data. The reason for such a good approximation may not be obvious, since the condition for the model above, that diffusion only takes place at the beginning, is not fulfilled. Therefore, we simplify Eq. (13) for low injection levels and get

$$\Delta n(t, z) = \Delta n_0(t, z) e^{-B p_0 t}. \qquad (27)$$

Moreover, $\Delta n_0(t, z) \approx A_1 U_1(z) e^{-D \beta_1^2 t}$ holds for long times, since $A_0 = 0$ for $S_f \neq 0$ or $S_b \neq 0$. Inserting this into (27) leads to

$$\Delta n(t, z) \approx A_1 U_1(z) e^{-(B p_0 + D \beta_1^2) t}. \qquad (28)$$

This shows that the time dependence of Δn_0 accounts for diffusion as well as for surface recombination. Furthermore, surface recombination can be understood as a bulk recombination with the corresponding lifetime $\tau_{sSRH} = \frac{1}{D \beta_1^2}$. To evaluate β_1, there are approximative solutions of (24) assuming $S_f = S_b = S$ or $S_f = 0$ found by graphic considerations.[11,14] In order to evaluate an approximative, but general solution, one can approximate $\tan x$ by

$$\tan x \approx \frac{8}{\pi^2} x \frac{\pi - x}{\pi - 2x} \text{ for } x \in [0, \pi] \qquad (29)$$

with an average relative error of 6% for $x \in [0, \pi]$. By this approximation, Eq. (24) becomes a third order equation in β_1, which can be solved analytically.

C. Impact of bulk defects

Now, we discuss the impact of deep bulk defects on the TRL-transients neglecting surface recombination. As in the first part of this work, we calculated a map, which shows the TRL-decay time depending on the density of deep defects and the injection level in the case of asymmetric capture cross sections $\sigma_n = 100 \sigma_p$. This map can be seen in Figure 4. While comparing it with Figure 3, in the first part of this work, in principle, no differences become obvious. A saturation of deep defects is visible
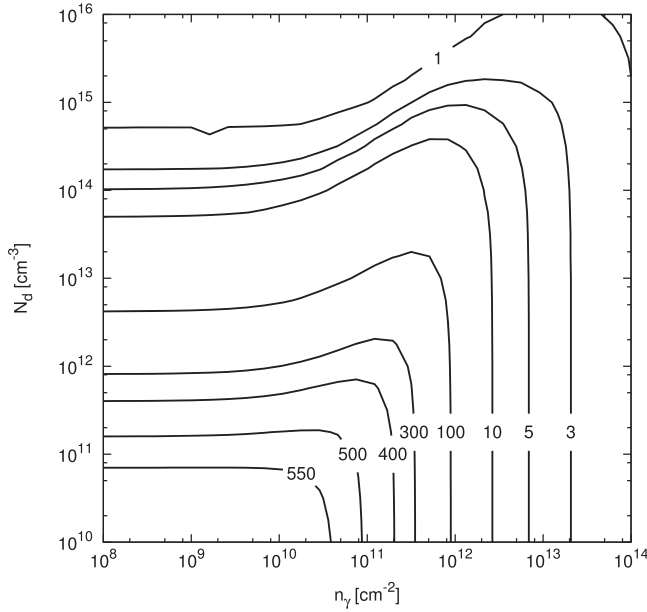
FIG. 4. Contour map of decay times in nanoseconds depending on the density of deep defects and on the injection level in a homogeneous semiconductor slab with asymmetric capture cross sections.

due to asymmetric carrier capture and majority carrier limited recombination. Moreover, the decay time shows a decrease for high injection levels due to bimolecular recombination and diffusion in contrast to the results in Sec. IV D in the first part, where the decline was only due to bimolecular recombination.

1. Low defect densities

First, we look at the transients calculated for a defect density $N_d = 10^{13} \, cm^{-3}$ in Figure 5. For low injection levels, the decay time is small, since all carriers recombine non-radiatively with a lifetime $\tau_{n0} = \frac{1}{\sigma_n v_n N_d}$. As the injection level increases, the decay time increases too, because there are not enough majority carriers in the defect level (for asymmetric carrier capture) and defect recombination becomes inefficient. In this case, the SRH-lifetime is $\tau_{n0} + \tau_{p0}$ with $\tau_{p0} = \frac{1}{\sigma_p v_p N_d}$. Since it is $\tau_{n0} + \tau_{p0} \gg \frac{1}{B p_0} = \tau_{rad}$ for low defect densities,
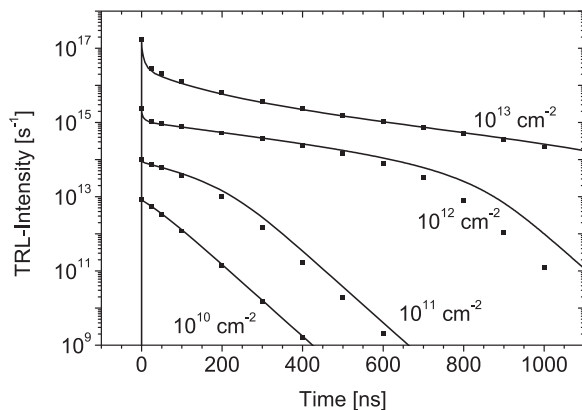
radiative recombination becomes the dominating recombination path and the transient's decay time is quite large.

After a certain time, the minority carrier density is such reduced that defect recombination becomes again efficient with lifetime τ_{n0}. The transients exhibit a biexponential decay. For further increased excitation, diffusion effects, and bimolecular recombination become apparent and one measures a third decay time or curved transients.

2. High defect densities

For low injection levels, the transients show the same principle behaviour. The luminescence decays with a small decay time $\tau = \tau_{n0}$, since the carriers recombine non-radiatively. Increasing the injection level increases the SRH-lifetime and one gets $\tau = \tau_{n0} + \tau_{p0}$. For high defect densities, it holds $\tau_{n0} + \tau_{p0} \ll \tau_{rad}$ and therefore the charge carriers keep recombining non-radiatively, but with a larger lifetime. For very high injection levels again diffusion effects cause a fast decay at short times.

3. Analytical approximation

To approximate the data one again has to solve the continuity equation. In the case that we have no trapping and $\tau_{p0} \gg \tau_{n0}$, the rate of Schockley-Read-Hall-recombination reads

$$R_{SRH}(t,z) = \frac{\Delta n(t,z)\big(p_0 + \Delta n(t,z)\big)}{\tau_{n0} \, p_0 + \tau_{p0} \, \Delta n(t,z)}. \tag{30}$$

Now, we again make the assumption that we can use the solution of the diffusion Eq. (4) as an initial value for the continuity equation without diffusion, but complemented with (30). Again, this is distinct from Ref. 11, where bimolecular recombination is not included. In this case, we have an ordinary differential equation that has no analytical solution. If we solve it numerically, we get the approximated data shown in Figures 5 and 6. We see that the decay of the intensity is approximated in a wide range. Only at the point of transition from majority limited ($\tau_{p0} + \tau_{n0}$) to minority limited recombination (τ_{n0}), there are considerable differences. The reason is that in this range the rate of recombination is very sensitive to the carrier density. This means, small differences in
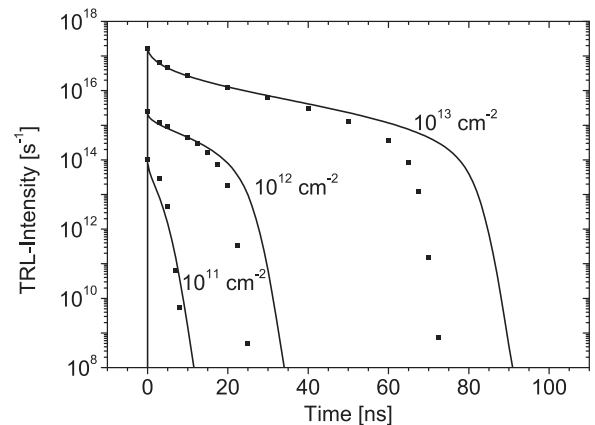

FIG. 5. TRL-transients for $N_d = 10^{13} \, cm^{-3}$ and different n_γ. The solid lines represent simulated data, the dots represent approximated data.

FIG. 6. TRL-transients for $N_d = 10^{15} \, cm^{-3}$ and different n_γ. The solid lines represent simulated data, the dots represent approximated data.

the carrier density due to non-correct treatment of diffusion at small times cause large differences in the rate of recombination at later times. By further calculations, we have shown that the above model yields good approximation even if the carrier lifetime and the carrier mobility are small that means $\tau_{Dif,car} > \tau_{n0} + \tau_{p0}$.

By distinguishing between high- and low injection levels the continuity equation can be solved analytically. For low injection levels, it is $\Delta n \ll \frac{\tau_{n0}}{\tau_{p0}} p_0$, and hence,

$$R_{SRH}(t,z) = \frac{\Delta n(t,z)\left(p_0 + \Delta n(t,z)\right)}{\tau_{n0}\,p_0}. \tag{31}$$

Then, the solution of the continuity equation reads

$$\Delta n(t,z) = \frac{p_0\,\Delta n_0(t,z)}{\left(p_0 + \Delta n_0(t,z)\,\mathrm{e}^{(B\,p_0+1/\tau_{n0})\,t} - \Delta n_0(t,z)\right)}$$

$$\approx p_0\,\Delta n_0(t,z)\,\mathrm{e}^{-(B\,p_0+1/\tau_{n0})\,t}, \tag{32}$$

and for the decay it holds for not too small defect densities $\tau \approx \tau_{n0}$.

For high injection levels, it is $\Delta n \gg \frac{\tau_{n0}}{\tau_{p0}} p_0$, and hence,

$$R_{SRH}(t,z) = \frac{\Delta n(t,z)\left(p_0 + \Delta n(t,z)\right)}{\tau_{p0}\,\Delta n(t,z)}. \tag{33}$$

In this case, the solution of the continuity equation reads

$$\Delta n(t,z) = \frac{\Delta n_0(t,z) + p_0 - p_0\left(1 + B\,\tau_{p0}\,\Delta n_0(t,z)\right)\mathrm{e}^{\left(1/\tau_{p0}-B\,p_0\right)t}}{-B\,\tau_{p0}\left(\Delta n_0(t,z) + p_0\right) + \left(1 + B\,\tau_{p0}\,\Delta n_0(t,z)\right)\mathrm{e}^{\left(1/\tau_{p0}-B\,p_0\right)t}}. \tag{34}$$

For reasonable defect densities, such that $\tau_{p0} \ll \tau_{rad}$ holds, Eq. (34) simplifies to

$$\Delta n(t,z) = \left(p_0 + \Delta n_0(t,z)\right)\mathrm{e}^{-\frac{t}{\tau_{p0}}} - p_0. \tag{35}$$

Equation (35) shows that indeed the TRL decay for high carrier densities, that is, for TRL intensities above $10^{14}\,\mathrm{s}^{-1}$ in Figs. 5 and 6, is determined by diffusion ($\Delta n_0(t,z)$) and majority carrier limited recombination (τ_{p0}).

D. Combination of bulk and surface defects

Now, we investigate the case of a combination of bulk and surface defects on the luminescence's decay. In Subsec. IV B, we already discussed that surface recombination contributes an excitation independent carrier lifetime to the minority bulk lifetime in case of a non-defective semiconductor slab. As can be seen in Figure 7, this still holds if there are deep defects in the bulk of the semiconductor. The principle effects of axial diffusion, bi- and monomolecular recombination can still be

FIG. 7. TRL-transients of a semiconductor slab with a defect density of $N_d = 10^{13}\,\mathrm{cm}^{-3}$ and asymmetric capture cross sections for varying injection levels and surface recombination velocities at the back contact.

found in the presence of surface recombination. In consequence, one cannot easily distinguish a TRL decay due to surface or bulk recombination.

1. Distinguishing front and back surface recombination

If the bulk lifetime is large, surface recombination may be the limiting recombination process. In this case, TRL-transients can exhibit different decays for front and back surface recombination, respectively, due to an inhomogeneous generation profile.

In Figure 8 TRL-transients are shown for a large, fixed bulk lifetime of 200 ns and two different carrier mobilities $\mu = 10\,\mathrm{cm}^2\,\mathrm{V}^{-1}\,\mathrm{s}^{-1}$ and $\mu = 100\,\mathrm{cm}^2\,\mathrm{V}^{-1}\mathrm{s}^{-1}$. Either the front or the back surface recombination velocity was adjusted, such that the effective lifetime is equal for both mobilities.

As can be seen, the TRL transient bends upwards for back surface recombination and small carrier mobilities. Directly after excitation, the carrier density at the back side is small compared to the average carrier density. Therefore, back surface recombination is small, too, leading to a large effective carrier lifetime $\tau_{eff} \approx \tau_{bulk}$. During homogenization, the carrier density at the back surface increases giving rise to an enhanced back surface recombination and a decreased effective lifetime $\tau_{eff} \approx \tau_{surf} < \tau_{bulk}$. This can also be seen by applying (b) in Eq. (9): an increase in Δn at the back side due to diffusion decreases the slope $\frac{\mathrm{d}}{\mathrm{d}t}I(t)$ and hence the PL-decay time.

According to Fig. 8, the TRL transient bends downwards for front surface recombination and small carrier mobilities. In this case, the carrier density at the front surface decreases due to homogenization causing an inhibited front surface recombination and an increasing effective carrier lifetime.

The time for which back surface recombination is diminished and front surface recombination is enlarged depends on the length of homogenization and thus on the
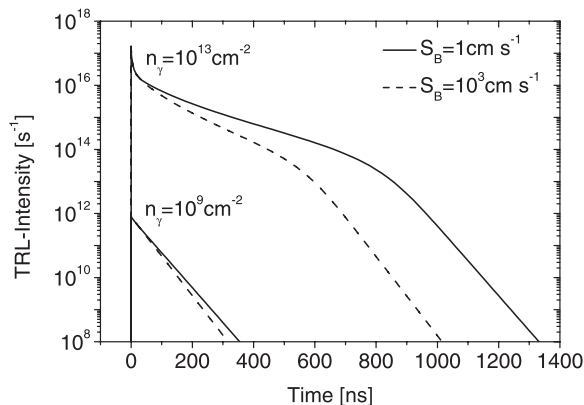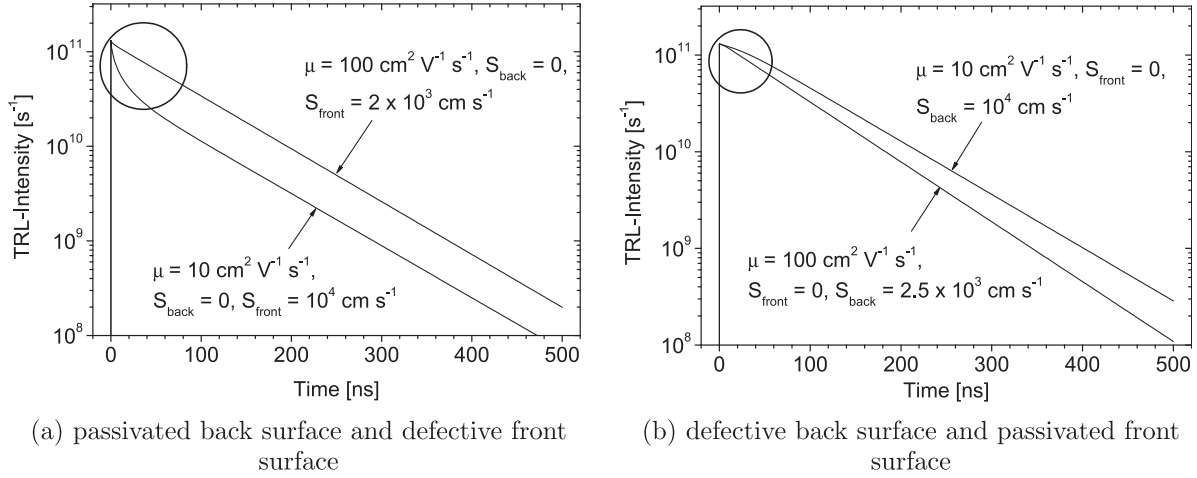
(a) passivated back surface and defective front
surface

(b) defective back surface and passivated front
surface

FIG. 8. TRL-transients of a semiconductor layer with a bulk lifetime of 200 ns and two carrier mobilities $\mu = 10 \, cm^2 \, V^{-1} \, s^{-1}$ and $\mu = 100 \, cm^2 \, V^{-1} s^{-1}$ for different front and back surface recombination velocities.

carrier mobility. Increasing the carrier mobility accelerates homogenization and prevents bending of the TRL transients as shown in Fig. 8.

E. Impact of space charges

In the first part of this work, we have shown that under the influence of space charges the decay time can increase, if the time-resolved luminescence starts from the steady state. For pulsed excitation experimentally the opposite is observed.[6,7] Therefore, we simulate the excitation of a defectless homojunction by one short laser pulse. The system n-Cu(In,Ga)Se$_2$/p-Cu(In,Ga)Se$_2$ may serve as a working example. The luminescence transients are shown in Figure 9.

1. High injection levels

If the excitation is turned off, there are charge carriers in the space charge region as well as in the quasi-neutral region. If the injection level is high (see label (1) in Fig. 9), the carrier density in the space charge region is large enough to screen the electric field of the junction. In consequence, there are no drift-effects. Hence, the luminescence decay is equal

for the homojunction as well as for the sole semiconductor layer and shows diffusion and bulk-recombination effects.

If the injection level decreases, small differences between the two cases become apparent. Now, the electric field cannot be fully screened. Hence, a small part of electron-hole-pairs is separated within the first 100 ps (label (2)), which leads to a reduction of $n(t, z) \cdot p(t, z)$ and therefore to a smaller luminescence intensity. After the separation, the recombination of the minority carriers generated in the quasi-neutral regions becomes apparent (label (3)) and the decay time equals the bulk-lifetime.

2. Low injection levels

If the excitation becomes further decreased drift effects increase. Now, the decay due to charge separation is very fast (label (2)) and a large number of charge carriers accumulate at the edges of the space charge region, where they are majority carriers (see Fig. 10). Afterwards again the charge carriers in the quasi-neutral region recombine (label (3)). After most of the minority carriers in the quasi-neutral regions are recombined, the majority carriers at the edges of the space charge region remain. They cannot recombine,
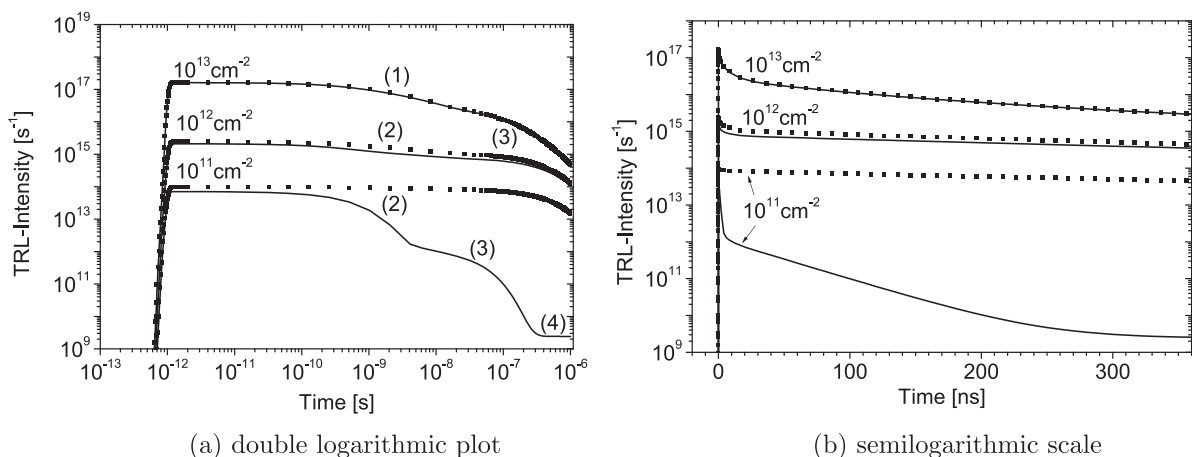

(a) double logarithmic plot

(b) semilogarithmic scale

FIG. 9. TRL-transients of a semiconductor-homojunction with $N_a = N_e = 10^{16} \, cm^{-3}$, $d_e = 0.5 \, \mu m$, and $d_a = 2.5 \, \mu m$ (lines) compared with that of a sole semiconductor layer with $N_a = 10^{16} \, cm^{-3}$ and $d_a = 3 \, \mu m$ (dots).
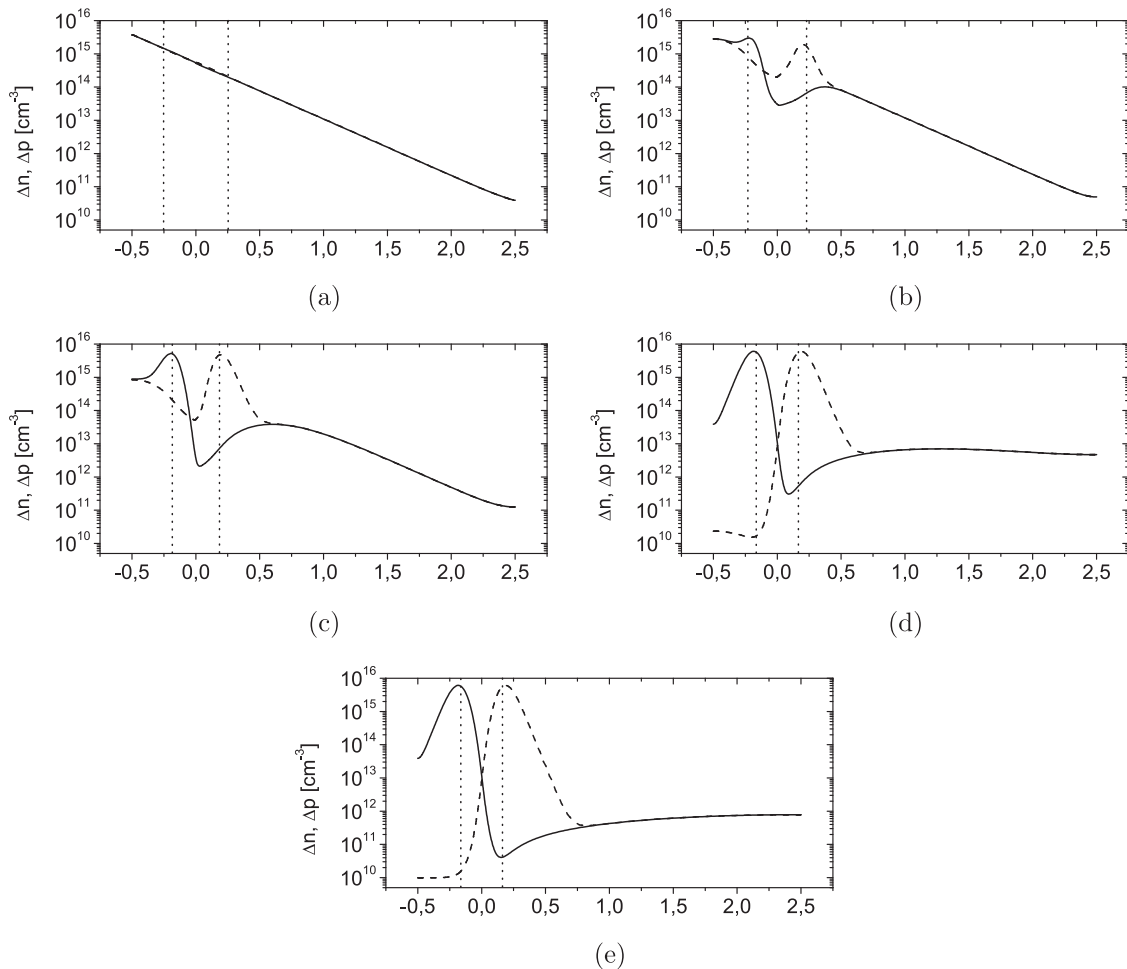
FIG. 10. Excess electron (solid) and hole (dashed) distribution in a semiconductor-homojunction for an injection level $n_\gamma = 10^{11}\,\text{cm}^{-2}$ for different times after excitation. Edges of SCR (dotted) are calculated according to Schottky approximation.

since the density of minorities as recombination partners is very low, and they cannot flow out, since the homojunction is under open circuit. Therefore, a large open circuit voltage builds up. Now, the charge storage effect that we have already explained in the first part of this work applies. The recombination is limited by a small diffusion current of the majority carriers across the space charge region and a very large decay time can be detected (label (4)). Since in real experiments, a luminescence's decay of only two or three orders of magnitude is measured, generally, only drift and diffusion effects as well as the bulk recombination can be measured, but no charge storage effects.

3. Estimation of drift-time

By supposing the Schottky-approximation to be valid, the luminescence intensity that originates from the space charge region in the p-doped semiconductor can be estimated. The calculations for a SCR in the n-doped semiconductor are equal. Therefore, we make some assumptions

- The electric field in the SCR is unscreened and has an average field strength E.
- The photogenerated excess carrier densities have exponential shape and move in opposite directions with the velocities v_n and v_p, respectively (see Figure 11).

- Charge separation is fast. Hence, no recombination has to be considered.
- No charge carriers from the quasi-neutral region are collected by the space charge region.

The two exponential curves in Figure 11 are shifted against each other with the velocities v_n and v_p leading to the following time dependence:
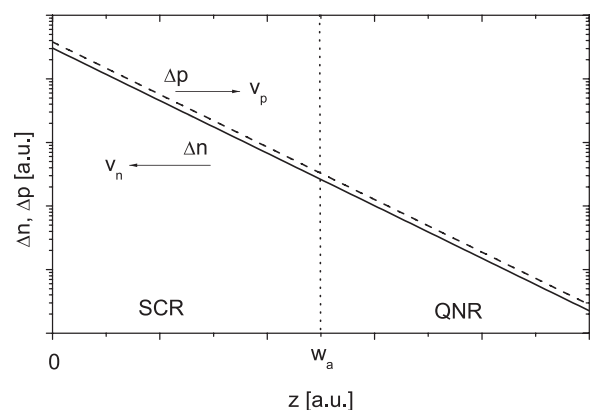

FIG. 11. Photogenerated density of electrons (solid) and holes (dashed) in the space charge region. For better visibility, the two curves are shifted. In reality, the densities are equal.

$$\Delta n(t,z) = \Delta n(0, z + v_n\, t)$$
$$\Delta p(t,z) = \Delta p(0, z - v_p\, t). \tag{36}$$

Inserting Eq. (36) into $R_{rad}(t,z) = B\,(n_0(z)\,\Delta p(t,z) + p_0(z)\,\Delta n(t,z) + \Delta n(t,z)\,\Delta p(t,z))$ and integrating over the SCR one gets

$$I(t) \propto \sinh(\alpha\,(w_a - (v_n + v_p)\,t)), \tag{37}$$

where w_a is the width of the space charge region in the p-semiconductor. With Eq. (37) one can estimate the time τ_{CS} for charge separation. It is

$$I(\tau_{CS}) = 0 \quad \Longleftrightarrow \quad \tau_{CS} = \frac{w_a}{v_n + v_p}. \tag{38}$$

Providing a symmetric doping of $N_A = N_D = 10^{16}\,\mathrm{cm}^{-3}$ and mobilities $\mu_n = \mu_p = 20\,\mathrm{cm}^2\,\mathrm{V}^{-1}\mathrm{s}^{-1}$ it is $E \approx 1.7 \times 10^4\,\mathrm{V}\,\mathrm{cm}^{-1}$, $v_n = v_p \approx 3.4 \times 10^5\,\mathrm{cm}\,\mathrm{s}^{-1}$, and $w_a \approx 250 \times 10^{-7}\,\mathrm{cm}$. Evaluation of Eq. (38) reveals $\tau_{CS} \approx 40\,\mathrm{ps}$. This means after 40 ps electrons and holes are separated and the space charge region is depleted from excess carriers. In reality, the time for charge separation will be longer than 40 ps since the space charge becomes screened leading to a diminished charge separation. In addition, the SCR collects charge carriers from the QNR. Thus, $I(t) = 0$ will not be fulfilled for a junction that is not in equilibrium.

At last, we investigate the dependence of (38) on the carrier mobility and electric field strength. From Schottky-approximation follows $w_a \propto E^{\frac{1}{2}}$ and $v \propto \mu E$. Inserting this into (38) reveals

$$\tau_{CS} \propto \frac{1}{\mu_n + \mu_p}\,\frac{1}{E^{\frac{1}{2}}}. \tag{39}$$

V. INFLUENCE OF MULTI-PULSE EXCITATION

Up to here, we have always considered the case of single-pulse excitation. At last, we focus on the impact of a multi-pulse excitation, meaning the photon current density in Eq. (1) is modified in the following way:

$$j_\gamma(t) = \frac{n_\gamma}{\sqrt{\pi}\,\tau_p}\sum_k e^{-\frac{(t - t_0 - kT)^2}{\tau_p^2}}, \tag{40}$$

where $f = T^{-1}$ is the frequency of the excitation. We simulated a multi-pulse excitation of a np-homojunction for varying excitation frequency, carrier lifetime and injection level, and concentrate on the output voltage which is shown in Figure 12. For each pulse charge carriers in the space charge region are generated and accumulate at the edges of the SCR as explained in Subsec. IV E. The charge carriers are stored for a long time. This is why the voltage is not complete decayed until the next pulse generates more charge carriers. Therefore, a bias photovoltage is applied even for pulsed luminescence experiments leading to a dark diffusion current. Due to this current, there is a bias luminescence shifting the background to higher TRL intensities. This hinders the determination of a decay time due to recombination. Hence, a low injection level
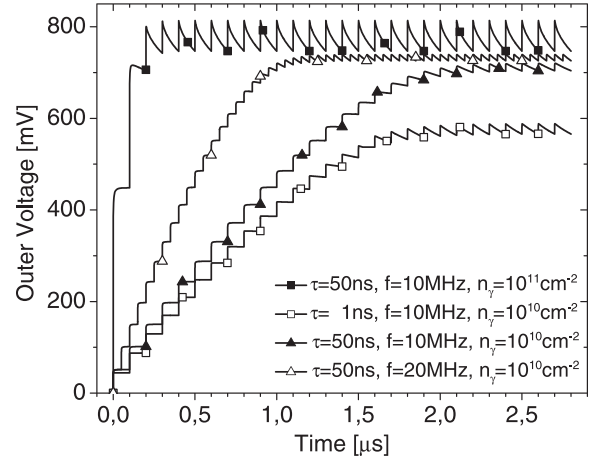

FIG. 12. Formation of a large photovoltage due to multi-pulse excitation with varying excitation frequency, carrier lifetime, and injection level.

is advisable, since this leads to a small bias photovoltage and hence to a low background luminescence intensity.

VI. CONCLUSION AND OUTLOOK

In the presented work, we have done one-dimensional simulations of time-resolved photoluminescence on semiconductors. First, we have shown that an initial state in a semiconductor layer can be defined by the number of photons per pulse per area and by the absorption coefficient. This initial state is largely independent of sample properties or the experimental setup and is hence suitable for comparison of different luminescence experiments.

In the next part, we have demonstrated that axial diffusion effects and bimolecular recombination have to be considered for high injection levels. Both lead to a decrease in the luminescence decay and can be found for short observation times. For longer times monomolecular recombination can be measured. This is a superposition of surface and bulk recombination and can be described by an effective bulk-lifetime. Therefore, recombination at grain boundaries can also be considered by one-dimensional simulations. By an excitation dependent measurement the minority and the majority carrier lifetime can be determined.

Moreover, we deduced an analytical model, which provides a good approximation for axial diffusion, bimolecular recombination, defect recombination, and surface recombination. This model can be used to fit experimental data and to deduce carrier lifetime and mobility.

In the last part, we analyzed the impact of space charges on the transient luminescence. We could reproduce the experimental finding, for which low injection levels the transient's decay time can increase and decrease due to space charge. This can be explained with different frequencies of a multi-pulse excitation. In the limit of single-pulse excitation, charge separation effects lead to a decrease of the decay time. For high frequencies, a bias voltage drops across the junction that causes a lowered space charge and therefore reduced charge separation. In this case, the diffusion of carriers over the barrier of the junction limits the recombination and leads to an increased decay time.

[1]M. Maiberg and R. Scheer, J. Appl. Phys. **116**, 123710 (2014).

[2]I. Yamakawa, M. Ichida, S. V. Sorokin, A. A. Toropov, A. Titkov, S. V. Ivanov, and A. Nakamura, J. Lumin. **87–89**, 384 (2000).

[3]S. Shirakata, Phys. Status Solidi A **210**, 1322 (2013).

[4]S. Shirakata and T. Nakada, Phys. Status Solidi C **6**, 1059 (2009).

[5]S. Shirakata, H. Ohta, and N. Iwado, Jpn. J. Appl. Phys., Part I **51**, 10NC13 (2012).

[6]W. K. Metzger, I. L. Repins, and M. A. Contreras, Appl. Phys. Lett. **93**, 022110-1–022110-3 (2008).

[7]W. K. Metzger, I. L. Repins, M. Romero, P. Dippo, R. N. Contreras, and D. Levi, Thin Solid Films **517**, 2360–2364 (2009).

[8]T. Sakurai, K. Taguchi, M. M. Islam, S. Ishiuuka, A. Yamada, K. Matsubara, S. Niki, and K. Akimoto, Jpn. J. Appl. Phys., Part I **50**, 05FC01 (2011).

[9]S. Shirakata, K. Ohkubo, Y. Ishii, and T. Nakada, Sol. Energy Mater. Sol. Cells **93**, 988 (2009).

[10]M. L. Timmons, T. S. Colpitts, R. Venkatasubramanian, B. M. Keyes, D. J. Dunlavy, and R. K. Ahrenkiel, Appl. Phys. Lett. **56**, 1850 (1990).

[11]R. K. Ahrenkiel, in *Minority Carriers in III-V Semiconductors: Physics and Applications* (Academic Press, Inc., 1993), Vol. 39, Chap. 2, pp. 39–150.

[12]W. K. Metzger, R. K. Ahrenkiel, J. Dashdorj, and D. J. Friedman, Phys. Rev. B **71**, 035301-1–035301-9 (2005).

[13]A. Kanevce, D. H. Levi, and D. Kuciauskas, Prog. Photovoltaics (2013).

[14]A. B. Sproul, J. Appl. Phys. **76**, 2851–2854 (1994).

5.2 Voltage dependent TRL for solar cell characterization

At the end of the preceding section it has been pointed out that the properties of a solar cell's absorber may change during the subsequent processing. In that case, an absorber characterization is advisable at the end of the cell preparation. However, the results in the previous section show that the luminescence decay may then be determined by recombination and charge carrier storage, and in particular by charge carrier drift. For this reason, the TRL of the solar cell will reveal the recombination in the absorber only in particular cases. Besides, the impact of drift on the TRL can hardly be estimated, because the electric field is determined by the stored charge carriers whose number in turn depends on the mobilities, the recombination lifetimes, the injection level, and the frequency of excitation. It is worth mentioning, that the latter is revealed by an increase of the photovoltage with increasing frequency as demonstrated in [Mai5], which is in accordance with the simulations presented in [Mai2]. This is also unveiled in the TRL transients by a slower decay at higher frequencies due to the increased amount of charge carriers screening the electric field [11, 22]. Altogether this means that the state of the solar cell is almost undetermined, which makes the analysis of TRL decays nearly impossible.

For this reason, the demand raised for the avoidance of charge storage in solar cells by the drain of the charge carriers. In [Mai5, Mai6] it is shown that this is achieved by electrical contacting of the cell. The electric field then is not screened and thus well-defined. With that, the TRL is also unaffected by charge storage. In particular, it is not influenced by mediated effects such as the dependence on the excitation frequency [Mai5]. The electrical contacting additionally allows a regulation of the electric field in order to study the drift of the charge carriers. This was already shown rudimentarily by Shirakata et. al. [9], who compared the TRL of a solar cell under short-circuit and open-circuit conditions. In this work, the voltage has been increased more systematically. The measurements reveal a bi-exponential decay of the luminescence. The fast initial decay depends on the voltage, whereas the second slow decay is nearly independent from the voltage. This is illustrated by figure 5.3. At the very beginning, the charge carrier densities are high making the semiconductor intrinsic. Therefore, the space charge region is expected to vanish. However, the potential drop across the solar cell must persist due to the fixed bias voltage (see figure 5.3 (a)). Because of the resulting electric field, the first decay time is mostly influenced by the drift and the drain of the charge carriers. If the voltage is increased, the potential drop will be reduced leading to a smaller electric field (see figure 5.3 (b)). This weakens the drift and drain of the charge carriers and the decay time increases. By time, the density of charge carriers decreases and the p-doped state of the absorber is reestablished. Then, the electric field is again confined to the equilibrium space charge region (see Fig. 5.3 (c)) and the luminescence is dominated by recombination in the quasi-neutral region. Since there is no electric field, the time constant of this second decay reveals the
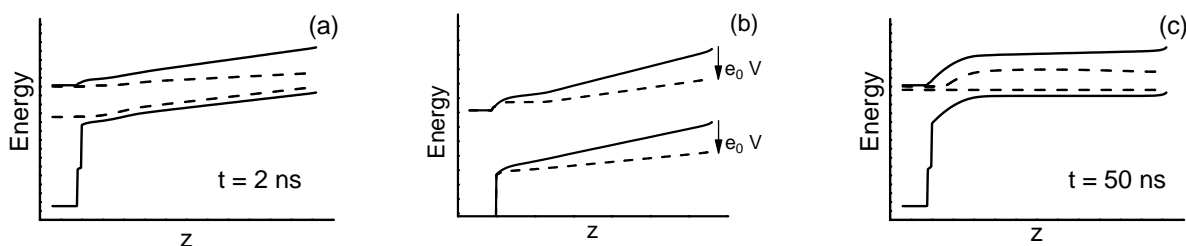
Figure 5.3: (a) Band energies (solid lines) and quasi-Fermi levels (dashed lines) in a solar cell under short-circuit conditions (a) 2 ns after excitation and (c) 50 ns after excitation. The subfigure (b) shows the band energies in the absorber 2 ns after the excitation for an applied voltage $V = 0$ (solid lines) and $V > 0$ (dashed lines).

recombination in the absorber, which is independent from the applied voltage.

In [Mai5, Mai6], an analytical expression for the voltage dependence of the initial decay time has been calculated presuming a homogeneous electric field. By fitting of this function to experimental data, recombination lifetimes and mobilities have been determined. The values of both quantities are not ambiguos, which has been discussed in [Mai6]. It is remarkable that a simulation of the TRL with these values yields decay curves that approximate the experimental TRL very well. For these reasons, the TRL under bias voltages comes out as a powerful method for the characterization of absorbers in solar cells. Furthermore, the non-correlation of the decay time and the solar cell parameters can be (at least partly) circumvented. Therefore, from the list at the beginning of this chapter only two problems remain; namely the origin of multi-exponential TRL decays and the reason for decay times in the range of the radiative limit. Both will be discussed in the next section.

Electrical characterization of Cu(In,Ga)Se$_2$-solar cells by voltage dependent time-resolved photoluminescence

Matthias Maiberg *, Conrad Spindler, Enrico Jarzembowski, Roland Scheer

Institute of Physics, Martin-Luther-University Halle-Wittenberg, 06120 Halle, Germany

ARTICLE INFO

ABSTRACT

Time-resolved photoluminescence (TRPL) is a promising method for the investigation of charge carrier dynamics and recombination kinetics in semiconductor devices. To characterize Cu(In,Ga)Se$_2$ (CIGSe) solar cells, we measured TRPL for different applied external forward voltages. We show that the TRPL decay time increases with increasing voltage in case of a high excitation intensity. This result is valid for a wide range of excitation frequencies of the laser. By simulation of the measured transients we determined semiconductor parameters which allow fitting the experimental photoluminescence transients for different voltages. The deduced quantities are the lifetime for deep defect assisted Schockley–Read–Hall recombination, doping density and charge carrier mobilities of the solar cell's absorber layer with values of 10 ns, 2×10^{15} cm^{-3} and 1 cm^2 V^{-1} s^{-1}, respectively, for a standard CIGSe solar cell. We further studied the appearance of a photovoltage in TRPL experiments with single-photon-counting methods. By experimental results we show a dependence of the open circuit voltage on the laser repetition rate, which influences the TRPL decay.

© 2014 Elsevier B.V. All rights reserved.

1. Introduction

Cu(In,Ga)Se$_2$ (CIGSe) has become a competitive absorber material for thin film solar cells. Though such CIGSe solar cells already exhibit efficiencies above 20% [1], important material parameters such as the minority carrier lifetime and the charge carrier mobilities are not accurately known. Hall measurements [2] on p-type CIGSe, for instance, bring out hole mobilities of $1 - 20$ cm^2 V^{-1} s^{-1} whereas time-of-flight measurements [3] lead to hole mobilities of $0.02 - 0.7$ cm^2 V^{-1} s^{-1}. The electron mobility, on the other hand, was determined to be $75 - 230$ cm^2 V^{-1} s^{-1} by time-resolved photoluminescence [2] and $0.02 - 0.05$ cm^2 V^{-1} s^{-1} by time-of-flight measurements [3].

Time-resolved photoluminescence (TRPL) under forward bias voltages may be a method for simultaneous determination of charge carrier mobilities and the minority carrier lifetime of a solar cell's absorber. To this end, we first study TRPL of an industrially prepared solar cell under open circuit conditions and under external bias voltages for different excitation frequencies. Then, we show by simulation that the electric field in the solar cell's space charge region can be varied by orders of magnitude compared to equilibrium by the application of a forward bias voltage and high excitation intensities meaning the photogenerated carrier density is in the range or above the absorber doping density. Therefore, the influence of charge carrier drift on the photoluminescence is varied.

Finally, we give experimental results on TRPL for different bias voltages of the industrial solar cell. By simulation and experimental results we determine the mobilities for electrons and holes of the solar cell's absorber layer.

2. Experimental

For measurement of TRPL at room temperature we use the setup shown schematically in Fig. 1. For excitation a pulsed diode laser with an excitation wavelength of 638 nm, a pulse length of 88 ps and a repetition frequency of $0.02 - 20$ MHz is used. The maximum pulse energy is 12.5 pJ which corresponds to 4×10^7 photons per pulse. The laser light is focused on the sample by a collecting lens (L$_1$) with a focus area of $A = (6.0 \pm 2.0) \times 10^{-5}$ cm^2. Hence, the maximum incident photon density per pulse is $n_\lambda = (6.7 \pm 2.3) \times 10^{11}$ cm^{-2}. By a second lens (L$_2$) the luminescence photons are collected and directed on a photomultiplier. To avoid detection of laser light, a long-pass filter with a cutoff wavelength of 850 nm in front of the detector was used. For time-correlated single photon counting the signal of the detector is analyzed by a PCI-card, which has a minimum channel width of 28 ps. However, the minimum time resolution is limited by the instrument response function and is about 700 ps for a chosen excitation frequency of 1 MHz. This frequency provides a good signal-to-noise ratio as well as sufficient long periods for a complete decay of luminescence for multi-pulse excitation. Since only one sample is studied, the quantum yield does not strongly change. Hence, a normalization of the transient's maxima for better comparison of the TRPL decay is justified.

* Corresponding author. Photovoltaics Group, Institut of Physics, Martin-Luther-University Halle-Wittenberg, Von-Danckelmann-Platz 3, 06120 Halle, Germany.
E-mail address: matthias.maiberg@physik.uni-halle.de (M. Maiberg).
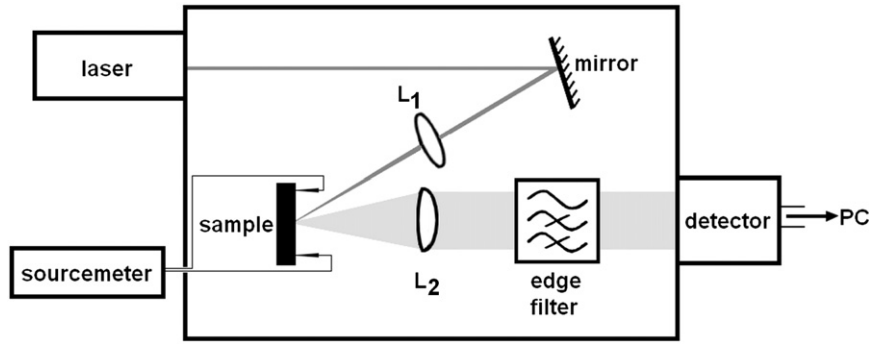
Fig. 1. Scheme of the setup for measurement of voltage-dependent transient photoluminescence.

2.1. Sample preparation

We study TRPL on an industrially produced absorber layer. Molybdenum as the back contact was sputtered on soda-lime glass. Thereon, the CIGSe absorber was deposited by a two-stage co-evaporation process with a final absorber thickness of 2.0 μm. CdS as a 50 nm thick buffer layer was deposited on the absorber layer by chemical bath deposition. The window layer of 100 nm thick intrinsic ZnO and 300 nm thick aluminum-doped ZnO was sputtered on the CdS layer.

2.2. Model for simulation

The simulation of voltage-dependent TRPL was done with Synopsys TCAD®. The simulations were one-dimensional. With the experimental focus area given above, lateral effects can be neglected. Since recombination velocities at the absorber/buffer and the absorber/Molybdenum interface are not conclusively known [4–6] interface recombination is considered by an effective bulk lifetime τ_{SRH} for deep defect assisted Shockley–Read–Hall (SRH) recombination. Since further experiments have revealed a Gallium gradient, we considered a V-shaped band gap gradient [7] with parameters as given in Table 1. To fit experimental photoluminescence the simulated data are convoluted with a Gaussian-shaped instrument response function. The most important simulation parameters are given in Table 1. The simulated incident photon density is about a third of the experimental photon density. In experiment, the intensity distribution has a Gaussian shape, whereas the intensity is homogeneous in simulation. Hence, there is no direct relation between experimental and theoretical photon densities. The excitation parameters lead to a maximum generated excess carrier density of $\Delta n_{max} = \Delta p_{max} = 2 \times 10^{16}$ cm^{-3}. Therefore, flat defects with densities up to 10^{15} cm^{-3} are saturated and are not considered in the

simulations. Additionally, it will be shown by experimental results that the luminescence's decay for forward bias voltages is not influenced by the frequency of excitation. In this case it is sufficient to simulate an excitation by only one laser pulse.

3. Results and discussion

3.1. Solar cells under open circuit

First, we consider a solar cell under open circuit conditions that is excited by one laser pulse. The photogenerated electrons and holes are separated by the electric field and remain at the edges of the space charge region. The charge carriers cannot recombine radiatively, since they are locally separated. This leads to a decrease of the photoluminescence intensity. The time for charge separation depends on the drift velocity, thus depending on the charge carrier mobility and the electric field strength. For a high electric field the drift velocity is large leading to a small charge separation time and hence to a fast decay of the luminescence intensity [8,9]. With each pulse, more charge carriers are stored at the edges of the space charge region. Therefore, a photovoltage builds up and the electric field becomes screened, causing a diminished charge separation time and an inhibited luminescence decay.

The number of charge carriers at the edges of the space charge region depends on excitation parameters, e.g. excitation intensity and repetition frequency, and also on the minority carrier lifetime [9]. Thus, the photovoltage and the TRPL decay depend on the repetition frequency as shown for the solar cell in Fig. 2.

Since the open circuit voltage depends on excitation parameters, the electrical boundary conditions are not accurately defined. Therefore,

Table 1
Main parameters used for simulation of TRPL.

Simulation parameter	Value
Window doping $N_{D,w}$	10^{18} cm^{-3}
Buffer doping $N_{D,b}$	4×10^{16} cm^{-3}
Absorber doping $N_{A,a}$	2×10^{15} cm^{-3}
Window thickness d_w	300 nm
Buffer thickness d_b	50 nm
Absorber thickness d	2 μm
Incident photon density n_γ	1.95×10^{11} cm^{-2}
Incident photon wavelength λ	638 nm
Absorber's absorption coefficient α	8 μm^{-1}
Absorber charge carrier lifetime τ_{SRH}	8 ns
Absorber charge carrier mobility μ_n, μ_p	0.9 cm^2 V^{-1} s^{-1}
Recombination at all interfaces S	0
Absorber minimum bandgap E_g	1.18 eV
Front band gap gradient ΔE_f	20 MeV
Back band gap gradient ΔE_b	40 MeV
Notch distance from buffer d_n	50 nm

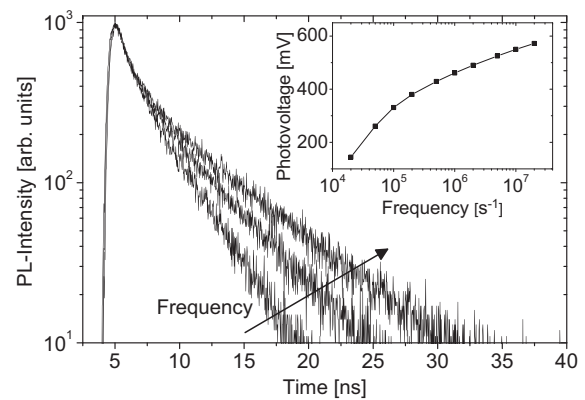**Fig. 2.** TRPL transients of a solar cell for a fixed pulse energy and repetition frequencies of 10^5, 10^6 and 10^7 s^{-1}. The inset shows the photovoltage for different excitation frequencies.
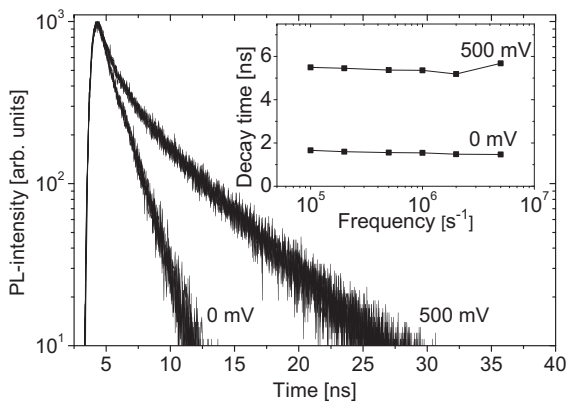
TRPL experiments with fixed forward bias voltages are considered in the following.
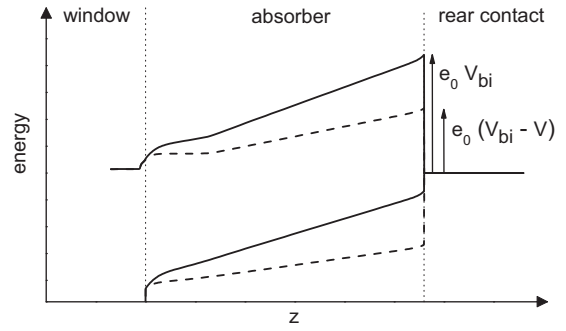
3.2. Solar cells under short circuit

Now, we consider a solar cell under short circuit conditions. Again, for each laser pulse the generated charge carriers are separated by the electric field. Since we are in the short circuit case, the charge carriers do not remain at the edges of the space charge region, but flow out of the cell. Hence, the electric field of the space charge region is unscreened and no photovoltage is build up. Therefore, the TRPL decay is independent of the number of laser pulse excitations and hence independent of the excitation frequency. This can be seen in Fig. 3. The independence of the repetition frequency and clearly-defined electrical boundary conditions are the advantages of TRPL under forward bias voltage, since it makes time-resolved photoluminescence experiments with single photon counting methods comparable.

3.3. Solar cells under forward bias voltages

Finally, we consider a solar cell under forward bias conditions that is excited by a laser pulse of high photon flux densities. Due to the high injection level the density of charge carriers generated at the front side of the absorber layer is in the range of the absorber doping density. Therefore, the space charge region becomes partly screened. Furthermore, the excess hole density at the back contact is higher than the excess electron density due to drift transport. Thus, the space charge region in the solar cell's absorber layer ranges up to the back contact. This is shown in Fig. 4 as a result of simulation. For short circuit conditions the drop of the electrical potential equals the built-in voltage V_{bi}. Since the space charge region ranges over the whole absorber layer the electric field is reduced compared to the equilibrium state by at least one order of magnitude with $E(z) \approx \frac{V_{bi}}{d}$, where d is the absorber thickness. If the applied voltage V increases, the potential drop decreases leading to a further reduced electric field $E(z) \approx \frac{V_{bi}-V}{d}$. Due to the electric field in the absorber the electrons drift toward the window layer. Contrary the holes drift to the rear contact. The separation of electrons and holes causes a luminescence decay. If the bias voltage is small (high electric field) the charge separation is very fast inducing a fast luminescence decay. For an increased forward bias voltage the electric field is decreased leading to an inhibited charge separation and hence to an increased luminescence decay time. Fig. 5 shows the TRPL transients at room temperature under increasing bias voltages. In agreement with expectation, the decay time becomes larger for increasing voltage bias. Using the

Fig. 4. Conduction and valence band in the absorber layer about 5 ns after excitation for short circuit case (solid) and 0.5 V (dashed). V_{bi} denotes the built-in voltage.
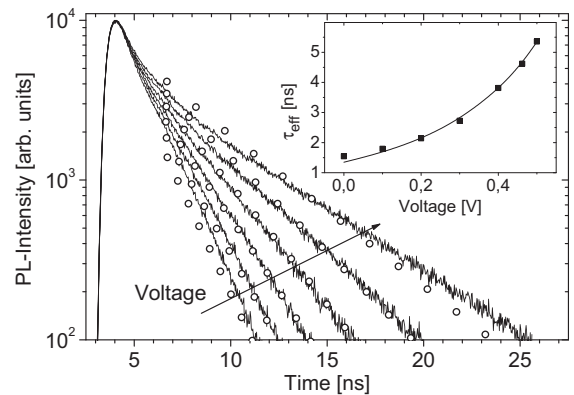
parameters listed in Table 1, the simulation fits the experimental data for $\mu_n = \mu_p = 0.9$ cm^2 V^{-1} s^{-1} and $\tau_b = 8$ ns. Deviations in the very initial decay may be caused by different instrument response functions in experiment and simulation besides the above-mentioned inaccurate photon density.

In order to describe the voltage dependence of the luminescence decay time τ_{eff} we have to solve the continuity equations of electrons and holes including drift, diffusion, mono- and bimolecular recombination. In the following this is done roughly for the electron continuity equation without deeper mathematical analysis. As shown in Ref. [9] the carrier density can be well-described by solving the continuity equation without any recombination and using the result as an initial value for the recombination equation. Therefore, we first solve the drift-diffusion-equation

$$\frac{\partial}{\partial t}n - \frac{\partial}{\partial z}\left(\mu_n\, n\, E + D_n\, \frac{\partial}{\partial z}n\right) = 0. \tag{1}$$

Here, D_n denotes the diffusion coefficient of electrons. The bias voltage is assumed to be small (large electric fields). Then, the dark current can be neglected. Furthermore, the electric field strength E as well as the absorber material properties is quite homogeneous according to the considerations above. Hence, it follows from Eq. (1)

$$\frac{\partial}{\partial t}n - \mu_n\, E\, \frac{\partial}{\partial z}n - D_n\, \frac{\partial^2}{\partial z^2}n = 0. \tag{2}$$

Fig. 3. TRPL transients of a solar cell for forward bias voltages of 0 and 500 mV, for repetition frequencies of 10^5, 2×10^5, 5×10^5, 10^6, 2×10^6 and 5×10^6 s^{-1}. The inset shows an almost constant PL decay time independent of excitation frequency.

Fig. 5. Experimental (lines) and simulated (dots) TRPL transients of a solar cell for external voltages of 0, 0.1, 0.2, 0.3, 0.4, 0.5 V. The inset shows the increase of the TRPL decay time with increasing forward voltages and a fit of these data by a function as given by Eq. (11).

A separation ansatz for Eq. (2) leads to the following representation of the solution:

$$n(t,z) = e^{-\frac{\mu_n E}{2 D_n} z} \sum_k \left(A_k \cos\left(\frac{\widetilde{C}_k z}{2 D_n}\right) + B_k \sin\left(\frac{\widetilde{C}_k z}{2 D_n}\right) \right) e^{-C_k t} \tag{3}$$

$$\widetilde{C}_k = \sqrt{4 D_n C_k - E^2 \mu_n^2} \neq 0.$$

The constants A_k, B_k and C_k have to be determined from initial values and boundary conditions. We choose the following boundary conditions for the electron current density:

$$j_n|_{z=d} \approx -\mu_n E n|_{z=d} = 0 \tag{4}$$

$$j_n|_{z=0} = v_{th,n} n|_{z=0}. \tag{5}$$

Eq. (5) means, that the electron supply from the window into the absorber is limited by the thermal velocity of electrons $v_{th,n}$. Conditions (Eq. (4)) mean, drift transport dominates the electron current due to a high electric field. The current in turn vanishes because of a passivated back contact. Combination of Eqs. (3), (4) and (5) leads to the following equation for the decay constants $0 < \widetilde{C}_1 < \widetilde{C}_2 < \ldots$

$$\tan\left(\frac{d \widetilde{C}_k}{2 D_n}\right) = \frac{\widetilde{C}_k}{2\left(E \mu_n - v_{th,n}\right)}. \tag{6}$$

The dominating decay of the electron density is determined by the smallest decay constant $\widetilde{C}_1$. By the approximation $\tan x \approx \frac{8}{\pi^2} x \frac{\pi - x}{\pi - 2 x} \ \forall x \in [0, \pi]$ (compare Ref. [9]) we find for large electric fields

$$\widetilde{C}_1 \approx \frac{2 D_n \pi}{d}$$
$$\Rightarrow C_1 \approx \frac{D_n \pi^2}{d^2} + \frac{\mu_n^2}{4 D_n} E^2 \approx \frac{\mu_n^2}{4 D_n} E^2. \tag{7}$$

$C_1 \approx \frac{\mu_n^2}{4 D_n} E^2 =: \frac{1}{\tau_{s,n}}$ describes the dominating decay of the electron density due to drift and diffusion. Inserting Eq. (3) into the recombination equation, the effective electron decay time $\tau_{eff,n}$ becomes

$$\frac{1}{\tau_{eff,n}} = \frac{1}{\tau_{b,n}} + \frac{1}{\tau_{s,n}} = \frac{1}{\tau_{b,n}} + \frac{\mu_n^2}{4 D_n} E^2 \tag{8}$$

with the electron bulk lifetime $\tau_{b,n}$. In principle, the transport is the same for electrons and holes. Therefore we find for holes

$$\frac{1}{\tau_{eff,p}} = \frac{1}{\tau_{b,p}} + \frac{1}{\tau_{s,p}} = \frac{1}{\tau_{b,p}} + \frac{\mu_p^2}{4 D_p} E^2. \tag{9}$$

The decay time of the electron and the hole density can now be used to estimate the decay of the luminescence intensity. Since we have bimolecular recombination due to high injection levels the rate of radiative recombination R_{rad} is

$$R_{rad} \sim n \ p \sim e^{-\frac{t}{\tau_{eff,n}}} e^{-\frac{t}{\tau_{eff,n}}}$$
$$\Rightarrow \frac{1}{\tau_{eff}} = \frac{1}{\tau_{eff,n}} + \frac{1}{\tau_{eff,p}}. \tag{10}$$

Rewriting Eq. (10) by $E \approx \frac{V_{bi} - V}{d}$ and the Einstein relation $D = V_T \mu$ ($V_T \approx 25$ mV for room temperature) yields

$$\frac{1}{\tau_{eff}} = \frac{1}{\tau_{b,n}} + \frac{1}{\tau_{b,p}} + \frac{\mu_n + \mu_p}{4 V_T d^2} (V_{bi} - V)^2. \tag{11}$$

Therefore, measuring the effective decay time τ_{eff} for different applied voltages V and fitting the data by the expression in Eq. (11) allow the determination of the bulk lifetime and the charge carrier mobility. The fit of the data which is shown in the inset of Fig. 5 leads to a bulk lifetime $\tau_{b,n} + \tau_{b,p} = 32$ ns and a charge carrier mobility $\mu_n < \mu_n + \mu_p = 3.2$ cm^2 V^{-1} s^{-1}. For symmetric carrier capture by deep defects it is $\tau_{b,n} = \tau_{b,p} = 16$ ns. This is in good agreement with the simulation.

Both, simulation and analytics, assume linear-shaped energy bands directly after excitation. In the presence of potential fluctuations this is still valid, since local space charges are screened for high excitation intensities.

4. Conclusion

In summary, we have presented photoluminescence decay of a solar cell under open circuit conditions and for different forward bias voltages. For a cell under open circuit a dependence of the photovoltage on the excitation frequency exists, which makes comparison and analysis of different TRPL experiments difficult. For a cell under forward bias voltage the TRPL decay does not depend on the excitation repetition frequency. Furthermore, we found by simulation that the electric field in the solar cell's space charge region is reduced due to high excitation intensities by at least one order of magnitude. Therefore, charge separation can be observed with TRPL. By comparison with simulated TRPL data we found for the carrier mobilities for electrons and holes $\mu_n = \mu_p \approx 0.9$ cm^2 V^{-1} s^{-1} and a bulk lifetime of $\tau_b \approx 20$ ns. However, by analytics we found $\mu_n + \mu_p < 3.2$ cm^2 V^{-1} s^{-1} and $\tau_b \approx 10$ ns. Both, simulations and analytics are in good agreement. Further simulations revealed that these values are unambiguous.

References

[1] M.A. Green, K. Emery, W. Warta, Y. Hishikawa, E.D. Dunlop, Solar cell efficiency tables (version 43), Prog. Photovolt. Res. Appl. 22 (2014) 1.
[2] D. Kuciauskas, J.V. Li, M.A. Contrera, J. Pankow, P. Dippo, Charge carrier dynamics and recombination in graded band gap CuIn$_{1 - x}$Ga$_x$Se$_2$ polycrystalline thin-film photovoltaic solar cell absorbers, J. Appl. Phys. 114 (2013) 154505-1.
[3] S.A. Dinca, E.A. Schiff, W.N. Shafarman, B. Egaas, R. Noufi, D.L. Young, Electron drift-mobility measurements in polycrystalline CuIn$_{1 - x}$Ga$_x$Se$_2$ solar cells, Appl. Phys. Lett. 100 (2012) 103901-1.
[4] W.K. Metzger, I.L. Repins, M. Romero, P. Dippo, R.N. Contreras, D. Levi, Recombination kinetics and stability in polycrystalline Cu(In, Ga)Se$_2$ solar cells, Thin Solid Films 517 (2009) 2360.
[5] W.K. Metzger, I.L. Repins, M.A. Contreras, Long lifetimes in high-efficiency Cu(In, Ga) Se$_2$ solar cells, Appl. Phys. Lett. 93 (2008) 022110-1.
[6] S. Shirakata, T. Nakada, Time-resolved photoluminescence in Cu(In, Ga)Se$_2$ thin films and solar cells, Thin Solid Films 515 (2007) 6151.
[7] W. Witte, D. Abou-Ras, K. Albe, G.H. Bauer, F. Bertram, C. Boit, R. Brüggemann, J. Christen, J. Dietrich, A. Eicke, D. Hariskos, M. Maiberg, R. Mainz, M. Meessen, M. Müller, O. Neumann, T. Orgis, S. Paetel, J. Pohl, H. Rodriguez-Alvarez, R. Scheer, H.-W. Schock, T. Unold, A. Weber, M. Powalla, Gallium gradients in Cu(In, Ga) Se$_2$ thin-film solar cells, Prog. Photovolt. Res. Appl. (2014) 1.
[8] W.K. Metzger, R.K. Ahrenkiel, J. Dashdorj, D.J. Friedman, Analysis of charge separation dynamics in a semiconductor junction, Phys. Rev. B 71 (2005) 035301-1.
[9] M. Maiberg, R. Scheer, Theoretical study of time-resolved luminescence in semiconductors. 2. pulsed excitation, J. Appl. Phys. 116 (12) (2014), http://dx.doi.org/10.1063/1.4896484.

Characterization of Cu(In,Ga)Se$_2$-solar cells by voltage dependent time-resolved photoluminescence

Matthias Maiberg,[1] Conrad Spindler,[1] Enrico Jarzembowski,[1] and Roland Scheer[1]

Institute of Physics, Martin-Luther-University Halle-Wittenberg, 06120 Halle, Germany

Time-resolved photoluminescence (TRPL) can give information on charge carrier dynamics and recombination kinetics in semiconductor devices. To characterize Cu(In,Ga)Se$_2$ (CIGSe) solar cells, we measured TRPL for different applied external forward voltages. We show that the TRPL decay time increases with increasing voltage in case of a high excitation intensity. By simulation of the measured transients we determined a set of parameters which allow to fit the experimental photoluminescence transients for different voltages. These parameters are the lifetime for deep defect assisted Schockley-Read-Hall recombination, the doping density and the charge carrier mobilities (electrons and holes) of the solar cell's absorber layer with values of 20 ns, 3×10^{15} cm^{-3} and 2 cm^2 V^{-1} s^{-1}, respectively, for a standard CIGSe solar cell. By further simulations we show that the determined lifetime and mobility values are unambiguous.

Cu(In,Ga)Se$_2$ (CIGSe) has become a competitive absorber material for thin film solar cells. Though such CIGSe solar cells already exhibit efficiencies up to 20.8%[1], important material parameters such as the minority carrier lifetime and the charge carrier mobilities are not accurately known. Hall measurements[2] on p-type CIGSe, for instance, bring out hole mobilities of $1 - 20$ cm^2 V^{-1}s^{-1} whereas time-of-flight measurements[3] lead to hole mobilities of $0.02 - 0.7$ cm^2 V^{-1}s^{-1}. The electron mobility, on the other hand, was determined to be $75 - 230$ cm^2 V^{-1}s^{-1} by time-resolved photoluminescence[2] and $0.02 - 0.05$ cm^2 V^{-1}s^{-1} by time-of-flight measurements.[3]

Time resolved photoluminescence (TRPL) may be a method that can be used for simultaneous determination of charge carrier mobilities and the minority carrier lifetime of the absorber. By application of an external forward voltage and by high excitation intensities the electric field in the solar cell's space charge region can be varied, thus, varying the influence of charge carrier drift on the photoluminescence. We give experimental results on TRPL for different bias voltages of the solar cell. By simulation, mathematical analysis and experimental results we determine the mobilities for electrons and holes of the solar cell's absorber layer. Finally, we show by simulations that the determination of charge carrier mobility and charge carrier lifetime is unambiguous if the charge carrier mobility is between 0.01 cm^2 V^{-1} s^{-1} and 20 cm^2 V^{-1} s^{-1} and if the minority carrier lifetime is greater than 10 ns.

For measurement of TRPL at room temperature we use the setup shown schematically in figure 1. For excitation a pulsed diode laser with an excitation wavelength of 638 nm, a pulse length of 88 ps and a repetition frequency of 1 MHz is used. The maximum pulse energy is 12.5 pJ. The laser light is focused on the sample by a collecting lens (L$_1$) with a focus area of $A = (6.0 \pm 2.0) \times 10^{-5}$ cm^2. Hence, the maximum incident photon density per pulse
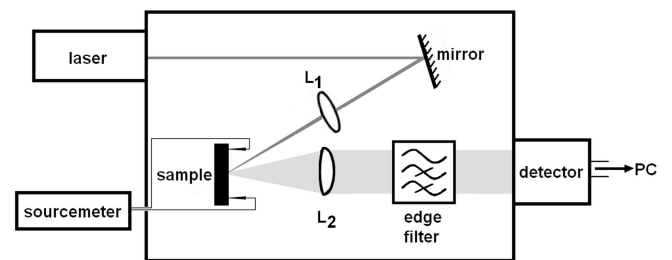

FIG. 1. Scheme of the setup for measurement of voltage dependent transient photoluminescence.

is $n_\lambda = (6.7 \pm 2.3) \times 10^{11}$ cm^{-2}. By a second lens (L$_2$) the luminescence photons are collected and focused on a photomulitplier. To avoid detection of laser light, a long-pass filter with a cutoff wavelength of 850 nm in front of the detector was used. For time-correlated single photon counting the signal of the detector is analyzed by a PCI-card, which has a minimum channel width of 28 ps. However, the minimum time resolution is limited by the instrument response function and is about 700 ps. For better comparison of the TRPL decay the transient's maxima are normalized.

The absorber layer of the solar cell was prepared by a three-stage co-evaporation process on a Molybdenum back contact sputtered on soda-lime glass. The final $\frac{[Ga]}{[Ga]+[In]}$-ratio was 0.3, the final $\frac{[Cu]}{[Ga]+[In]}$-ratio was 0.91 and the final absorber thickness was 2.8 µm. CdS as a 50 nm thick buffer layer was deposited on the absorber layer by chemical bath deposition. The window layer of 100 nm thick intrinsic ZnO and 300 nm thick aluminium doped ZnO was sputtered on the CdS layer. Finally, an Ni/Al-grid was deposited by electron beam evaporation. The simulation of voltage dependent TRPL was done with Synopsys TCAD®. The simulations were onedimensional. With the experimental focus area above lateral effects can be neglected. Since re-

simulation parameter	value
window doping $N_{D,w}$	10^{18} cm^{-3}
buffer doping $N_{D,b}$	4×10^{16} cm^{-3}
absorber doping $N_{A,a}$	3×10^{15} cm^{-3}
window thickness d_w	300 nm
buffer thickness d_b	50 nm
absorber thickness d	2.8 µm
incident photon density n_γ	2.77×10^{11} cm^{-2}
incident photon wavelength λ	638 nm
absorber's absorption coefficient α	8 µm^{-1}
absorber charge carrier lifetime τ_{SRH}	21 ns
absorber charge carrier mobility μ_n, μ_p	1.95 cm^2 V^{-1} s^{-1}
recombination at all interfaces S	0
absorber minimum bandgap E_g	1.15 eV
front band gap gradient ΔE	60 meV
back band gap gradient ΔE	120 meV
notch distance from buffer d_n	650 nm

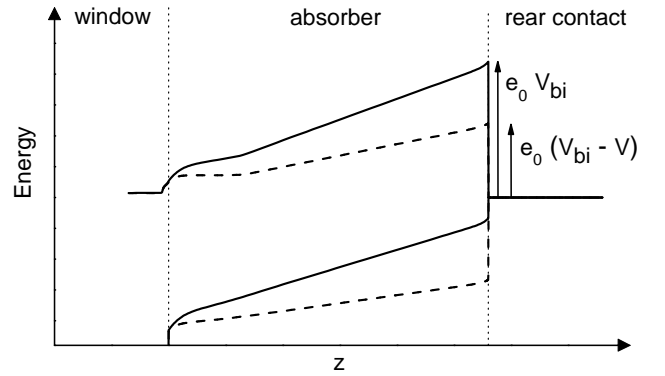TABLE I. Main parameters used for simulation of TRPL.

FIG. 2. Conduction and valence band in the absorber layer about 5 ns after excitation for short circuit conditions (solid) and for an applied voltage of 0.5 V (dashed). V_{bi} denotes the built-in voltage.

combination velocities at the absorber/buffer and the absorber/Molybdenum interface are not conclusively known[4–6] interface recombination is turned off, but is considered by an effective bulk lifetime τ_{SRH} for deep defect assisted SRH-recombination. Since further experiments on absober layers have revealed a Gallium gradient, we considered a V-shaped band gap gradient with parameters as given in table I.[7] To fit experimental photoluminescence the simulated data are convoluted with a Gaussian shaped instrument response function. The most important simulation parameters are given in table I. The incident photon density in the simulations is about a half of the experimental photon density. In experiment, the intensity distribution has a Gaussian shape, whereas the intensity is homogeneous in simulation. Hence, there is no direct relation between experimental and theoretical photon density. The excitation parameters lead to a maximum generated excess carrier density of $\Delta n_{max} = \Delta p_{max} = 2 \times 10^{16}$ cm^{-3}. Therefore, flat defects with densities up to 10^{15} cm^{-3} are saturated and are not considered in the simulations. Additionally, further experiments and simulations have shown, that the luminescence's decay is not influenced by the frequency of excitation.[8] Hence, it is sufficient to simulate an excitation by only one laser pulse.

First, we consider a solar cell under short circuit conditions that is excited by a laser pulse of high photon flux densities. Due to the high injection level the density of charge carriers generated at the front side of the absorber layer is in the range of the absorber doping density. Therefore, the space charge region becomes partly screened. Furthermore, the excess hole density at the back contact is higher than the excess electron density due to drift transport. Thus, the space charge region in the solar cell's absorber layer ranges up to the back contact. This is shown in figure 2. In the short circuit case the drop of the electrical potential equals the built-in voltage V_{bi}. Since the space charge region ranges over the whole absorber layer the electric field is reduced

compared to the equilibrium state by at least one order of magnitude with $E(z) \approx \frac{V_{bi}}{d}$, where d is the absorber thickness. If the applied voltage V increases, the potential drop decreases leading to a further reduced electric field $E(z) \approx \frac{V_{bi}-V}{d}$. Due to the electric field in the absorber the holes drift to the rear contact and contribute to the photocurrent. Accordingly, the electrons are collected by the emitter. The separation of electrons and holes reduces the number of recombination partners. This causes a luminescence decay. If the bias voltage is small (high electric field) the charge separation is very fast inducing a fast luminescence decay. For an increased forward bias voltage the electric field is decreased leading to an inhibited charge separation and hence to an increased luminescence decay time. Figure 3 shows experimental TRPL transients at room temperature under increasing bias voltages. In agreement with expectation, the decay time becomes larger for increasing voltage bias. Using the parameters listed in table I, the model fits the experimental data for $\mu_n = \mu_p = 1.95$ cm^2 V^{-1} s^{-1} and $\tau_b = 21$ ns. In order to describe the voltage dependence of the luminescence decay time τ_{eff} we have to solve the continuity equations of electrons and holes including drift, diffusion, mono- and bimolecular recombination. In the following this is roughly done for the electron continuity equation without any deep mathematical analysis. As shown in Ref.[9] the carrier density can be well described by solving the continuity equation without any recombination and using the result as an initial value for the recombination equation. Therefore, we first solve the drift-diffusion-equation

$$\frac{\partial}{\partial t}n - \frac{\partial}{\partial z}\left(\mu_n\, n\, E + D_n\, \frac{\partial}{\partial z}n\right) = 0. \qquad (1)$$

Here, D_n denotes the diffusion coefficient of electrons. The bias voltage is assumed to be small (large electric fields). Then, the dark current can be neglected. Furthermore, the electric field strength E as well as the absorber material properties are quite homogeneous accord-
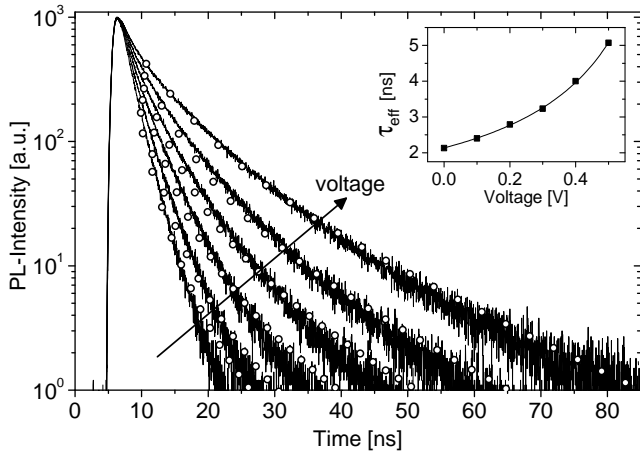
FIG. 3. Experimental and simulated TRPL transients for external voltages of 0, 0.1, 0.2, 0.3, 0.4, 0.5 V.

ing to the considerations above. Hence, it follows from equation (1)

$$\frac{\partial}{\partial t}n - \mu_n E \frac{\partial}{\partial z}n - D_n \frac{\partial^2}{\partial z^2}n = 0. \qquad (2)$$

A separation ansatz for equation (2) leads to the following representation of the solution:

$$n(t,z) = e^{-\frac{\mu_n E}{2 D_n} z} \sum_k \left(A_k \cos\left(\frac{\widetilde{C}_k z}{2 D_n}\right) + B_k \sin\left(\frac{\widetilde{C}_k z}{2 D_n}\right) \right) e^{-C_k t}$$

$$\widetilde{C}_k = \sqrt{4 D_n C_k - E^2 \mu_n^2} \neq 0. \qquad (3)$$

The constants A_k, B_k and C_k have to be determined from initial values and boundary conditions. We choose the following boundary conditions for the electron current density:

$$j_n|_{z=d} \approx -\mu_n E \ n|_{z=d} = 0 \qquad (4)$$

$$j_n|_{z=0} = v_{th,n} \ n|_{z=0}. \qquad (5)$$

Equation (5) means, that the electron supply from the window into the absorber is limited by the thermal velocity of electrons $v_{th,n}$. Conditions (4) means, drift transport dominates the electron current due to a high electric field. The current in turn vanishes because of a passivated back contact. Combination of (3), (4) and (5) leads to the following equation for the decay constants $0 < \widetilde{C}_1 < \widetilde{C}_2 < \ldots$

$$\tan\left(\frac{d \widetilde{C}_k}{2 D_n}\right) = \frac{\widetilde{C}_k}{2 \left(E \mu_n - v_{th,n} \right)}. \qquad (6)$$

The dominating decay of the electron density is determined by the smallest decay constant $\widetilde{C}_1$. By the approximation $\tan x \approx \frac{8}{\pi^2} x \frac{\pi - x}{\pi - 2 x} \ \forall x \in [0, \pi]$ (compare Ref.[9])

we find for large electric fields

$$\widetilde{C}_1 \approx \frac{2 D_n \pi}{d}$$

$$\Rightarrow C_1 \approx \frac{D_n \pi^2}{d^2} + \frac{\mu_n^2}{4 D_n} E^2 \approx \frac{\mu_n^2}{4 D_n} E^2. \qquad (7)$$

$C_1 \approx \frac{\mu_n^2}{4 D_n} E^2 =: \frac{1}{\tau_{s,n}}$ describes the dominating decay of the electron density due to drift and diffusion. Inserting (3) into the recombination equation, the effective electron decay time $\tau_{eff,n}$ becomes

$$\frac{1}{\tau_{eff,n}} = \frac{1}{\tau_{b,n}} + \frac{1}{\tau_{s,n}} = \frac{1}{\tau_{b,n}} + \frac{\mu_n^2}{4 D_n} E^2 \qquad (8)$$

with the electron bulk lifetime $\tau_{b,n}$. In principle, the transport is the same for electrons and holes. Therefore we find for holes

$$\frac{1}{\tau_{eff,p}} = \frac{1}{\tau_{b,p}} + \frac{1}{\tau_{s,p}} = \frac{1}{\tau_{b,p}} + \frac{\mu_p^2}{4 D_p} E^2. \qquad (9)$$

The decay time of the electron and the hole density can now be used to estimate the decay of the luminescence intensity. Since we have bimolecular recombination due to high injection levels the rate of radiative recombination R_{rad} is

$$R_{rad} \sim n \, p \sim e^{-\frac{t}{\tau_{eff,n}}} e^{-\frac{t}{\tau_{eff,n}}}$$

$$\Rightarrow \frac{1}{\tau_{eff}} = \frac{1}{\tau_{eff,n}} + \frac{1}{\tau_{eff,p}}. \qquad (10)$$

Rewriting equation (10) by $E \approx \frac{V_{bi} - V}{d}$ and the Einstein relation $D = V_T \mu$ ($V_T \approx 25 \, \text{mV}$ for room temperature) yields

$$\frac{1}{\tau_{eff}} = \frac{1}{\tau_{b,n}} + \frac{1}{\tau_{b,p}} + \frac{\mu_n + \mu_p}{4 V_T d^2} \left(V_{bi} - V \right)^2. \qquad (11)$$

Therefore, measuring the effective decay time τ_{eff} for different applied voltages V and fitting the data by the expression in equation (11) allows the determination of the bulk lifetime and the charge carrier mobility. The fit of the data which is shown in the inset of figure 3 leads to a bulk lifetime $\tau_{b,n} + \tau_{b,p} = 30 \, \text{ns}$ and a charge carrier mobility $\mu_n < \mu_n + \mu_p = 1.55 \, \text{cm}^2 \, \text{V}^{-1} \, \text{s}^{-1}$. For symmetric carrier capture by deep defetcs it is $\tau_{b,n} = \tau_{b,p} = 15 \, \text{ns}$. This is in good agreement with the simulation.

Both, simulation and analytics, assume linear shaped energy bands directly after excitation. In the presence of potential fluctuations this is still valid, since local space charges are screened for high excitation intensities.

Finally, we adress the unambiguousness of the determined parameters. Charge carrier lifetime and charge carrier mobility are determined by measuring the decay time τ_{0mV} for short circuit conditions and the decay
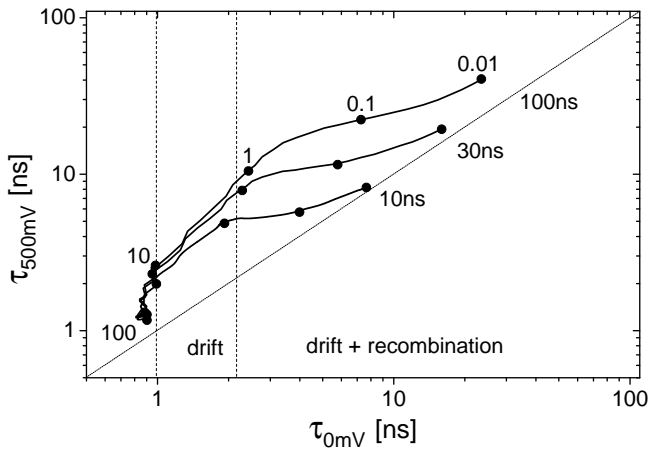
FIG. 4. Decay times τ_{0mV} for $0\,\text{V}$ and τ_{500mV} for $500\,\text{mV}$ for bulk lifetimes $\tau_b = 10, 30, 100\,\text{ns}$, charge carrier mobilites $\mu_n = \mu_p = 0.01\ldots 100\,\text{cm}^2\ \text{V}^{-1}\ \text{s}^{-1}$ and absorber thickness $d = 2.8\,\mu\text{m}$.

time τ_{500mV} for a voltage of $500\,\text{mV}$. Here, the decay time τ is defined by $I_{PL}(t_0 + \tau) = I_{PL}(t_0)/e$ and $I_{PL}(t_0) = I_{PL,max}$. To study if the map $(\tau_{0mV}, \tau_{500mV}) \to (\tau_b, \mu)$ is unique, we calculated decay times for $\tau_b = \tau_{SRH} = 10, 30, 100\,\text{ns}$ and equal mobilities for electrons and holes $\mu = 0.01\ldots 100\,\text{cm}^2\ \text{V}^{-1}\ \text{s}^{-1}$. The results are shown in figure 4. For very small mobilities ($\approx 0.01\,\text{cm}^2\ \text{V}^{-1}\ \text{s}^{-1}$) recombination of charge carriers is much faster than drift transport. Thus, the luminescence decay is independent of the carriers' drift leading to equal decay times $\tau_{0mV} \approx \tau_{500mV}$. Already for charge carrier mobilities larger than $0.02\,\text{cm}^2\ \text{V}^{-1}\ \text{s}^{-1}$, drift and recombination contribute equally to the decay time. Small deviations in the bulk lifetime cause large variations of τ_{500mV}. Furthermore, the isolines for constant bulk lifetime do not intersect. This means, charge carrier mobility and bulk lifetime can be clearly determined and with high precision from $(\tau_{0mV}, \tau_{500mV})$. If the mobility is even higher ($\approx 1\,\text{cm}^2\ \text{V}^{-1}\ \text{s}^{-1}$) the drift determines the luminescence decay and the mobility can be well determined from τ_{0mV}. However, the isolines are close together. Thus, the charge carrier lifetime can not be clearly ascertained. In this case, one can make use of the luminescence transient's shape to determine

the bulk lifetime with more accuracy. Finally, for high charge carrier mobilities $> 20\,\text{cm}^2\ \text{V}^{-1}\ \text{s}^{-1}$ we are in the limit of the time resolution and charge carrier lifetime and charge carrier mobility can not be determined.

Further simulations revealed that the simulation do not fit the experimental TRPL if the electron mobility is smaller than $1\,\text{cm}^2\ \text{V}^{-1}\text{s}^{-1}$ or larger than $3\,\text{cm}^2\ \text{V}^{-1}\ \text{s}^{-1}$. Therefore, unequal carrier mobilities are excluded by simulations.

For the experiment given in figure 3 we get $\tau_{0mV} \approx 1.8\,\text{ns}$ and $\tau_{500mV} \approx 5.5\,\text{ns}$ and conclude $\mu = 1.95\,\text{cm}^2\ \text{V}^{-1}\text{s}^{-1}$ and $\tau_b = 21\,\text{ns}$. According to the considerations above, the value of the charge carrier mobility is unique and of high precision. However, the determined charge carrier lifetime is subject to uncertainties.

In summary, we have presented photoluminescence decay of a solar cell under different forward voltages. By simulation we have shown that the electric fields are reduced due to high excitation intensities by at least one order of magnitude. Therefore, charge separation can be observed with TRPL. By comparison with simulated TRPL data we found a carrier mobility for electrons and holes of $\mu \approx 1\ldots 2\,\text{cm}^2\ \text{V}^{-1}\ \text{s}^{-1}$ and a bulk lifetime of $\tau_b \approx 20 - 30\,\text{ns}$. Further simulations revealed that these values are unambiguous.

[1] M. A. Green, K. Emery, W. Warta, Y. Hishikawa, and E. D. Dunlop, Progress in Photovoltaics: Reaseach and Applications **22** (2014).

[2] D. Kuciauskas, J. V. Li, M. A. Contrera, J. Pankow, and P. Dippo, Journal of Applied Physics **114** (2013).

[3] S. A. Dinca, E. A. Schiff, W. N. Shafarman, B. Egaas, R. Noufi, and D. L. Young, Applied Physics Letters **100** (2012).

[4] W. K. Metzger, I. L. Repins, M. Romero, P. Dippo, R. N. Contreras, and D. Levi, Thin Solid Films **517** (2009).

[5] W. K. Metzger, I. L. Repins, and M. A. Contreras, Applied Physics Letters **93** (2008).

[6] S. Shirakata and T. Nakada, Thin Solid Films **515**, 6151 (2007).

[7] W. Witte, D. Abou-Ras, K. Albe, G. H. Bauer, F. Bertram, C. Boit, R. Brüggemann, J. Christen, J. Dietrich, A. Eicke, D. Hariskos, M. Maiberg, R. Mainz, M. Meessen, M. Müller, O. Neumann, T. Orgis, S. Paetel, J. Pohl, H. Rodriguez-Alvarez, R. Scheer, H.-W. Schock, T. Unold, A. Weber, and M. Powalla, Progress in Photovoltaics: Research and Applications (2014).

[8] M. Maiberg, C. Spindler, E. Jarzembowski, and R. Scheer, Thin Solid Films , to be published.

[9] M. Maiberg and R. Scheer, Journal of Applied Physics , to be published.

5.3 The impact of minority carrier trapping

So far, the impact of drift, diffusion, bulk recombination, and surface recombination on the TRL decay have been investigated in general in [Mai1, Mai2]. It came out that the effect of drift and diffusion of charge carriers on the TRL decay can be neglected for low excitations of absorber layers. The luminescence decay time then equals the effective recombination lifetime of the minority charge carriers and Eq. (5.1.1) holds. Accordingly, a correlation between V_{oc} and τ_{decay} has been postulated and confirmed by several experiments. Furthermore, it has been found that multi-exponential decay curves occur only for high excitations or in the presence of space charges. For this reason, for absorber layers always mono-exponential decay curves are expected with decay times in the range of 10 ns (see footnote 1).

Although the above theoretical findings often have been confirmed by experiments, there are observations which are not compatible with the understanding of TRL so far. The still persisting discrepancies are:

- For absorbers often a bi-exponential luminescence decay is observed [2, 14, 61, 62].

- For absorbers often decay times beyond 100 ns occur [Mai7, 17, 19, 23].

- The decay time of the absorber does not correlate with the open-circuit voltage.

The reason for these discrepancies is twofold: Either the model is incomplete or fundamental assumptions are wrong. For instance, the assumption of zero space charges in absorber layers is incorrect, since thin-film semiconductors often are compensated and reveal electric fields due to inhomogeneities of the defect densities. These space charges may explain the bi-exponential decay curves and the non-correlation of τ_{decay} and V_{oc}. However, they may not explain decay curves with time constants above 100 ns.[20]

As another possibility, several authors propose to take minority carrier traps into consideration [2, 19]. As p-type semiconductors are studied in this work, the considered traps must be donor-like defects and close to the conduction band in accordance with the findings in section 2.4.2.[21] Therefore, at the time of generation the traps are unoccupied as illustrated in the right figure 5.4 ①. Afterwards, the electrons start to recombine. Simultaneously, they are captured by the trap, which leads to the pronounced initial decay of the luminescence with a decay time $\tau_{decay,1}$ (see ② in fig. 5.4). By time, the electron density is reduced and the conduction band becomes almost empty. The radiative recombination then is borne by electrons which are reemitted to the conduction band. This process is thermally activated and may become very slow. Consequently, the luminescence intensity is low and decays slowly with a decay time $\tau_{decay,2}$ as marked by ③ in figure 5.4.

---

[20]This will be shown in the next section 5.4.

[21]Acceptor like traps are also allowed. In that case, the trap energy must be smaller than 50 meV to comply with the trap condition (2.4.22). As shown below, such shallo defects would not affect the room-temperature TRL.
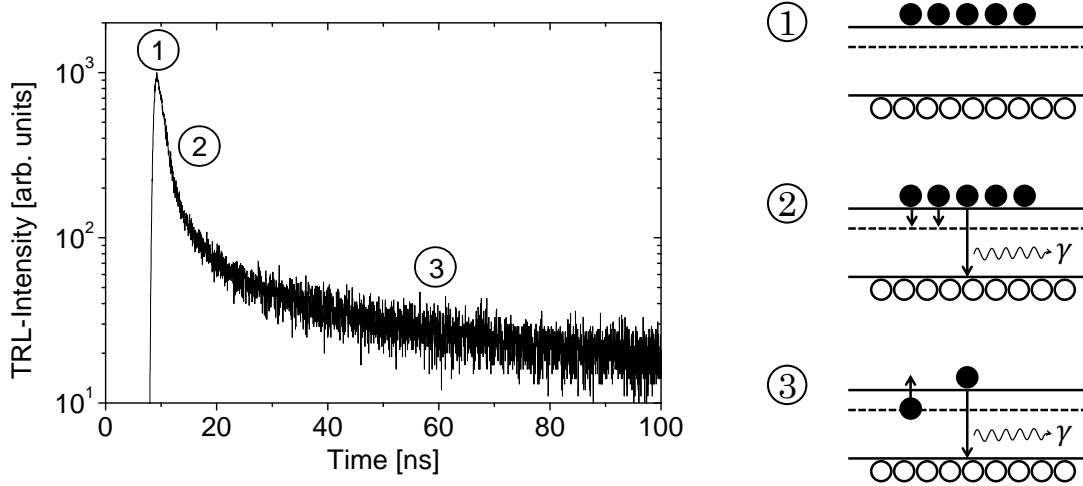
Figure 5.4: *left:* Bi-exponential luminescence decay measured on a CZTSe absorber layer. With kind permission of Stefan Hartnauer. *right:* ① Charge carriers are generated and the trap is empty of electrons. ② Electrons recombine and additionally they are captured by the trap leading to a pronounced decay. ③ The conduction band is almost empty and the radiative recombination is limited by the electron supply by emission of electrons from the trap. This can become very slow.

In [Mai3], analytical expressions for the two decay times have been obtained by solution of the rate equations (2.4.14) in the limit of low excitations:

$$\tau_{decay,1}^{-1} \approx \frac{1}{\tau_c} + \frac{1}{\tau_e} + \frac{1}{\tau_n}\left(1 - \frac{\tau_c}{\tau_e}\right) \xrightarrow{\tau_e \gg \tau_c} \frac{1}{\tau_c} + \frac{1}{\tau_n} \tag{5.3.1a}$$

$$\tau_{decay,2}^{-1} \approx \frac{\tau_c}{\tau_e}\frac{1}{\tau_n}. \tag{5.3.1b}$$

Here, τ_c is the capture time, τ_e is the emission time, and τ_n is an abbreviated symbol for $\tau_{eff,r}$. Expression (5.3.1a) is equal to the result of Ahrenkiel et al. [2]. Expression (5.3.1b), however, is not equal to his findings since he did not account for recapturing of electrons in contrast to the approach in this work.

In [Mai3], TRL decays for different τ_e and τ_c are given. It is shown that minority carrier trapping indeed may lead to bi-exponential luminescence decays of sole absorbers even under low excitations. It is demonstrated that the first decay time can become much smaller than the recombination lifetime, whereas the second decay time can become much larger than the recombination lifetime. This unveils that the recombination lifetime in the TRL decay is obscured by minority carrier traps. For the purpose of a lifetime measurement in terms of TRL, minority carrier trapping therefore must be switched off. To this end, in [Mai3] various methods have been discussed. Several authors suggest to occupy the traps using increased excitations or a bias illumination in addition to the pulsed excitation [2, 3]. These approaches work very well for transient conductivity measurements as demonstrated in [3]. For transient luminescence measurements, however, the calculations in [Mai3] reveal undesired high injection effects that occur when applying both techniques. For this reason, bias illumination and increased excitations are inappropri-

ate to get rid off trapping effects in TRL experiments. In order to avoid high injection effects, it has been suggested in [Mai3] to use low excitations and to empty the traps instead of filling them by a faster reemission of charge carriers. The faster reemission is achieved by an increase of the temperature. This reduces both, the impact of carrier capture and of carrier emission, and the decay curves become mono-exponential and reveal the recombination in the absorber as shown in [Mai3]. The experimental realization of the proposed temperature and excitation increase has been examined for $Cu_2ZnSnSe_4$ in [Mai8] and for $Cu(In,Ga)Se_2$ in [Mai7]. The measurements yield decay curves that exhibit all pecularities of trapping: bi-exponential decays with very long decay times that strongly decrease at elevated temperatures. The trap properties of the investigated absorbers have been quantified by means of simulations, which give a trap density of $10^{15} \ldots 10^{16}\,cm^{-3}$, a trap energy of approximately $200\,meV$, and a capture cross-section for electrons of about $10^{-13}\,cm^2$. These values are in accordance with the findings of admittance spectroscopy measurements [63, 64] and of theoretical calculations using the supercell method [65]. In particular, this knowledge about the trap properties allows a discrimination of the minority carrier trapping from the recombination in the TRL. This enables the determination of the recombination lifetime, which comes out as $1 \ldots 10\,ns$ [Mai7, Mai8].

Finally, the question concerning the correlation of the open-circuit voltage and the decay time from Fig. 1.2 has been discussed in [Mai9] with regard to the impact of minority carrier trapping. This question is not easy to answer, because a pulsed excitation for TRL and a steady state excitation for V_{oc} must be compared. These difficulties particularly emerge when traps are studied, since trapping is actually a transient phenomenon. In the stationary case, trapping does not occur and shallow defects act as recombination centers. This suggests that the effective recombination lifetime is smaller when V_{oc} is measured compared to TRL. However, at least under low excitations the contribution of traps to the steady state recombination can be disregarded and the same effective recombination lifetime can be used for the calculation of V_{oc} and τ_{decay}. On the basis of this result, in [Mai9] the open-circuit voltage has been calculated as a function of the decay time. To this end, $V_{oc}(\tau_n)$ has been taken from [16] for QNR-recombination and $\tau_n(\tau_{decay})$ has been taken from equation (5.3.1b). Using the definition of the capture and the emission time, this can be rewritten as $\tau_n = \frac{n^*}{N_t}\tau_{decay}$. The combination of both led to the following dependence of the open-circuit voltage on the decay time:

$$V_{oc}\left(\tau_{decay};\, \frac{n^*}{N_t}\right) = \frac{k\,T}{e_0}\,\log\frac{J_{sc}(\frac{n^*}{N_t}\tau_{decay})}{J_0(\frac{n^*}{N_t}\tau_{decay})}. \tag{5.3.2}$$

It is J_0 the saturation current density, and J_{sc} again denotes the short-circuit current density. In Eq. (5.3.2) V_{oc} is a function of τ_{decay} but with a parameter n^*/N_t, which can reach any positive value. Accordingly, equation (5.3.2) describes an entire family of curves as indicated in figure 5.5. The solid red curves are boundaries to the measured data
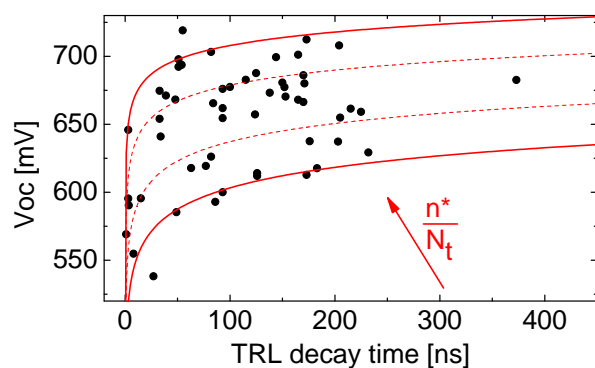
Figure 5.5: Scatter plot of the open-circuit voltage V_{oc} of approximately 60 CIGSe solar cells measured as a function of the decay time τ_{decay} of the absorber. The red curves are calculated $V_{oc}(\tau_{decay})$ graphs according to equation (5.3.2) for constant n^*/N_t ratios of 1, 0.15, 0.015, 0.003 (from top to bottom). With kind permission of Enrico Jarzembowski.

and correspond to $n^*/N_t = 0.003$ and $n^*/N_t = 1$, respectively. Thus, for each solar cell $0.003 \leq n^*/N_t \leq 1$ must hold, which is a restriction to the trap properties. On the basis of the fixed trap energy, which has been revealed in the TRL measurements [Mai7], n^* can be treated as a material constant. Thus, for all cells only the trap density is allowed to vary in the range $10^{15}\,\mathrm{cm}^{-3} \lesssim N_t \lesssim 10^{17}\,\mathrm{cm}^{-3}$. Here, it is pointed out that only by measuring V_{oc} as a function of the decay time boundaries to the trap density in CIGSe can be determined. In particular, these values are in good agreement with the densities determined by temperature and excitation dependent TRL [Mai7]. This is a remarkable result since it combines minority carrier trapping, TRL, and electrical measurements. At the end of [Mai7], this finding is further pursued with regard to the often reported correlation of V_{oc} and τ_{decay} [5–8, 11, 14, 17, 23], which is, however, in contradiction to figure 5.5. This has to do with the small open-circuit voltages below $600\,\mathrm{mV}$ in all of these works. For these rather small voltages, the curves in figure 5.5 approximate each other. But then, the decay time is not disturbed by trapping and it correlates with the open-circuit voltage.

In conclusion, in [Mai3] a theory of TRL decays governed by minority carrier trapping has been deduced, which is more general than that of Ahrenkiel et al. [2]. It has been demonstrated that trapping may explain bi-exponential decays that are observed on sole semiconductor layers. For verification of traps, a temperature and excitation increase has been proposed which has been carried out in [Mai7, Mai8] for CIGSe and CZTSe. The observed luminescence characteristics cannot be explained by charge carrier drift [Mai9]. Only a model that includes shallow defects is capable to describe the temperature and excitation dependence of the bi-exponential decay curves correctly. As a consequence of trapping, the solar cell parameters cannot be predicted unambiguosly by measuring the TRL decay time. However, it is admitted that there are even more reasons for the non-correlation. In the previous section it has been addressed that the impact of the overlying layers or resistances on the V_{oc} are not revealed by the TRL of the absorber. Furthermore, the absorptivity, mobility, acceptor density, and diode quality factor may vary between different solar cells, which is reflected in V_{oc} but not in the decay time. Further origins for the non-correlations are material inhomogeneities, which are adressed in the next section.

Theoretical study of time-resolved luminescence in semiconductors. III. Trap states in the band gap

Matthias Maiberg,[a] Torsten Hölscher, Setareh Zahedi-Azad, and Roland Scheer
Institute of Physics, Martin-Luther-University Halle-Wittenberg, 06120 Halle, Germany

In the third part of this series, we study the influence of trap states in the band gap of semiconductors on the time-resolved luminescence decay (TRL) after a pulsed excitation. The results based on simulations with Synopsys TCAD® and analytical approximations are given for p-doped Cu(In,Ga)Se$_2$ as a working example. We show that a single trap can be mostly described by two parameters which are assigned to minority carrier capture and emission. We analyze their influence on the luminescence decay and study the difference between a single trap and an energetic Gaussian trap distribution. It is found that trap states artificially increase the TRL decay and obscure the recombination dynamics. Thus, there is a demand for experimental methods which can reveal the recombination of minority carriers in a TRL experiment without trapping effect. In this regard, a variation of the device temperature, the excitation frequency, the injection level, as well as a bias illumination may be promising approaches. We study these methods, discuss advantages and disadvantages, and show experimental TRL for prove of concept. At the end, we validate our approach of simulating only band-to-band radiative recombination although photoluminescence spectra often exhibit free-to-bound radiative recombination of charge carriers. © 2015 AIP Publishing LLC. [http://dx.doi.org/10.1063/1.4929877]

I. INTRODUCTION

In the first and second part of this work, the influence of excitation, diffusion, deep defects, and space charges on the transient luminescence of a homogeneous semiconductor was investigated by one-dimensional simulations.[1,2] We found that the decay of the luminescence intensity equals the decay of the minority carriers if a homogeneous semiconductor layer without space charges is excited with low injection levels. On the contrary, high injection levels can cause bimolecular recombination and diffusion of charge carriers. Curved transients can also arise from a spatial defect distribution. Both lead to curved, multi-exponential luminescence transients. Then, the decay time is not well-defined since it is not constant with time.

In the third part of this work, the time-resolved luminescence (TRL) is studied for semiconductors that contain trap states for minority carriers. Such shallow defects are often used to explain biexponential luminescence decays with very long decay times up to the radiative recombination lifetime.[3,4] In Cu(In,Ga)Se$_2$, for instance, the radiative lifetime amounts to a few hundred nanoseconds up to microseconds depending on the acceptor density.[5] In the case of biexponential transients due to minority carrier trapping, the luminescence decay may not reveal the carrier recombination, and therefore, the minority carrier lifetime should not easily be determined from simple TRL measurements. On the other hand, in some cases, a correlation between the TRPL decay time and the open circuit voltage has been revealed experimentally. Examples for measurements on Cu(In,Ga)Se$_2$ and CdTe, where the decay times were below 100 ns, can be

found in Refs. 4, and 6–9. The contradiction between experimental correlation and theoretical uncorrelation of the TRPL decay time and the minority carrier lifetime defines the need for a more thorough study on the impact of trapping in TRL experiments.

The theoretical description of minority carrier trapping is based on the rate equations of Shockley, Read, and Hall.[10,11] Ahrenkiel calculated analytical approximate solutions making the following assumptions: the initial fast decay can be assigned to carrier capture and carrier recombination. For later times, the recombination is limited by the rate of electron emission to the conduction band.[12] In the present work, a more general solution of TRL is given including minority carrier traps. An exact analytic expression is given if a low trap occupation is supposed. Using these results, it is shown that long decay times are not only influenced by carrier emission (as assumed by Ahrenkiel) but also by carrier re-capturing. As many experimentalists actually are interested in carrier recombination, TRL experiments with disabled carrier trapping are desirable. Different methods for trapping suppression are proposed such as an increase of the injection level, a variation of the device temperature, as well as application of a bias illumination. We show that elevated temperature is most easily employed and using this approach we present a practical example. At the end, we shortly concentrate on the validity of our simulations which implicitly assume that the luminescence comes from radiative band-to-band recombination while in TRL experiments often photon energies being smaller than the band gap are detected. The latter can be assigned to radiative free-to-bound recombination. We discuss that the decay by band-to-band and free-to-bound transitions mostly occur on the

[a]Electronic mail: matthias.maiberg@physik.uni-halle.de

same time scale if we exclude inhomogeneous band gaps and non-local recombination.

II. SIMULATION PARAMETERS

In this work, the same simulation parameters as in the second part are used. Since numerous experimental parameters in the simulations will be varied, a list of the most important standard simulation parameters is given in Table I. Using these parameters, the effective electron density comes out as $n^* = 9 \times 10^{13} \, \text{cm}^{-3}$, the capture time as $\tau_c = 100 \, \text{ns}$, and the emission time as $\tau_e = 120 \, \text{ns}$ (compare Equation (5) in Section III).

III. BASICS ON MINORITY CARRIER TRAPS

A. Rate equations

First, the trapping dynamics of a single minority carrier trap is investigated and we look for an approximate analytic description. The transition rates provided by Shockley, Read, and Hall[10,11] are applied to a trap state in a p-type semiconductor. For the electron density n in the conduction band, the hole density p in the valence band, and the density of electrons in the trap state n_t the following rate equations are found (neglecting any carrier current):

$$\frac{\mathrm{d}}{\mathrm{d}t}n = G - R_n + e_e - e_c,$$
$$\frac{\mathrm{d}}{\mathrm{d}t}p = G - R_p + h_e - h_c, \tag{1}$$
$$\frac{\mathrm{d}}{\mathrm{d}t}n_t = e_c - e_e + h_e - h_c.$$

Here, G is the generation rate, R is the recombination rate, e_e is the electron emission rate, e_c is the electron capture rate,

TABLE I. Main simulation parameters used in all simulations if not stated otherwise.

Simulation parameter	Value
Trap density N_t	$10^{14} \, \text{cm}^{-3}$
Trap distribution width ΔE	0
Electron capture cross-section σ_n	$10^{-14} \, \text{cm}^2$
Hole capture cross-section σ_p	$10^{-18} \, \text{cm}^2$
Thermal velocity v_n, v_p	$10^7 \, \text{cm} \, \text{s}^{-1}$
Trap distribution maximum $E_c - E_t$	$0.26 \, \text{eV}$
Device temperature T	$300 \, \text{K}$
SRH-related carrier lifetime τ_{SRH}	$20 \, \text{ns}$
Free carrier mobility $\mu = \mu_n = \mu_p$	$20 \, \text{cm}^2 \text{V}^{-1} \text{s}^{-1}$
Surface recombination velocity S	0
Absorber acceptor density N_a	$10^{16} \, \text{cm}^{-3}$
Absorber thickness d	$3 \, \mu\text{m}$
Absorber bandgap E_g	$1.15 \, \text{eV}$
Effective density of states N_v, N_c	$2 \times 10^{18} \, \text{cm}^{-3}$
Excitation wavelength λ	$900 \, \text{nm}$
Absorption coefficient α	$3.8 \, \mu\text{m}^{-1}$
Excitation frequency f	$10^6 \, \text{Hz}$
Pulse length τ_{pulse}	$100 \, \text{fs}$
Photon density per pulse n_γ	$10^9 \, \text{cm}^{-2}$

h_e is the hole emission rate, and h_c is the hole capture rate. The latter are given by[10,11]

$$e_e = \sigma_n v_n n^* n_t,$$
$$e_c = \sigma_n v_n n (N_t - n_t),$$
$$h_e = \sigma_p v_p p^* (N_t - n_t), \tag{2}$$
$$h_c = \sigma_p v_p p n_t.$$

In the above equation, N_t is the trap density, $\sigma_{n,p}$ denotes the capture cross-section, and $v_{n,p}$ denotes the thermal velocity of electrons and holes, respectively. Further, it is $n^* = N_c \, \mathrm{e}^{-\frac{E_c - E_t}{kT}}$ the electron density and $p^* = N_v \, \mathrm{e}^{-\frac{E_t - E_v}{kT}}$ the hole density if the Fermi-level lies at the defect level E_t.

The trap state shall be donator like and close to the conduction band. Otherwise it would be occupied even in equilibrium and electrons could not be captured. Furthermore, we demand $\sigma_n v_n n^* \gg \sigma_p v_p p$. Otherwise defect assisted recombination of electrons would be more probable than electron trapping. Recombination, however, for systematic reasons shall only be included in the recombination lifetime τ_n and take place via the trap states. Altogether, it is $h_e, h_c \ll G, R, e_e, e_c$ and it follows:

$$\frac{\mathrm{d}}{\mathrm{d}t}n = G - R_n + \sigma_n v_n n^* n_t - \sigma_n v_n n (N_t - n_t),$$
$$\frac{\mathrm{d}}{\mathrm{d}t}p = G - R_p, \tag{3}$$
$$\frac{\mathrm{d}}{\mathrm{d}t}n_t = \sigma_n v_n n (N_t - n_t) - \sigma_n v_n n^* n_t,$$
$$p(t=0) = p_0, \quad n(t=0) = n_0, \quad n_t(t=0) = n_{t0},$$

where n_0 and p_0 are the equilibrium carrier densities, and n_{t0} is the equilibrium occupied trap density with $n_{t0} \ll N_t$ for donor like defects near the conduction band. For reasons of simplicity, low injection levels are studied, that means the generated carrier density $\Delta n_0 = \Delta p_0$ is much smaller than p_0, much larger than n_0, and not much larger than N_t. Then we have monomolecular recombination with the rates $R_n = \frac{n - n_0}{\tau_n} \approx \frac{n}{\tau_n}$ and $R_p = \frac{p - p_0}{\tau_p} \approx 0$, where τ_n and τ_p are the recombination lifetimes of electrons and holes, respectively, considering all recombination paths. For this reason, the rate equation for holes is decoupled from those of n and n_t and (3) can be simplified

$$\frac{\mathrm{d}}{\mathrm{d}t}n = G - \frac{n}{\tau_n} + \sigma_n v_n n^* n_t - \sigma_n v_n n (N_t - n_t),$$
$$\frac{\mathrm{d}}{\mathrm{d}t}n_t = \sigma_n v_n n (N_t - n_t) - \sigma_n v_n n^* n_t, \tag{4}$$
$$n(t=0) = n_0, \quad n_t(t=0) = n_{t0}.$$

Additionally, it follows $n_t \ll N_t$ due to low injection levels. With the notation $\frac{1}{\tau_e} = \sigma_n v_n n^*$ and $\frac{1}{\tau_c} = \sigma_n v_n N_t$ we get

$$\frac{\mathrm{d}}{\mathrm{d}t}n = G - \left(\frac{1}{\tau_n} + \frac{1}{\tau_c} \right) n + \frac{n_t}{\tau_e},$$
$$\frac{\mathrm{d}}{\mathrm{d}t}n_t = \frac{n}{\tau_c} - \frac{n_t}{\tau_e}, \tag{5}$$
$$n_t(0) = n_{t0}, \quad n(0) = n_0.$$

Comparing the definition of τ_e and τ_c with the electron capture and emission rates in (2), τ_e can be seen as the average time for emission and τ_c can be seen as the average time for capturing of an electron by the shallow defect. Finally, the laser excitation pulse is assumed to be short with a pulse length $\tau_{pulse} \ll \tau_c, \tau_n$. Then Equation (5) becomes

$$
\begin{aligned}
\frac{d}{dt}n &= -\left(\frac{1}{\tau_n} + \frac{1}{\tau_c}\right)n + \frac{n_t}{\tau_e}, \\
\frac{d}{dt}n_t &= \frac{n}{\tau_c} - \frac{n_t}{\tau_e}, \\
n_t(0) &= n_{t0}, \quad n(0) = n_0 + \Delta n_0 \approx \Delta n_0.
\end{aligned}
\tag{6}
$$

Equation (6) shows that the impact of a shallow defect on a luminescence decay can be fully described by only two parameters τ_e and τ_c, which in turn depend on σ_n, v_n, N_t, and E_t. The equation system (6) may be written in the form

$$
\frac{d}{dt}\mathbf{n}(t) = \mathbf{A}\,\mathbf{n}(t) \tag{7a}
$$

with

$$
\mathbf{n}(t) = \begin{pmatrix} n(t) \\ n_t(t) \end{pmatrix} \text{ and } \mathbf{A} = \begin{pmatrix} -\left(\dfrac{1}{\tau_n} + \dfrac{1}{\tau_c}\right) & \dfrac{1}{\tau_e} \\ \dfrac{1}{\tau_c} & -\dfrac{1}{\tau_e} \end{pmatrix}. \tag{7b}
$$

The solution of (7) can be found by the fundamental matrix and yields

$$
n(t) = \frac{a\,(1 - \tau_e \lambda_2)}{\tau_e}\, e^{-\lambda_2 t} - \frac{b\,(1 - \tau_e \lambda_1)}{\tau_e}\, e^{-\lambda_1 t}
$$

$$
n_t(t) = \frac{a}{\tau_c}\, e^{-\lambda_2 t} - \frac{b}{\tau_c}\, e^{-\lambda_1 t}
$$

with

$$
\begin{aligned}
a &= \frac{\tau_e \Delta n_0 - n_{t0}\tau_c(1 - \tau_e \lambda_1)}{(\lambda_1 - \lambda_2)\tau_e} \\
b &= \frac{\tau_e \Delta n_0 - n_{t0}\tau_c(1 - \tau_e \lambda_2)}{(\lambda_1 - \lambda_2)\tau_e} \\
\lambda_1 &= \frac{1}{2}(\omega_1 + \omega_2), \quad \lambda_2 = \frac{1}{2}(\omega_1 - \omega_2) \\
\omega_1 &= \frac{1}{\tau_n} + \frac{1}{\tau_e} + \frac{1}{\tau_c}, \quad \omega_2 = \sqrt{\left(\frac{1}{\tau_n} + \frac{1}{\tau_e} + \frac{1}{\tau_c}\right)^2 - \frac{4}{\tau_n \tau_e}}.
\end{aligned}
\tag{8}
$$

The result is a biexponential decay with a short decay time $1/\lambda_1$ and a long decay time $1/\lambda_2$.

B. Impact of carrier capture and emission on luminescence decay

Now, the electron capture and emission are varied and the general effects on the electron kinetics are studied. For very large capture times compared to the effective recombination lifetime τ_n, the electrons recombine before they can be captured by the shallow defect. Therefore, the traps have only a minor influence on the luminescence decay and the decay is mono-exponential (see Fig. 1(a)). This is independent of electron emission and can be revealed by

Equation (8), which gives $\lambda_1 = \frac{1}{\tau_n}$ and $\lambda_2 = \frac{1}{\tau_e}$ for $\tau_c \gg \tau_n$ and hence $n(t) = \Delta n_0\, e^{-\frac{t}{\tau_n}}$.

If the capture time is in the range or even smaller than the effective lifetime, most of the electrons are captured and trapped until being re-emitted to the conduction band after the emission time. Now two limiting cases have to be distinguished: If the emission time is much smaller than the recombination lifetime and capture time, the electrons are instantaneously re-emitted to the conduction band and they are hardly trapped. In this case, the electron density decays mono-exponentially with the recombination lifetime τ_n (see Fig. 1(b)). Evaluation of Equation (8) gives $\lambda_1 = \frac{1}{\tau_e}$ and $\lambda_2 = \frac{1}{\tau_n}$ for $\tau_e \ll \tau_n, \tau_c$ and leads to $n(t) = \Delta n_0\, e^{-\frac{t}{\tau_n}}$.

In the other case, the emission time is in the range or larger than the capture and recombination time and the electrons are trapped and are slowly re-emitted to the conduction band. Since the conduction band is almost empty due to electron capture and electron recombination for times $t \gg \tau_n$, the recombination of electrons with an abundant hole is limited by the electron supply by re-emission from the shallow defect. If the emission time is large, the re-emission is very small leading to a small electron supply and a large luminescence decay time (see Fig. 1(b)). If the capture time is small, too, the electrons are directly re-captured. This further reduces the electron supply and further increases the luminescence decay time (see Fig. 1(a)). This can also be calculated from Equation (8). For $\tau_e > \tau_c$ we find by a Taylor Series of (8)
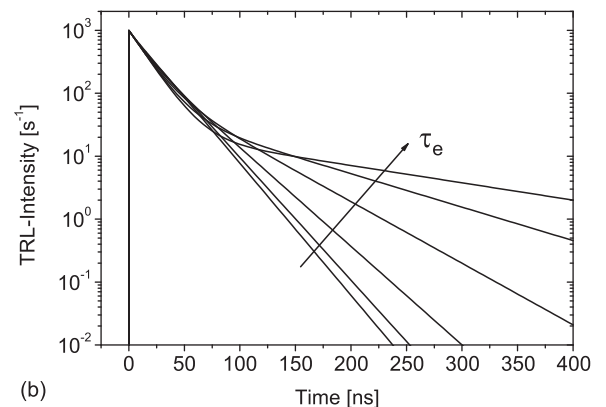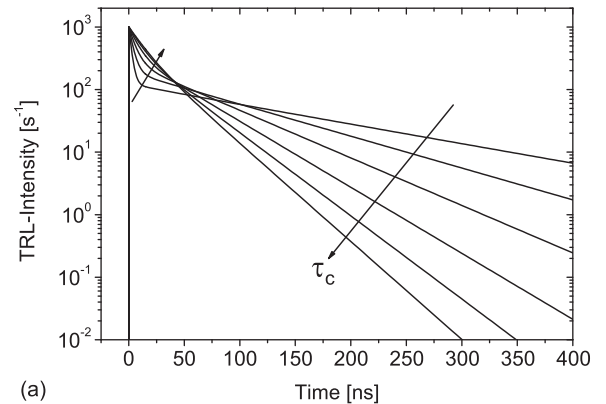

(a)

(b)

FIG. 1. TRL-transients of a semiconductor layer with a carrier SRH-lifetime of $\tau_{SRH} = 20$ ns $\approx \tau_n$, a trap density $N_t = 10^{14}$ cm^{-3} and varying capture or emission time.

$$\lambda_1 = \frac{1}{\tau_n} + \frac{1}{\tau_c} + \frac{1}{\tau_e}\left(1 - \frac{\tau_c}{\tau_n}\right)$$
$$\lambda_2 = \frac{\tau_c}{\tau_e\,\tau_n}. \tag{9}$$

This shows that the long decay time $1/\lambda_2$ is not only influenced by τ_e but also by τ_c according to the considerations above. This is in contrast to the result of Ahrenkiel *et al.*[12] who found $\lambda_1 = \frac{1}{\tau_n} + \frac{1}{\tau_c}$ and $\lambda_2 = \frac{1}{\tau_e}$, which is only valid for $\tau_n > \tau_c \gtrsim \tau_e$.

Furthermore, Figure 1 illustrates that the electron capture affects both decay times $1/\lambda_1$ and $1/\lambda_2$ whereas the electron emission mostly affects the long decay time $1/\lambda_2$. Now, in experiments it can occur that for very small capturing times the initial decay cannot be seen due to limited experimental time resolution. Then, only the second long decay can be detected which does not correlate with the recombination lifetime τ_n. In such a case, the luminescence decay time would exhibit no correlation to the open-circuit voltage of a solar cell device.

C. Impact of a trap distribution on the luminescence decay

The results above calculated for a single trap can be generalized if there is not a single shallow defect but a Gaussian trap distribution with a trap density $\tilde{N}_t(E)$ according to

$$\frac{d\tilde{N}_t}{dE} = \frac{N_t}{\sqrt{2\pi}\,\Delta E}\, e^{-\frac{(E_c - E_t - E)^2}{2\Delta E^2}}, \tag{10}$$

where N_t is the total density of traps, ΔE describes the energetic width of the distribution, and E_t denotes the position of the distribution's maximum in the bandgap. We demand that each trap state can only interact with the conduction band but not with other trap states. Figure 2(a) shows the occupied trap states after 1 ns and after 256 ns. It can be seen that states closer to the conduction band are emptied much faster than the states deeper in the band gap, since the emission rate e_e increases with decreasing $E_c - E_t$. Therefore, the initial decay of the transients in Figure 2(b), which is mostly uninfluenced by carrier emission, is independent of ΔE, since the carrier capture depends only on the total density of defects. For later times, the luminescence decay becomes curved with increasing trap distribution broadness, since the decay is now a superposition of an infinite number of exponential decays with different emission times.

D. Impact of multi-pulse excitation on trap occupation

Finally, the trap occupation is studied if the semiconductor is excited by more than one laser pulse with a frequency $f = 1/T_p$, where T_p is the pulse period. Then, the trap will not be fully emptied up to the next laser excitation if T_p is in the range or smaller than the decay time of the luminescence.
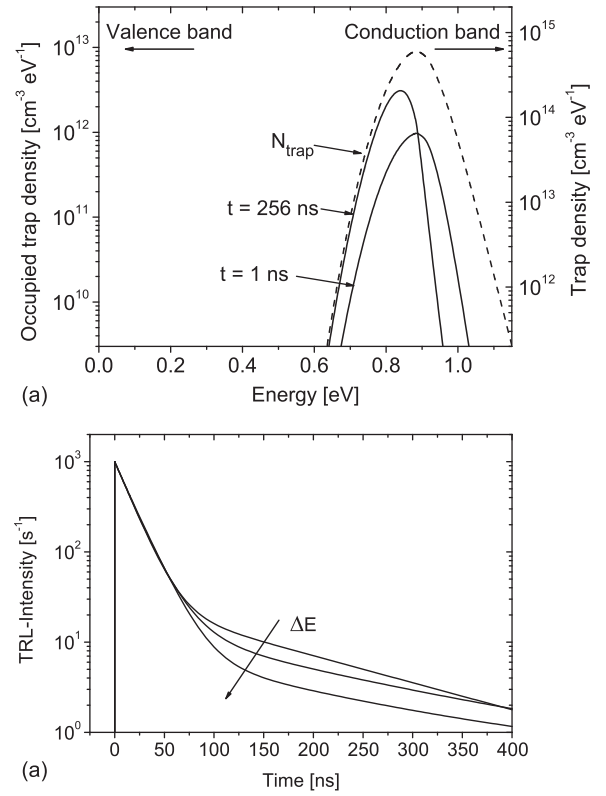

(a)

(a)

FIG. 2. Trap occupation and TRL-transients of a semiconductor layer with a carrier SRH-lifetime of $\tau_{SRH} = 20\,\text{ns}$, a trap density $N_t = 10^{14}\,\text{cm}^{-3}$, and a Gaussian trap distribution with maximum at $E_c - E_t = 0.26\,\text{eV}$ and varying energetic width ΔE. The incident photon density is $n_\gamma = 10^9\,\text{cm}^{-2}$ per pulse.

Due to incomplete evacuation of the traps at the time of the next excitation, the trap occupation immediately before the $k-$ th excitation $n_{t0,k}$ increases with each laser excitation and it is $n_{t0,0} < n_{t0,1} < n_{t0,2} < \ldots$. This is shown in Figure 3(a). In turn, this leads to an increased carrier emission with each laser excitation ($e_e \propto n_t$). Both effects compensate each other and we find a "steady state" trap occupation $n_{t0,k-1} \approx n_{t0,k}$ for a large number of excitations. From Equation (8), we find

$$n_{t0,k} = A\,\frac{1 - (-B)^k}{1 + B} \tag{11a}$$

with

$$A = \frac{\Delta n_0}{\tau_c}\,\frac{e^{-\lambda_2 T_p} - e^{-\lambda_1 T_p}}{\lambda_1 - \lambda_2}$$
$$B = \frac{1}{\tau_e}\,\frac{(1 - \tau_e\,\lambda_1)\,e^{-\lambda_2 T_p} - (1 - \tau_e\,\lambda_2)\,e^{-\lambda_1 T_p}}{\lambda_1 - \lambda_2}. \tag{11b}$$

By evaluation of B one finds $-1 < B < 0$ (since it is $\lambda_1 > \lambda_2$) which induces $n_{t0,k}$ to converge. Physically, this corresponds to a "steady state" trap occupation as we have stated above. The steady state trap occupation $n_{t,s}$ immediately before the next laser excitation is

$$\Rightarrow n_{t,s} = \lim_{k\to\infty} n_{t0,k} = \Delta n_0\,\frac{\tau_e}{\tau_c}\,\frac{e^{T_p\lambda_1} - e^{T_p\lambda_2}}{(1 - \tau_e\,\lambda_1)\,e^{T_p\lambda_1} + \tau_e\,(\lambda_1 - \lambda_2)\,e^{T_p(\lambda_1 + \lambda_2)} - (1 - \tau_e\,\lambda_2)\,e^{T_p\lambda_2}}. \tag{12}$$
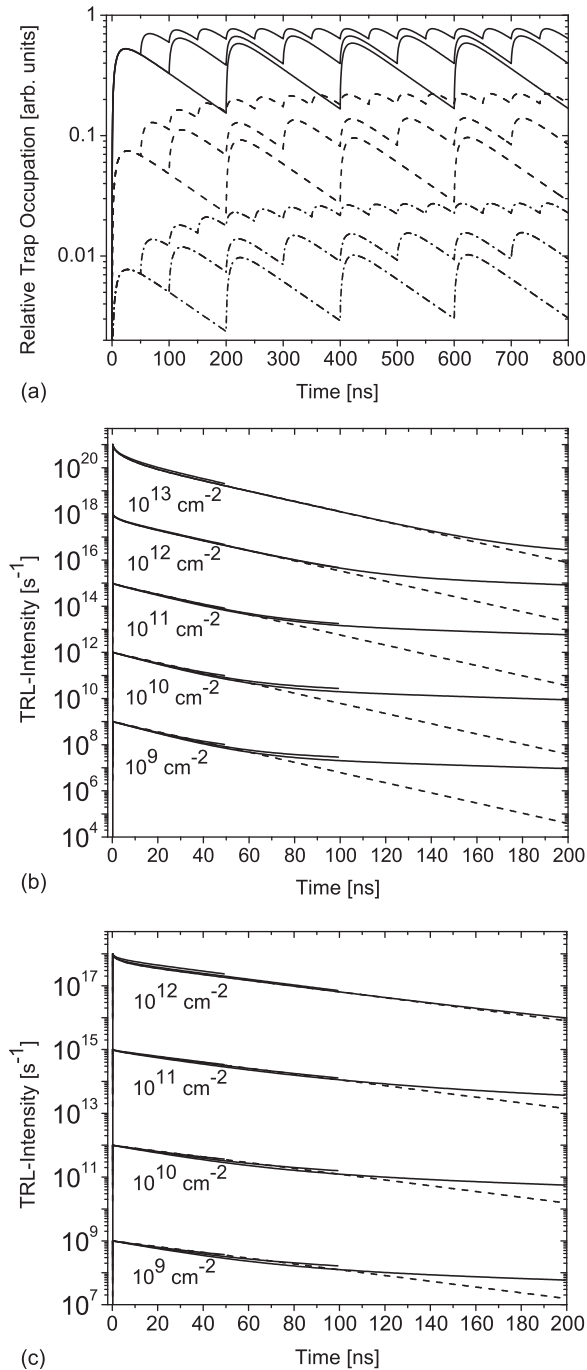
FIG. 3. Trap occupation and TRL-transients of a semiconductor layer with a single trap for different excitation period $T_p = 50, 100, 200$ ns, different carrier SRH-lifetimes and different injection levels. Capture time $\tau_c = 100$ ns and emission time $\tau_e = 120$ ns.

This result is valid as long as $n_{t,s} \ll N_t$ and $\Delta n_0 \ll p_0$ holds. Equation (12) already shows that the trap occupation can be increased if the period T_p is reduced ($\lambda_1 > \lambda_2$) or if the injection level Δn_0 is increased, which will be discussed in detail in Section IV A.

The last question is, how many laser excitations are needed to saturate the trap occupation. From Equation (11), we find for the necessary number of laser excitations to reach 99% of the saturation value

$$k_{99\%} \geq \frac{\log 0.01 - \log(1.01 + B)}{\log |B|} \quad (13)$$

with B as in Equation (11). This means $n_{t,k_{99\%}} = 0.99\, n_{t,s}$. Inserting the values from Table I with $\tau_n \approx \tau_{SRH}$ gives $k_{99\%} = 4$ for $T_p = 200$ ns, $k_{99\%} = 6$ for $T_p = 100$ ns and $k_{99\%} = 10$ for $T_p = 50$ ns. Hence, it is sufficient to simulate only the first ten laser excitations to retrieve the full information.

IV. TRL WITH SUPPRESSED CARRIER TRAPPING

As carrier trapping can strongly influence the luminescence decay—thus hindering the determination of the minority carrier lifetime—trapping has to be switched off in the TRL experiment. To do so we look at Equation (3). We have to demand $R_n - G \gg \sigma_n v_n n (N_t - n_t) - \sigma_n v_n n^* n_t$. To reduce electron capture ($\sim N_t - n_t$), the traps have to be filled such that $n_t \approx N_t$ holds, which can be achieved by an increased injection level (increased Δn_0), by a reduced device temperature (reduced n^*), or by a bias light illumination. In turn, occupied traps lead to an increased emission ($\sim n_t$) to the conduction band. This has to be compensated by an increased injection level (increased R_n) or by a reduced device temperature (reduced n^*). Alternatively, electron emission may be increased in order to reduce the trap effect. This calls for an elevated device temperature. In the following, it will be discussed in detail that trapping effects can be reduced by increased excitation intensities and frequencies, by a variation of the device temperature, or by bias illumination.

A. Trap filling using increased injection levels

First, we study how the impact of shallow defects on a luminescence decay can be reduced by increased injection levels and excitation frequencies. As Equation (12) suggests, the average trap occupation can be increased by increased excitation intensities and frequencies. This is shown in Figure 3(a). Furthermore, this figure demonstrates the independence of the trap occupation dynamics from the excitation pulse number k even at the very beginning, as it has been calculated in Sec. III D.

Looking at Figures 3(b) and 3(c), indeed the influence of electron capture on the luminescence decay vanishes with increased excitation intensity and frequency.

For high injection levels $n_t \approx N_t$ can be assumed. Then we have $\frac{dn}{dt} = -R_n + e_e - e_c \approx -\frac{n}{\tau_n} + \sigma_n v_n n^* N_t$ (see Eq. 1). Hence, electron emission e_e can be neglected as long as the electron density fulfills $n(t) \gg \tau_n \sigma_n v_n n^* N_t$. When the electron trapping is negligible, $n(t) = \Delta n_0 e^{-\frac{t}{\tau_n}}$ can be assumed. Using this, the condition for negligible electron emission can be formulated as follows:

$$\Delta n_0 \gg \frac{\tau_n}{\tau_c} e^{\frac{T_p}{\tau_n}} n^*, \quad (14)$$

where T_p is the period of excitation. This has two consequences: First, the electron emission can be neglected for increased excitation intensities. Second, the influence of

electron emission depends on the effective electron lifetime τ_n. If the lifetime time is large, the electron density decays slowly (see Figure 3(c)). Therefore, in Figure 3(c) less intensity (compared to Figure 3(b)) is needed to make electron emission negligible.

The problem of increased injection levels is that the high intensities, necessary to switch off electron capture and to make electron emission negligible, lead to bimolecular recombination or to hole limited recombination,[1,2] which hinders to determine the low injection minority carrier lifetime. This can be seen in Figure 3(b) where the transients bend at the highest injection levels.

B. Trap filling and reduced carrier emission by reduced device temperatures

Next to the excitation energy, the sample temperature may provide an experimental parameter to reduce trap effects. Again, we look at Equation (12). The average trap occupation increases if the emission time τ_e increases, because the electrons are trapped for longer times. The emission time is defined by $\tau_e = (\sigma_n v_n n^*)^{-1}$. The capture cross-section σ_n and the electron velocity v_n are only weakly temperature dependent. However, the electron density n^* strongly depends on the temperature and can be reduced by decreased device temperatures leading to increased τ_e. Therefore, a decrease of the temperature should increase the average trap occupation. This is shown in Figure 4(a). It can be seen that the trap occupation can be increased by about one order of magnitude if the temperature is reduced from 300 K to 225 K for an incident photon density of $n_\gamma = 10^9\,\mathrm{cm}^{-2}$ per pulse. In consequence, for 300 K a photon density of about $n_\gamma = 10^{11}\,\mathrm{cm}^{-2}$ per pulse is necessary to fill the traps, whereas for 225 K a photon density of about $n_\gamma = 10^{10}\,\mathrm{cm}^{-2}$ per pulse is sufficient to fill the traps.

The temperature dependent photoluminescence decay is shown in Figures 4(b) and 4(c). The impact of trapping is reduced by increased recombination lifetimes, by increased excitation intensities and by reduced device temperatures. Further, the effect of a reduction of the temperature is smaller for low injection levels than for high injection levels. To understand this, we again look at the condition for negligible electron emission

$$\Delta n_0 \gg \tau_n \sigma_n v_n n^*(T)\, n_t\, \mathrm{e}^{\frac{T_p}{\tau_n}} \overset{T\downarrow, n_\gamma\uparrow}{\approx} \frac{\tau_n}{\tau_c}\, \mathrm{e}^{\frac{T_p}{\tau_n}} n^*(T), \quad (15)$$

where T means the device temperature. This again explains that the impact of electron emission can be reduced if τ_n or the excitation intensity increases. For low intensities, n^* decreases with reduced temperature and n_t increases with reduced temperature. Both effects mostly compensate and their combined influence of the temperature is small. For high intensities, $n_t \approx N_t$ is fixed and independent of the temperature. Then, again n^* decreases with reduced temperature and a strong dependence on the device temperature can be seen.

C. Trap filling using bias light illumination

In this section, it is demonstrated, how traps can be filled by a bias light illumination. The case shown in Figure 5 is
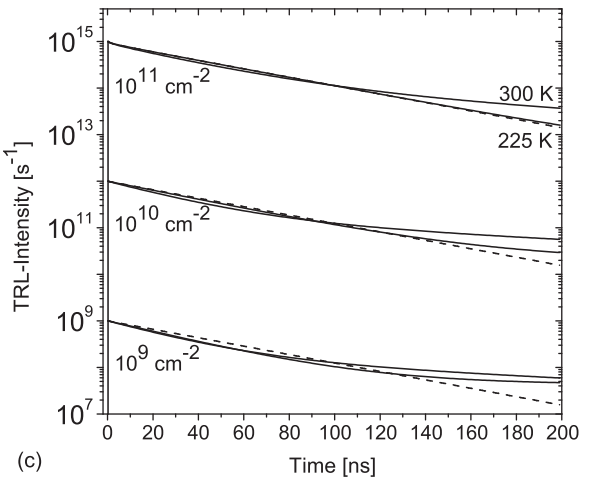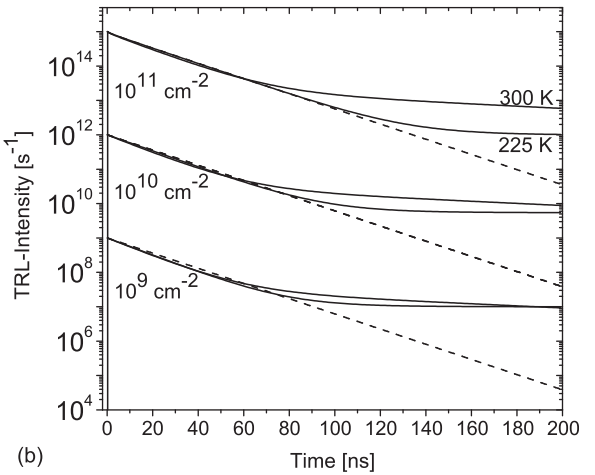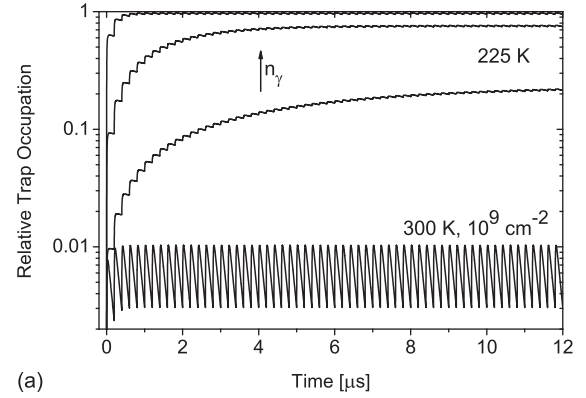

(a)

(b)

(c)

FIG. 4. Trap occupation and TRL-transients (after 60 excitations) of a semiconductor layer with a single trap for reduced device temperatures $T = 225$, 300 K, different carrier SRH-lifetimes and different injection levels $n_\gamma = 10^9$, 10^{10}, $10^{11}\,\mathrm{cm}^{-2}$ per pulse.

considered in the following. A constant bias light with photon energies smaller than the band gap is used. Superposed is the pulsed light with photon energies larger than the band gap. This can be described by

$$\frac{\mathrm{d}}{\mathrm{d}t}n = G - R_n + e_e - e_c$$
$$\frac{\mathrm{d}}{\mathrm{d}t}n_t = e_c - e_e + G_b, \quad (16)$$
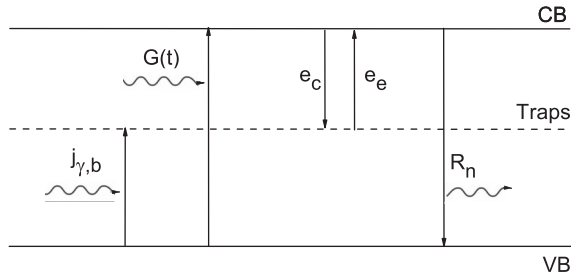
FIG. 5. Allowed transitions of electrons in a semiconductor with a trap state in the band gap. The semiconductor is excited by constant bias light $j_{\gamma,b}$ with photon energies smaller than the band gap and by pulsed laser light $G(t)$ with photon energies larger than the band gap.

which is analogue to Equation (4), but now a generation rate G_b has to be added for the transition of electrons from the valence band into the trap state by absorption of a photon. For the bias generation rate into the trap, we set

$$G_b = j_{\gamma,b}\, \alpha_T \left(N_t - n_t\right). \tag{17}$$

Here, a linear dependence of the transition rate on the photon flux density of the bias light $j_{\gamma,b}$ is assumed. α_T accounts for the transition probability of an electron from the valence band into the trap state by absorption of a photon. Under steady state conditions, this leads to a bias occupation $n_{t,b}$ of trap states and to a bias electron and hole density n_b and p_b. These can be calculated from Equation (16) if low excitations $p_b \approx p_0$ and monomolecular recombination $R_n \approx \frac{n_b}{\tau_n}$ are assumed

$$n_b = \frac{-\alpha_T j_{\gamma,b} - \sigma_n v_n n^* + \sqrt{\Omega}}{2\,\sigma_n v_n} < \frac{\tau_n}{\tau_c}\, n^*$$

$$n_{t,b} = \frac{\sigma_n v_n n^* + (1 + 2\,\sigma_n v_n N_t \tau_n)\alpha_T j_{\gamma,b} - \sqrt{\Omega}}{2\,\sigma_n v_n \alpha_T j_{\gamma,b} \tau_n} < N_t \tag{18}$$

$$\Omega = \left(\alpha_T j_{\gamma,b} + \sigma_n v_n n^*\right)^2 + 4\sigma_n^2 v_n^2 n^* N_t\, \alpha_T j_{\gamma,b} \tau_n.$$

The carrier densities saturate for large $\alpha_T j_{\gamma,b}$ values. Far away from saturation, a Taylor Series in $\alpha_T j_{\gamma,b}$ yields

$$n_b \approx \tau_n N_t\, \alpha_T j_{\gamma,b}$$

$$n_{t,b} \approx \left(1 + \frac{\tau_n}{\tau_c}\right) \tau_e N_t\, \alpha_T j_{\gamma,b}. \tag{19}$$

Now the luminescence decay under bias light illumination is studied. This can be described by

$$\frac{\mathrm{d}}{\mathrm{d}t} n = -R_n + e_e - e_c$$

$$\frac{\mathrm{d}}{\mathrm{d}t} n_t = e_c - e_e + G_b \tag{20}$$

$$n(t=0) = n_b + \Delta n_0,\ \ n_t(t=0) = n_{t,b},$$

where n_b and $n_{t,b}$ are defined as in (18) and Δn_0 is the electron density generated per laser pulse. Figure 6 shows that a bias generation into the trap state can reduce carrier capturing. However, there may be a large background luminescence due to the steady state electron density n_b. Again, this must be compensated by an increased excitation and we ask
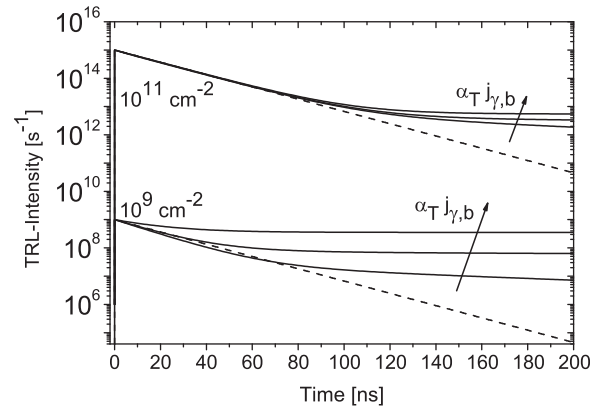

FIG. 6. TRL-transients of a semiconductor layer for carrier SRH-lifetimes $\tau_{SRH} = 20\,\mathrm{ns} \approx \tau_n$ and for different bias generation rates $\alpha_T j_{\gamma,b} = 0,\ 7 \times 10^6,\ 10^8\,\mathrm{s}^{-1}$ and different injection levels $n_\gamma = 10^9, 10^{11}\,\mathrm{cm}^{-2}$. Dashed lines are related to luminescence decay without shallow defects and solid lines to luminescence decay with impact of shallow defects.

for the necessary intensity. The conditions $n(t) \gg n_{t,b}$ and $R_n \gg e_e$ for $0 \le t \le T_p$ lead to

$$\Delta n_0 \gg \max\left\{\frac{n^*}{\tau_c},\, N_t\, \alpha_T j_{\gamma,b}\right\} \cdot \tau_n\, \mathrm{e}^{\frac{T_p}{\tau_n}}. \tag{21}$$

Equation (21) yields the condition $\alpha_T j_{\gamma,b} < \frac{1}{\tau_e}$. Otherwise the background luminescence would be higher than the luminescence due to carrier emission. In that case, a bias illumination would be of no advantage. On the other hand, we demand $n_{t,b} > 0.1\,N_t$ in order to reach a trap filling from the bias illumination. From this, we find $\alpha_T j_{\gamma,b} > \left(10\,\tau_e \left(1 + \frac{\tau_n}{\tau_c}\right)\right)^{-1}$. Both conditions limit the useful values of $\alpha_T j_{\gamma,b}$ to

$$\left(10\,\tau_e \left(1 + \frac{\tau_n}{\tau_c}\right)\right)^{-1} \le \alpha_T j_{\gamma,b} \le \frac{1}{\tau_e}. \tag{22}$$

Inserting the parameters from Table I gives $7 \times 10^6\,\mathrm{s}^{-1} < \alpha_T j_{\gamma,b} < 9 \times 10^6\,\mathrm{s}^{-1}$. This shows that bias illumination is only useful for traps that exhibit small emission times and can only be used for trap filling. However, the electron emission must be compensated by increased injection levels.

D. Reduced carrier trapping by increased device temperatures

In the foregoing Sections IV A–IV C, ways to reduce electron capture, i.e., increase τ_c, by trap occupation have been discussed. However, all measures A-C as a side effect also increase the electron emission making high injection levels necessary to compensate for. In this section, we follow another idea: If the device temperature increases, the emission time τ_e decreases. If the temperature is increased such that $\tau_e \ll \tau_c$ holds, the electrons are trapped but almost directly re-emitted to the conduction band. This already has been shown in Figure 1(b) and has been calculated in Section III B. We now look at the luminescence decay in Figure 7. The impact of trapping can indeed be diminished if the device temperature is moderately increased. The origin is the almost instantaneous re-emission of the electrons to the
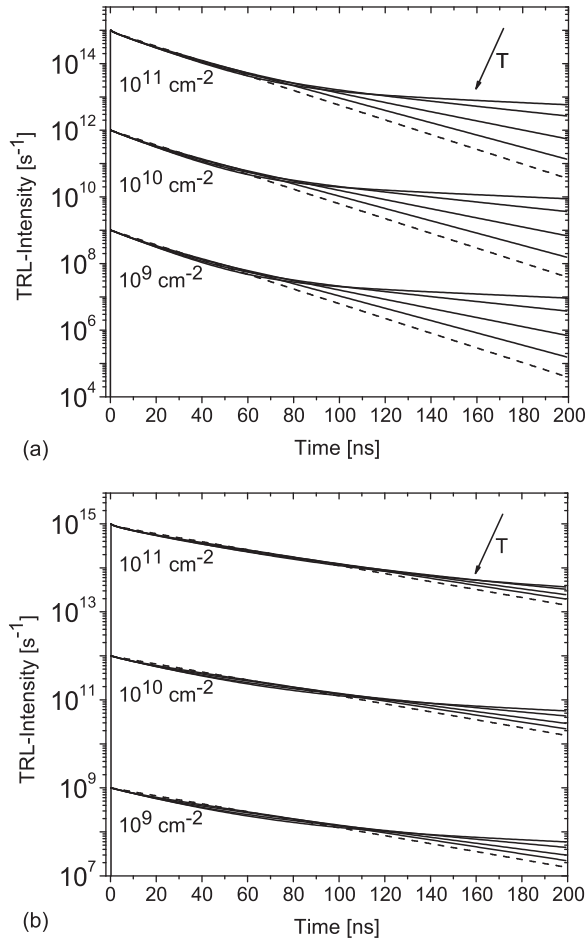
FIG. 7. TRL-transients (after 20 excitations) of a semiconductor layer with a single trap for increased device temperatures $T = 300, 325, 350, 375\,\text{K}$ and different injection levels $n_\gamma = 10^9, 10^{10}, 10^{11}\,\text{cm}^{-2}$ per pulse. Dashed lines are without shallow defects and solid lines with shallow defects.

conduction band. This effect already happens for low injection levels and no high photon densities are needed, such that bimolecular and hole limited recombination can be avoided. It also occurs for a moderate temperature increase. From Section III B, $\tau_e < \tau_n$, τ_c can be estimated for negligible electron trapping leading to the condition

$$n^*(T) > \frac{1}{\sigma_n v_n \tau_n}, \frac{1}{\sigma_n v_n \tau_c}, \qquad (23)$$

which is independent from the excitation.

On the other hand, also the Shockley-Read-Hall lifetime $\tau_{SRH,(n,p)}$ is providing a competing temperature effect. The Shockley-Read-Hall lifetime is defined by $\tau_{SRH,(n,p)} = (v_{n,p} N_d \sigma_{d,(n,p)})^{-1}$, where N_d is the density of deep defects and $\sigma_{d,(n,p)}$ is the capture cross-section of the deep defect. For the thermal velocity it holds $v_{n,p} \propto T^{1/2}$. At room temperature, a localized defect performs harmonic oscillations with amplitude $A_d \propto E^{1/2} \propto T^{1/2}$. The capture cross-section is assumed to be circular shaped, thus $\sigma_{d,(n,p)} \propto A_d^2 \propto T$. Altogether we find $\tau_{SRH,(n,p)} \propto T^{-3/2}$. In experiment, the temperature coefficient of Shockley-Read-Hall (SRH) recombination typically is even larger than 3/2, e.g., for silicon the temperature coefficient is ~ 3.[13] This has to be regarded in temperature dependent TRL experiments.

E. Experimental TRL under increased temperatures

The above considerations show that a slight increase of the device temperature leads to a strong decrease of minority carrier trapping even for low injection levels. In the following, this is demonstrated experimentally for the semiconductor Cu(In,Ga)Se$_2$. In Cu(In,Ga)Se$_2$, it was found by two wavelength excited photoluminescence spectroscopy that one possible trap state lies approximately 800 meV above the valence band maximum.[14] Electrical spectroscopy techniques also reveal a defect state in Cu(In,Ga)Se$_2$ with energies between 100 meV and 250 meV.[15–19] Both observations may have a common origin and may be interpreted as a shallow trap state with about 200 meV activation energy. The setup used for the experiments is described in Ref. 20. By using the metallic molybdenum back contact of the cell as a heating element with electric current passing through it the sample temperature can be increased. The resulting photoluminescence is shown in Figure 8. The luminescence decay time at room temperature is $\sim 300\,\text{ns}$ and decreases strongly by a factor of four if the temperature is increased by 30 K. Now we show that this experimental result cannot be due to the SRH temperature dependence. Therefore, we assume $\tau_{SRH,(n,p)}(T) \propto T^{-3}$ also for CIGSe which is equal to $\tau_{SRH,(n,p)}(T) = \tau_{SRH,(n,p)}(\text{RT})\left(\frac{T}{\text{RT}}\right)^{-3}$ if we normalize to room temperature (RT). We know for low excitations of semiconductors without traps[1,2] that the decay time equals the minority carrier lifetime and the minority carrier lifetime equals the Shockley-Read-Hall lifetime. By that we find the theoretical temperature effect $\tau_{SRH,n}(329\,\text{K})/\tau_{SRH,n}(296\,\text{K}) \approx 0.75$ which is much smaller than the experimental temperature effect $\tau_{decay}(329\,\text{K})/\tau_{decay}(296\,\text{K}) \approx 0.25$. This means, the temperature effect of the Shockley-Read-Hall lifetime is too small to explain the experimental findings. This is also demonstrated in the inset of Figure 8 which shows simulated decay times with and without traps as a function of temperature. Next we show that also fluctuations of the electrostatic potential cannot explain the experimental data. In CIGSe, the band gap and the net-doping density are fluctuating
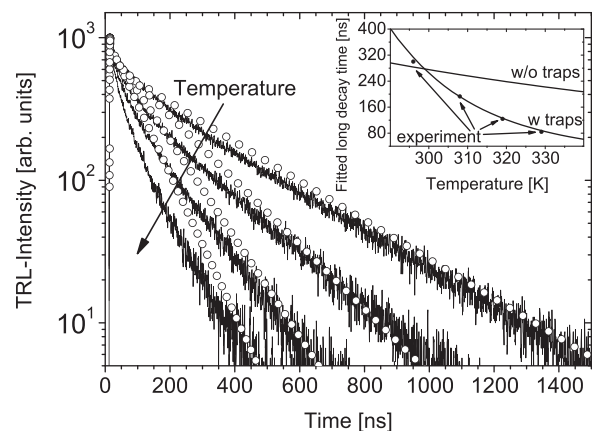

FIG. 8. Experimental (lines) and simulated (dots) TRL data of a Cu(In,Ga)Se$_2$ layer under increasing temperatures of $T = 296, 308, 319, 329\,\text{K}$ and low photon density of $n_\gamma = 9 \times 10^9\,\text{cm}^{-2}$ per pulse. The inset shows the dependence of the decay time of the simulated data (lines) and the experimental data (dots) on the temperature. Simulation with parameters as in Tables II and III.

leading to a fluctuation of conduction and the valence band with deviations up to 80 meV on a sub-micron length scale.[21,22] Such a fluctuation of the electrostatic potential is attended by large electric fields which cause a decay time much smaller than the recombination lifetime due to charge separation effects (see Fig. 9 in Ref. 2). In turn, for decay times of a few hundred nanoseconds, this would mean recombination lifetimes larger than the radiative recombination lifetime which does not make sense physically. Therefore, we assign the temperature effect in CIGSe to electron traps. Using the values described in the Appendix, the TRL can be simulated. The simulated transients are shown in Figure 8 and approximate the experimental TRL well. Residual deviation can be due to inhomogeneous defect distribution in the sample.

V. TRAPS WITH CARRIER RECOMBINATION

In Section V, we want to focus on the validity of our simulations compared to real photoluminescence experiments. In all simulations, the luminescence intensity is calculated from the radiative band-to-band recombination. However, photoluminescence spectroscopy often shows radiative recombination due to electronic free-to-bound transitions. One may ask, under which circumstances the decay by both recombination paths are equal. Band gap gradients or tunnelling assisted non-local recombination are excluded and Equations (1) and (2) are chosen to be the starting point. Now, $h_c \ll e_c$, e_e can no longer be assumed, since we are interested in defect assisted recombination. Since donor like defects near the conduction band are studied it is $\sigma_n v_n n \gg \sigma_p v_p p^*$. Further $p_0 \gg n(t) \gg n_0$ is assumed. This leads to

$$
\begin{aligned}
\frac{\mathrm{d}}{\mathrm{d}t} n &= -\left(\frac{1}{\tau_n} + \sigma_n v_n N_t\right) n + \sigma_n v_n n^* n_t \\
\frac{\mathrm{d}}{\mathrm{d}t} n_t &= \sigma_n v_n N_t n - \left(\sigma_n v_n n^* + \sigma_p v_p p_0\right) n_t.
\end{aligned} \tag{24}
$$

With the assumption $h_c \lesssim e_e$ (24) can be solved yielding

$$
\frac{\frac{\mathrm{d}}{\mathrm{d}t} n_t}{\frac{\mathrm{d}}{\mathrm{d}t} n} \approx \frac{1}{2} + \frac{p_0 v_p \sigma_p}{2 n^* v_n \sigma_n} + \frac{1}{2 \sigma_n} \sqrt{\psi} = \text{constant} \tag{25a}
$$

with

$$
\psi = \sigma_n^2 + \frac{4 \sigma_n^2 N_t}{n^*} + \frac{\sigma_p v_p N_t}{v_n^2 n^{*2}} + \frac{1}{v_n^2 n^{*2} \tau_n^2} - \frac{2 \sigma_n}{v_n n^* \tau_n}
$$
$$
- \frac{2 \sigma_p v_p p_0}{v_n^2 n^{*2} \tau_n}. \tag{25b}
$$

From Equation (25) follows $\frac{\mathrm{d}}{\mathrm{d}t} n_t \approx \frac{B}{\delta \sigma_p v_p} \frac{\mathrm{d}}{\mathrm{d}t} n$ for all times with an appropriate number δ. Integration of this leads to

$$
\underbrace{B p_0 n}_{R_{BTB}} \approx \delta \underbrace{\sigma_p v_p p_0 n_t}_{R_{FTB}}, \tag{26}
$$

where R_{BTB} is the rate of radiative band-to-band recombination and R_{FTB} is the rate of radiative free-to-bound recombination. Both rates are proportional. Hence, they have the same time dependence and finally they exhibit the same decay times. The reason is that we have to demand capture

times $\tau_c \lesssim \tau_n$. Otherwise the defect would not have any impact on the electron density in the conduction band (see Sec. III B). Further, it is known from luminescence spectroscopy that the defects are close to the conduction band and therefore the emission time τ_e is small. In summary, such defects are communicating very fastly with the conduction band. A variation of the electron density in the conduction band leads to an almost immediate variation of the occupied defects and vice versa. Therefore, the decay is almost equal for band-to-band and free-to-bound recombination and the decay time does not depend on the emission wavelength even if the recombination time is not constant as assumed in (24) but a function of time $\tau_n(t)$.

By time-resolved photoluminescence in Cu(In,Ga)Se$_2$ measured at different emission wavelengths, it is revealed that the decay time is mostly independent from the wavelength.[4,8,9] In some cases, however, the decay time decreases with increasing wavelength. The effect becomes stronger if the temperature is reduced which indicates a temperature activated red shift.[8,9] This may be due to potential fluctuations which are predominant in Cu(In,Ga)Se$_2$ and Cu$_2$ZnSnSe$_4$.[23,24]

VI. CONCLUSIONS

In the present work, the impact of minority carrier trapping on the luminescence decay has been studied. We have seen that trapping can cause a biexponential decay, where the first fast decay can be assigned to carrier capture and recombination, whereas the second slow decay can be assigned to carrier emission, re-capture, and recombination. Due to incomplete emission, the trap occupation may depend on the excitation frequency which has to be considered in simulations. The impact of trapping can be reduced by increased excitation intensities and frequencies. Though this is very easy to realize, bimolecular and hole limited recombination are disadvantages. A small variation of the device temperature can decrease the injection level necessary to reduce carrier trapping. Here, a temperature increase has a larger effect than a reduction of the temperature. We consider temperature increase as the method of choice, which we have also demonstrated experimentally. Using CIGSe as an example, we show that by fitting experimental decay curves recombination parameters and trapping parameters can be derived. Finally it has been demonstrated that trap states can be filled by a bias illumination with photon energies smaller than the band gap.

TABLE II. Main parameters used for simulation of TRL.

Simulation parameter	Value
Absorber thickness d	2.8 μm
Absorber's absorption coefficient α	8 μm^{-1}
Absorber charge carrier mobility $\mu_{n,p}$	2 cm^{2}V^{-1}s^{-1}
Recombination at all interfaces $S_{n,p}$	10 cm s^{-1}
Minimum absorber bandgap E_g	1.17 eV
Notch distance from front side d_n	780 nm
Band gap gradient to front side ΔE_f	40 meV
Band gap gradient to back side ΔE_b	100 meV
Temperature coefficient b of $\tau_{SRH,(n0,p0)}$	3
Hole capture-cross section by trap σ_p	10^{-18} cm^2

TABLE III. Acceptor density N_a, SRH-lifetimes $\tau_{SRH,n0}$ and $\tau_{SRH,p0}$ of electrons and holes trap energy $E_c - E_t$, trap density N_t, trap distribution FWHM, and electron capture cross-section σ_n extracted from simulation of TRL.

Acceptor density	SRH-lifetime		Trap parameter			
	Electron	Hole	Energy below CB	FWHM	Density	Electron capture cross section
5×10^{16} cm^{-3}	6 ns	2 μs	185 meV	30 meV	3×10^{16} cm^{-3}	2×10^{-13} cm^2

However, due to thermal emission to the conduction band this causes a bias induced free electron density and leads to a bias luminescence. In Section V, it has been shown that the decay of band-to-band luminescence and the decay of free-to-bound luminescence is almost equal as long as the shallow optically active defects which give rise to the TRL signal are close the conduction band.

APPENDIX: SIMULATION PARAMETERS USED IN SECTION V E

Simulation of TRL was done with Synopsys TCAD®. With the experimental laser excitation diameter of about 70 μm, lateral effects can be neglected and one-dimensional simulations are sufficient. Since recombination velocities at the CIGSe/Mo and the CIGSe/air interface are not conclusively known,[7,25,26] interface recombination is set to a low value, but is taken into account by an effective bulk recombination time $\tau_{SRH,(n0,p0)}$ for deep defect assisted SRH recombination.[10,11] Here, the lifetimes exhibit a temperature dependence according to $\tau_{SRH,(n,p)}(T) \propto T^{-b}$ where the temperature coefficient b is assumed to be 3 as in Silicon.[13] For the carrier mobilities, we chose values as determined by earlier voltage dependent TRL on similar absorber layers.[20] These have to be distinguished from the "standard" mobilities for simulation of Table I. As further experiments on CIGSe layers revealed a Gallium gradient, a V-shaped band gap gradient is considered.[27,28] For simulation of trapping and detrapping of charge carriers by a donor like defect with an energetic Gaussian distribution, we again use the equations of Shockley, Read and Hall (see Eqs. (1), (2), and (6)). The hole capture cross-section of the trap defect is chosen much smaller than the capture cross-section of electrons (see Table II) in order to avoid capture of a hole and thereby distinguishing from recombination centers. To fit experimental photoluminescence, the simulated data are convoluted with a Gaussian shaped instrument response function. The most important simulation parameters are given in Table I.

By finding the best approximation of experimental TRL by simulated ones, we derive the trap parameters, acceptor density, and effective SRH lifetime summarized in Table III.

[1]M. Maiberg and R. Scheer, J. Appl. Phys. **116**, 123710 (2014).
[2]M. Maiberg and R. Scheer, J. Appl. Phys. **116**, 123711 (2014).
[3]R. Scheer, A. Pérez-Rodríguez, and W. K. Metzger, Prog. Photovolt.: Res. Appl. **18**, 467 (2010).
[4]B. Ohnesorge, R. Weigand, G. Bacher, A. Forchel, W. Riedl, and F. H. Karg, Appl. Phys. Lett. **73**, 1224 (1998).
[5]R. Scheer and H.-W. Schock, *Chalcogenide Photovoltaics: Physics, Technologies, and Thin Film Devices* (Wiley-Vch, 2011).
[6]W. K. Metzger, D. Albin, D. Levi, P. Sheldon, X. Li, B. M. Keyes, and R. K. Ahrenkiel, J. Appl. Phys. **94**, 3549 (2003).
[7]S. Shirakata and T. Nakada, Thin Solid Films **515**, 6151 (2007).
[8]S.-I. Shimakawa, K. Kitani, S. Hayashi, T. Satoh, Y. Hashimoto, Y. Takahashi, and T. Negami, Phys. Status Solidi **203**, 2630 (2006).
[9]S.-I. Shimakawa, Y. Hashimoto, S. Hayashi, T. Satoh, and T. Negami, Sol. Energy Mater. Sol. Cells **92**, 1086 (2008).
[10]W. Shockley and W. T. Read, Phys. Rev. **87**, 835 (1952).
[11]R. N. Hall, Phys. Rev. **87**, 387 (1952).
[12]R. K. Ahrenkiel, N. Call, S. W. Johnston, and W. K. Metzger, Sol. Energy Mater. Sol. Cells **94**, 2197–2204 (2010).
[13]M. S. Tyagi and R. V. Overstraeten, Solid-State Electron. **26**, 577 (1983).
[14]A. Gupta, N. Hiraoka, T. Sakurai, A. Yamada, S. Ishizuka, S. Niki, and K. Akimoto, J. Cryst. Growth **378**, 162 (2013).
[15]M. Igalson and P. Zabierowski, Opto-Electron. Rev. **11**(4), 261 (2003).
[16]T. Eisenbarth, T. Unold, R. Caballero, C. A. Kaufmann, and H.-W. Schock, J. Appl. Phys. **107**, 034509 (2010).
[17]G. Brammertz, M. Buffière, S. Oueslati, H. ElAnzeery, K. Ben Messaoud, S. Sahayaraj, C. Köble, M. Meuris, and J. Poortmans, Appl. Phys. Lett. **103**, 163904 (2013).
[18]T. Paul Weiss, A. Redinger, J. Luckas, M. Mousel, and S. Siebentritt, Appl. Phys. Lett. **102**, 202105 (2013).
[19]E. Kask, M. Grossberg, R. Josepson, P. Salu, K. Timmo, and J. Krustok, Mater. Sci. Semicond. Process. **16**, 992 (2013).
[20]M. Maiberg, C. Spindler, E. Jarzembowski, and R. Scheer, Thin Solid Films **582**, 379 (2015).
[21]T. Gokmen, O. Gunawan, T. K. Todorov, and D. B. Mitzi, Appl. Phys. Lett. **103**, 103506 (2013).
[22]J. H. Werner, J. Mattheis, and U. Rau, Thin Solid Films **480–481**, 399 (2005).
[23]D. Kuciauskas, J. V. Li, M. A. Contrera, J. Pankow, and P. Dippo, J. Appl. Phys. **114**, 154505 (2013).
[24]M. J. Romero, H. Du, G. Teeter, Y. Yan, and M. Al-Jassim, Phys. Rev. B **84**, 165324 (2011).
[25]W. K. Metzger, I. L. Repins, M. Romero, P. Dippo, R. N. Contreras, and D. Levi, Thin Solid Films **517**, 2360–2364 (2009).
[26]W. K. Metzger, I. L. Repins, and M. A. Contreras, Appl. Phys. Lett. **93**, 022110 (2008).
[27]T. Orgis, M. Maiberg, and R. Scheer, J. Appl. Phys. **114**, 214506 (2013).
[28]W. Witte, D. Abou-Ras, K. Albe, G. H. Bauer, F. Bertram, C. Boit, R. Brüggemann, J. Christen, J. Dietrich, A. Eicke, D. Hariskos, M. Maiberg, R. Mainz, M. Meessen, M. Müller, O. Neumann, T. Orgis, S. Paetel, J. Pohl, H. Rodriguez-Alvarez, R. Scheer, H.-W. Schock, T. Unold, A. Weber, and M. Powalla, Prog. Photovolt.: Res. Appl. **23**(6), 717–733 (2014).

Investigation of long lifetimes in Cu(In,Ga)Se$_2$ by time-resolved photoluminescence

Matthias Maiberg, Torsten Hölscher, Setareh Zahedi-Azad, Wolfgang Fränzel, and Roland Scheer

Institute of Physics, Martin-Luther-University Halle-Wittenberg, 06120 Halle, Germany

The main objective of time-resolved photoluminescence (TRPL) is to characterize minority carrier recombination in semiconductors. However, trap states in the band gap can lead to artificially long decay times thus distorting the measured minority carrier lifetime. In this work, we propose to measure TRPL under elevated temperature and excitation in order to reduce minority carrier trapping. Taking three Cu(In,Ga)Se$_2$ layers as examples, we show that the decay time decreases with increasing temperature—in accordance with simulations. Under increasing excitation, the decay time can become smaller due to trap saturation but also can become larger due to asymmetric hole and electron lifetimes. By comparison of simulation and experiment, we can find the energy, the density, and the electron capture cross-section of the trap which in the present example of Cu(In,Ga)Se$_2$ films gives values of $\sim$200 meV, $\sim$10^{15} cm^{-3}, and $\sim$10^{-13} cm^2, respectively. © 2015 AIP Publishing LLC. [http://dx.doi.org/10.1063/1.4931632]

One of the most important parameters characterizing the quality of doped semiconductors is the minority carrier lifetime. A well-established method for its determination in silicon or GaAs is the measurement of time-resolved photoluminescence (TRPL).[1] However, in thin film semiconductors such as Cu(In,Ga)Se$_2$ and Cu$_2$ZnSnSe$_4$ the luminescence decay is often biexponential with first and second decay time, the latter often being much larger than the former. The reason for two decay times (as well as their correlation with the minority carrier lifetime) is still not accurately known.[2–5] One possibility is the presence of minority carrier trap states in the band gap. The so called N$_2$ defect in Cu(In,Ga)Se$_2$, for instance, which is revealed by admittance and two-photon spectral photoluminescence, would have an appropriate activation energy for minority carrier trapping of 250 meV.[6,7] Then, we expect a decrease of the second decay time with increasing temperature due to enhanced detrapping.[8] Further, for increasing excitation the traps may saturate.

In this work, we perform TRPL measurements on co-evaporated Cu(In,Ga)Se$_2$ (CIGSe) films at measurement temperatures between 296 K and 334 K and under different injection levels. We indeed find the predicted dependencies expected for absorber layers with minority carrier traps.[8] Considering minority carrier trapping in simulations, we can determine the trap density, trap activation energy, and trap electron capture cross-section as well as the carrier lifetimes by approximation of experimental and simulated TRPL.

Three different CIGSe absorbers were selected in order to demonstrate the variety of effects to be observed in CIGSe thin films. In the following, we call them CIGSe1, CIGSe2, and CIGSe3. The layers were grown on different Mo coated soda-lime substrates which we refer to by Mo(A) and Mo(B). The samples were prepared by the standard three-stage co-evaporation method[9] with similar deposition times and temperatures in the first and second stage. The final $\frac{[Cu]}{[Ga]+[In]}$ and $\frac{[Ga]}{[Ga]+[In]}$ concentrations as well as KF treatment are summarized in Table I. It is worth mentioning that TRPL measurements were carried out on fresh absorbers immediately after preparation.

For the measurement of TRPL, the time-correlated single photon counting setup described in Ref. 10 is used. The time resolution of the setup is about 1 ns. First, a variation of the excitation is performed. For photoexcitation, a 638 nm pulsed diode laser with a pulse length of 88 ps and a repetition frequency of 500 kHz is used. The maximum incident photon density per pulse is $n_\lambda = (9 \pm 2) \times 10^{11}$ cm^{-2} which is denoted in the following by $I = 100\%$. After this, the temperature is increased under constant excitation starting at room temperature. To this end, the molybdenum thin film layer is contacted at two opposite sides of the substrate and a voltage is applied. Due to the electrical current through the Mo layer, the temperature can be adjusted between room temperature and 340 K. Each temperature and excitation variation needs about 1 h of time. Afterwards excitation and temperature are reset to the start values to retrieve possible degradation during the measurement. Only for the temperature variation on sample CIGSe1, the decay time reduces to 75% compared to the beginning which can be assigned to temperature induced degradation. Since the quantum yield of all samples was similar, the transients' maxima are normalized and the background is subtracted.

Simulation of TRPL was done with Synopsys TCAD®. With the experimental laser excitation diameter of about 70 μm, lateral effects can be neglected and one-dimensional simulations are sufficient. Since recombination velocities at the CIGSe/Mo and the CIGSe/air interface are not conclusively known,[3,4,11] interface recombination is set to a low value but is taken into account by an effective bulk recombination time $\tau_{SRH,(n0,p0)}$ for deep defect assisted Shockley-Read-Hall (SRH) recombination.[12,13] Here, the lifetimes exhibit a temperature dependence according to Equation (1) where the temperature coefficient b is assumed to be 3 as in silicon.[14] For CIGSe1, $b = 5$ is used to account for an additional decrease of the lifetime because of degradation during

TABLE I. CIGSe processing parameters.

Sample	Final $\frac{[Cu]}{[Ga]+[In]}$	Final $\frac{[Ga]}{[Ga]+[In]}$	KF-treatment	Substrate
CIGSe1	0.88	0.76	Post deposition	Mo(A)
CIGSe2	0.85	0.32	No	Mo(A)
CIGSe3	0.85	0.32	No	Mo(B)

the temperature measurement. For the carrier mobilities, we chose values as determined by voltage dependent TRPL on similar absorber layers.[10] As further experiments on CIGSe layers revealed a gallium gradient, a V-shaped band gap gradient is considered.[15,16] For simulation of trapping and detrapping of charge carriers by a donor like defect with an energetic Gaussian distribution, we again use the equations of Shockley, Read, and Hall.[8,12,13] The hole capture cross-section of the trap defect is chosen much smaller than the capture cross-section of electrons (see Table III) in order to avoid capture of a hole and thereby distinguishing trap states from recombination centers. To fit experimental photoluminescence, the simulated data are convoluted with a Gaussian shaped instrument response function. The most important simulation parameters are given in Table II.

Figure 1 shows the TRPL of absorber layer CIGSe1. For fixed excitation, we find a decrease of the long decay time with increasing temperature, and we have considered three alternative explanations for this behaviour. In the first place, this may be due to a smaller electron recombination lifetime τ_n at higher temperatures. The electron recombination lifetime is defined by $R_n = \frac{\Delta n}{\tau_n}$, where R_n is the rate of electron recombination with the abundant holes and Δn is the excess electron density. A rough calculation[8] predicts a temperature dependence of the SRH lifetime according to

$$\tau_{SRH,n0}(T) = \tau_{SRH,n0}(300\,\mathrm{K})\left(\frac{T}{300\,\mathrm{K}}\right)^{-b}, \quad (1)$$

with $b = 5$ for CIGSe1. For measurement at different temperatures we use low injection levels, thus, the generated minority carrier density Δn_0 is much smaller than the doping density. Furthermore, Shockley-Read-Hall recombination is dominating. Then it is $\tau_n \approx \tau_{SRH,n0}$ and we would have[17,18]

$$I_{PL}(t;T) \sim \Delta n(t;T) \sim e^{-\frac{t}{\tau_{SRH,n0}(T)}}. \quad (2)$$

However, this theoretical dependence of the luminescence decay on the temperature $(\tau_{SRH,n0}(334\,\mathrm{K})/\tau_{SRH,n0}(296\,\mathrm{K}) \approx 0.5)$ comes out too weak to explain the strong temperature dependence in experiments $(\tau_{decay}(334\,\mathrm{K})/\tau_{decay}(296\,\mathrm{K}) \approx 0.2)$.

TABLE III. Main parameters used for simulation of TRPL.

Simulation parameter	Value
Absorber thickness d	2.8 μm
Absorber's absorption coefficient α	8 μm^{-1}
Absorber charge carrier mobility $\mu_{n,p}$	2 cm^2 V^{-1} s^{-1}
Recombination at all interfaces $S_{n,p}$	10 cm s^{-1}
Minimum absorber bandgap E_g	1.41 eV (CIGSe1)
	1.17 eV (CIGSe2/3)
Notch distance from front side d_n	340 nm (CIGSe1)
	780 nm (CIGSe2/3)
Band gap gradient to front side ΔE_f	80 meV (CIGSe1)
	40 meV (CIGSe2/3)
Band gap gradient to back side ΔE_b	230 meV (CIGSe1)
	100 meV (CIGSe2/3)
Temperature coefficient b of $\tau_{SRH,(n0,p0)}$	5 (CIGSe1)
	3 (CIGSe2/3)
Hole capture-cross section by trap σ_p	10^{-18} cm^2

In the second place, the temperature effect may arise from fluctuations of the electrostatic potential with amplitudes being up to 80 mV.[19,20] If so, we expect a decay time smaller than the recombination lifetime (see Fig. 9 in Ref. 18). In turn, for decay times of a few hundred nanoseconds, this leads to recombination lifetimes larger than the radiative recombination lifetime which does not make sense physically.

In the third place, the temperature effect on the second decay may be due to thermally enhanced detrapping of electrons from trap states more than 100 meV below the conduction band. Then, we find for the long decay time[8]

$$\tau_{decay} \approx \frac{\tau_e\,\tau_n}{\tau_c}, \quad (3a)$$

with

$$\tau_c^{-1} = \sigma_n v_n N_t \quad \tau_e^{-1} = \sigma_n v_n N_c\, e^{-\frac{E_c-E_t}{kT}}, \quad (3b)$$

where τ_n is the recombination, τ_c is the capture, and τ_e is the emission time. E_c–E_t is the energy of the trap below the conduction band, N_c is the effective density of states of the conduction band, v_n is the thermal velocity of electrons, σ_n is the capture cross-section of electrons, and N_t is the density of trap states. Again, $\tau_n \approx \tau_{SRH,n0}$ is assumed and with Equations (1) and (3) we find

$$\tau_{decay} \sim e^{\frac{E_c-E_t}{kT}} \cdot T^{-b}. \quad (4)$$

Thus, the trap effect predicts the decay time to strongly decrease with temperature.

TABLE II. Acceptor density N_a, SRH-lifetimes $\tau_{SRH,n0}$ and $\tau_{SRH,p0}$ of electrons and holes trap energy E_c–E_t, trap density N_t, trap distribution FWHM, and electron capture cross-section σ_n extracted from simulation of TRPL of sample CIGSe1, CIGSe2, and CIGSe3. Other simulation parameters from Table III.

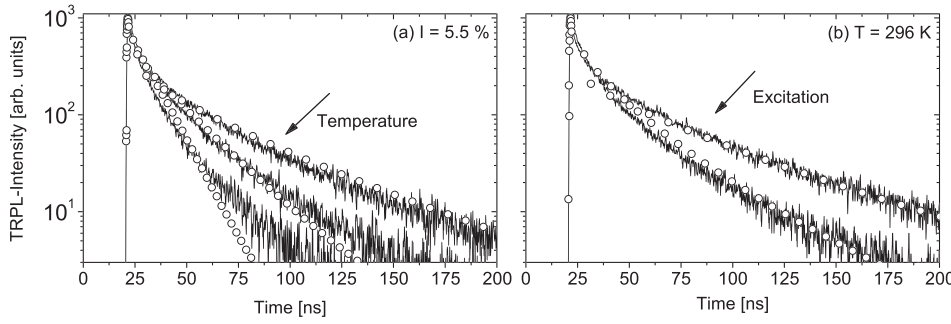| Sample	Acceptor density (cm^{-3})	SRH-lifetime		Trap parameter			
		Electron (ns)	Hole	Energy below CB (meV)	FWHM (meV)	Density (cm^{-3})	Electron capture cross section (cm^2)
CIGSe1	7×10^{15}	2	130 ns	220	30	4×10^{15}	2×10^{-13}
CIGSe2	1.6×10^{16}	4	2 μs	185	35	1.1×10^{16}	2×10^{-13}
CIGSe3	5×10^{16}	6	2 μs	185	30	3×10^{16}	2×10^{-13}

FIG. 1. Experimental (lines) and simulated (circles) TRPL-transients of absorber layer CIGSe1 for (a) $I = 5.5\%$ and temperature $T = 296$, 315, and 334 K and (b) for 296 K and $I = 1\%$, 18%. Parameters for simulation from Tables II and III.

For fixed temperature and increasing excitation, a decrease of the long time part of the transient is found. This may have two reasons. First, due to bimolecular recombination, the recombination time τ_n can decrease with increasing excitation. This would lead to a decrease of the decay time regardless of trap states. Second, the electron supply from the trap states becomes negligible if[8]

$$\Delta n_0 \gg \frac{\tau_n}{\tau_c} \, e^{\frac{T_p}{\tau_n}} N_c \, e^{-\frac{E_c - E_t}{kT}} \qquad (5)$$

holds for the photogenerated electron density with T_p being the period of excitation. This means, the traps are saturated, trapping effects are reduced and only recombination (with shorter decay times) affects the luminescence decay. After these considerations, we adjust trap parameters in the simulation in order to find the best approximation of experimental by simulated TRPL. The thereby obtained parameters are given in Table III.

Next, the TRPL of sample CIGSe2 is analyzed which is illustrated in Figure 2. Again, a strong decrease of the long decay time with increasing temperature is found due to a decrease of the recombination time and thermally enhanced detrapping as discussed above. The intensity dependence, however, shows a behaviour being different from that of sample CIGSe1, i.e., an increase of the decay time with increasing excitation. To understand this, the SRH lifetime of electrons is studied. For defects with mid-bandgap energy in a p-type semiconductor, the SRH-recombination rate is given by

$$R_{SRH} = \frac{p_0 + \Delta p}{\tau_{n0}(p_0 + \Delta p) + \tau_{p0}\Delta n} \, \Delta n, \qquad (6)$$

with p_0 being the equilibrium hole density and Δn and Δp being the excess electron and hole density. By defining the electron SRH-lifetime by $\tau_{SRH,n} := \frac{\Delta n}{R_{SRH}}$, it comes out as

$\tau_{SRH,n} = \tau_{n0} + \tau_{p0} \frac{\Delta n}{p_0 + \Delta p}$. Considering the two limiting cases $\Delta p \ll p_0$ and $\Delta p \gg p_0$, the electron SRH-lifetime becomes

$$\tau_{SRH,n} \approx \begin{cases} \tau_{SRH,n0} & \text{for } \Delta p \ll p_0, \\ \tau_{SRH,n0} + \dfrac{\Delta n}{\Delta p}\tau_{SRH,p0} & \text{for } \Delta p \gg p_0. \end{cases} \qquad (7)$$

It is always $\frac{\Delta n}{\Delta p} > 0$ regardless of electron trapping because Δn and Δp are positive quantities. According to Equation (7), the high injection electron SRH-lifetime $\tau_{SRH,n0} + \frac{\Delta n}{\Delta p}\tau_{SRH,p0}$ then is larger than the low-injection electron SRH-lifetime τ_{n0}. This shows that the Shockley-Read-Hall lifetime of electrons increases with excitation regardless of electron trapping. Then, also the decay time increases for higher excitation in agreement with Equation (3a). In experiment, the maximum excess hole density is $\Delta p_{max} \approx p_0$, thus, being between the two limiting cases of Equation (7). The material parameters determined by simulation are given in Table III. Trap energy, electron capture cross-section, and electron SRH-lifetime are in the same range as for CIGSe1. The trap energy is slightly reduced due to the lower band gap. However, the hole SRH-lifetime is now larger than for CIGSe1. According to Equation (7), this causes a stronger increase of the electron SRH-lifetime with excitation compared to CIGSe1 which leads to different trends. Further, the acceptor density is increased. Since Cu(In,Ga)Se$_2$ is a compensated semiconductor, the density of donor traps is increased, too, which causes stronger carrier trapping and longer decay times.

Finally, the TRPL of absorber layer CIGSe3 shown in Figure 3 is studied. Here, the well-known temperature dependence of the TRPL decay is found but now the decay does hardly depend on the excitation intensity. This can be understood by the parameters in Table III, where the acceptor is increased. Due to the compensation in CIGSe, this also leads to increased trap densities which can barely be
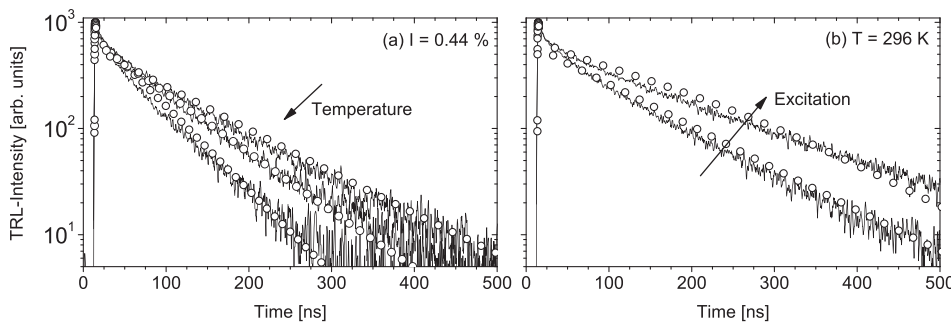

FIG. 2. Experimental (lines) and simulated (circles) TRPL-transients of absorber layer CIGSe2 for (a) $I = 0.44\%$ and temperature $T = 296$, 304, and 313 K and (b) for 296 K and $I = 0.7\%$, 5.6%. Parameters for simulation from Tables II and III.
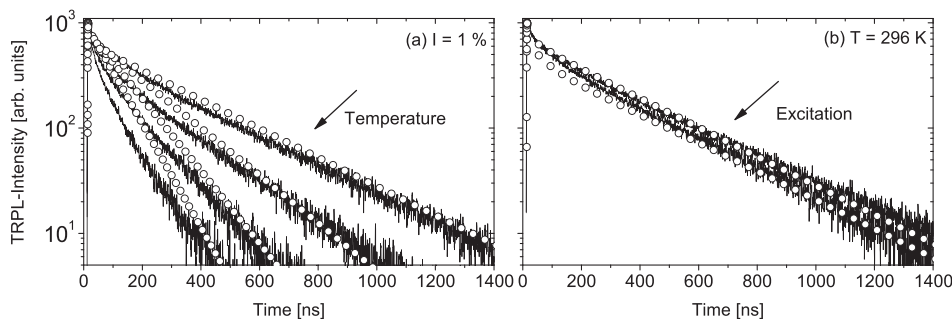
FIG. 3. Experimental (lines) and simulated (circles) TRPL-transients of absorber layer CIGSe3 for (a) $I = 1\%$ and temperature $T = 296$, 308, 319, and 329 K and (b) for 296 K and $I = 0.3\%$, 18%. Parameters for simulation from Tables II and III.

saturated. Therefore, trapping is dominating and recombination of charge carriers with asymmetric lifetimes is not apparent. One explanation for higher acceptor densities may be a higher Na content[21,22] as a consequence of the different substrate. On the other hand, sodium induces a reduction of donor states located at grain boundaries, thus, leading to an increased net hole density.[23,24] Since the donor traps in this work are apparently not passivated by sodium, they are presumably located in the grain interior. The effect of an improved bulk quality by Na as shown in Ref. 28 is not reflected in the simulation parameters.

The donor trap energy of ~ 0.2 eV determined for all samples has also been revealed by admittance, two-photon, and capacitance spectroscopy, however, with much smaller capture cross-sections of $\sim 10^{-16}$ cm^2.[6,7,25] Furthermore, capacitance measurements revealed an acceptor density of 10^{16} cm^{-3} which is in agreement with the values in Table III.[26] Finally, the decrease of the recombination lifetime with higher gallium content is consistent with JV-measurements.[27]

In summary, photoluminescence decay of three different CIGSe absorber layers was presented. The decay time strongly decreases at slight temperature increase. Excluding other origins, minority carrier trapping has been identified as source of the strong temperature effect. A donor trap about 200 meV below the conduction band is appropriate to simulate the temperature dependent transients which is in agreement with defect activation energies determined by spectral photoluminescence and admittance spectroscopy.

At increased excitation either trapping effects are reduced due to trap saturation or the recombination lifetime is increased due to deep defect saturation. Both effects can counterbalance or dominate each other, thus, leading to a decrease, an increase or nearly no excitation dependence. This study suggests that in typical CIGSe layers the carrier dynamics is governed by recombination and trapping, both acting on similar time scales. We find that small changes in material parameters can influence trapping and recombination.

[1]R. K. Ahrenkiel, N. Call, S. W. Johnston, and W. K. Metzger, Sol. Energy Mater. Sol. Cells **94**, 2197 (2010).

[2]I. Repins, C. Beall, N. Vora, C. DeHart, D. Kuciauskas, P. Dippo, B. To, J. Mann, W.-C. Hsu, A. Goodrich, and R. Noufi, Sol. Energy Mater. Sol. Cells **101**, 154 (2012).

[3]W. K. Metzger, I. L. Repins, and M. A. Contreras, Appl. Phys. Lett. **93**, 022110 (2008).

[4]S. Shirakata and T. Nakada, Thin Solid Films **515**, 6151 (2007).

[5]S.-I. Shimakawa, K. Kitani, S. Hayashi, T. Satoh, Y. Hashimoto, Y. Takahashi, and T. Negami, Phys. Status Solidi **203**, 2630 (2006).

[6]T. Eisenbarth, T. Unold, R. Caballero, C. A. Kaufmann, and H.-W. Schock, J. Appl. Phys. **107**, 034509 (2010).

[7]A. Gupta, N. Hiraoka, T. Sakurai, A. Yamada, S. Ishizuka, S. Niki, and K. Akimoto, J. Cryst. Growth **378**, 162 (2013).

[8]M. Maiberg, S. Zahedi-Azad, T. Hölscher, and R. Scheer, J. Appl. Phys. **118**, 105701 (2015).

[9]K. Ramanathan, M. A. Contreras, C. L. Perkins, S. Asher, F. S. Hasoon, J. Keane, D. Young, M. Romero, W. Metzger, R. Noufi *et al.*, Prog. Photovoltaics: Res. Appl. **11**, 225 (2003).

[10]M. Maiberg, C. Spindler, E. Jarzembowski, and R. Scheer, Thin Solid Films **582**, 379 (2015).

[11]W. K. Metzger, I. L. Repins, M. Romero, P. Dippo, R. N. Contreras, and D. Levi, Thin Solid Films **517**, 2360 (2009).

[12]W. Shockley and W. T. Read, Phys. Rev. **87**, 835 (1952).

[13]R. N. Hall, Phys. Rev. **87**, 387 (1952).

[14]M. S. Tyagi and R. V. Overstraeten, Solid-State Electron. **26**, 577 (1983).

[15]T. Orgis, M. Maiberg, and R. Scheer, J. Appl. Phys. **114**, 214506 (2013).

[16]W. Witte, D. Abou-Ras, K. Albe, G. H. Bauer, F. Bertram, C. Boit, R. Brüggemann, J. Christen, A. Dietrich, A. Eicke, D. Hariskos, M. Maiberg, R. Mainz, M. Meessen, M. Müller, O. Neumann, T. Orgis, S. Paetel, J. Pohl, H. Rodriguez-Alvarez, R. Scheer, H.-W. Schock, T. Unold, A. Weber, and M. Powalla, Prog. Photovoltaics: Res. Appl. **23**, 717 (2015).

[17]M. Maiberg and R. Scheer, J. Appl. Phys. **116**, 123710 (2014).

[18]M. Maiberg and R. Scheer, J. Appl. Phys. **116**, 123711 (2014).

[19]T. Gokmen, O. Gunawan, T. K. Todorov, and D. B. Mitzi, Appl. Phys. Lett. **103**, 103506 (2013).

[20]J. H. Werner, J. Mattheis, and U. Rau, Thin Solid Films **480–481**, 399 (2005).

[21]E. Jarzembowski, M. Maiberg, F. Obereigner, K. Kaufmann, S. Krause, and R. Scheer, Thin Solid Films **576**, 75 (2015).

[22]J. Hedström, L. Stolt, J. Kessler, M. Ruckh, K.-O. Velthaus, and H.-W. Schock, Appl. Phys. Lett. **62**, 597 (1993).

[23]D. Cahen and R. Noufi, Appl. Phys. Lett. **54**, 558 (1989).

[24]L. Kronik, D. Cahen, and H.-W. Schock, Adv. Mater. **10**, 31 (1998).

[25]M. Igalson and P. Zabierowski, Opto-Electron. Rev. **11**, 261 (2003).

[26]U. Rau and M. Schmidt, Thin Solid Films **387**, 141 (2001).

[27]M. A. Contreras, L. M. Mansfield, B. Egaas, J. Li, M. Romero, R. Noufi, E. Rudiger-Voigt, and W. Mannstadt, Prog. Photovoltaics: Res. Appl. **20**, 843 (2012).

[28]A. Rockett, Thin Solid Films **480–481**, 2 (2005).

Investigation of long decay times in $Cu_2ZnSnSe_4$ by time-resolved photoluminescence

Matthias Maiberg,[1] Torsten Hölscher,[1] Stefan Hartnauer,[1] and Roland Scheer[1]

Institute of Physics, Martin-Luther-University Halle-Wittenberg, 06120 Halle, Germany

In this work we present time-resolved photoluminescence (TRPL) measurements on $Cu_2ZnSnSe_4$ and alloyed $Cu_2ZnSnSe_4$-$CuInSe_2$ layers. In the latter case we find one-exponential decays. In the first case the decay is bi-exponential indicating a large amount of minority carrier traps. By approximation of experimental $Cu_2ZnSnSe_4$ TRPL by simulated decay curves we determine the trap energy, the trap density, and the electron capture cross-section of the trap with reasonable values of $\sim 10^{15}\,\mathrm{cm^{-3}}$, $\sim 250\,\mathrm{meV}$, and $10^{-13}\,\mathrm{cm^{-2}}$. The trap density of the alloyed $Cu_2ZnSnSe_4$-$CuInSe_2$ layers, however, is estimated to $\leq 10^{13}\,\mathrm{cm^{-3}}$.

Keywords: transient, photoluminescence, trap states, $Cu_2ZnSnSe_4$

One of the most important material parameters of doped semiconductors is the minority carrier lifetime. The measurement of transient photoluminescence (TRPL) is a prevalent method for its determination in silicon or GaAs.[1] For co-evaporated $Cu_2ZnSnSe_4$ (CZTSe) and $Cu(In,Ga)Se_2$ (CIGSe), however, the luminescence decay is often bi-exponential and the reason for two decay times as well as their correlation with the minority carrier lifetime is still not accurately known.[2–5] One reason for a bi-exponential decay may be the trapping of minority carriers[6], which has already been approved by time-resolved photoluminescence in $Cu(In,Ga)Se_2$.[7] Therefore, it is evident to find a large amount of trap states also in $Cu_2ZnSnSe_4$ due to the similar electronic structure. Defects with energies suitable for trapping are revealed by spectral photoluminescence and admittance spectroscopy with activation energies of $70\,\mathrm{meV}$-$200\,\mathrm{meV}$ whereas defects deeper in the band gap are predicted by theoretical calculations with energy values of $\sim 300\,\mathrm{meV}$ below the conduction band edge.[8–12] It now depends on the capture cross-sections of these defects, whether they will act as recombination centers or as minority carrier traps. In the first case, a one-exponential decay of the time-resolved photoluminescence is expected, and in the latter case the decay will be bi-exponential with a long decay time decreasing with increasing excitation and temperature.[6] Hence, the transients' shape and dependence on excitation and temperature can be used to discriminate recombination centers from minority carrier traps.

In this work, we verify minority carrier traps in CZTSe by finding the expected dependencies of the luminescence decay from temperature and excitation. By the approximation of the experimental luminescence by simulation we can determine the density, activation energy and electron capture cross-section of the trap, as well as the minority carrier lifetime and the acceptor density. Thereby, we further show that the alloying with $CuInSe_2$ reduces the amount of minority carrier traps in $Cu_2ZnSnSe_4$-$CuInSe_2$ (CZTISe).

Three slightly different chalcogenide samples were prepared on a glass substrate coated with molybdenum

TABLE I. Thickness and elemental composition determined by EDX of the $Cu_2ZnSnSe_4$ (CZTSe1 and CZTSe2) and $Cu_2ZnSnSe_4$-$CuInSe_2$ (CZTISe) layers.

Sample	Thickness	Final $\frac{[Zn]}{[Sn]}$	Final $\frac{[Cu]}{[In]+[Zn]+[Sn]}$	Final $\frac{[In]}{[In]+[Zn]+[Sn]}$
CZTISe	$1.6\,\mathrm{\mu m}$	1.39	0.84	0.08
CZTSe1	$2\,\mathrm{\mu m}$	1.27	0.82	0
CZTSe2	$2.4\,\mathrm{\mu m}$	1.82	0.68	0

by means of a two-stage Cu-rich/Cu-free co-evaporation process being similar to that described in section 3.3 "Process C" of Ref. 13. By this process, two $Cu_2ZnSnSe_4$ layers CZTSe1 and CZTSe2, and one alloyed $Cu_2ZnSnSe_4$-CuInSe2 layer CZTISe were prepared, the latter by additional incorporation of indium in both stages. Further information on alloyed CZTSe can be found in Ref. 14 and 15. After the preparation, the elemental composition was determined by energy dispersive X-ray spectroscopy (EDX) with the values summarized in table I.

For the measurement of TRPL the setup described in Ref. 16 is used with an equal workflow for all samples. First, a variation of the injection level is performed. To this end, a pulsed diode laser with an excitation wavelength of $638\,\mathrm{nm}$, a pulse length of $88\,\mathrm{ps}$, and a repetition frequency of $\sim 1\,\mathrm{MHz}$ is used. The maximum incident photon density per pulse is $n_\lambda = (9 \pm 2) \times 10^{11}\,\mathrm{cm^{-2}}$ which in the following is denoted by $I = 100\%$. Afterwards, the temperature is varied starting at room temperature. We use the molybdenum back contact layer as a heating element. Due to the electrical current through the Mo layer, the CZT(I)Se temperature can be adjusted between room temperature and $340\,\mathrm{K}$. After each variation, excitation and temperature are reset to the start values. By doing so, degradation during the measurement may be retrieved. However, it comes out that all samples do not exhibit any degradation. At the end, the transients' maxima are normalized and the background is subtracted which is reasonable since the quantum yield

TABLE II. Main parameters used for simulation of TRPL.

simulation parameter	value
max. incident photon density n_γ	9×10^{11} cm^{-2}
incident photon wavelength λ	638 nm
absorber's absorption coefficient α	8 μm^{-1}
absorber charge carrier mobility $\mu_{n,p}$	5 cm^2 V^{-1} s^{-1}
recombination velocity at all interfaces $S_{n,p}$	10 cm s^{-1}
absorber bandgap E_g	1 eV
hole capture cross-section by trap σ_p	10^{-18} cm^2
width of energetic trap distribution ΔE	50 meV

of all samples was similar.

The simulation of TRPL was done with Synopsys TCAD®. With a laser excitation diameter of about 70 μm lateral effects can be neglected, thus, one-dimensional simulations are sufficient. Since recombination velocities at the absorber/molybdenum and the absorber/air interface are not conclusively known[3,4,17] interface recombination is set to a low value, but is considered by an effective bulk recombination time $\tau_{SRH,(n0,p0)}$ for deep defect assisted Shockley-Read-Hall (SRH) recombination.[18,19] Here, the lifetimes are further supposed to be temperature dependent according to equation (1). In order to simulate minority carrier trapping and detrapping we again use the equations of Shockley, Read, and Hall[18,19] and apply them to a donor like defect near the conduction band. Here, the hole capture cross-section of the trap defect is chosen much smaller than the capture cross-section of electrons to distinguish the trap state from recombination centers. To fit experimental photoluminescence the simulated data are convoluted with a Gaussian shaped instrument response function to account for the time resolution of the measurement setup which is approximately 1 ns. The most important simulation parameters are given in table II.

First, the TRPL of sample CZTISe is studied which is shown in figure 1. The decay of the luminescence is one-exponential with a decay time of a few nanoseconds. The decay time decreases slightly if the temperature increases. This may in the first place be due to a smaller electron recombination lifetime τ_n at higher temperatures. Here, the electron recombination lifetime is defined by $R_n = \frac{\Delta n}{\tau_n}$, where R_n is the rate of electron recombination with an abundant hole and Δn is the excess electron density. A rough calculation[6] predicts a temperature dependence of the SRH lifetime according to

$$\tau_{SRH,n0}(T) = \tau_{SRH,n0}\,(300\,\text{K}) \left(\frac{T}{300\,\text{K}}\right)^{-b}, \quad (1)$$

where b is around 3, e.g. in silicon b is between 2.7 and 3.4.[20] For measurement at different temperatures low in-

jection levels were used leading to a generated minority carrier density Δn_0 much smaller than the doping density. Furthermore, Shockley-Read-Hall recombination is dominating. Then it is $\tau_n \approx \tau_{SRH,n0}$ and we have[21,22]

$$I_{PL}(t;T) \sim \Delta n(t;T) \sim \mathrm{e}^{-\frac{t}{\tau_{SRH,n0}(T)}}. \quad (2)$$

Equation (2) describes a temperature dependent luminescence decay with a decay time

$$\tau_{decay}(T) \approx \tau_{SRH,n0}(T) \sim \left(\frac{T}{300\,\text{K}}\right)^{-b}. \quad (3)$$

From experiment we find a decrease of the decay time by about 25% if the temperature is increased by 40 K. From equation (3) the temperature coefficient in CZTSe then becomes $b \approx 2.7$. A similar dependence is revealed during the excitation variation where we find a slight decrease of the luminescence decay time if the injection level is increased. This may be due to additional bimolecular recombination at increased excitation which reduces the electron recombination lifetime. Both effects are included in the simulation of TRPL, so that the experimental data can be approximated by simulation (see Fig. 1) using the material parameters from table II and III. We note that the TRPL effects described for CZTISe is typical and has been found on several samples.

We now study TRPL on CZTSe layers that were processed without incorporation of indium. The luminescence decay for CZTSe1 having a moderate Zn/Sn excess of 1.27 is shown in figure 2. For this sample, the luminescence decay is different from the previous: First, the decay is bi-exponential. Second, we find a strong decrease of the decay time of about 75% for a temperature increase of 40 K, which cannot be traced back to the decrease of the Shockley-Read-Hall lifetime. Both lead to the need for consideration of other (additional) effects. As mentioned in the introduction, minority carrier trapping may explain bi-exponential luminescence decays and strong temperature dependencies. Then, it holds for the long decay time[6]

$$\tau_{decay} \approx \frac{\tau_e\,\tau_n}{\tau_c} \quad (4a)$$

with

$$\tau_c = (\sigma_n\,v_n\,N_t)^{-1} \quad (4b)$$

$$\tau_e = \left(\sigma_n\,v_n\,N_c\,\mathrm{e}^{-\frac{E_c - E_t}{kT}}\right)^{-1}, \quad (4c)$$

where τ_n is the recombination time, τ_c is the capture time, τ_e is the emission time, $E_c - E_t$ is the energy of the trap below the conduction band, N_c is the effective density of states of the conduction band, v_n is the thermal velocity of electrons, σ_n is the capture cross-section of electrons by the trap, and N_t is the density of trap states. Again, we assume $\tau_n \approx \tau_{SRH,n0}$ due to the low injection levels, and with equation (1) and (4) we then find

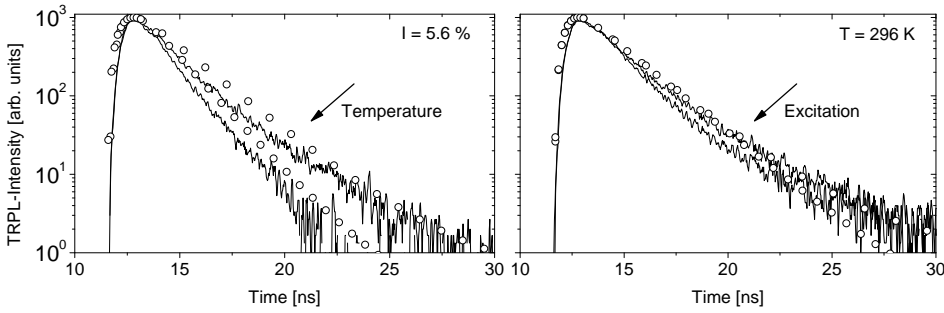$$\tau_{decay} \sim \mathrm{e}^{\frac{E_c - E_t}{kT}} \cdot T^{-b}. \quad (5)$$

FIG. 1. Experimental (lines) and simulated (dots) TRPL-transients of absorber layer CZTISe for (a) $I = 5.6\%$ and temperature $T = 296$, 334 K and (b) for 296 K and $I = 1$, 50%. Parameters for simulation from table II and III.

TABLE III. Acceptor density N_a, SRH-lifetimes $\tau_{SRH,(n0,p0)}(300\,\text{K})$ of electrons and holes, temperature coefficient b of the SRH-lifetime, trap energy $E_c - E_t$, trap density N_t, and electron capture cross-section σ_n extracted from simulation of TRPL of sample CZTISe, CZTSe1, and CZTSe2. Other simulation parameters from Table II.

sample	acceptor density	SRH-recombination		trap parameter		
		lifetime	temperature coefficient	energy below CB	electron capture cross-section	density
CZTISe	$5 \times 10^{16}\,\text{cm}^{-3}$	2 ns	2.7	250 meV	$4 \times 10^{-13}\,\text{cm}^2$	$\leq 10^{13}\,\text{cm}^{-3}$
CZTSe1	$5 \times 10^{16}\,\text{cm}^{-3}$	2 ns	2.7	250 meV	$4 \times 10^{-13}\,\text{cm}^2$	$1 \times 10^{15}\,\text{cm}^{-3}$
CZTSe2	$3 \times 10^{16}\,\text{cm}^{-3}$	2 ns	2.7	250 meV	$4 \times 10^{-13}\,\text{cm}^2$	$3 \times 10^{15}\,\text{cm}^{-3}$

Thus, the trap effect predicts the decay time to strongly decrease with temperature.

For fixed room temperature and increasing excitation we find decay times that are mostly constant and only the intensity of the second, long time part reduces. This is due to the limited electron supply from the trap states, which becomes negligible if[6]

$$\Delta n_0 \gg \frac{\tau_n}{\tau_c}\, e^{\frac{T_p}{\tau_n}}\, N_c\, e^{-\frac{E_c - E_t}{kT}} \qquad (6)$$

holds for the photogenerated electron density Δn_0 with T_p being the period of excitation. This means, on these time scales there are enough charge carriers for recombination and the recombination is not limited by the electron supply from the trap. Hence, trapping effects are reduced and only recombination (with shorter decay times) affects the luminescence decay. As the figure shows, this can be confirmed by simulation using the material parameters listed in table II and III.

It comes out, that the time-resolved photoluminescence of both samples can be approximated by means of simulation using equal material parameters, e.g. acceptor density, lifetime, temperature coefficient, trap energy, and electron capture cross-section. The independence of the lifetime and the acceptor density from the alloying with indium is in accordance with the experimental finding that the open-circuit voltage as a measure of recombination does not change for such low amounts of indium.[14] Furthermore, it shows that the acceptor density is not influenced by the alloying with indium. This is due to the same principle copper deficiency in both samples (see table I), since copper vacancies V_{Cu} are the dominating acceptor states in CZTSe.[12]

The only difference in the parameters of both samples is

the trap density which is smaller by orders of magnitudes if indium is incorporated. A possible donor state with an activation energy of approximately 300 meV would be the Zn_i defect.[12] It can now be concluded, that the incorporation of indium reduces the density of Zn_i defects. This is in agreement with in-situ XRD measurements at elevated temperatures, which show that the amount of the secondary ZnSe phase is reduced by indium below the detection limit.[13] Hence, less ZnSe is dissolved in the kesterite and therefore, the amount of Zn_i trap states may be reduced.

We also performed TRPL measurements on a second CZTSe sample CZTSe2 with higher Zn/Sn ratio. Since the decay is almost similar to that of CZTSe1 in figure 2, a presentation of the results is omitted and only the simulation parameters are listed in table III. Now, two parameters change. First, the trap density is slightly increased which can be traced back to an increased density of Zn_i defects due to the increased amount of Zn (see Tab. I). Furthermore, the acceptor density is smaller, though the density of copper vacancies is expected to be larger due to the lower copper content. However, an increased amount of indium and a reduced amount of copper lead to a higher density of Zn_{Cu} and Sn_{Cu} defects, which both act as donors thereby compensating the increasing acceptor density.[12]

In summary, we have presented photoluminescence decays of slightly different CZT(I)Se layers at different temperatures and excitations. We found bi-exponential decays on $Cu_2ZnSnSe_4$ layers and one-exponential decays for alloyed $Cu_2ZnSnSe_4$-$CuInSe_2$ layers. Both led to the conclusion that there must be a large amount of minority carrier traps 10^{15} cm^{-3} in CZTSe, that can be substantially reduced by alloying with $CuInSe_2$. It further comes
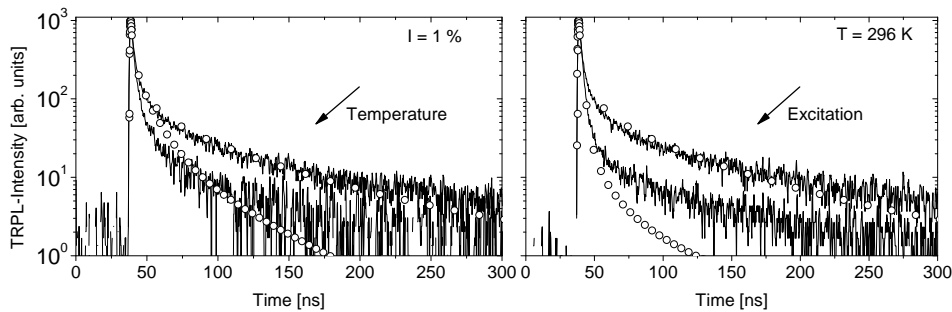
FIG. 2. Experimental (lines) and simulated (dots) TRPL-transients of absorber layer CZTSe1 for (a) $I = 1\%$ and temperature $T = 296$, 335 K and (b) for $T = 296$ K and $I = 1$, 50 %. Parameters for simulation from table II and III.

out, that the recombination lifetimes and acceptor densities are rather independent from the indium content, however, the latter depends on the Cu and Zn content. These effects can be explained by the defect model of Chen et. al.[12] where - according to the present work - the following defects are the most important: copper vancies V_{Cu} as acceptor states, Zn_{Cu} and Sn_{Cu} as donor states, and Zn_i as trap states. The trap states still are sufficiently shallow for not being active as recombination sites. Deeper defects must be present which are not suppressed by alloying.

[1] R. K. Ahrenkiel, N. Call, S. W. Johnston, and W. K. Metzger, Solar Energy Materials & Solar Cells **94** (2010).

[2] I. Repins, C. Beall, N. Vora, C. DeHart, D. Kuciauskas, P. Dippo, B. To, J. Mann, W.-C. Hsu, A. Goodrich, and R. Noufi, Solar Energy Materials and Solar Cells **101**, 154 (2012).

[3] W. K. Metzger, I. L. Repins, and M. A. Contreras, Applied Physics Letters **93** (2008).

[4] S. Shirakata and T. Nakada, Thin Solid Films **515**, 6151 (2007).

[5] S.-i. Shimakawa, K. Kitani, S. Hayashi, T. Satoh, Y. Hashimoto, Y. Takahashi, and T. Negami, Physica Status Solidi **203**, 2630 (2006).

[6] M. Maiberg, T. Hölscher, S. Zahedi-Azad, and R. Scheer, Journal of Applied Physics **118**, 105701 (2015).

[7] M. Maiberg, T. Hölscher, S. Zahedi-Azad, W. Fränzel, and R. Scheer, Applied Physics Letters **107** (2015), in press.

[8] G. Brammertz, M. Buffière, S. Oueslati, H. ElAnzeery, K. Ben Messaoud, S. Sahayaraj, C. Köble, M. Meuris, and J. Poortmans, Applied Physics Letters **103**, 163904 (2013).

[9] T. Paul Weiss, A. Redinger, J. Luckas, M. Mousel, and S. Siebentritt, Applied Physics Letters **102**, 202105 (2013).

[10] E. Kask, M. Grossberg, R. Josepson, P. Salu, K. Timmo, and J. Krustok, Materials Science in Semiconductor Processing **16**, 992 (2013).

[11] K. Hönes, E. Zscherpel, J. Scragg, and S. Siebentritt, Physica B: Condensed Matter **404**, 4949 (2009).

[12] S. Chen, A. Walsh, X.-G. Gong, and S.-H. Wei, Advanced Materials **25**, 1522 (2013).

[13] S. Hartnauer, L. A. Wägele, F. Syrowatka, G. Kaune, and R. Scheer, physica status solidi (a) **212**, 356 (2015).

[14] S. Hartnauer, L. A. Wägele, E. Jarzembowski, and R. Scheer, Thin Solid Films **582**, 272 (2015), e-MRS 2014 Spring Meeting, Symposium A, Thin-Film Chalcogenide Photovoltaic Materials.

[15] S. Schorr, M. Tovar, H.-J. Hoebler, and H.-W. Schock, Thin Solid Films **517**, 2508 (2009).

[16] M. Maiberg, C. Spindler, E. Jarzembowski, and R. Scheer, Thin Solid Films **582**, 379 (2015).

[17] W. K. Metzger, I. L. Repins, M. Romero, P. Dippo, R. N. Contreras, and D. Levi, Thin Solid Films **517** (2009).

[18] W. Shockley and W. T. Read, Physical Review **87**, 835 (1952).

[19] R. N. Hall, Physical Review **87**, 387 (1952).

[20] M. S. Tyagi and R. v. Overstraeten, Solid-State Electronics **26**, 577 (1983).

[21] M. Maiberg and R. Scheer, Journal of Applied Physics **116**, 123710 (2014).

[22] M. Maiberg and R. Scheer, Journal of Applied Physics **116**, 123711 (2014).

Verification of minority carrier traps in Cu(In,Ga)Se$_2$ and Cu$_2$ZnSnSe$_4$ by means of time-resolved photoluminescence

Matthias Maiberg[1], Torsten Hölscher, Enrico Jarzembowski, Stefan Hartnauer, Setareh Zahedi-Azad, Wolfgang Fränzel, Roland Scheer

Institute of Physics, Martin-Luther-University Halle-Wittenberg, 06120 Halle, Germany

Abstract

The decay of the room-temperature time-resolved photoluminescence (TRPL) on thin-film semiconductors such as Cu(In,Ga)Se$_2$ and Cu$_2$ZnSnSe$_4$ often is bi-exponential. This can be traced back either to fluctuations of the electrostatic potential or to minority charge carrier trapping. We show by means of simulations that both effects can be discriminated by a measurement of the TRPL decay at different excitation intensities and temperatures. Application of the standard semiconductor theory yields, that the bi-exponential photoluminescence decay in Cu(In,Ga)Se$_2$ and Cu$_2$ZnSnSe$_4$ must result from a strong minority carrier trapping. By simulation of experimental TRPL decay curves we can determine the minority carrier lifetime, the trap energy, the trap density, and the doping density of these materials with values in the ranges of $1 - 10\,\mathrm{ns}$, $200\,\mathrm{meV}$, $10^{15} - 10^{16}\,\mathrm{cm}^{-3}$, and $10^{15} - 10^{17}\,\mathrm{cm}^{-3}$. These yield reasonable solar cell parameters and they also explain the non-correlation of the open-circuit voltage and the luminescence decay time.

Keywords: transient, photoluminescence, minority carrier traps, Cu(In,Ga)Se$_2$, Cu$_2$ZnSnSe$_4$

1. Introduction

Time-resolved photoluminescence (TRPL) is a well-established technique for the measurement of minority carrier lifetimes in Cu(In,Ga)Se$_2$ (CIGSe) and Cu$_2$ZnSnSe$_4$ (CZTSe). However, due to the polycrystallinity of these materials, the decay is very complex and still not well-understood. This is demonstrated by the increased amount of recently published theoretical papers [1, 2, 3, 4, 5, 6].

In the first place, the photoluminescence decay is governed by the recombination of charge carriers. In that case, a mono-exponential decay is predicted with a decay time being equal to the minority recombination lifetime [1, 2, 7]. The latter is related to the open-circuit voltage V_{oc} of a solar cell, for which reason a correlation of the decay time and the solar cell parameters is expected. For CdTe and CIGSe, this correlation has already been approved in the 1990's [8, 9]. However, more recent and detailed experiments show that the photoluminescence decay is not necessarily mono-exponential,

nor does the decay correlate with the PV parameters [10, 11, 12, 13]. It has been suggested that this may be due to minority carrier traps or due to potential fluctuations [14, 15, 3, 4]. Both may influence the decay time without affecting the recombination, thus, without impact on the PV parameters.

In this paper, we compare minority carrier traps and potential fluctuations to each other, and show that both can be distinguished by means of TRPL under elevated temperatures and excitations. Afterwards, we show that the bi-exponential photoluminescence decay observed on CIGSe and CZTS must result from a strong minority carrier trapping. Equipped with this information, we can simulate the experimental decay curves. An outcome of the simulations are the trap parameters. Furthermore, we can derive V_{oc} as a function of the decay time and show that the non-correlation of both is also due to minority carrier traps.
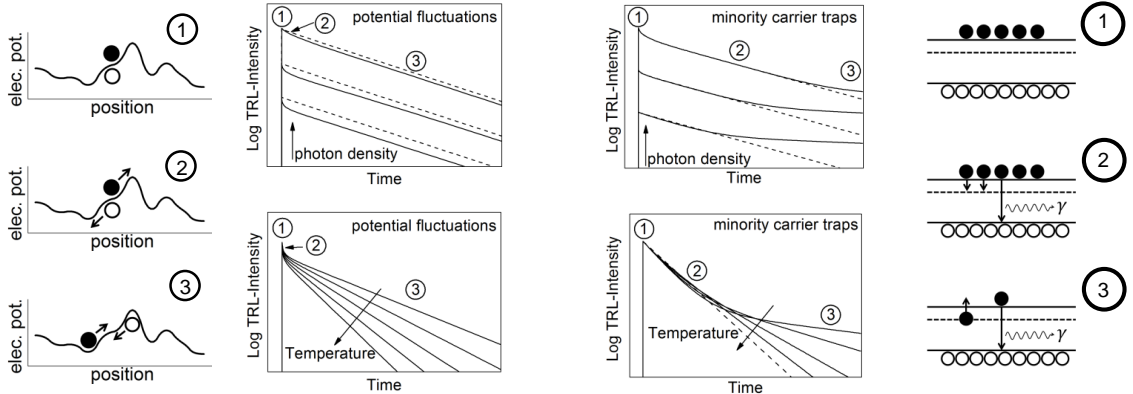
---

[1]matthias.maiberg@physik.uni-halle.de

Figure 1: Schematic photoluminescence decay of an absorber layer governed by recombination and potential fluctuations (left figures), or by recombination and minority carrier traps (right figures). The dashed lines show the room-temperature TRPL without potential fluctuations and minority carrier traps.

2. Theory of bi-exponential decays

2.1. Potential fluctuations

In CIGSe and CZTSe, potential fluctuations can reach values between 20 and 100 meV at temperatures below 10 K [16, 17, 18] but at room-temperature they are reduced to only a few meV [19, 17]. As a result, electric fields occur and charge carriers being generated by light separate due to the drift (see figure 1). The simultaneous recombination and charge separation leads to a fast initial decay of the photoluminescence with a decay time being smaller than the recombination lifetime τ_r [2, 4]. Afterwards, the charge carriers recombine which is limited by the thermally activated overcoming of the potential barriers. It turns out that the barriers at room-temperature are too small in order to strongly affect the recombination. For this reason the second decay time equals the recombination lifetime τ_r.

If the excitation is increased, the potential barriers are screened [4]. Without electric fields the charge carriers do not drift and the TRPL approximates the decay curves of an absorber without potential fluctuations (see figure 1). Thereby, in particular the first TRPL decay vanishes.

If the temperature is increased, in the first place the defect related recombination lifetime will decrease according to a power law [3, 20, 21]

$$\tau_r \sim T^{-b}, \quad b \approx 2 \dots 4. \quad (1)$$

Consequently, both decay times decrease at elevated temperatures. Especially the second decay time, which is equal to the recombination lifetime τ_r, decreases according to the power law in Eq. (1).

2.2. Minority carrier traps

In CIGSe and CZTSe numerous shallow defects have been found with energies of $E_t = 100 - 300$ meV being suitable for minority carrier trapping [22, 23, 24, 25, 26, 27, 28, 29]. These defects may capture photogenerated charge carriers. The simultaneous recombination and capturing of charge carriers leads to a fast initial decay (see figure 1). Thereby, the first decay time can become much smaller than the recombination lifetime depending on the capture cross-section and the density N_t of the traps [3, 14]. The second decay appears, when the conduction band is almost empty. The recombination is then limited by the electron supply from the trap resulting in a very slow decay with the decay time [3]

$$\tau_{dec} = \frac{N_t}{n^*} \tau_r, \quad n^* = N_c \, e^{-\frac{E_t}{kT}} \quad (2)$$

being larger than τ_r. Here, it is N_c the effective density-of-states of the conduction band.

If the excitation is increased the number of charge carriers in the conduction band will increase. Therefore, the onset of the second decay in the TRPL indicating an almost empty conduction band shifts to later times. In consequence, the first decay becomes more pronounced. Thereby, the excitation does only affect the intensities but not the decay times.

For increased temperatures, the reemission becomes

2

stronger which leads to less trapping of the charge carriers. At the same time, the recombination lifetime decreases again. From Eq. (1) and (2) then follows

$$\tau_{dec} \sim T^{-b}\, e^{\frac{E_t}{kT}}. \qquad (3)$$

Due to the additional exponential term, the temperature dependence of the decay time is much stronger for minority carrier trapping than for potential fluctuations.

3. Experimental application

3.1. Measurement setup

In order to discriminate the effect of potential fluctuations from minority carrier traps, excitation and temperature dependent TRPL is performed on a CZTSe and different CIGSe absorbers. Details on the preparation of the absorbers can be found in Ref. [20, 30]. For the measurement, the setup described in Ref. [31, 20] is used with an equal workflow for all samples. First, a variation of the injection level is performed. To this end, a pulsed diode laser with an excitation wavelength of 638 nm and a maximum incident photon density per pulse of $n_\lambda = (9 \pm 2) \times 10^{11}\,\mathrm{cm}^{-2}$ is used. Afterwards, the temperature is varied starting at room-temperature up to 340 K. After each variation, excitation and temperature are reset to the start values. By doing so, no degradation during the measurement could be retrieved. At the end, the transients' maxima are normalized and the background is subtracted.

3.2. Application to CZTSe absorbers

The transients for the CZTSe absorber are shown in figure 2. The decay at room-temperature under low injection conditions is bi-exponential with a long decay time of approximately 300 ns, which is far above the often reported recombination lifetime of approximately $1 - 10$ ns [10, 32]. Such a long decay time being much larger than the minority carrier lifetime is the first indication for a strong minority carrier trapping, since potential fluctuations will yield decay times smaller than the recombination lifetime. This is also verified by the excitation dependence, for which the first decay becomes more pronounced while the second decay time is not influenced. We remind, that for potential fluctuations a vanishing first decay would be expected. Thirdly, the second decay time decreases by more than 75 % if the temperature is increased by approximately 40 K. The simple power-law dependence in

Eq. (1) as expected for potential fluctuations cannot explain this strong decrease. Instead, the temperature dependence of Eq. (3) must be applied, which is the third indication for minority carrier traps. Based on these findings, the TRPL is simulated including minority carrier trapping. These simulations yield the trap-values $N_t = 10^{15}\,\mathrm{cm}^{-3}$, $E_t \approx 250\,\mathrm{meV}$, $N_A = 5 \times 10^{16}\,\mathrm{cm}^{-3}$, and $\tau_r = 2$ ns. For further information on the simulations see Ref. [1, 2, 3, 20].

3.3. Application to CIGSe absorbers

For the CIGSe absorbers, in principle the same dependence of the TRPL on the excitation and the temperature is found [20]. For the same reasons, the time-resolved photoluminescence must be governed by a strong minority carrier trapping even in CIGSe. The experimental decay curves are then again approximated by simulations, which yield $N_t = 5 \times 10^{15} - 5 \times 10^{16}\,\mathrm{cm}^{-3}$, $E_t \approx 200\,\mathrm{meV}$, $N_A = 5 \times 10^{15} - 5 \times 10^{16}\,\mathrm{cm}^{-3}$, and $\tau_r = 1 - 10$ ns [20].

4. Relation of TRPL to JV-parameters

The above results show that the recombination in an absorber is obscured by minority carrier trapping. At the end of this paper we study the consequences for the absorber characterization by means of TRPL. To this end, the open-circuit voltage of CIGSe solar cells has been measured as a function of the decay time, that reveals a strong scattering as show in figure 3. We now ask, if this scattering is due to the impact of minority carrier trapping. Primarily, it is pointed out that minority carrier trapping is a transient phenomenon and does not influence neither the steady state nor the transient recombination. According to this, under low excitations the same effective recombination lifetime τ_r can be used for the determination of V_{oc} (steady state excitation) and the decay time τ_{dec} (pulsed excitation). Based on that, the open-circuit voltage and the decay time can be related. First, the open-circuit voltage is given as a function of τ_r by

$$V_{oc} = \frac{kT}{e_0} \log \frac{J_{sc}}{J_0} \quad \text{with} \quad J_0(\tau_r) = e_0\, n_i^2\, \frac{\sqrt{D_n}}{N_A}\, \frac{1}{\sqrt{\tau_r}}, \quad (4)$$

which is valid for a solar cell in the limit of QNR-recombination [33]. In this equation, J_0 is the saturation current density and J_{sc} is the short-circuit current density. For an accurate description, it must be kept in mind that also J_{sc} depends on τ_r. This can be modelled by evaluating the product of

3

Figure 2: Experimental (lines) and simulated (dots) TRPL-transients of a CZTSe absorber for (a) $I = 1\%$ and temperature $T = 296, 335\,\mathrm{K}$ and (b) for $T = 296\,\mathrm{K}$ and $I = 1, 50\%$.
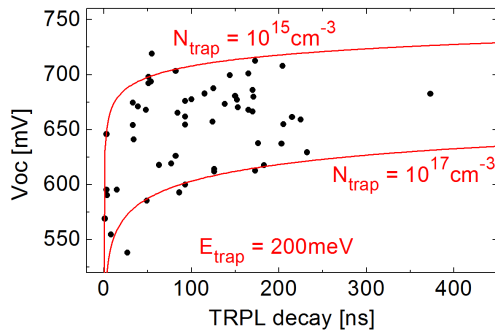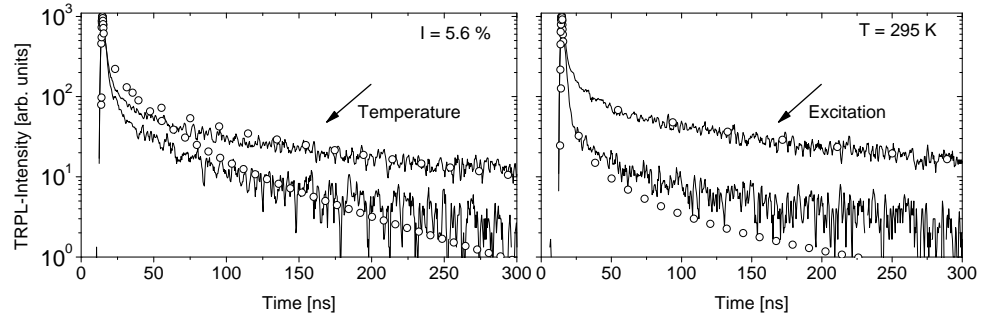

Figure 3: Scatter plot of the open-circuit voltage V_{oc} of CIGSe solar cells measured as a function of the decay time of the absorber. The curves are calculated $V_{oc}(\tau_{dec})$ graphs according to equation (6) for $n^* \approx 9 \times 10^{14}\,\mathrm{cm}^{-3}$ (this corresponds to $E_t = 200\,\mathrm{meV}$) and for $N_t = 10^{15}, 10^{17}\,\mathrm{cm}^{-3}$.

the generation function $G_{ph}(z)$ and the charge carrier collection function $\eta(z)$ [33]:

$$J_{sc}(\tau_r) = e_0 \int_0^d G_{ph}(z)\,\eta(z,\tau_r)\mathrm{d}z$$

$$\approx J_{sc,0}\,\frac{\sqrt{D_n}\,\alpha_{eff}\,\sqrt{\tau_r}}{1 + \sqrt{D_n}\,\alpha_{eff}\,\sqrt{\tau_r}}. \qquad (5)$$

For reasons of simplicity, the thickness d of the absorber is assumed to be much larger than the diffusion length. Furthermore, the generation function is arranged according to Lambert-Beer's law with an effective absorption coefficient α_{eff}, and the charge carrier collection function is arranged by $\eta(z,\tau_r) = \mathrm{e}^{-\frac{z}{\sqrt{D_n\,\tau_r}}}$. Together with equation (5), the open-circuit voltage in equation (4) is a well-defined function of the recombination lifetime τ_r. In order to rewrite V_{oc} as a function of τ_{dec}, equation (2) is used. Inserting this into equation (4) yields

$$V_{oc}\left(\tau_{dec};\,\frac{n^*}{N_t}\right) = \frac{kT}{e_0}\,\log\frac{J_{sc}(\frac{n^*}{N_t}\,\tau_{dec})}{J_0(\frac{n^*}{N_t}\,\tau_{dec})}. \qquad (6)$$

Here, V_{oc} is a function of τ_{dec} parametrized by n^*/N_t. Accordingly, equation (6) describes an entire family of curves, which already demonstrates that there is no clear correlation between V_{oc} and τ_r. The function (6) is now evaluated for typical CIGSe solar cell values of $N_A = 5 \times 10^{15}\,\mathrm{cm}^{-3}$, $J_{sc,0} = 25\,\mathrm{mAcm}^{-2}$, and $n_i = 10^9\,\mathrm{cm}^{-3}$ [33], and diffusion constant of $D_n = 0.05\,\mathrm{cm}^2\mathrm{s}^{-1}$ [31]. Furthermore, the electron density is fixed to $n^* = 9 \times 10^{14}\,\mathrm{cm}^{-3}$, which follows from the above determined trap energy $E_t = 200\,\mathrm{meV}$. Thus, only the trap density N_t is allowed to vary. As the figure 3 shows, the lower and the upper boundary to the measured data can be achieved for trap density values of $10^{15}\,\mathrm{cm}^{-3} \leq N_t \leq 10^{17}\,\mathrm{cm}^{-3}$ which exactly matches the trap density values determined by simulation of the TRPL [20]. This is a remarkable result since it combines minority carrier trapping, TRPL, and electrical measurements. In turn, only by measuring V_{oc} as a function of the decay time boundaries to the trap density in CIGSe could be determined.

Although the model of minority carrier trapping may explain the recently found non-correlation of the decay time and the open-circuit voltage, it is still open why earlier papers reported a clear correlation between both, though [34, 12, 35, 8, 9, 11, 36, 13]. A thorough study of these works reveals that the open-circuit voltage at that time was below $600\,\mathrm{meV}$. For so small voltages, the curves in figure 3 approximate each other due to a higher recombination, for which reason minority carrier trapping becomes less important. Then, the decay time is not disturbed by trapping and it correlates with the open-circuit voltage. Hence, the problem of the non-correlation only occured in the recent years after the solar cells had become more efficient.

4

5. Conclusion

In this work, we have shown that the impact of minority carrier traps and potential fluctuations on the TRPL can be distinguished by measurements at elevated temperatures and excitations. We have discussed for the two semiconductors CIGSe and CZTSe that potential fluctuations may not explain the observed photoluminescence decay, for which reason both materials must contain a substantial amount of minority carrier traps. These have a density of $N_t = 10^{15} - 10^{17}\,\mathrm{cm}^{-3}$ and an energy of $E_t \approx 200\,\mathrm{meV}$. Based on this result, we could calculate the open-circuit voltage as a function of the decay time for absorbers containing traps. It came out that there is an entire range of possible open-circuit voltages for each decay time as a consequence of a varying n^*/N_t ratio. Hence, the solar cell parameters cannot be predicted unambiguously by measuring the TRPL decay time. However, this model is still very inaccurate, because it implies equal absorptivity, diffusion constant, and acceptor density in all solar cells, and it neglects the impact of other effects on the V_{oc} such as resistances and the quality of the overlying layers.

6. Acknowledgement

[1] M. Maiberg, R. Scheer, Theoretical study of time-resolved luminescence in semiconductors. 1. decay from the steady state, Journal of Applied Physics 116 (2014) 123710.

[2] M. Maiberg, R. Scheer, Theoretical study of time-resolved luminescence in semiconductors. 2. pulsed excitation, Journal of Applied Physics 116 (2014) 123711.

[3] M. Maiberg, T. Hölscher, S. Zahedi-Azad, R. Scheer, Theoretical study of time-resolved luminescence in semiconductors. 3. trap states in the band gap, Journal of Applied Physics 118 (2015) 105701.

[4] M. Maiberg, R. Scheer, Theoretical study of time-resolved luminescence in semiconductors. 4. lateral inhomogeneities, Journal of Applied PhysicsSubmitted.

[5] J. Dashdorj, R. Ahrenkiel, W. Metzger, Modeling of recombination lifetimes in charge-separation device structures, Materials Research Society Symposium Proceedings 799.

[6] A. Kanevce, D. H. Levi, D. Kuciauskas, The role of drift, diffusion, and recombination in time-resolved photoluminescence of cdte solar cells determined through numerical simulation, Progress in Photovoltaics 22 (2014) 1138 – 1146.

[7] R. K. Ahrenkiel, Minority-carrier lifetime in iii-v semiconductors, in: Minority Carriers in III-V Semiconductors: Physics and Applications, Vol. 39, Academic Press, INC., 1993, Ch. 2, pp. 39–150.

[8] B. Ohnesorge, R. Weigand, G. Bacher, A. Forchel, W. Riedl, F. H. Karg, Minority-carrier lifetime and efficiency of Cu(In,Ga)Se$_2$ solar cells, Applied Physics Letters 73 (9) (1998) 1224–1226.

[9] W. K. Metzger, D. Albin, D. Levi, P. Sheldon, X. Li, B. M. Keyes, R. K. Ahrenkiel, Time-resolved photoluminescence studies of CdTe solar cells, Journal of Applied Physics 94 (5) (2003) 3549–3555.

[10] I. Repins, C. Beall, N. Vora, C. DeHart, D. Kuciauskas, P. Dippo, B. To, J. Mann, W.-C. Hsu, A. Goodrich, R. Noufi, Co-evaporated Cu$_2$ZnSnSe$_4$ films and devices, Solar Energy Material & Solar Cells 101 (2012) 154–159.

[11] W. K. Metzger, I. L. Repins, M. A. Contreras, Long lifetimes in high-efficiency cu(in,ga)se$_2$ solar cells, Applied Physics Letters 93 (2008) 022110.

[12] S. Shirakata, T. Nakada, Time-resolved photoluminescence in cu(in,ga)se$_2$ thin films and solar cells, Thin Solid Films 515 (2007) 6151–6154.

[13] S.-i. Shimakawa, K. Kitani, S. Hayashi, T. Satoh, Y. Hashimoto, Y. Takahashi, T. Negami, Characterization of cu(in,ga)se$_2$ thin films by time-resolved photoluminescence, Physica Status Solidi 203 (11) (2006) 2630–2633.

[14] R. K. Ahrenkiel, N. Call, S. W. Johnston, W. K. Metzger, Comparison of techniques for measuring carrier lifetime in thin-film and multicrystalline photovoltaic materials, Solar Energy Materials & Solar Cells 94.

[15] R. Scheer, A. Pérez-Rodríguez, W. K. Metzger, Advanced diagnostic and control methods of processes and layers in cigs solar cells and modules, Progress in Photovoltaics: Research and Applications 18 (2010) 467–480.

[16] T. Gokmen, O. Gunawan, T. K. Todorov, D. B. Mitzi, Band tailing and efficiency limitation in kesterite solar cells, Applied Physics Letters 103 (2013) 103506.

[17] J. Larsen, K. Burger, L. Gutay, S. Siebentritt, Temperature dependence of potential fluctuations in chalcopyrites, in: Photovoltaic Specialists Conference (PVSC), 2011 37th IEEE, 2011, pp. 000396–000401.

[18] S. Siebentritt, N. Papathanasiou, M. C. Lux-Steiner, Potential fluctuations in compensated chalcopyrites, Physica B: Condensed Matter 376 - 377 (2006) 831 – 833.

[19] M. J. Romero, H. Du, G. Teeter, Y. Yan, M. Al-Jassim, Mowafak, Comparative study of the luminescence and intrinsic point defects in the kesterite Cu$_2$ZnSnS$_4$ and chalcopyrite Cu(In,Ga)Se$_2$ thin films used in photovoltaic applications, Physical Review B 84 (2011) 165324.

[20] M. Maiberg, T. Hölscher, S. Zahedi-Azad, W. Fränzel, R. Scheer, Investigation of long lifetimes in Cu(In,Ga)Se$_2$ by time-resolved photoluminescence, Applied Physics Letters 107 (2015) 122104.

[21] M. S. Tyagi, R. v. Overstraeten, Minority carrier recombination in heavily-doped silicon, Solid-State Electronics 26 (6) (1983) 577–597.

[22] G. Brammertz, M. Buffière, S. Oueslati, H. ElAnzeery, K. Ben Messaoud, S. Sahayaraj, C. Köble, M. Meuris, J. Poortmans, Characterization of defects in 9.7% efficient Cu$_2$ZnSnSe$_4$-CdS-ZnO solar cells, Applied Physics Letters 103 (16) (2013) 163904.

[23] T. Paul Weiss, A. Redinger, J. Luckas, M. Mousel, S. Siebentritt, Admittance spectroscopy in kesterite solar cells: Defect signal or circuit response, Applied Physics Letters 102 (20) (2013) 202105.

[24] E. Kask, M. Grossberg, R. Josepson, P. Salu,

5.4 Beyond the one-dimensional model

Up to now, all simulations have been one-dimensional and inhomogeneities only have been considered on the axial scale, e.g. in a pn-junction. However, most of the thin-film semiconductors such as CIGSe are highly inhomogeneous even on the lateral scale. This becomes apparent especially by electron microscopy that reveals the polycrystallinity of the material with grain sizes of approximately 1 µm [16, 63]. Further evidence for the fluctuations is given by measurements of the micro-photoluminescence and quasi-Fermi level splitting. These unveil different characteristic fluctuation lengths of $20 - 30\,\mu m$ determined by PL mapping [66], $3-6\,\mu m$ measured from the quasi-Fermi level splitting [67], or $< 1\,\mu m$ as estimated by near-field photoluminescence [68]. These results indicate that there must be a diversity of material inhomogeneities each acting on a different length scale. For this work, this leads to the question how such material non-uniformities affect the time-resolved luminescence. This issue has been adressed in [Mai4] by means of three-dimensional simulations.

For non-homogeneous recombination lifetimes, it has already been shown in [Mai1] that the TRL decay curves may bend depending on the lifetime-distribution and the standard deviation σ_τ of the distribution. In [Mai4] it has been shown, that the effect also depends on the length scale of the inhomogeneities. If the length scale is small, the charge carriers will be able to diffuse to the position of highest recombination, that is, the smallest recombination lifetime will govern the luminescence decay. An increase of σ_τ will further
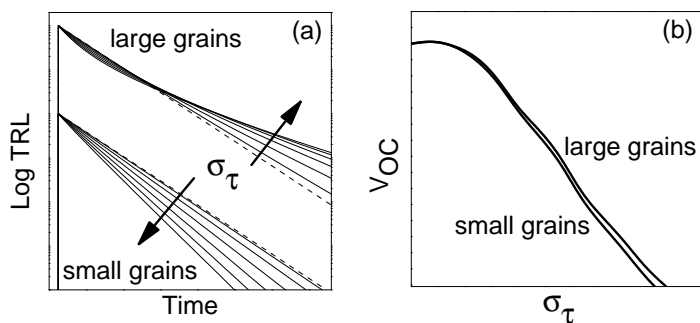

Figure 5.6: (a) TRL decay and (b) open-circuit voltage for a fluctuating recombination lifetime with fixed average and varying standard deviation σ_τ. The dashed lines mark $\sigma_\tau = 0$. For "small grains", the fluctuation length is in the range of the average diffusion length and for "large grains" it is above.

reduce the minimum lifetime, and consequently the luminescence will decline faster. This is illustrated in Fig. 5.6 (a). In Fig. 5.6 (b) it is shown that also the open-circuit voltage will become smaller with increasing σ_τ. It is pointed out that the correlation of the decay time and the open-circuit voltage is not corrupted. Contrary to that, it has been shown for large length scales that no recombination lifetime is preferred. Then, the TRL becomes a sum of exponential decays, which yields bent decay curves. Remarkably, this equality of high and low recombination lifetimes in the TRL is not reflected in V_{oc} (see fig. 5.6 (b)). Instead, the smallest recombination lifetime still dominates the open-circuit voltage. In consequence, the decay time and the open-circuit voltage become anti-correlated.

Apart from the lifetime there are further inhomogeneous physical properties in CIGSe. One of these is the band gap due to alloy, non-stoichiometry, or strain induced fluctutations. Such non-uniformities of the band gap may become detrimental for the solar cell's performance, since they increase the saturation current density thereby reducing the photovoltaic parameters [69, 70]. In contrast, the results in [Mai4] reveal a negligible impact of band gap fluctuations on the luminescence decay. This may be another reason for the non-correlation of the decay time and the open-circuit voltage.

Similar to the non-uniform composition and band gap also the doping densities can be considered inhomogeneous. This leads to a varying net-doping density and consequently to a fluctuation of the electrostatic potential [71]. As a result of these potential fluctuations, electric fields come up which make the charge carriers drift in-plane. In [Mai4], it has been demonstrated that this drift leads to bi-exponential decay curves with a first decay being related to drift and a second decay, that is related to recombination. Despite the similarity to the transient luminescence of a junction, it is pointed out that the TRL decay governed by potential fluctuations does not exhibit a third decay, which earlier has been assigned to the diffusion current across the barrier. The reason is that the potential drop of potential fluctuations - in particular at room-temperature - is much smaller than the built-in voltage in solar cells [71, 72]. In consequence of the missing contribution of the diffusion current to the TRL decay, the decay time for potential fluctuations is always smaller than the recombination lifetime, while it can become much larger than the recombination lifetime for minority carrier traps.

It is pointed out that the TRL for potential fluctuations is bi-exponential under low excitations. Accordingly, in principle there is no difference to the bi-exponential decay for minority carrier trapping. In order to distinguish both effects, the temperature and excitation dependence have been studied for potential fluctuations in [Mai4]. The results have been compared in [Mai9] to the earlier findings for the case of minority carrier traps [Mai3]. It has been found, that the temperature dependence is much smaller for potential fluctuations than for minority carrier trapping because of the smaller energy barriers. Under excitation increase, a vanishing first decay is expected for potential fluctuations, while it should become more pronounced for minority carrier traps. Thus, measurements of TRL under elevated excitations and temperatures enable an unambiguous discrimination of the effect of minority carrier traps and potential fluctuations. Based on this finding, it has been demonstrated in [Mai9] that the TRL decay curves on $Cu(In,Ga)Se_2$ and $Cu_2ZnSnSe_4$ are governed by minority carrier trapping.

In [Mai1–Mai3, Mai5–Mai9], the excitation in the simulations has been considered uniform in-plane. However, in real experiments the excitation in general is localized. This may lead to lateral diffusion currents and inhomogeneous trap and defect occupation. In [Mai4], this case of a local excitation and a global detection of the luminescence has been investigated. It has been shown that the same effect of lowly and highly excited

regions being combined under a local excitation on the TRL cannot be simulated by a uniform excitation with average photon density. In other words, an accurate simulation of micro-TRL requires the consideration of a local excitation. Furthermore, the case of a local excitation and a local detection of the luminescence has been studied. It has been calculated that the resolution of such an experiment is limited by the size of the excitation spot and by the diffusion length.

Concluding, in [Mai4] the effect of material and excitation inhomogeneities on the TRL decay have been studied by three-dimensional simulations. It has been mentioned that lifetime non-uniformities, band gap, and potential fluctuations may reduce the open circuit voltage by an increase of the saturation current. Regarding the TRL, however, the effect is not straight forward. Lifetime and potential inhomogeneities lead to bi- or multi-exponential decays whereas band gap fluctuations do not have a strong impact on the luminescence decay. Accordingly, material inhomogeneities may be another reason for the non-correlation of the decay time and V_{oc}. For the purpose of the detection of such fluctuations, micro-TRL experiments could be performed. It has been demonstrated, that an accurate simulation of such experiments requires the consideration of localized excitations. Another possibility, which goes beyond the scope of this work, is the measurement of spectrally time-resolved luminescence. Thereby, band gap fluctuations appear by a red shift in the transient luminescence spectra, whereas potential fluctuations are revealed by a blue shift [71, 72].

Theoretical study of time-resolved luminescence in semiconductors. 4. Lateral inhomogeneities

Matthias Maiberg,[1, a)] Frank Bertram,[2] and Roland Scheer[1]

[1] *Institute of Physics, Martin-Luther-University Halle-Wittenberg, Von-Danckelmann-Platz 3, 06120 Halle, Germany*

[2] *Institute of Experimental Physics, Otto-von-Guericke University, Universitätsplatz 2, 39106 Magdeburg, Germany*

In the fourth part of this series, we study the impact of lateral inhomogeneities on the time-resolved luminescence decay (TRL) after a pulsed excitation by means of simulation with Synopsys® TCAD and analytical approximation. This work consists of two parts: In the first part, the effect of excitations being inhomogeneous on a lateral scale is investigated. It turns out that for localized excitations there may be a strong lateral diffusion of charge carriers thereby limiting the resolution of a micro-TRL experiment. In this case, a replacement of the inhomogeneous excitation in the simulation by a homogeneous excitation and an average photon density is not allowed, especially due to bi-molecular recombination and due to defect saturation depending non-linear on the excitation. In the second part, we consider a homogeneous excitation and study inhomogeneous material parameters, namely inhomogeneous charge carrier lifetimes, band gaps, and doping densities. We find that their effects strongly depend on their characteristic lengths of variation. For length scales smaller than the diffusion length, inhomogeneous material parameters can lead to curved luminescence decays.

Keywords: simulation, luminescence, semiconductor, inhomogeneities

I. INTRODUCTION

The method of time-resolved luminescence is used to determine material parameters, e.g. the minority carrier lifetime in a semiconductor. However, due to the size of the excited area the obtained data are mostly mean values averaged over a typical region of 10^{-4} cm^2.[1,2] Especially in polycrystalline semiconductors such as Cu(In,Ga)Se$_2$ (CIGSe) with grain diameters of approximately 1 µm,[3] the determined values are averaged over 10,000 grains each exhibiting (slightly) different material parameters. This can be illustrated by the spatially resolved measurement of the photoluminescence or the quasi-Fermi level splitting, both revealing inhomogeneities on a micrometer and sub-micrometer scale.[4–7] The reasons for these inhomogeneities in CIGSe can be various. For example, the measurement of the time-resolved microphotoluminescence shows that the luminescence decay time may vary on a micrometer and sub-micrometer scale by about 30%, which may in the first place be due to a minority carrier lifetime being different in each grain.[5] It is found that this variation of the lifetime cannot be due to non-uniform grain boundaries only.[4] Accordingly, also the bulk properties must differ from grain to grain. This includes amongst others a fluctuating band gap due to a non-uniform composition, which is revealed by the measurement of the spectral microphotoluminescence and the quasi-Fermi-level splitting. Reported values in CIGSe for the band gap inhomogeneities are in the range of $10 - 80$ meV.[7–9] Apart from these variations in defect density and composition, also

a local variation of the doping density must be considered leading to fluctuations of the electrostatic potential. Since CIGSe is very prone to such potential fluctuations because of the high compensation, the deviation of the potential may become up to $20 - 100$ meV.[6,8–11] All these non-uniformities may limit the performance of solar cells.[8,12] The impact thereby depends on the strength and the length scale of the inhomogeneities, which in turn depend on material properties like the Ga and Cu content in the case of Cu(In,Ga)Se$_2$.[5,10] Therefore, it is indispensable to investigate all these inhomogeneities in order to develop a microscopic model of the semiconductor, which then allows the optimization of the semiconductor processing. As time-resolved luminescence (TRL) is a method of choice for such an investigation, the impact of inhomogeneities in general on the TRL decay is studied in this work by three-dimensional simulation with Synopsys® TCAD. This work is divided into two parts. In the first part, the effect of laterally inhomogeneous excitations is studied. Here, it is discussed if the previous simplification in the parts I-III[2,13,14], namely the approximation of a local excitation in the simulations by a uniform excitation with average photon density, is justified. Afterwards, the impact of lateral diffusion induced by the generation profile is investigated and consequences for the resolution of a micro-TRL experiment are deduced. In the second part, the impact of inhomogeneous material properties is studied keeping the excitation laterally homogeneous. We start with inhomogeneous charge carrier lifetimes, for which the ratio of the structure size and the diffusion length will turn out as a crucial parameter for the impact on the TRL decay. After this, the impact of electrostatic fluctuations due to band gap or doping density inhomogeneities is studied. It will be shown that

---

a)Electronic mail: matthias.maiberg@physik.uni-halle.de

the effect is rather similar to that of space charges described in Ref. 13 and 14, but now also the temperature dependence will be shown in order to detect such potential fluctuations in experiments. At the end, we give a summary of TRL decay curves which have been observed in all the simulations of the four parts of this work. This will allow a classification of semiconductor decay curves in order to narrow down the effects governing a concrete luminescence decay.

II. EXCITATION INHOMOGENEITIES

In the first part of this paper we study excitations being inhomogeneous on the lateral scale. For systematic reasons we demand homogeneous material parameters, in particular homogeneous absorption coefficient, carrier mobilities, and defect densities. With regard to TRL experiments we suppose Gaussian shaped incident photon flux densities of the form

$$j_\gamma(x,y,t) = \frac{N_\gamma}{\pi^{3/2}\,\sigma_r^2\,\tau_p}\, e^{-\frac{(x-x_0)^2}{\sigma_r^2}}\, e^{-\frac{(y-y_0)^2}{\sigma_r^2}}\, e^{-\frac{(t-t_0)^2}{\tau_p^2}}, \quad (1)$$

that impinge at $z = 0$ perpendicular to the semiconductor surface. In (1), N_γ is the number of incident photons per pulse, τ_p is the pulse length, σ_r is the standard deviation in x and y direction. x_0 and y_0 refer to the center of excitation and t_0 corresponds to the excitation peak maximum. Here we chose $t_0 = 1\,\mathrm{ps}$ and $\tau_p = 100\,\mathrm{fs}$ as in Ref. 2, 13, and 14. Integration of (1) over time yields the incident photon density per pulse

$$n_\gamma(x,y) = \frac{N_\gamma}{\pi\,\sigma_r^2}\, e^{-\frac{(x-x_0)^2}{\sigma_r^2}}\, e^{-\frac{(y-y_0)^2}{\sigma_r^2}}. \quad (2)$$

In experiments, it is common to define an average photon density instead of specifying an expression like in (2). To this end, the region of excitation $\mathbf{A_p}$ is defined by the $1/e^2$ decay of n_γ, more precisely by

$$\mathbf{A_p} := \{(x,y) \in \mathbb{R}^2 : n_\gamma(x,y) \geq \frac{1}{e^2}\, n_\gamma(x_0,y_0)\}. \quad (3)$$

Then, the area of the excitation spot becomes

$$A_p = ||\mathbf{A_p}||_2 = 2\,\pi\,\sigma_r^2 = \frac{\pi}{2\log 2}\, FWHM_r^2, \quad (4)$$

where $FWHM_r = 2\,\sigma_r\,\sqrt{\log 2}$ is the full width of half maximum in x and y direction. In this work, we will use both terms, $FWHM_r$ and σ_r for convenience. Knowing the area A_p and the number of photons N_γ the average incident photon density $n_{\gamma,av}$ of a Gaussian shaped excitation pulse can be defined by

$$n_{\gamma,av} = \frac{N_\gamma}{A_p} = \frac{N_\gamma}{2\,\pi\,\sigma_r^2}. \quad (5)$$

The rate of electron-hole pair generation is given by $G = R\,\alpha\,j_\gamma\,e^{-\alpha z}$ where R is the reflection coefficient at
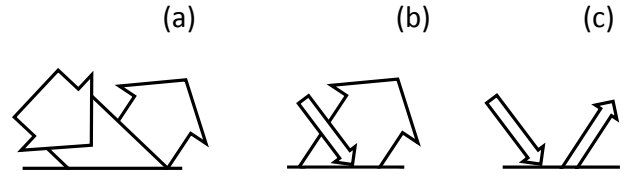

FIG. 1. (a) uniform excitation and global detection of the luminescence (b) local excitation but global detection of the luminescence (c) local excitation and local detection of the luminescence

the front surface and α is the absorption coefficient. Assuming excitations with pulse lengths shorter than both diffusion and recombination time constants we find for the generated charge carrier density (compare Ref. 14):

$$\Delta n_0(x,y,z) \approx R\,\alpha\,\frac{N_\gamma}{\pi\,\sigma_r^2}\, e^{-\frac{(x-x_0)^2}{\sigma_r^2}}\, e^{-\frac{(y-y_0)^2}{\sigma_r^2}}\, e^{-\alpha z}. \quad (6)$$

From this, we find the maximum generated charge carrier density $\Delta n_{0,max}$ and from equation (5) the average generated charge carrier density $\Delta n_{0,av}(z)$ for which holds

$$\Delta n_{0,max} = R\,\alpha\,\frac{N_\gamma}{\pi\,\sigma_r^2} \quad (7a)$$

$$\Delta n_{0,av}(z) = \frac{1}{2}\,\Delta n_{0,max}\, e^{-\alpha z}. \quad (7b)$$

A crucial parameter for the excitation in this work is the standard deviation σ_r. If it is chosen sufficiently small such as in micro-photoluminescence experiments, the charge carrier densities will become much larger than the doping density according to equation (7). This will lead to high injection effects, that depend non-linearily on the excitation. We will show that some high injection effects occuring by local excitation cannot be simulated by a laterally homogeneous (uniform) excitation with average photon density. Afterwards, the in-plane diffusion as a consequence of the local excitation will be studied and its impact on the luminescence decay will be investigated. In this regard, problems for the resolution of TRL mapping on the micrometer scale arise. These will be adressed at the end of the first part.

A. Comparability with one-dimensional simulations

In the parts I-III of this work,[2,13,14] the excitation was assumed uniform in-plane and the overall radiative recombination was taken as the luminescence intensity. This is illustrated by the pictogram 1 (a). In experiments such as micro-photoluminescence or micro-cathodoluminescence, the excitation is localized (see fig. 1 (b)). For this reason, precise simulations of luminescence experiments actually must be three-dimensional with overproportional longer computation times. In the following, it is discussed if this higher dimensionality can be circumvented by replacing in the simulations the local excitation in equation (2) by a uniform excitation

with an average photon density as defined in equation (5). The discussions are based on equation (9) in Ref. 14, that gives an expression for the slope of the luminescence intensity $I(t)$ derived for the one-dimensional case. However, for the purpose of the following considerations it must be generalized to three dimensions, first. This yields the following equation:

$$
\frac{\mathrm{d}}{\mathrm{d}t}I(t) = -B \underbrace{\int_V (n\,R_p + p\,R_n)\,\mathrm{d}\mathbf{r}}_{(a)}
$$
$$
\underbrace{-B \int_{\partial V} (S_p\,n\,\Delta p + S_n\,p\,\Delta n)\,\mathrm{d}S}_{(b)}
$$
$$
\underbrace{+B \int_V \mathbf{E}\,(\mu_p\,p\,\nabla_{\mathbf{r}}n - \mu_n\,n\,\nabla_{\mathbf{r}}p)\,\mathrm{d}\mathbf{r}}_{(c)}
$$
$$
\underbrace{-B \int_V (D_p + D_n)\,\nabla_{\mathbf{r}}n \nabla_{\mathbf{r}}p\,\mathrm{d}\mathbf{r}}_{(d)}
$$
$$
\underbrace{+B \int_V p\,(e_e - e_c)\,\mathrm{d}\mathbf{r}}_{(e)}. \tag{8}
$$

The quantities in equation (8) are as follows: B is the coefficient of radiative recombination, R_p and R_n are the net-recombination rates, D_p and D_n are the diffusion constants, S_p and S_n are the space-dependent surface recombination velocities, and μ_p and μ_n are the charge carrier mobilities of electrons and holes, respectively. Furthermore, it is V the volume of the semiconductor, ∂V the surface of the semiconductor, $\nabla_{\mathbf{r}}$ the nabla operator, $\mathbf{E}$ the electric field strength with $\mathbf{E}|_{\partial V} = 0$, and e_e and e_c are the emission and capture rates of electrons by an electron trap in the band gap. The terms (a) and (b) describe volume and surface recombination and are always negative. The terms (c) and (d) describe drift and diffusion of charge carriers and can be positive or negative. The term (e) describes trapping and de-trapping of electrons (see Ref. 2).

1. Low injection levels

We begin the considerations with low injection conditions. This requires excess carrier densities being smaller than the density of majority carriers (holes) and a density of occupied traps being smaller than the total trap density, that is $\Delta n,\ \Delta p,\ n_0 \ll p_0$ and $n_t \ll N_t$. In consequence, the recombination rate of electrons can be writ-ten as $R_n = \frac{\Delta n}{\tau_n}$ and equation (8) becomes

$$
\frac{\mathrm{d}}{\mathrm{d}t}I(t) = -B\,p_0\,\frac{1}{\tau_n}\underbrace{\int_V \Delta n\,\mathrm{d}\mathbf{r}}_{(a)} \underbrace{-B\,p_0 \int_{\partial V} S_n\,\Delta n\,\mathrm{d}S}_{(b)} +
$$
$$
\underbrace{+B\,p_0\,\sigma_n\,v_n\,n^* \int_V n_t\,\mathrm{d}\mathbf{r} - B\,p_0\,\sigma_n\,v_n\,N_t \int_V \Delta n\,\mathrm{d}\mathbf{r}}_{(e)}. \tag{9}
$$

First, it is pointed out that the drift and diffusion terms (c) and (d) in equation (8) become 0 for low injection conditions. The other integrands in term (a), (b), and (e) of equation (9) are linear in Δn and n_t, respectively. Therefore, the luminescence decay depends only on the total number of (trapped) electrons but not on their distribution. Then, for local and for uniform excitations with equal average photon densities the luminescence intensities decay equally.

2. Bimolecular recombination and axial diffusion

If a semiconductor is excited by a high, laterally inhomogeneous excitation there will be regions having a generated carrier density smaller than the doping density and regions having a generated charge carrier density larger than the doping density. For the latter, the TRL decay will exhibit characteristics of bimolecular recombination and axial diffusion (see Ref. 14). We now ask, if the same effect of lowly and highly excited regions being combined under one Gaussian pulse on the TRL decay can also be achieved by a uniform excitation being either low or high. For the considerations we naturally omit lateral diffusion of charge carriers but allow axial diffusion. Defect and trap saturation effects are first neglected and discussed separately. The radiative recombination can then be written as follows (see equation (32) in Ref. 14):

$$
R_{rad}(t,z,r) = B\,p_0^2\,\mathrm{e}^{\frac{t}{\tau_n}} \times
$$
$$
\times \frac{\Delta n_0(t,z,r)\,(p_0 + \Delta n(t,z,r))}{\left(\Delta n_0(t,z,r) - \mathrm{e}^{\frac{t}{\tau_n}}\,(p_0 + \Delta n_0(t,z,r))\right)^2}. \tag{10}
$$

Here, the in-plane distance r from the middle of the excitation spot has been introduced by $r^2 = (x - x_0)^2 + (y - y_0)^2$. The charge carrier density $\Delta n_0(t,z,r)$ is the solution of the homogeneous diffusion equation, that is without recombination term. For $t = 0$, it equals the generated charge carrier density, which either will be close to the doping density p_0 or far below. Then, equation (10) can be expanded by powers of $\Delta n_0/p_0$ which yields

$$
R_{rad}(t,z,r) \approx B\,p_0\,\Delta n_0(t,z,r)\,\mathrm{e}^{-\frac{t}{\tau_n}}
$$
$$
- B\,\Delta n_0(t,z,r)^2\left(\mathrm{e}^{-\frac{t}{\tau_n}} - 2\,\mathrm{e}^{-2\frac{t}{\tau_n}}\right). \tag{11}
$$

As in-plane diffusion of charge carriers has been omitted, the density $\Delta n_0(t,z,r)$ can be expressed by $\Delta n_0(t,z,r) = n_\gamma(r)\,f(t,z)$ with the photon density per

pulse $n_\gamma(r)$ as in equation (2) and a function $f(t,z)$ describing the axial diffusion (see equation (4) in Ref. 14). Equation (11) then becomes

$$R_{rad}(t,z,r) \approx B\, p_0\, n_\gamma(r)\, f(t,z)\, \mathrm{e}^{-\frac{t}{\tau_n}}$$
$$- B\, n_\gamma(r)^2\, f(t,z)^2 \left(\mathrm{e}^{-\frac{t}{\tau_n}} - 2\,\mathrm{e}^{-2\frac{t}{\tau_n}} \right). \quad (12)$$

The photon density $n_\gamma(r)$ must now be related to the average photon density $n_{\gamma,av}$. To this end, we write $n_\gamma(r) = n_{\gamma,av}\, \Theta(\sqrt{2}\sigma_r - r) + \eta(r)$ using the Heaviside step function Θ. This includes a new function $\eta(r)$, which is the difference between the Gaussian function and the average value. This function fulfilles

$$\int_0^\infty r\,\eta(r)\,\mathrm{d}r = 0, \int_0^{\sqrt{2}\sigma_r} r\,\eta(r)\,\mathrm{d}r = -n_{\gamma,av}\,\sigma_r^2/\mathrm{e}^2, \quad (13a)$$

$$\text{and} \quad \int_0^\infty r\,\eta(r)^2\,\mathrm{d}r = 2\,n_{\gamma,av}^2\,\sigma_r^2/\mathrm{e}^2. \quad (13b)$$

By this, equation (12) can be integrated over the volume V which gives an approximation to the luminescence intensity for the localized excitation. All integrals containing $\eta(r)$ or $\eta(r)^2$ vanish and it remains

$$I(t) \approx \int_V \left(B\, p_0\, n_{\gamma,av}\, f(t,z)\, \mathrm{e}^{-\frac{t}{\tau_n}} \right.$$
$$\left. - B\, n_{\gamma,av}^2\, f(t,z)^2 \left(\mathrm{e}^{-\frac{t}{\tau_n}} - 2\,\mathrm{e}^{-2\frac{t}{\tau_n}} \right) \right) \mathrm{d}V. \quad (14)$$

However, the integrand is the rate of radiative recombination if the semiconductor is excited uniformly with an average photon density $n_{\gamma,av}$ (see eq. (12) and replace $n_\gamma(r)$ by $n_{\gamma,av}$). This shows that in first and second order approximation the effect of bimolecular recombination and axial diffusion due to a localized excitation can also be obtained by a uniform excitation with an average photon density. In figure 2 (1), this result also has been approved by simulation. It can be seen, that the decay curve for a localized excitation indeed can be simulated by a uniform excitation. Note, that these simulations also include lateral diffusion. Accordingly, the result in equation (14) will be still correct if the above assumption of negligible lateral diffusion is not made.

3. Trap and deep defect saturation

Next, the impact of a high and localized excitation on the saturation of deep and shallow defects is studied. The effects as revealed by simulation are exemplified in figure 2 (2) and (3). First, it is obvious that the decay of the transients depends on the size of the excitation spot which indicates an impact of the lateral diffusion of charge carriers. However, as shown below it cannot be the lateral diffusion itself that influences the luminescence decay. Instead, the lateral diffusion leads to the reduction of charge carrier densities in highly excited regions which in turn reduces the saturation of defects. Secondly, the figure demonstrates that the saturation effects are more pronounced if the excitation spot becomes
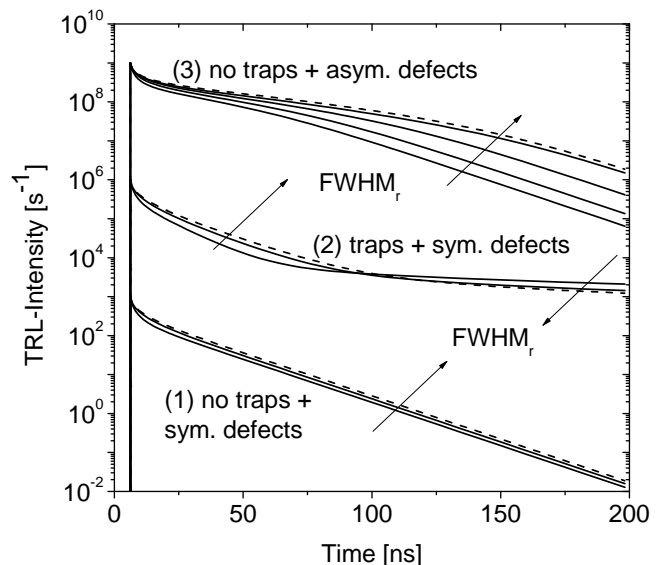

FIG. 2. TRL-transients of a semiconductor layer which is excited uniformly (dashed lines) and locally (full lines) with $FWHM_r = 1, \ldots, 10\,\mu m$. The electron and hole SRH-lifetimes and charge carrier mobilities are $\tau_{SRH} = 20\,\mathrm{ns}$ and $\mu = 20\,\mathrm{cm}^2\,\mathrm{V}^{-1}\,\mathrm{s}^{-1}$. For the simulation of trapping (2), the trap parameters are $N_t = 10^{15}\,\mathrm{cm}^{-3}$, $E_t = 260\,\mathrm{meV}$, and $\sigma_n = 10^{-14}\,\mathrm{cm}^{-2}$. For the simulation of defects with asymmetric lifetimes (3), the hole SRH-lifetime is $\tau_{SRH} = 200\,\mathrm{ns}$. The average photon density per pulse is always $n_{\gamma,av} = 3 \times 10^{12}\,\mathrm{cm}^{-2}$ (corresponds to $\Delta n_{0,max} = 20\,N_a$). For visibility, the curves are shifted.

larger than the diffusion length $L = 1\,\mu m$. Then, the diffusion currents are small and charge carrier densities are hardly reduced by diffusion which preserves the defect saturation. Furthermore, highly and lowly excited regions compensate each other, for which reason the decay of the transients are equal to that of a homogeneous excitation with equal average photon density.

All in all, local excitations with excitation diameters larger than the diffusion length can be simulated by uniform excitations if the average photon density is equal. Errors are made for small excitation spot sizes, because lateral diffusion leads to different charging and discharging of defects.

B. Direct impact of lateral diffusion on TRL decay

In the following, the effect of lateral charge carrier diffusion on the global TRL decay is studied. In other words, we again consider local excitation and global detection as illustrated by figure 1 (b). To study the influence of lateral diffusion on the TRL decay we focus on term (d) in equation (8). This term describes the direct impact of diffusion on the TRL decay. For its evaluation, a homogeneous semiconductor with $\nabla_\mathbf{r} p_0 = \nabla_\mathbf{r} n_0 = \nabla_\mathbf{r} D_n = \nabla_\mathbf{r} D_p = 0$ is assumed. Furthermore, Δn and Δp must be known as functions of time. However, for this estimation knowledge about the maximum diffusion

current is sufficient. Since this maximum current flows at the very beginning, $\Delta n = \Delta p = \Delta n_0(x, y, z)$ with Δn_0 from equation (6) is used. By this, the following two integrals can be evaluated:

$$\int_V \nabla_{\mathbf{r}} n \nabla_{\mathbf{r}} p \, d\mathbf{r} = \frac{1}{4} \pi \alpha \sigma_r^2 \left(1 - e^{-2\alpha d} \right) \quad (15a)$$

$$\int_V \frac{\partial}{\partial z} n \frac{\partial}{\partial z} p \, d\mathbf{r} = \frac{1}{4} \frac{\pi}{\alpha} \left(2 + \alpha^2 \sigma_r^2 \right) \left(1 - e^{-2\alpha d} \right) \quad (15b)$$

with d being the semiconductor thickness. Equation (15a) describes the impact of lateral **and** axial diffusion on the TRL decay, whereas in equation (15b) only axial diffusion is allowed. By divison of (15b) by (15a) the contribution of the impact of axial diffusion to that of total diffusion is found to be:

$$\frac{\text{axial diffusion}}{\text{total diffusion}} = \frac{\alpha^2 \sigma_r^2}{2 + \alpha^2 \sigma_r^2} \overset{\alpha \sigma_r \gg 1}{\approx} 1. \quad (16)$$

This shows that the impact of axial diffusion on the TRL decay is dominating for strong absorption (α) or for broad excitations (σ_r). For typical values of $\alpha = 4\,\mu m^{-1}$ and $\sigma_r = 10\,\mu m$ equation (16) yields 0.999 and even for $\sigma_r = 1\,\mu m$ as in micro-luminescence experiments the ratio is 0.889, which shows that the impact of lateral diffusion can mostly be neglected. Accordingly, no curved decay due to lateral diffusion is expected. However, it is pointed out that this is true only if the global luminescence from the whole semiconductor is considered. If only a confined region is considered, these statements are no longer valid which will be discussed in the next section II C

C. TRL mapping

Above it has been calculated, that the impact of axial charge carrier diffusion on the global luminescence decay is dominating against lateral diffusion impact. This is no longer true for local-local luminescence mapping experiments, when the luminescence decay is observed spatially resolved as illustrated in figure 1 (c). To make this clear, we consider the following experiment: For mapping of the luminescence decay time an excitation as in equation (1) is used with $FWHM_r = 1\,\mu m$. The resulting luminescence is observed spatially resolved and we ask for the region the luminescence comes from. Therefore, we calculate the luminescence from a cylindrical region with center (x_0, y_0) and diameters of $d_{cyl} = 1, \ldots, 50\,FWHM_r$ which is shown in figure 3. In reality, such an experiment could be realized by a cover layer which is transparent only for the excitation but exhibits a pinhole for the luminescence. An example may be a metal layer letting pass an electron beam. Another realization could be confocal TRPL.

First, it is obvious (see (1) in Fig. 3) that the luminescence intensity at $t \approx 0$ from the cylinder with
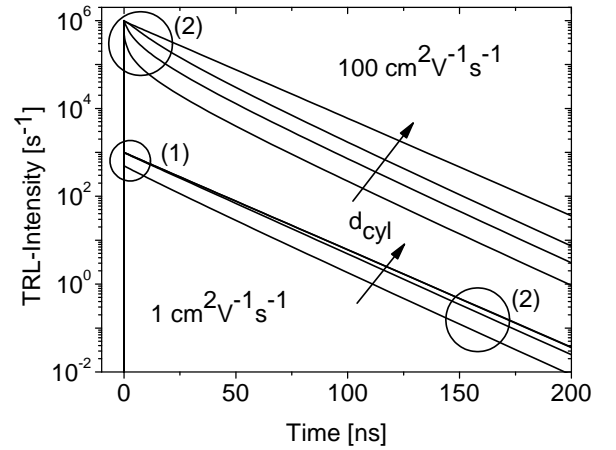

FIG. 3. TRL-transients of a semiconductor layer that is excited by a Gaussian laser pulse focused to $FWHM_r = 1\,\mu m$ with $n_{\gamma,av} = 10^9\,cm^{-2}$. The intensity is calculated by integrating the radiative recombination in cylindrical regions around (x_0, y_0) with diameters of $d_{cyl} = 1\,FWHM_r$, $2\,FWHM_r$, $5\,FWHM_r$, $50\,FWHM_r$. The carrier SRH-lifetime is $\tau_{SRH} = 20\,ns$ and the carrier mobilities are $\mu = 1, 100\,cm^2\,V^{-1}\,s^{-1}$.

$d_{cyl} = 1\,FWHM_r$ is only $\sim 45\%$ of the total luminescence approximated by $d_{cyl} = 50\,FWHM_r$. This is in accordance with the fact, that also only 50% of the excited semiconductor are within $1\,FWHM_r$. Already for $d_{cyl} = 2\,FWHM_r$ the luminescence intensity is $\sim 90\%$ of the total intensity and the difference becomes negligible. Secondly, the luminescence intensity in the cylinders decays faster than the total luminescence due to the evacuation of charge carriers (see (2) in Fig. 3). This means, though lateral diffusion does not affect the global luminescence decay it may affect the local luminescence decay. This limits the spatial resolution of charge carrier lifetime mappings.

An estimation of the resolution shall be carried out in the following. To this end, the electron density must be known as a function of space and time which can be obtained by the solution of the inhomogeneous diffusion equation. Due to the symmetric excitation we use cylindrical coordinates r, φ, z with $x = x_0 + r \cos \varphi$, $y = y_0 + r \sin \varphi$, and $z = z$. Then, the initial-boundary-problem reads

$$\frac{\partial}{\partial t} \Delta n - D_n \Delta_{\mathbf{r}} \Delta n = -R_n \quad (17a)$$

$$\frac{\partial}{\partial z} \Delta n \Big|_{z=0} = S_f \, \Delta n|_{z=0} \quad (17b)$$

$$\frac{\partial}{\partial z} \Delta n \Big|_{z=d} = -S_b \, \Delta n|_{z=d} \quad (17c)$$

$$\lim_{r \to \pm \infty} \Delta n = 0 \quad (17d)$$

$$\Delta n|_{t=0} = \Delta n_0 \quad (17e)$$

where $\Delta_{\mathbf{r}}$ is the Laplacian operator, S_f and S_b are the front and back surface recombination velocities, and Δn_0 is given by equation (6). The recombination rate is ar-

ranged by $R_n = \frac{\Delta n}{\tau_n}$ with the recombination lifetime τ_n which is valid for low excitation intensities. The exact solution of (17) can then be found by a separation ansatz. This leads to Bessel functions which are difficult to process further. Thus, only an approximate solution is searched for that can be obtained by replacing (17b) and (17c) by $\lim_{z \to +\infty} \Delta n = 0$ which is fulfilled for thick absorbers. In this limit, the solution reads

$$\Delta n(t,r,z) = \frac{N_\gamma R \alpha}{2\pi \left(\sigma_r^2 + 4 D_n t\right)} \left(1 + \mathrm{erf}\left(\frac{z - 2 D_n \alpha t}{2 \sqrt{D_n t}}\right)\right)$$

$$\mathrm{e}^{-\alpha z + D_n \alpha^2 t}\, \mathrm{e}^{-\frac{r^2}{\sigma_r^2 + 4 D_n t}}\, \mathrm{e}^{-\frac{t}{\tau_n}} \qquad (18)$$

with $\mathrm{erf}(x)$ being the error function. Approximately knowing the time-dependent electron density we can calculate the rate $R_{rad} = B\, p_0\, \Delta n$ of radiative recombination. From this, we calculate the function $A(t)$ defined by:

$$A(t) = \frac{2\pi \int_0^{d_{cyl}/2} \int_0^\infty R_{rad}\, r\, \mathrm{d}z \mathrm{d}r}{2\pi \int_0^\infty \int_0^\infty R_{rad}\, r\, \mathrm{d}z \mathrm{d}r} = 1 - \mathrm{e}^{-\frac{d_{cyl}^2}{16 D_n t + 4\sigma_r^2}}. \quad (19)$$

$A(t)$ gives the fraction of luminescence that comes from a cylinder with diameter d_{cyl} in relation to the total (global) luminescence. Hence, the time-dependence of A describes the evacuation of charge carriers out of the cylinder. If the time-dependence of A is weak, the evacuation will be slow and the decay of the luminescence from the cylinder will only exhibit the recombination of the charge carriers. This means for the estimation of the resolution of a TRL mapping we have to determine d_{cyl} such that the time-dependence of A is weak. In other words, we require that $A(t)$ stays close to $A(0)$. This is expressed by

$$A(3\tau_n) \geq 0.9\, A(0), \qquad (20)$$

which allows a 10% deviation within $[0, 3\tau_n]$. This equation must now be rewritten for d_{cyl} using $A(t)$ from equation (19). This is not possible analytically. However, by applying a Taylor approximation equation (19) can be linearized and the result becomes approximately

$$d_{cyl} = \begin{cases} 2\sqrt{\log 10}\, \sqrt{\sigma_r^2 + 12 L_n^2}, & \text{for } L_n > 0.15\, \sigma_r, \\ < 2\sqrt{3}\, \sigma_r, & \text{for } L_n \leq 0.15\, \sigma_r. \end{cases} \quad (21)$$

Here, $L_n = \sqrt{D_n \tau_n}$ is the diffusion length. In figure 3, it was $FWHM_r = 1\,\mu\mathrm{m}$, $\tau_n = 20\,\mathrm{ns}$, and $D_n = 0.026\,\mathrm{cm}^2\mathrm{V}^{-1}\mathrm{s}^{-1}$. Equation (21) then yields $d_{cyl} \approx 3\,\mu\mathrm{m}$. This means, if the size of the pinhole is chosen to $3\,\mu\mathrm{m}$, the recombination of the charge carriers can be observed with an error of less then 10%. For $D_n = 2.6\,\mathrm{cm}^2\mathrm{V}^{-1}\mathrm{s}^{-1}$, however, equation (21) yields $d_{cyl} \approx 24\,\mu\mathrm{m}$. This shows that the resolved region is broad due to charge carrier diffusion. Therefore, TRL mapping is possible only in particular cases.

The second problem in TRL mappings is the quantum yield of the experimental setup. In typical TRL mappings with laser excitation the number of photons per pulse is approximately $N_\gamma = 10^7$ to achieve a good signal to noise ratio. However, if the light is focused to a
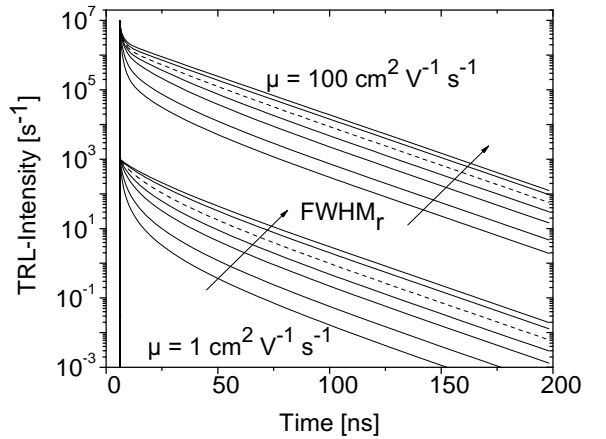

FIG. 4. TRL-transients of a semiconductor layer with a carrier SRH-lifetime of $\tau_{SRH} = 20\,\mathrm{ns}$ and carrier mobilities $\mu = 1, 100\,\mathrm{cm}^2\,\mathrm{V}^{-1}\,\mathrm{s}^{-1}$. The semiconductor is excited by a Gaussian laser pulse with $N_\gamma = 10^7$ photons focused on varying spot sizes with $FWHM_r = 1, 2, 5, 10, 20, 50, 100\,\mu\mathrm{m}$. The dashed curve marks $\Delta n_{0,max} \approx N_A$.

spot size with $FWHM_r = 1\,\mu\mathrm{m}$ the maximum generated electron density $\Delta n_{0,max}$ will be in the range of $10^{19} \ldots 10^{20}\,\mathrm{cm}^{-3}$. This is far above the limit of low excitations and leads to strong bimolecular recombination and defect saturation.[13,14] Figure 4 shows the TRL decay for a semiconductor excited by $N_\gamma = 10^7$ photons per pulse that are focused to different spot sizes $FWHM_r = 1 \ldots 100\,\mu\mathrm{m}$. For large spot diameters, the photon density is low and hence the semiconductor is only weakly excited. Then, the above considerations on the TRL-mapping can be applied. For small spot sizes, however, the photon density per pulse becomes large and the semiconductor is highly excited. The transition is marked by the dashed curve, for which the maximum charge carrier density equals the doping density. It can be seen, that the curves with small $FWHM_r$ strongly bend which can be assigned to bimolecular recombination and axial diffusion (since the effect of lateral diffusion can be excluded according to (16)).

All in all, one has to make a compromise between the TRL-mapping resolution given by σ_r, the signal-to-noise ratio determined by N_γ, and the accuracy of the lifetime measurement perturbed by high injection effects and the evacuation of charge carriers.

III. SEMICONDUCTOR INHOMOGENEITIES

In contrary to the previous considerations, in this part we assume a homogeneous excitation and study semiconductors with inhomogeneous material parameters. As mentioned in the introduction, in polycrystalline materials these are primarily fluctuating minority carrier lifetimes, band gaps, and doping densities.

A. Inhomogeneous carrier lifetime

If a polycrystalline semiconductor is excited by light, the spot may cover 10,000s of grains. If each grain has a distinct defect density, there will be a multitude of minority carrier lifetimes jointly affecting the luminescence decay. In Ref. 13 we have already shown under the assumption of negligible diffusion currents that the effect strongly depends on the exact distribution of the minority carrier lifetimes. Thereby, we studied equal and Gaussian lifetime distributions, and equal and Gaussian defect distributions. We found that lifetime distributions being symmetric cannot lead to strongly curved luminescence transients. However, equal and Gaussian defect distributions lead to asymmetric lifetime distributions and may result in strongly curved luminescence transients. These results will be tested in the following by three-dimensional simulations. In order to do so, the simulated semiconductor is divided into a mesh of 11×11 vertical, columnar grains. Electron Shockley- Read-Hall lifetimes are then assigned randomly and pairwise independently to the grains. The latter means, a correlation of lifetimes between neighboring grains is not considered. But in contrast to the analytical approach, the simulation accounts for carrier transport between different grains. Grain boundary recombination and potential barriers are omitted.

1. Simulated lifetime distributions

Prior to presenting the results of the simulation, we introduce the simulated lifetime probability functions $f(\tau)$, their average, and their standard deviation. To this end, we define the n-th moment of τ by

$$\langle \tau^n \rangle = \int_0^\infty \tau^n f(\tau) \mathrm{d}\tau. \tag{22}$$

Here, the integration is carried out only for values larger than zero, since only positive lifetimes are physically reasonable. By this notation, the average μ_τ and the standard deviation σ_τ of τ are defined by

$$\mu_\tau = \langle \tau \rangle, \qquad \sigma_\tau = \sqrt{\langle \tau^2 \rangle - \langle \tau \rangle^2}. \tag{23}$$

These definitions are now applied to the four lifetime probability density functions. First, equally distributed lifetimes are considered for which the probability density function is given by

$$f(\tau) = \begin{cases} \frac{1}{\tau_2 - \tau_1}, & \tau_1 \leq \tau < \tau_2, \\ 0, & \text{else.} \end{cases} \tag{24}$$

τ_1 and τ_2 are two parameters. Using equation (22) and (23) yields the average and the standard deviation for equally distributed lifetimes:

$$\mu_\tau = \frac{1}{2} \left(\tau_1 + \tau_2 \right), \qquad \sigma_\tau = \frac{1}{2\sqrt{3}} \left(\tau_2 - \tau_1 \right). \tag{25}$$
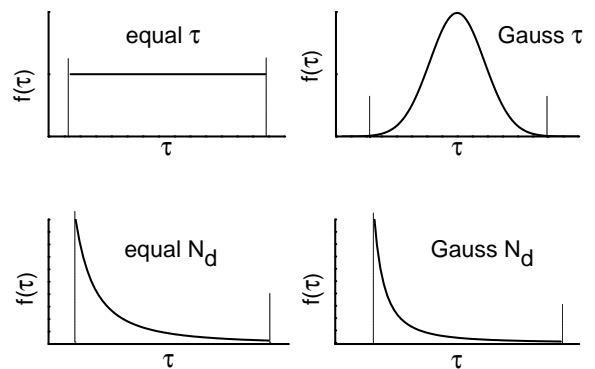

FIG. 5. Schematic graph of the four studied lifetime probability density functions $f(\tau)$ for the case of an equally and Gaussian distributed lifetime τ, and for an equally and Gaussian distributed defect density N_d.

The parameters τ_1 and τ_2 can now be expressed by $\tau_1 = \mu_\tau - \sqrt{3}\,\sigma_\tau$ and $\tau_2 = \mu_\tau + \sqrt{3}\,\sigma_\tau$. Since only positive lifetimes are reasonable ($\tau_1, \tau_2 \geq 0$) it follows $\sigma_\tau \leq \frac{1}{\sqrt{3}}\mu_\tau$. This means, for a given average μ_τ, the distribution can not be broadened arbitrarily.

If the lifetimes are Gaussian distributed, the probability density function will approximately be given by

$$f(\tau) = \begin{cases} \frac{1}{\sqrt{2\pi}\,\sigma_\tau} \mathrm{e}^{-\frac{(\tau - \mu_\tau)^2}{2\sigma_\tau^2}}, & \mu_\tau - 3\sigma_\tau \leq \tau < \mu_\tau + 3\sigma_\tau, \\ 0, & \text{else} \end{cases} \tag{26}$$

Again, only positive lifetimes are reasonable for which follows $\sigma_\tau \leq \frac{1}{3}\mu_\tau$. Thus, the broadness for both distributions - the equal and the Gaussian lifetime distribution - have an upper limit due to their symmetry around the average. This is shown schematically in figure 5.

We now consider a defect density N_d, which is equally distributed. The probability density function is then similar to Eq. (24):

$$f(N_d) = \begin{cases} \frac{1}{N_{d,2} - N_{d,1}}, & N_{d,1} \leq N_d < N_{d,2}, \\ 0, & \text{else.} \end{cases} \tag{27}$$

With the substitution $\tau = (\sigma_n v_n N_d)^{-1}$, this can be transformed into a probability density function of lifetimes:

$$f(\tau) = \begin{cases} \frac{\tau_1 \tau_2}{\tau_1 - \tau_2} \frac{1}{\tau^2}, & \tau_2 < \tau \leq \tau_1, \\ 0, & \text{else,} \end{cases} \tag{28}$$

with $\tau_i := (\sigma_n v_n N_{d,i})^{-1}$. Again, the distribution is described by two parameters τ_1 and τ_2. Unfortunately, a relation to the average and standard deviation μ_τ and σ_τ is not possible analytically and must be done numerically. By the implicit function theorem, however, it can be shown that τ_1 and τ_2 always exist for an arbitrary $\mu_\tau > 0$ and $\sigma_\tau > 0$. In turn this means that σ_τ has no upper limits for an equal defect distribution!

Finally, we assume a Gaussian distribution of deep defects N_d with average μ_d and standard deviation σ_d:

$$f(N_d) = \begin{cases} \frac{1}{\sqrt{2\pi}\,\sigma_d}\,e^{-\frac{(N_d-\mu_d)^2}{2\,\sigma_d^2}}, & \mu_d - 3\,\sigma_d \leq N_d < \mu_d + 3\,\sigma_d, \\ 0, & \text{else,} \end{cases}$$

(29)

With the transformation $\tau = (\sigma_n\,v_n\,N_d)^{-1}$, the probability density function of lifetimes becomes

$$f(\tau) = \begin{cases} \frac{1}{\sqrt{2\pi}\sigma_n\,\sigma_d\,v_n\,\tau^2}\,e^{-\left(\frac{1-\sigma_n\,v_n\,\mu_d\,\tau}{\sqrt{2}\,\sigma_n\,\sigma_d\,v_n\,\tau}\right)^2}, & \tau_2 < \tau \leq \tau_1, \\ 0, & \text{else} \end{cases}$$

(30)

with $\tau_2 = (\mu_d + 3\,\sigma_d)^{-1}$ and $\tau_1 = (\mu_d - 3\,\sigma_d)^{-1}$. Again, the two parameters σ_d and μ_d or equivalently τ_1 and τ_2 have to be determined numerically for each given μ_τ and σ_τ. It turns out that also in this case σ_τ has no upper limits. Hence, a symmetric defect distribution leads to an asymmetric lifetime distribution (as shown in Fig. 5), which enables an unlimited broadening of the distribution.

2. Resulting TRPL

Now, we study the impact of each distribution on the luminescence decay. To this end, the average of each lifetime distribution is fixed to $\mu_\tau = 20$ ns, and the standard deviation σ_τ is varied from 0 ns up to $\frac{\mu_\tau}{\sqrt{3}} \approx 11.5$ ns for the equal lifetime distribution, up to $\frac{\mu_\tau}{3} \approx 6.5$ ns for the Gaussian lifetime distribution, and up to 20 ns for equal and Gaussian defect distributions. The charge carrier mobility is 20 cm² V⁻¹ s⁻¹ which yields an average diffusion length of $L_n \approx 1\,\mu$m. In order to study the effect of lateral diffusion, we therefore chose two sizes of the grains: 1 μm and 6 μm. The results are shown in Fig. 6. First, we focus on the decay for a large grain size of 6 μm which is much larger than the diffusion length. Then, the luminescence transients bend with increasing broadness σ_τ of the underlying distribution $f(\tau)$. The effect is smaller for the equal and Gaussian lifetime distribution, since here the standard deviation cannot be increased arbitrarily. In turn, the effect is larger for the equal and Gaussian defect distribution, since here the standard deviation has no upper limits.

Due to the grain size being larger than the diffusion length, most of the charge carriers recombine in the same grain where they have been generated. This means, the lifetime distribution is only little changing during the decay and the luminescence intensity can be calculated by

$$I(t) = I_0 \int_0^\infty f(\tau)e^{-\frac{t}{\tau}}\,d\tau$$

(31)

with a normalization factor I_0. For each of the four distributions, the integrals have been evaluated in Ref. 13 and the result is drawn in figure 6 (dashed lines) for the largest values of σ_τ. It can be seen, that these theoretical curves are upper limits for the simulated transients. The difference may have two reasons. First, the random sample of 121 lifetimes in the simulation may be too small. Then, especially the high lifetimes with low probability density as for the equally and Gaussian distributed defect densities may be not sufficiently represented. Secondly, lateral diffusion is not completely switched off. This means, charge carriers diffuse to grains with small charge carrier lifetime, since these form sinks for the charge carriers. This weakens the impact of grains with high lifetime and strengthens the impact of grains with low lifetimes. For this reason, the transients decay faster than the theoretical ones.

The effect is more pronounced, if the grain size is reduced. Then, grains with high minority carrier lifetimes have almost no impact on the luminescence decay, which is only determined by grains with small minority carrier lifetime. Therefore, all transients decay faster with increasing σ_τ, though the average lifetime is always fixed to 20 ns. Thereby, the effect is again smaller for the equal and Gaussian lifetime distribution due to the limitation of σ_τ. In summary, we find curved transients due to lifetime distributions if diffusion of charge carriers is small, that is if the average diffusion length is larger than the grain size.

B. Inhomogeneous band gap

The above discussed fluctuations of the lifetime may strongly affect the TRL and the solar cell parameters. However, estimates show that in the case of CIGSe the effect is too small in order to explain the intensity inhomogeneities that are observed in micro TRPL[4]. Hence, apart from the lifetime there must be other inhomogeneous physical properties. One of these may be the band gap due to alloy-, non-stoichiometry, or strain induced fluctuations. This assumption is supported by the observed correlation of the quasi-Fermi level splitting and the gallium content in CIGSe (which in turn results in an inhomogeneous band gap). The analysis of these data yields band gap fluctuations of $10-80$ meV[7–9]; in $Cu_2ZnSnSe_4$ these are even larger with $70-90$ meV due to order-disorder phenomena[9]. Such strong non-uniformities of the band gap are detrimental for the solar cell's performance, since they increase the saturation current density thereby reducing the photovoltaic parameters[8,12].

In this section, we study the impact of a fluctuating band gap on the TRL decay. We first study the impact of a fluctuating band gap on the bulk properties, in particular on the absorption coefficient and the recombination lifetimes. It will turn out, that these properties have only negligible impact on the integral luminescence decay. For investigation of the impact on surface recombination we must account for a V-shaped band gap grading which has been often observed in CIGSe. The band gap
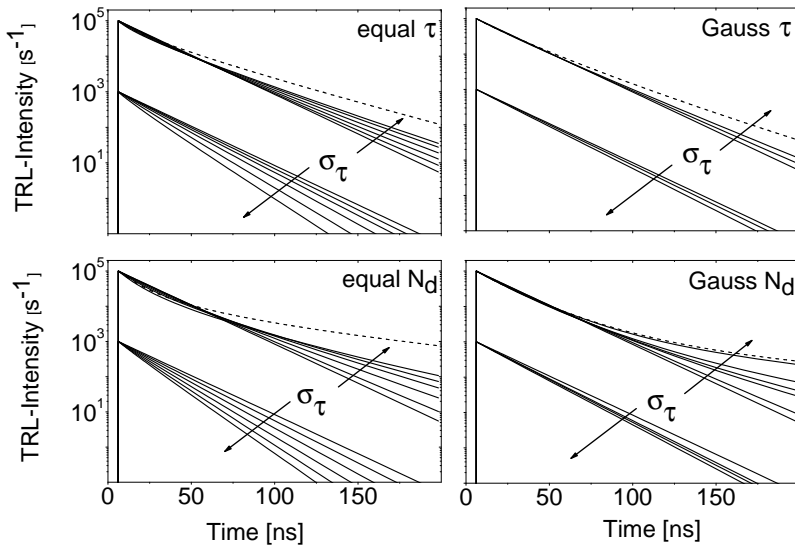
FIG. 6. Simulated TRL-transients of a semiconductor with 121 grains. For each grain, the SRH-lifetime is determined using a random number generator and by a transformation the lifetime is calculated according to one of the four lifetime distributions. The average SRH-lifetime is always 20 ns. The standard deviation σ_τ is varied from 0 ns up to 11.5 ns for equally distributed lifetimes, up to 6.5 ns for Gaussian distributed lifetimes, and up to 20 ns for both defect distributions. For the largest σ_τ, the theoretical TRL-transients are calculated after equation (31) (dashed lines). The simulations were done for a large grain size of 6 μm (upper graphs) and a small grain size of 1 μm (lower graphs). The photon density per pulse is $n_\gamma = 10^9 \, \text{cm}^{-2}$ and the charge carrier mobility is $20 \, \text{cm}^2 \, \text{V}^{-1} \, \text{s}^{-1}$ leading to an average diffusion length of 1 μm.

gradient towards the back side is found to be laterally homogeneous whereas the front band gap gradient may fluctuate.[15] Thereby, the fluctuation length exceeds the size of the grains and becomes approximately 3 μm.

1. Impact on photon absorption

If the band gap varies, this will simultaneously cause a variation of the absorption coefficient. To estimate its fluctuation strength, the absorption coefficient is related to the band gap by[16]

$$\alpha(\hbar\omega) = C_1 \sqrt{\hbar\omega - E_g}. \tag{32}$$

It is C_1 a specific material constant and $E_g = E_g(x,y,z)$ is the space-dependent band gap. We rewrite the band gap using the constant average band gap $E_{g,av}$ and the space-dependent fluctuation $\delta E_g = \delta E_g(x,y,z)$:

$$E_g = E_{g,av} + \delta E_g. \tag{33}$$

For CIGSe with $E_{g,av} = 1.15 \, \text{eV}$ we take an average value of $\delta E_g \approx 50 \, \text{meV}$.[7] Thus, the deviations of the band gap from the average value are small and Eq. (32) can be expanded by orders of δE_g:

$$\alpha(\hbar\omega) = C_1 \sqrt{\hbar\omega - E_{g,av}} - \frac{1}{2} C_1 \frac{\delta E_g}{\sqrt{\hbar\omega - E_{g,av}}} \tag{34a}$$

$$= \alpha_{av} + \delta\alpha. \tag{34b}$$

In the first term of Eq. (34a), only the average band gap enters which is therefore assigned to the average absorption coefficient α_{av}. The second term is then the fluctuation $\delta\alpha$ of the absorption coefficient for which it holds

$$\frac{\delta\alpha}{\alpha_{av}} = -\frac{\delta E_g}{2(\hbar\omega - E_{g,av})}. \tag{35}$$

For typical values of $E_g = 1.15 \, \text{eV}$, $\hbar\omega = 1.9 \, \text{eV}$, and $\delta E_g = 50 \, \text{meV}$ this yields $\delta\alpha/\alpha_{av} \approx 3\%$. With equation (7), then also the fluctuation $\delta\Delta n_{0,max}$ of the maximum generated charge carrier density can be estimated, which becomes

$$\frac{\delta\Delta n_{0,max}}{\Delta n_{0,max,av}} = \frac{\delta\alpha}{\alpha_{av}} \approx 3\%. \tag{36}$$

Both effects are very small. Therefore, the impact of band gap fluctuations on the photon absorption and charge carrier generation can be neglected.

2. Impact on bulk recombination

For the study of the impact of a band gap fluctuation on the bulk recombination we consider two cases: radiative band-to-band recombination and defect assisted SRH-recombination. In the first case, the recombination rate is given by $R_{rad} = B(np - n_0 p_0)$. For a p-type semiconductor we then find for the radiative lifetime of electrons

$$\tau_{rad,n} = \frac{\Delta n}{R_{rad}} = \frac{1}{B(p_0 + \Delta p)}. \tag{37}$$

We now estimate the fluctuation strength of the radiative lifetime due to the band gap fluctuation. The hole density p_0 shall be constant, since in semiconductors such as CIGSe band gap fluctuations are related mainly to the conduction band. Furthermore, the transition rate B is assumed to be constant, since the variations due to the fluctuating band gap are small. It remains the excess hole density Δp, which varies weakly according to Eq. (36). Again, we write the excess hole density as a superposition of the average generated charge carrier density Δp_{av} and the fluctuation $\delta\Delta p$. Inserting this into Eq.

(37) and expanding it by powers of $\delta\Delta p$ yields

$$\tau_{rad,n} = \frac{1}{B\,(p_0 + \Delta p_{av})} - \frac{\delta\Delta p}{B\,(p_0 + \Delta p_{av})^2} \quad (38a)$$

$$= \tau_{rad,n,av} + \delta\tau_{rad,n}. \quad (38b)$$

Again, the first term is the average radiative recombination lifetime of electrons, since only the average charge carrier densities enter. Therefore, the second term must be the variation due to the band gap fluctuation for which holds

$$\frac{\delta\tau_{rad,n}}{\tau_{rad,n,av}} = \frac{\delta\Delta p}{p_0 + \Delta p_{av}}. \quad (39)$$

For the evaluation of equation (39), low and high injections must be distinguished. One finds

$$\frac{\delta\tau_{rad,n}}{\tau_{rad,n,av}} \leq \begin{cases} \frac{\delta\Delta p}{p_0} \approx 0 & \text{for low injections} \\ \frac{\delta\Delta p}{\Delta p_{av}} \approx 3\% & \text{for high injections.} \end{cases} \quad (40)$$

for the parameters stated above. The same is done for recombination assisted by defects deep in the band gap. For a p-type semiconductor, the SRH-lifetime of electrons then becomes

$$\tau_{SRH,n} = \frac{\Delta n}{R_{SRH}} = \tau_{n0} + \tau_{p0}\,\frac{\Delta n}{p_0 + \Delta p}. \quad (41)$$

Here, the lifetimes τ_{n0} and τ_{p0} do not depend on the band gap. Hence, only fluctuation of Δn and Δp must be considered. Expansion of Eq. (41) by orders of $\delta\Delta n$ and $\delta\Delta p$ then yields the variation $\delta\tau_{SRH,n}$ of the electron SRH-recombination lifetime. The resulting expression is very long for which reason it is not shown here. The discrimination into low and high excitations yields

$$\frac{\delta\tau_{SRH,n}}{\tau_{SRH,n,av}} \leq \begin{cases} \frac{\tau_{p0}}{\tau_{n0}}\,\frac{\delta\Delta n}{p_0} \approx 0 & \text{for low injections} \\ \frac{\delta\Delta n}{\Delta n_{av}} + \frac{\delta\Delta p}{\Delta p_{av}} \approx 6\% & \text{for high injections.} \end{cases} \quad (42)$$

According to the equations (40) and (42), the variation of the bulk lifetime due to band gap fluctuation is negligible for low injection conditions. For high excitations, it becomes less than approximately 10%. Such small lifetime inhomogeneities will not substantially influence the luminescence decay as discussed in the previous section.

3. Impact on front surface recombination

Finally, we discuss the impact on the front surface recombination. Above it was pointed out that in CIGSe often V-shaped band gap gradients are found.[17,18] Such a band gap grading may reduce surface recombination of charge carriers, since it hinders the charge carrier transport towards the surface. Hence, a laterally fluctuating band gap grading may influence the surface recombination and thus the luminescence decay. From luminescence measurements it is known that only the front gradient of the band gap varies.[15] The band gap gradient towards the back surface is constant. This is exemplified
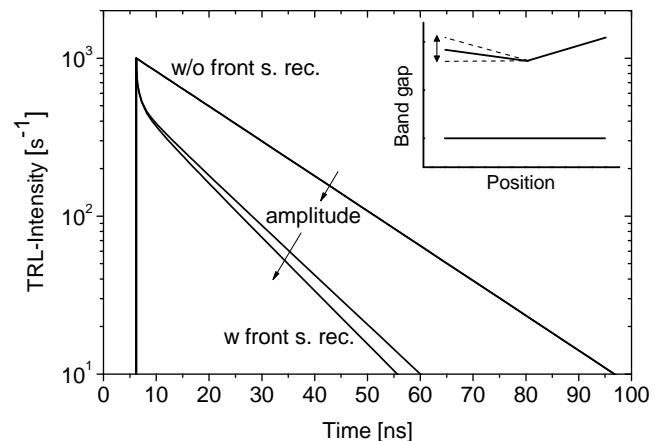

FIG. 7. TRL-transients of a semiconductor layer with V-shaped band gap gradient with a minimum band gap of 1.15 eV within a distance of 0.8 μm from the front surface, a front surface gradient of 60 meV, and a back surface gradient of 120 meV. Thereby, the front surface gradient is fluctuating sinusoidally with amplitudes 0 and 1, and a period of 3 μm. Furthermore, the front surface recombination velocities were 0 and 10^7 cm s^{-1}, the charge carrier mobilities were 20 cm^2 V^{-1} s^{-1}, and the bulk SRH-lifetimes were 20 ns. The photon density per pulse was $n_\gamma = 10^9$ cm^{-2}.

in the inset of figure 7.

For the simulation, we vary the front band gap gradient sinusoidally with a period of 3 μm. The amplitude of the variation is thereby increased from 0 to 1, where zero corresponds to no fluctuation, and 1 corresponds to no front surface gradient in the minima. We further vary the recombination velocity at the front surface. If this is zero, the band gap fluctuation will not affect the luminescence decay (see Fig. 7), because the semiconductor is not limited by surface recombination. This means, the recombination is not influenced by the transport of charge carriers towards the front surface and hence it is unaffected by the fluctuation. However, if the surface recombination velocity is 10^7 cm s^{-1} the semiconductor will be limited by front surface recombination, the recombination will depend on the transport of charge carriers towards the front surface (which makes the transient bend), and the band gap fluctuation will influence the luminescence decay.

C. Inhomogeneous doping density

At the end of this work we study fluctuations of the electrostatic potential. Since these are predominant in compensated semiconductors such as Cu(In,Ga)Se$_2$ and Cu$_2$ZnSnSe$_4$ it is assumed that they result from an inhomogeneous net-doping due to an inhomogeneous ratio of donors and acceptors. Therefore in the simulations, we again divide the semiconductor into 121 grains and distribute acceptor and donor densities randomly. The acceptor density N_A follows a Gaussian distribution (compare Eq. (26)) with average μ_A and standard deviation
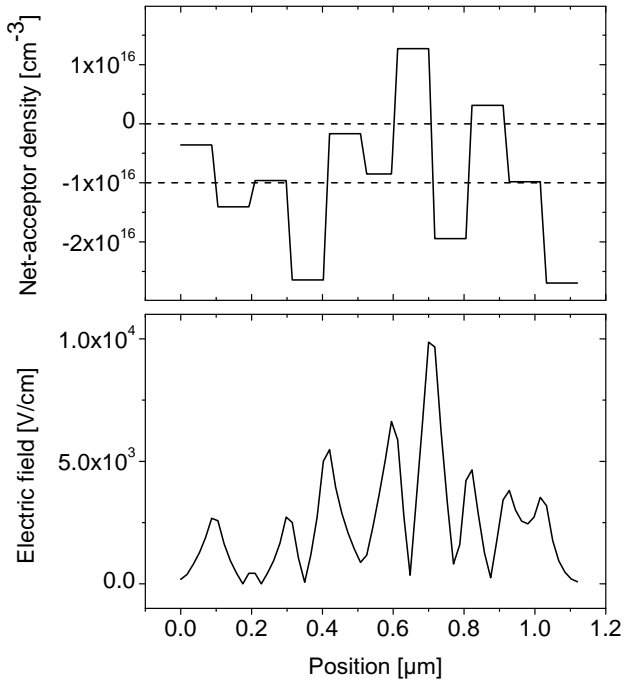
FIG. 8. Cross-section of the net-doping density for a grain size of 100 nm, an average net-p-doping of $N_{A,av} = \mu_{net} = 10^{16}\,\mathrm{cm}^{-3}$, and a doping fluctuation of $\sigma_{dop} = 9.6 \times 10^{15}\,\mathrm{cm}^{-3}$. The dashed lines mark $N_{A,net} = 0$ and $N_{A,net} = N_{A,av}$. The lower figure shows the resulting electric field strength.
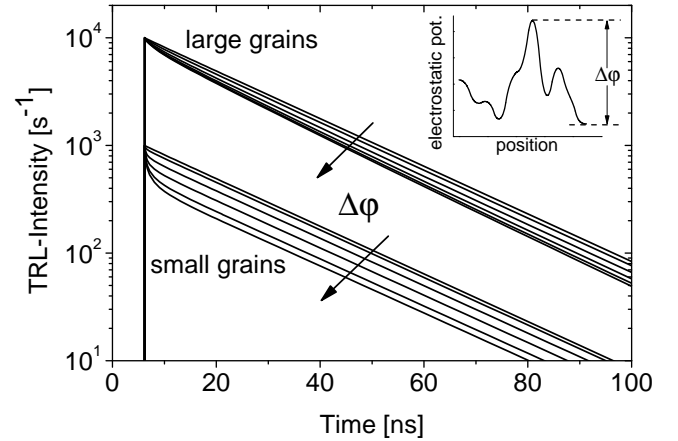

FIG. 9. Simulated TRL-transients of a semiconductor with 121 grains. For each grain, the net-acceptor (or net-donor) density is determined using a random number generator and by a transformation the density is calculated according to a Gaussian distribution. The average net-p doping of $N_{A,av} = 10^{16}\,\mathrm{cm}^{-3}$ is fixed. The strength σ_{dop} of fluctuation is varied such that the strength of potential fluctuation becomes $\Delta\varphi = 0, 30, 55, 75, 90, 100\,\mathrm{mV}$. The inset shows an exemplary cross-section of the electrostatic potential. Furthermore, two grain sizes 100 nm and 1 µm are chosen. The photon density per pulse is $n_\gamma = 10^9\,\mathrm{cm}^{-2}$, the bulk SRH-lifetimes are 20 ns, and the mobilities are $20\,\mathrm{cm}^2\,\mathrm{V}^{-1}\,\mathrm{s}^{-1}$.

σ_{dop}. Correspondingly the donor density N_D follows a Gaussian distribution with average μ_D and standard deviation σ_{dop}. The net p-doping $N_{A,net} = N_A - N_D$ is then again Gaussian distributed with average $\mu_{net} = \mu_A - \mu_D$ and standard deviation $\sigma_{net} = \sqrt{2}\,\sigma_{dop}$. An example for such an inhomogeneous net-doping is given in figure 8.

Due to the inhomogeneous net-p-doping, the semiconductor becomes a series of p-p-junctions (see $z < 0.6\,\mu\mathrm{m}$ in Fig. 8). For strong doping fluctuations the net-p-doping can become negative which results in a net-n-doping. Then, there may be also p-n-junctions (see $z > 0.6\,\mu\mathrm{m}$ in Fig. 8). Both lead to an electric field on a lateral scale as demonstrated in figure 8. Expressions for the maximum electric field strength and the space charge widths are summarized in the appendix A.

1. Impact of net-doping fluctuation strength and length on the TRL decay

We now vary these electric fields by net-doping fluctuations of different fluctuation strengths and study the impact on the TRL decay. As the net-doping inhomogeneities increase, the potential drop across the p-p junctions increases according to equation (A3). In the following, we adjust the doping fluctuation strength σ_{dop} such that the width $\Delta\varphi$ of the resulting potential fluctuation (see the inset of figure 9) becomes $\Delta\varphi =$

0, 30, 55, 75, 90, 100 mV. Thereby, the average net-acceptor density is fixed by $N_{A,av} = 10^{16}\,\mathrm{cm}^{-3}$, which leads to a room temperature screening length $\sim 40\,\mathrm{nm}$ (see equation A8). On this basis, for the study of the effect of the characteristic fluctuation length we also consider the two grain sizes 100 nm and 1 µm, which are either in the range of the screening length or much larger. The resulting TRL-decay is shown in figure 9 which illustrates three important findings on lateral potential fluctuations: First, the luminescence decay becomes bi-exponential due to the impact of potential fluctuations. Thereby, only the first decay time is influenced by the potential fluctuation strength $\Delta\varphi$ (or equivalently by the maximum electric field strength E_{max}), which indicates that the first decay includes the separation of charge carriers by drift, and the second decay describes the bulk recombination of charge carriers.

Secondly, the effect of a potential fluctuation becomes less for increased characteristic length scales. This is due to the arising quasi-neutral region in the semiconductor if the structure size exceeds the screening length. Accordingly, even for constant fluctuation strength $\Delta\varphi$, the average electric field becomes reduced and the drift effects in the TRL decay diminish.

Thirdly, the decay time is always smaller than that for a semiconductor without potential fluctuations which is similar to the results in Ref. 13 and 14. This is in contrast to the expectation that the charge carriers are preserved from recombination by the potential barriers. A reason why preservation from recombination is not found here may be the small barrier height of at most 100 mV which

is much smaller than the barrier height of a typical pn-junction ($\sim 800\,\text{mV}$). Furthermore, it must be taken into account that the electrostatic potential equalizes at the metallic back contact. This means, the electrostatic potential close to the contact is homogeneous which leads to a path of higher conductivity and reduces the effect of charge separation.

2. Temperature and excitation dependence of TRL-decay due to doping inhomogeneities

Now, we study the effect of potential fluctuations under different experimental conditions. Therefore, we simulate the TRL for a fixed fluctuation strength of $\Delta\varphi = 90\,\text{mV}$ and vary the temperature and excitation intensity. The results are shown in figure 10. In the left subfigure, the effect of a temperature increase is illustrated. It comes out that both decay times become smaller for higher temperatures. The decrease of the second decay is due to a decreasing bulk SRH-lifetime of the charge carriers, which can be expressed by[1,2,19]

$$\tau_{bulk} \sim T^{-b}. \tag{43}$$

The decrease of the first decay time indicates a temperature dependent drift of the charge carriers. In the simulations, however, the mobility is assumed to be constant. Hence, the electric field must depend on the temperature, more precisely the electric field increases with increasing temperature. This comes out from equation (A10), which predicts a larger electric field at elevated temperatures due to the higher diffusity of the charge carriers. However, this is only true for small temperature increases. For high temperatures, when the semiconductor becomes intrinsic, the electric field becomes smaller due to screening.

In the right subfigure of Fig. 10, the influence of an increasing injection level is shown. Two effects can be found. First, the potential fluctuations can be screened if the injection level is increased. This is due to the higher charge carrier densities that screen the space charge. Secondly, the screening effect is more pronounced for larger characteristic lengths of the fluctuation. This is due to the smaller space charge, thus, less charge carriers are necessary for screening.

IV.   CONCLUSIONS

In this work we studied the impact of lateral inhomogeneities on the time-resolved luminescence decay. For systematic reasons we distinguished inhomogeneities of the excitation and inhomogeneities of the semiconductor material properties.

For laterally inhomogeneous excitations with high injection levels we found that contrary to axial diffusion, the lateral diffusion of charge carriers does not directly affect the decay of the luminescence. However, indirectly lateral diffusion influences the decay via the occupation of deep and shallow defects in the band gap. We then studied the spatial resolution of a micro-TRL experiment, which is limited by the diffusion length of the charge carriers and by the size of the excitation spot. Due to this, the resolved spot size can be more than ten times larger than the width of the excitation spot, if the diffusion length is sufficiently large. This means, micro-TRL is not applicable in all cases. The approximation of an inhomogeneous excitation profile by a homogeneous excitation with an average photon density is possible for low injection levels and even for high injection levels, if the excitation spot is large. This can facilitate the simulation. However, for small excitation spots and high injection levels, the occupation of defects in the band gap is strongly determined by lateral diffusion. Hence, simulations must be performed under consideration of the inhomogeneous excitation profile.

In the second part, we studied inhomogeneous material parameters. First, we considered inhomogeneous bulk-recombination lifetimes. Thereby, we divided the simulated semiconductor into 121 grains on a quadratic mesh, where each grain has uniform properties, and distributed SRH-lifetimes randomly on the grains according to different distribution functions. It comes out, that the effect is larger for asymmetric lifetime distributions than for symmetric lifetime distributions. Furthermore, the effect does strongly depend on the characteristic length of the inhomogeneities. For length scales smaller than the diffusion length, regions of high recombination attract carrier and the decay is increased. For large length scales, the effect of lateral diffusion is reduced and the decay exhibits multiple decay times according to the lifetime distribution. This leads to curved transients. Next, we studied inhomogeneities of the band gap. It is found, that these are small and the effects on the bulk properties (absorption coefficient, bulk-lifetime) are negligible. Only an laterally inhomogeneous band gap gradient may influence the luminescence decay, if the semiconductor is limited by surface recombination. At the end we studied inhomogeneities of the doping density since these cause fluctuations of the electrostatic potential which are often observed. These fluctuations lead to bi-exponential luminescence decays. Thereby, the first smaller decay time is mostly determined by charge carrier separation due to drift, and the second larger decay time is determined by bulk recombination. A third decay time which is longer than the bulk-recombination lifetime is not observed, probably due to the small barrier heights and the paths of higher conductivity at the metallic back contact. A moderate increase of the temperature leads to a decrease of both decay times due to smaller recombination lifetimes and higher electric fields. A screening of the space charge at higher temperatures is not found, since this requires much higher temperatures. However, the space charge can be screened, if the excitation intensity is increased.
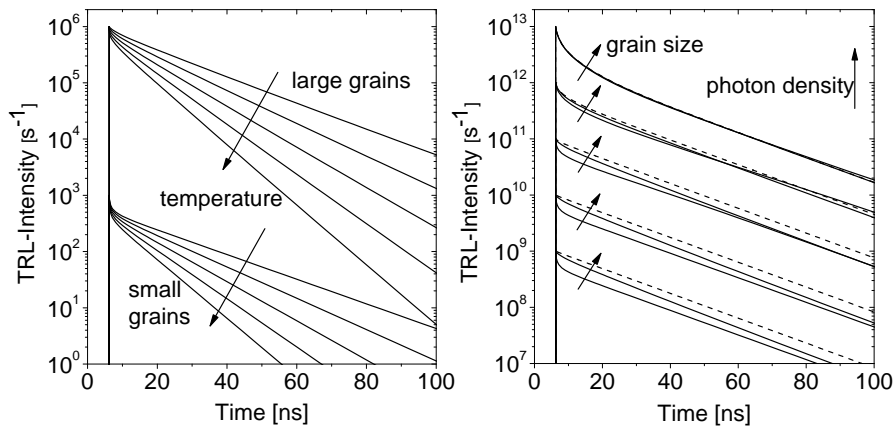
FIG. 10. Simulated TRL-transients of a semiconductor with 121 grains each with a size of 100 nm and 1 μm. For each grain, the net-doping density is asigned randomly according to a Gaussian distribution. The average net-p doping of $N_{A,av} = 10^{16}$ cm^{-3} and the fluctuation strength of $\Delta\varphi = 90$ mV are fixed. The bulk SRH-lifetimes are 20 ns and the mobilities are 20 cm^2 V^{-1} s^{-1}. In the left figure, the incident photon density is $n_\gamma = 10^9$ cm^{-2} and the temperature is $T = 300, 325, 350, 375, 400$ K. In the right figure, the temperature is $T = 300$ K and the incident photon density is $n_\gamma = 10^9, 10^{10}, 10^{11}, 10^{12}, 10^{13}$ cm^{-2}. The dashed line shows the TRL decay for a semiconductor without potential fluctuations.

V. SUMMARY OF TRL DECAY CURVES

At the end of this work, we give a summary of all the decay curves that have been simulated for a **blank** semiconductor layer in the parts I-IV. In order to provide a base for the interpretation of **low-injection** and **spectrally integrated** TRL decay curves, we classify the transients into mono-exponential, bi-exponential, and multi-exponential decays.

A. Mono-exponential decays

Effects that may lead to mono-exponential luminescence decays are radiative band-to-band and non-radiative SRH-recombination in the volume or at the surface of the semiconductor layers. Also minority carrier trapping may yield mono-exponential decay curves if the capture time is below the time-resolution of the experimental setup. A summary of the different excitation dependencies is given in table I.

TABLE I. Overview of the different dependencies under excitation increase for mono-exponential decay under low injection (dashed curve).

| bimolecular recombination and axial diffusion | recombination via deep defects with asymmetric lifetimes | minority carrier trapping with capture times below exp. resolution |

Effects leading to mono-exponential decays but without excitation dependence:

- SRH-recombination with symmetric lifetimes
- a distribution of lifetimes with small structure sizes
- surface recombination with small recombination velocities or large mobilities

B. Bi-exponential decays

Effects that may lead to bi-exponential luminescence transients are surface recombination in semiconductors with small charge carrier mobilities and low bulk recombination, the drift of charge carriers due to potential fluctuations, and the trapping of minority charge carriers. A summary of the different excitation and temperature dependencies of the TRL is given in table II.

TABLE II. Overview of the different dependencies under excitation and temperature increase for bi-exponential decays under low injection (dashed curve).

| drift due to potential fluctuations | minority carrier trapping with capture times above exp. resolution | temperature dependence for pot. fluctuations and for minority carrier traps |

Effects leading to bi-exponential decays but without excitation dependence:

- surface recombination with large recombination velocities, low bulk recombination, and small carrier mobilities

C. Multi-exponential decays

In the simulations, also multi-exponential decays of the luminescence under low-excitation have been observed. The following list provides a summary of effects that may lead to multi-exponential decays, but for which the TRL decay does not exhibit any excitation dependence.

- (mostly asymmetric) distribution of lifetimes with large structure sizes

- diffusion of charge carriers out of an observation volume

- photon recycling

D. Effects without impact on the TRL decay

Finally we give a list of effects, that do not have (a strong impact) on the luminescence decay.

- charge carrier diffusion at low injections

- lateral charge carrier diffusion at high injections

- band gap fluctuations in semiconductors limited by bulk recombination

Appendix A: Electric field of p-n and p-p-junctions

For a junction of a p-type semiconductor with acceptor density N_A and a n-type semiconductor with donor density N_D, the maximum electric field strength E_{max}, and the space charge widths w_p and w_n in the p- and n-type semiconductor, respectively, are[20]:

$$E_{max} = \sqrt{\frac{2\,N_A\,N_D}{\varepsilon_0\,\varepsilon_r\,(N_A + N_D)}\left(E_g - k_B\,T\,\log\frac{N_c\,N_v}{N_A\,N_D}\right)} \quad \text{(A1a)}$$

$$w_p = \sqrt{\frac{2\,k_B\,T\,\varepsilon_0\,\varepsilon_r}{e_0^2}\,\frac{N_D}{N_A\,(N_A + N_D)}\,\log\frac{N_A\,N_D}{n_i^2}} \quad \text{(A1b)}$$

$$w_n = \sqrt{\frac{2\,k_B\,T\,\varepsilon_0\,\varepsilon_r}{e_0^2}\,\frac{N_A}{N_D\,(N_A + N_D)}\,\log\frac{N_A\,N_D}{n_i^2}}. \quad \text{(A1c)}$$

Here, N_v is the effective density-of-states of the valence band, N_c the effective density-of-states of the conduction band, n_i the intrinsic charge carrier density, k_B is the Boltzmann constant, e_0 the elementary charge, ε_0 the dielectric permittivity of vacuum, and ε_r the relative permittivity of the material.

For a junction of two p-type semiconductors, the results are strongly different. For this reason, they are derived below for the following space dependent acceptor density

$$N_A(z) = \begin{cases} N_{A,l} & z < 0 \\ N_{A,h} & z > 0 \end{cases} \quad \text{(A2)}$$

with $N_{A,h} > N_{A,l}$. In the limits of impurity exhaustion and Boltzmann approximation, the built-in voltage V_{bi} then becomes

$$\begin{aligned} e_0\,V_{bi} &= \lim_{z\to-\infty}(E_f - E_v) - \lim_{z\to+\infty}(E_f - E_v) \\ &= -k_B\,T\,\log\frac{N_{A,l}}{N_v} + k_B\,T\,\log\frac{N_{A,h}}{N_v} \\ &= k_B\,T\,\log\frac{N_{A,h}}{N_{A,l}}. \end{aligned} \quad \text{(A3)}$$

Thereby, E_f denotes the Fermi-level and E_v is the valence band edge. In contrast to a p-n-junction, there are no

positively ionized donors. Thus, the positive space charge results from an excess of mobile holes. These are then screened with Debye's screening length which motivates the following ansatz for the space charge density ϱ

$$\varrho = \begin{cases} A_l\,\mathrm{e}^{\frac{z}{w_l}} & z < 0 \\ A_h\,\mathrm{e}^{\frac{-z}{w_h}} & z > 0. \end{cases} \quad \text{(A4)}$$

with parameters A_l, A_h, w_l, $w_h > 0$ that have to be determined by a self-consistent solution of Poisson's equation and the two continuity equations. The electron current equation can be omitted due to the negligible number of electrons. The Poisson equation is solved by twice integration of equation (A4) which gives the electric field $E(z)$ and the electrostatic potential $\varphi(z)$. Since both must be continuous functions, this leads to the following conditions

$$A_l\,w_l - A_h\,w_h = 0 \quad \text{(A5a)}$$

$$A_l\,w_l^2 + A_h\,w_h^2 = \varepsilon_0\,\varepsilon_r\,V_{bi}. \quad \text{(A5b)}$$

Using these conditions, Poisson's equation is solved self-consistently. What remains, is the solution of the hole current equation. In equilibrium, the hole current Γ_p must vanish. Hence, it must be

$$p(z)\,E(z) - \frac{k_B\,T}{e_0}\,\frac{\mathrm{d}p(z)}{\mathrm{d}z} = 0. \quad \text{(A6)}$$

Since the amount of electrons can be neglected, the hole density can be expressed by $p(z) = \frac{1}{e_0}\varrho(z) + N_A(z)$. Furthermore, $E(z)$ is known from integration of the space charge density. Inserting both into equation (A6) yields

$$k_B\,T\,\varepsilon_0\,\varepsilon_r - e_0^2\,N_{A,l}\,w_l^2 = e_0\,A_l\,w_l^2\,\mathrm{e}^{\frac{z}{w_l}} \quad \text{for } z < 0 \quad \text{(A7a)}$$

$$k_B\,T\,\varepsilon_0\,\varepsilon_r - e_0^2\,N_{A,h}\,w_h^2 = e_0\,A_h\,w_h^2\,\mathrm{e}^{-\frac{z}{w_h}} \quad \text{for } z > 0 \quad \text{(A7b)}$$

It comes out, that the terms on the right hand sides of each equation can be neglected. Then, the parameters w_l and w_h are given by

$$w_l = \sqrt{\frac{k_B\,T\,\varepsilon_0\,\varepsilon_r}{e_0^2\,N_{A,l}}}, \qquad w_h = \sqrt{\frac{k_B\,T\,\varepsilon_0\,\varepsilon_r}{e_0^2\,N_{A,h}}}. \quad \text{(A8)}$$

By equations (A5) and (A8), the constants A_l and A_h can be determined:

$$A_l = \frac{e_0^2}{k_B\,T}\,\frac{N_{A,l}\,\sqrt{N_{A,h}}}{\sqrt{N_{A,l}} + \sqrt{N_{A,h}}}\,V_{bi}, \quad \text{(A9a)}$$

$$A_h = \frac{e_0^2}{k_B\,T}\,\frac{\sqrt{N_{A,l}}\,N_{A,h}}{\sqrt{N_{A,l}} + \sqrt{N_{A,h}}}\,V_{bi}. \quad \text{(A9b)}$$

The quantities A_l, A_h, w_l, w_h in Eqs. (A8) and (A9) are parameters of a self-consistent solution of the two continuity equations and Poisson's equation. The latter allows the calculation of the maximum electric field strength which becomes

$$E_{max} = \frac{A_l\,w_l}{\varepsilon_0\,\varepsilon_r} = \sqrt{\frac{k_B\,T}{\varepsilon_0\,\varepsilon_r}}\,\frac{\sqrt{N_{A,l}}\sqrt{N_{A,h}}}{\sqrt{N_{A,l}} + \sqrt{N_{A,h}}}\,\log\frac{N_{A,h}}{N_{A,l}}. \quad \text{(A10)}$$

[1] M. Maiberg, T. Hölscher, S. Zahedi-Azad, W. Fränzel, and R. Scheer, Applied Physics Letters **107**, 122104 (2015).

[2] M. Maiberg, C. Spindler, E. Jarzembowski, and R. Scheer, Thin Solid Films **582**, 379 (2015).

[3] R. Scheer and H.-W. Schock, *Chalcogenide Photovoltaics: Physics, Technologies, and Thin Film Devices* (WILEY-VCH, 2011).

[4] K. Bothe, G. H. Bauer, and T. Unold, Thin Solid Films **403-404**, 453 (2002).

[5] T. Sakurai, K. Taguchi, M. M. Islma, S. Ishiuuka, A. Yamada, K. Matsubara, S. Niki, and K. Akimoto, Japanese Journal of Applied Physics **50**, 05FC01 (2011).

[6] M. J. Romero, H. Du, G. Teeter, Y. Yan, and M. M. Al-Jassim, Physical Review B **84**, 165324 (2011).

[7] L. Gütay, C. Lienau, and G. H. Bauer, Applied Physics Letters **97**, 052110 (2010).

[8] J. H. Werner, J. Mattheis, and U. Rau, Thin Solid Films **480-481**, 399 (2005).

[9] T. Gokmen, O. Gunawan, T. K. Todorov, and D. B. Mitzi, Applied Physics Letters **103**, 103506 (2013).

[10] S. Siebentritt, N. Papathanasiou, and M. C. Lux-Steiner, Physica B **376-377**, 831 (2006).

[11] J. Larsen, K. Burger, L. Gutay, and S. Siebentritt, in *Photovoltaic Specialists Conference (PVSC), 2011 37th IEEE* (2011) pp. 000396–000401.

[12] P. O. Grabitz, U. Rau, and J. Werner, physica status solidi a **202**, 2920 (2005).

[13] M. Maiberg and R. Scheer, Journal of Applied Physics **116**, 123710 (2014).

[14] M. Maiberg and R. Scheer, Journal of Applied Physics **116**, 123711 (2014).

[15] G. H. Bauer, S. J. Heise, S. Knabe, O. Neumann, R. Brüggemann, D. Hariskos, and W. Witte, Energy Procedia **10**, 208 (2011).

[16] K. Seeger, *Semiconductor Physics*, 9th ed. (Springer, 2004).

[17] T. Orgis, M. Maiberg, and R. Scheer, Journal of Applied Physics **114**, 214506 (2013).

[18] W. Witte, D. Abou-Ras, K. Albe, G. H. Bauer, F. Bertram, C. Boit, R. Brüggemann, J. Christen, J. Dietrich, A. Eicke, D. Hariskos, M. Maiberg, R. Mainz, M. Meessen, M. Müller, O. Neumann, T. Orgis, S. Paetel, J. Pohl, H. Rodriguez-Alvarez, R. Scheer, H.-W. Schock, T. Unold, A. Weber, and M. Powalla, Progress in Photovoltaics: Research and Applications **23**, 717 (2015).

[19] M. S. Tyagi and R. v. Overstraeten, Solid-State Electronics **26**, 577 (1983).

[20] S. M. Sze and K. K. Ng, *Physics of Semiconductor Devices*, 3rd ed. (Wiley, 2007).

6 Summary and suggestions for further studies

The goal of this work was to essentially improve the current understanding of room-temperature time-resolved luminescence in thin-film semiconductors by putting the numerous distinct phenomena into order and interpreting them with the help of simulations. In order to do so, all equations needed for describing generation, transport, and recombination of charge carriers have been derived first. Many simplifying assumptions have thereby been made, that are, however, fulfilled for thin-film semiconductors such as Cu(In,Ga)Se$_2$ in a wide parameter range. On the basis of these equations, the effective recombination lifetime has been introduced as an important material parameter of semiconductors, relating the density of excess carriers to the recombination rate. It could be shown that this quantity in special cases can be determined from the luminescence decay, which gives a reason for the high interest in TRL as a characterization technique. Based on the example of band-to-band recombination under high extitations, however, it has been demonstrated that the equality of the effective recombination lifetime and the decay time is not universal. Thus, there are cases in which the measurement of the effective recombination lifetime by means of TRL would yield wrong results. Therefore, in order to retrieve such artificial effects and to increase the significance of a TRL decay, more thourough studies have been performed in chapter 5 of this work.

The first step consisted in the investigation of the effects of charge carrier drift, diffusion, recombination via defects, direct band-to-band recombination, and photon recycling on the TRL decay of thin-film semiconductors, because so far these have been studied only for bulk semiconductors [20, 24, 59]. As a first result it turned out that photon recycling basically can be neglected due to the mainly subbandgap luminescence. This essentially simplified further simulations. The other effects - recombination, drift, and diffusion - are non-linear effects in terms of the behaviour of the TRL decay under excitation increase. For this reason, these have been discussed for low and high excitations separately.

The diffusion of charge carriers does always occur. However, such a diffusion current influences the luminescence decay directly only under high injection conditions. Under low injection levels, it can be disregarded. In contrast, the drift of charge carriers occurs only in electric fields, e.g. in the space charge region of semiconductor junctions. In this case, the luminescence decay under low excitations exhibits at least two time constants, with a fast initial decay due to charge separation and a second slow decay that reveals the recombination lifetime. Under high excitations, the electric field can be screened partially. This

reduces the impact of drift and makes the decay curve mono-exponential. Concerning the recombination of charge carriers, the behaviour under excitation increase is inverse: the decay of the luminescence is mono-exponential under low excitations, but under high excitations the luminescence decay will become either faster and multi-exponential if bimolecular recombination is dominating, or slower and concave bi-exponential due to an inhibited defect recombination. Altogether this means that the luminescence of sole absorber layers under low excitation does not exhibit drift or diffusion effects. Instead, the decay is governed only by recombination and the decay time equals the effective recombination lifetime. This relation implies that the open-circuit voltage of a solar cell is a function of the low injection decay time of the absorber. Based on this assumption, it could be estimated that the decay times for CIGSe absorbers must be in the range of a few $10 \, \mathrm{ns}$ in order to achieve typical open-circuit voltages of $700 \ldots 800 \, \mathrm{mV}$ [18]. In experiment, however, noticeably longer decay times have been observed, which additionally do not correlate with the solar cell parameters either (see figure 6.1). In the first instance, this may be due to a change of the absorber properties through the subsequent processing. For this reason, a technique has been developed that allows the characterization of the absorber after finishing the cell process. This is achieved by a measurement of TRL under varying bias voltage. The advantages of this method are manyfold. For instance, the absorber in the cell is protected from degradation effects by the adjacent layers. Furthermore, the electric field in the solar cell can be adjusted which allows the discrimination of the recombination from the drift. By doing so, recombination lifetimes have been determined with values of $10 - 20 \, \mathrm{ns}$. These lie exactly in the expected range. Thus, it could be indeed the case that an absorber is modified through the further processing. In that case, it is advisable to perform lifetime measurements on complete cells in order to determine the relevant recombination lifetime. But then, it still poses the question for the origin of bi-exponential decay curves with time-constants of several $100 \, \mathrm{ns}$ (see figure 6.1) observed on absorbers, because all studied recombination mechanisms lead to mono-exponential decays under low excitations.

One approach to solve the problem was to consider potential fluctuations. These are variations of the electrostatic potential due to inhomogeneities of the doping density. In consequence, electric fields are created even in absorber layers, that make the charge carriers drift and lead to a bi-exponential luminescence decay. As an outcome of absorption measurements, these potential fluctuations already have been determined to be below $100 \, \mathrm{meV}$. The simulations have shown that these fluctutations are too small in order to substantially influence the luminescence decay. Even the simulation of an inhomogeneous recombination lifetime or band gap did not yield the above described bi-exponential decays with long decay times. For this reason, the current model of absorbers has been extended by shallow defects that may capture and reemit charge carriers. By these, the charge carriers are preserved only but they do not recombine. Because of the additional capture,
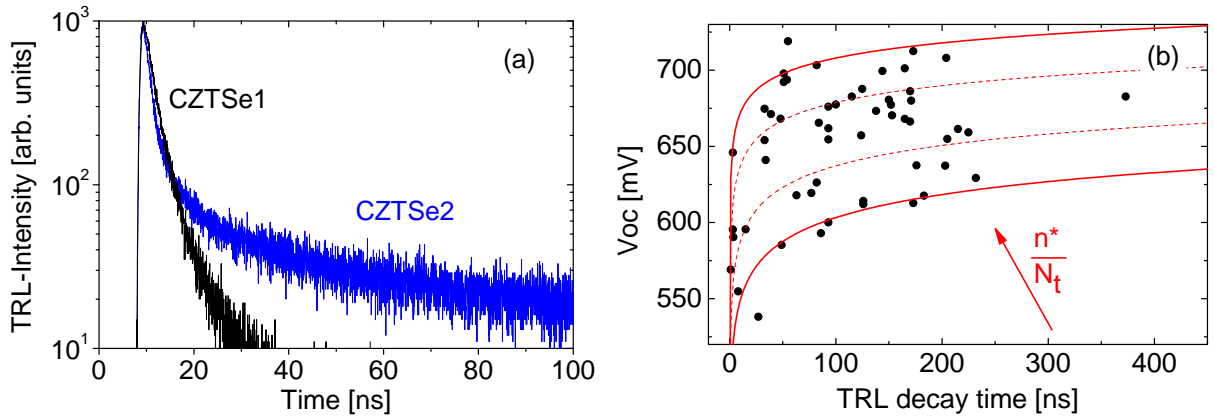
Figure 6.1: (a) One- and bi-exponential luminescence decay of two different $Cu_2ZnSnSe_4$ absorber layers and (b) luminescence decay time (determined from the $1/e$ decay) of $Cu(In,Ga)Se_2$ absorbers measured immediately after preparation process vs. open-circuit voltage of final solar cell. The red curves are theoretical $V_{oc}(\tau_{decay})$ curves calculated after equation (5.3.2) for $n^*/N_t = 1$, 0.15, 0.015, 0.003. With kind permission of Stefan Hartnauer and Enrico Jarzembowski.

the charge carrier densities decay faster compared to the case of pure recombination. Afterwards, the charge carriers are stored in the trap for a characteristic time and then they are thermally reemitted to the energy bands and recombine. Depending on the barrier height, this emission may become very slow leading to a slow, second luminescence decay. Thus, the model extended by traps finally could explain the bi-exponential decay curves. Accordingly, the black graph in figure 6.1 (a) is related to a semiconductor with only little shallow defects, and the blue curve is related to a semiconductor with similar recombination but with a high density of traps. In the end, this hypothesis of a dominant minority carrier trapping has been further confirmed in terms of a combination of experiment and simulation. First of all, the transients show a strong temperature dependence which is in agreement with the expectations due to the thermally activated reemission. Apart from this qualitative argument, the decay curves could be approximated by simulated ones as well. A result of the simulations are the recombination lifetime, the trap energy, and the trap density in the absorber with values that are in accordance with admittance and spectral luminescence experiments. Therefore, the trap model could reasonably describe all transients observed on absorbers, and only the relation remained of the TRL decay to electric quantities, such as the open-circuit voltage. In order to deal with this problem, it has been shown first that traps do not influence the open-circuit voltage but only the decay time. Hence, traps act as an independent variable for which reason V_{oc} does not correlate with τ_{decay}. For a more detailed investigation, the open-circuit voltage has been calculated as a function of τ_{decay} which yielded the red curves in figure 6.1 (b). It turned out, the there is an entire range of possible open-circuit voltages for one single decay time. This is due to differences in the trap density, for instance because of a different preparation.
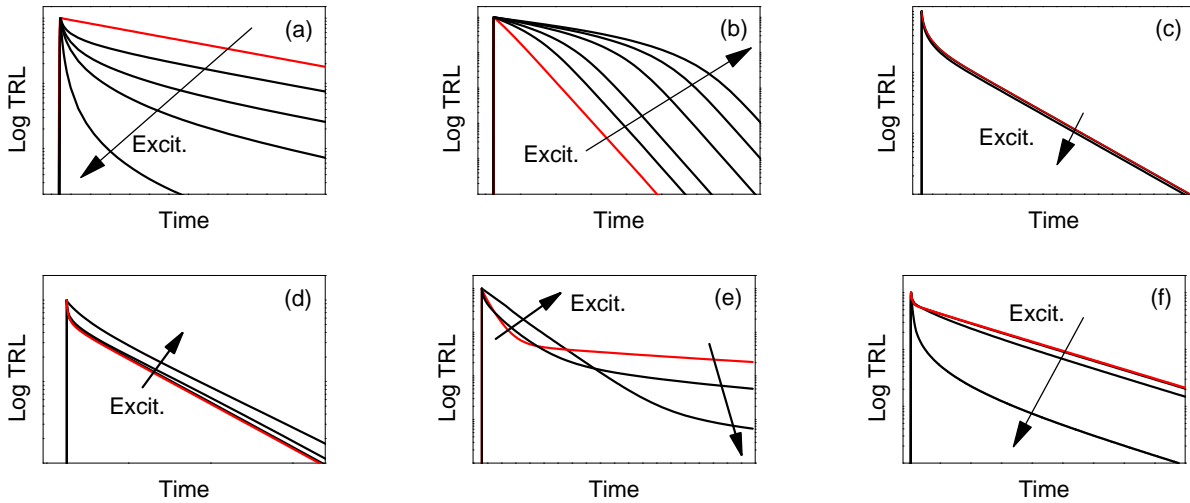
Figure 6.2: Sketch of the dependencies under excitation increase (the red curve marks a low injection excitation) for dominating (a) bimolecular recombination (b) asymmetric defect recombination (c) front surface recombination (d) potential fluctuations (e) minority carrier trapping (f) minority carrier trapping with capture times below the resolution of the experimental setup.

Altogether, the goals of this work have been attained. A model has been found, that is capable to describe the luminescence transients observed on thin-film absorbers. This model is one-dimensional and includes the drift, the diffusion, the recombination, and the trapping of charge carriers. Each single effect brings a different excitation dependence of the TRL decay about - these are sketched in figure 6.2. This shows, that the consideration of minority carrier traps is indispensable in order to describe the observed transients. This minority carrier trapping hinders the characterization of the recombination, which is important in particular for an application in photovoltaics. Thus, trapping should be avoided, e.g. by measurements under slightly increased temperatures.

Despite the outstanding progress in the application of TRL to thin-film semiconductors and its analyzation, several problems are still not dealt with. Building on that, the following concerns for further studies are proposed:

- The microscopic model of thin-film semiconductors that has been developed in this work describes the observed TRL decays very well. However, so far there is still a lack of combined simulations of time-resolved luminescence (temperature, excitation, and voltage dependent), current-voltage measurements, quantum efficiency measurements, and so on. In doing so, the model will be further validated and improved. In particular, this will reveal the role of grain boundaries and local shunts, that are not included in the presented one-dimensional model.

- The material parameters so far have been determined by manually changing the input values for simulations until the simulated decay curves approximate the experimental luminescence transients. This is time-consuming, for which reason a fit

routine must be developed in order to determine material parameters from the luminescence decay automatically. This is indispensable for the in-line application of TRL and for the optimization of preparation processes.

- With regard to the prior point, it is unclear how semiconductors are affected by material compositions, growth conditions, and processing. It is proposed to systematically vary the material preparation and to study the effect in order to retrieve correlations.

- Finally, the measurement routine proposed in this work requires measurements on sole absorber layers or complete solar cells. However, most published works show TRL on absorbers covered with a thin semiconducting layer that shall protect the absorber. The impact of this additional layer on the TRL decay is still not accurately known and needs further investigations.

Bibliography

[1] K. Seeger. *Semiconductor Physics: An introduction.* 8th ed. Springer, 2002.

[2] R. K. Ahrenkiel, N. Call, S. W. Johnston, and W. K. Metzger. "Comparison of techniques for measuring carrier lifetime in thin-film and multicrystalline photovoltaic materials". In: *Solar Energy Materials & Solar Cells* 94 (2010), pp. 2197–2204.

[3] D. Macdonald, R. A. Sinton, and A. Cuevas. "On the use of a bias-light correction for trapping effects in photoconductance-based lifetime measurements of silicon". In: *Journal of Applied Physics* 89 (2001), pp. 2772–2778.

[4] L. Janßen. "Herstellung und Untersuchung von beidseitig passivierten kristallinen Siliziumsolarzellen". PhD thesis. Rheinisch-Westfälische Technische Hochschule Aachen, 2009.

[5] B. Ohnesorge, R. Weigand, G. Bacher, A. Forchel, W. Riedl, and F. H. Karg. "Minority-carrier lifetime and efficiency of Cu(In,Ga)Se$_2$ solar cells". In: *Applied Physics Letters* 73.9 (1998), pp. 1224–1226.

[6] B. M. Keyes, P. Dippo, W. K. Metzger, J. AbuShama, and R. Noufi. "Changes in the dominant recombination mechanism of polycrystalline Cu(In,Ga)Se$_2$ occuring during growth". In: *Journal of Applied Physics* 94 (2003), pp. 5584–5590.

[7] W. K. Metzger, D. Albin, D. Levi, P. Sheldon, X. Li, B. M. Keyes, and R. K. Ahrenkiel. "Time-resolved photoluminescence studies of CdTe solar cells". In: *Journal of Applied Physics* 94.5 (2003), pp. 3549–3555.

[8] S.-i. Shimakawa, Y. Hashimoto, S. Hayashi, T. Satoh, and T. Negami. "Annealing effects on Zn$_{1-x}$Mg$_x$O/CIGS interfaces characterized by ultraviolet light excited time-resolved photoluminescence". In: *Solar Energy Material & Solar Cells* 92 (2008), pp. 1086–1090.

[9] S. Shirakata. "Photoluminescence characterization of photovoltaic effect in ZnO/CdS/Cu(In,Ga)Se$_2$ heterostructure". In: *Physica Status Solidi A* 210 (2013), pp. 1322–1327.

[10] S. Shirakata, H. Ohta, and N. Iwado. "Characterization of Cu(In,Ga)Se$_2$ Solar Cell Fabrication Process by Photoluminescence". In: *Japanese Journal of Applied Physics* 51 (2012), 10NC13.

[11] S. Shirakata and T. Nakada. "Time-resolved photoluminescence in Cu(In,Ga)Se$_2$ thin films and solar cells". In: *Thin Solid Films* 515 (2007), pp. 6151–6154.

[12] D. Kuciauskas, J. V. Li, M. A. Contrera, J. Pankow, and P. Dippo. "Charge carrier dynamics and recombination in graded band gap CuIn$_{1-x}$Ga$_x$Se$_2$ polycrystalline thin-film photovoltaic solar cell absorbers". In: *Journal of Applied Physics* 114 (2013), p. 154505.

Bibliography

[13] T. Sakurai, K. Taguchi, M. M. Islma, S. Ishiuuka, A. Yamada, K. Matsubara, S. Niki, and K. Akimoto. "Time-Resolved Microphotoluminescence Study of Cu(In,Ga)Se$_2$". In: *Japanese Journal of Applied Physics* 50 (2011), 05FC01.

[14] S.-i. Shimakawa, K. Kitani, S. Hayashi, T. Satoh, Y. Hashimoto, Y. Takahashi, and T. Negami. "Characterization of Cu(In,Ga)Se$_2$ thin films by time-resolved photoluminescence". In: *Physica Status Solidi* 203.11 (2006), pp. 2630–2633.

[15] I. Repins, C. Beall, N. Vora, C. DeHart, D. Kuciauskas, P. Dippo, B. To, J. Mann, W.-C. Hsu, A. Goodrich, and R. Noufi. "Co-evaporated Cu$_2$ZnSnSe$_4$ films and devices". In: *Solar Energy Material & Solar Cells* 101 (2012), pp. 154–159.

[16] R. Scheer and H.-W. Schock. *Chalcogenide Photovoltaics: Physics, Technologies, and Thin Film Devices*. WILEY-VCH, 2011.

[17] W. K. Metzger, I. L. Repins, and M. A. Contreras. "Long lifetimes in high-efficiency Cu(In,Ga)Se$_2$ solar cells". In: *Applied Physics Letters* 93 (2008), p. 022110.

[18] P. Jackson, R. Wuerz, D. Hariskos, E. Lotter, W. Witte, and M. Powalla. "Effects of heavy alkali elements in Cu(In,Ga)Se$_2$ solar cells with efficiencies up to 22.6%". In: *Physica Status Solidi RRL* (2016).

[19] R. Scheer, A. Pérez-Rodríguez, and W. K. Metzger. "Advanced diagnostic and control methods of processes and layers in CIGS solar cells and modules". In: *Progress in Photovoltaics: Research and Applications* 18 (2010), pp. 467–480.

[20] R. K. Ahrenkiel. "Minority-Carrier Lifetime in III-V Semiconductors". In: *Minority Carriers in III-V Semiconductors: Physics and Applications*. Vol. 39. Academic Press, INC., 1993. Chap. 2, pp. 39–150.

[21] S. Shirakata, K. Ohkubo, Y. Ishii, and T. Nakada. "Effects of CdS buffer layers on photoluminescence properties of Cu(In,Ga)Se$_2$ solar cells". In: *Solar Energy Materials & Solar Cells* 93 (2009), pp. 988–992.

[22] S. Shirakata and T. Nakada. "Photoluminescence and time-resolved photoluminescence in Cu(In,Ga)Se$_2$ thin films and solar cells". In: *Physica Status Solidi C* 6 (2009), pp. 1059–1062.

[23] W. K. Metzger, I. L. Repins, M. Romero, P. Dippo, R. N. Contreras, and D. Levi. "Recombination kinetics and stability in polycrystalline Cu(In,Ga)Se$_2$ solar cells". In: *Thin Solid Films* 517 (2009), pp. 2360 –2364.

[24] W. K. Metzger, R. K. Ahrenkiel, J. Dashdorj, and D. J. Friedman. "Analysis of charge separation dynamics in a semiconductor junction". In: *Physical Review B* 71 (2005), p. 035301.

[25] A. Kanevce, D. H. Levi, and D. Kuciauskas. "The role of drift, diffusion, and recombination in time-resolved photoluminescence of CdTe solar cells determined through numerical simulation". In: *Progress in Photovoltaics* 22 (2014), 11381146.

[26] A. Jüngel. *Transport Equations for Semiconductors*. Lecture notes in Physics 773. Springer, 2009.

[27] G. Czycholl. *Theoretische Festkörperphysik*. 3rd ed. Springer, 2008.

[28] S. Selberherr. *Analysis and Simulation of Semiconductor Devices*. Springer Verlag, 1984.

[29] D. Vasileska and S. M. Goodnick. *Computational Electronics*. Morgan & Claypool, 2006.

[30] E. A. B. Cole. *Mathematical and Numerical Modelling of Heterostructure Semiconductor Devices: From Theory to Programming*. Springer, 2009.

[31] S. L. Chuang. *Physics of Optoelectronic Devices*. WILEY-VCH, 1995.

[32] W. Shockley and W. T. Read. "Statistics of the Recombinations of Holes and Electrons". In: *Physical Review* 87 (1952), pp. 835–842.

[33] R. N. Hall. "Electron-Hole Recombination in Germanium". In: *Physical Review* 87 (1952), p. 387.

[34] P. T. Landsberg. *Recombination in Semiconductors*. Cambridge University Press, 1991.

[35] A. M. Stoneham and R. H. Bartram. "Non-radiative de-excitation of deep centres". In: *Solid-State Electronics* 21 (1978), pp. 1325–1329.

[36] P. Würfel. *Physics Of Solar Cells*. 2nd ed. Wiley-VCH, 2009.

[37] R. H. Bube. *Photoelectronic Properties of Semiconductors*. Cambridge University Press, 1992.

[38] I. Pelant and J. Valenta. *Luminescence Spectroscopy of Semiconductors*. Oxford University Press, 2012.

[39] *Sentaurus Device User Guide*. Synopsys®. Sept. 2011.

[40] H. Haug and S. W. Koch. *Qunatum Theory of the Optical and Electronic Properties of Semiconductors*. 5th ed. World Scientific, 2009.

[41] S. M. Sze and K. K. Ng. *Physics of Semiconductor Devices*. 3rd ed. Wiley, 2007.

[42] J. L. Balenzategui and A. Mart. "Detailed modelling of photon recycling: application to GaAs solar cells". In: *Solar Energy Materials & Solar Cells* 90 (2006), pp. 1068–1088.

[43] W. Becker. *Advanced Time-Correlated Single Photon Counting Techniques*. Berlin: Springer Verlag, 2005.

[44] D. Abou-Ras, T. Kirchartz, and U. Rau. *Advanced Characterization Tequnices for Thin Film Solar Cells*. Weinheim: WILEY-VCH, 2011.

[45] B. Lax and S. F. Neustadter. "Transient Response of a p-n Junction". In: *Journal of Applied Physics* 25 (1954), pp. 1148–1154.

[46] R. E. Bank, D. J. Rose, and W. Fichtner. "Numerical Methods for Semiconductor Device Simulation". In: *IEEE Transactions on Electron Devices* 30 (1983), pp. 1031–1041.

[47] S. J. Polak, C. d. Heijer, and W. Schilders. "Semiconductor device modelling from the numerical point of view". In: *International Journal for Numerical Methods in Engineering* 24 (1987), pp. 763–838.

[48] D. Scharfetter and H. Gummel. "Large-signal analysis of a silicon read diode oscillator". In: *IEEE Transactions on Electron Devices* 16 (1969), pp. 64–77.

[49] W. M. J. Coughran, J. Cole, P. Lloyd, and J. K. White. *Semiconductors Part I*. Vol. 50. IMA Volumes in Mathematics and its Applications. Springer Verlag, 1994.

[50] R. E. Bank, W. M. Coughran, W. Fichtner, E. H. Grosse, D. J. Rose, and R. K. Smith. "Transient Simulation of Silicon Devices and Circuits". In: *IEEE Transactions on Computer-Aided Design* 4 (1985), pp. 436–451.

[51] R. E. Bank and D. J. Rose. "Global approximative Newton Methods". In: *Numerical Mathematics* 37 (1981), pp. 279–295.

[52] Y. Saad and M. H. Schultz. "GMRES: A Generalized Minimal Residual Algorithm for Solving Nonsymmetric Linear Systems". In: *SIAM Journal on Scientific and Statistical Computing* 7 (1986), pp. 856–869.

[53] J.-R. Ohm and H. D. Lüke. *Signalübertragung: Grundlagen der digitalen und analogen Nachrichtenübertragungssysteme*. Vol. 10. Springer, 2007.

[54] G. W. t Hooft and C. van Opdorp. "Determination of bulk minoritycarrier lifetime and surface/interface recombination velocity from photoluminescence decay of a semi-infinite semiconductor slab". In: *Journal of Applied Physics* 60.3 (1986), pp. 1065–1070.

[55] R. K. Ahrenkiel. "Measurement of minority-carrier lifetime by time-resolved photoluminescence". In: *Solid-State Electronics* 35.3 (1992), pp. 239–250.

[56] A. B. Sproul. "Dimensionless solution of the equation describing the effect of surface recombination on carrier decay in semiconductors". In: *Journal of Applied Physics* 76 (1994), p. 2851.

[57] R. K. Ahrenkiel, B. M. Keyes, and D. J. Dunlavy. "Non-linear recombination processes in photovoltaic semiconductors". In: *Solar Cells* 30 (1991), pp. 163–176.

[58] I. L. Repins, B. J. Stanbery, D. L. Young, S. S. Li, W. K. Metzger, C. L. Perkins, W. N. Shafarman, M. E. Beck, L. Chen, V. K. Kapur, D. Tarrant, M. D. Gonzalez, D. G. Jensen, T. J. Anderson, X. Wang, L. L. Kerr, B. Keyes, S. Asher, A. Delahoy, and B. Von Roedern. "Comparison of device performance and measured transport parameters in widely-varying Cu(In,Ga) (Se,S) solar cells". In: *Progress in Photovoltaics: Research and Applications* 14.1 (2006), pp. 25–43.

[59] Y. Rosenwaks, B. R. Thacker, R. K. Ahrenkiel, A. J. Nozik, and I. Yavneh. "Photogenerated carrier dynamics under the influence of electric fields in III-V semiconductors". In: *Physical Review B* 50 (1994), pp. 1746–1754.

[60] J. Dashdorj, R. Ahrenkiel, and W. Metzger. "Modeling of recombination lifetimes in charge-separation device structures". In: *Materials Research Society Symposium Proceedings* 799 (2004), Z4–5.

[61] L. Q. Phuong, M. Okano, Y. Yamada, A. Nagaoka, K. Yoshino, and Y. Kanemitsu. "Temperature-dependent photocarrier recombination dynamics in Cu2ZnSnS4 single crystals". In: *Applied Physics Letters* 104.8 (2014), p. 081907.

[62] I. L. Repins, H. Moutinho, S. G. Choi, A. Kanevce, D. Kuciauskas, P. Dippo, C. L. Beall, J. Carapella, C. DeHart, B. Huang, and S. H. Wei. "Indications of short minority-carrier lifetime in kesterite solar cells". In: *Journal of Applied Physics* 114.8 (2013), p. 084507.

[63] S. Siebentritt and U. Rau, eds. *Wide-Gap Chalcopyrites*. Vol. 86. Springer Series in Materials Science. Springer Berlin Heidelberg, 2006.

[64] M. Igalson and P Zabierowski. "Electron traps in Cu(In,Ga)Se$_2$ absorbers of thin film solar cells studied by junction capacitance techniques". In: *Opto-Electronics Review* 11 (2003), pp. 261–267.

[65] S. Chen, A. Walsh, X.-G. Gong, and S.-H. Wei. "Classification of Lattice Defects in the Kesterite Cu2ZnSnS4 and Cu2ZnSnSe4 Earth-Abundant Solar Cell Absorbers". In: *Advanced Materials* 25.11 (2013), pp. 1522–1539.

[66] K. Bothe, G. Bauer, and T. Unold. "Spatially resolved photoluminescence measurements on Cu(In,Ga)Se2 thin films". In: *Thin Solid Films* 403-404 (2002), pp. 453 – 456.

[67] G. H. Bauer, S. J. Heise, S. Knabe, O. Neumann, R. Brüggemann, D. Hariskos, and W. Witte. "Depth dependent optoelectronic properties of Cu(In,Ga)Se$_2$ with lateral resolution in the micro/submicro scale from luminescence studies". In: *Energy Procedia* 10 (2011), pp. 208–212.

[68] L. Gütay, C. Lienau, and G. H. Bauer. "Subgrain size inhomogeneities in the luminescence spectra of thin film chalcopyrites". In: *Applied Physics Letters* 97.5 (2010), p. 052110.

[69] J. H. Werner, J. Mattheis, and U. Rau. "Efficiency limitations of polycrystalline thin film solar cells: case of Cu(In,Ga)Se$_2$". In: *Thin Solid Films* 480-481 (2005), pp. 399–409.

[70] P. O. Grabitz, U. Rau, and J. H. Werner. "Modeling of spatially inhomogeneous solar cells by a multi-diode approach". In: *physica status solidi (a)* 202.15 (2005), pp. 2920–2927.

[71] M. J. Romero, H. Du, G. Teeter, Y. Yan, and M. Al-Jassim Mowafak. "Comparative study of the luminescence and intrinsic point defects in the kesterite Cu$_2$ZnSnS$_4$ and chalcopyrite Cu(In,Ga)Se$_2$ thin films used in photovoltaic applications". In: *Physical Review B* 84 (2011), p. 165324.

[72] J. Larsen, K. Burger, L. Gutay, and S. Siebentritt. "Temperature dependence of potential fluctuations in chalcopyrites". In: *Photovoltaic Specialists Conference (PVSC), 2011 37th IEEE*. 2011, pp. 000396–000401.

Acknowledgements

Selbstständigkeitserklärung

Hiermit versichere ich ausdrücklich, dass ich die vorliegende Dissertation mit dem Thema

„Numerical and analytical study of time-resolved luminescence in thin-film semiconductors"

selbstständig verfasst habe und in dieser Form erstmalig einreiche. Es sind keine anderen als die angegebenen Quellen und Hilfsmittel benutzt und sämtliche Zitate kenntlich gemacht worden. Andere Promotionsversuche als diesen habe ich nicht unternommen.

Halle, den 22. August 2016

M.Sc. Matthias Maiberg

Lebenslauf

Persönliche Angaben

Geburt	**23. März 1988 in Bernburg (Saale)**.
Geschlecht	**Männlich**.
Nationalität	**Deutsch**.

Akademischer Werdegang

10/2007–09/2010	**Martin-Luther-Universität Halle-Wittenberg**, Bachelorstudium in Physik mit Abschlussnote 1,4.
10/2010–10/2012	**Martin-Luther-Universität Halle-Wittenberg**, Masterstudium in Physik mit Abschlussnote 1,2.
04/2012–09/2012	**Martin-Luther-Universität Halle-Wittenberg**, Bachelorstudium in Mathematik mit Anwendungsfach mit Abschlussnote 1,4.
seit 10/2012	**Martin-Luther-Universität Halle-Wittenberg**, Wissenschaftlicher Mitarbeiter mit Aussicht auf Erlangung des Doktorgrades.

Angaben zu Vorstrafen

Es liegen weder Vorstrafen vor, noch ist ein Ermittlungsverfahren eingeleitet.

Halle, 22. August 2016